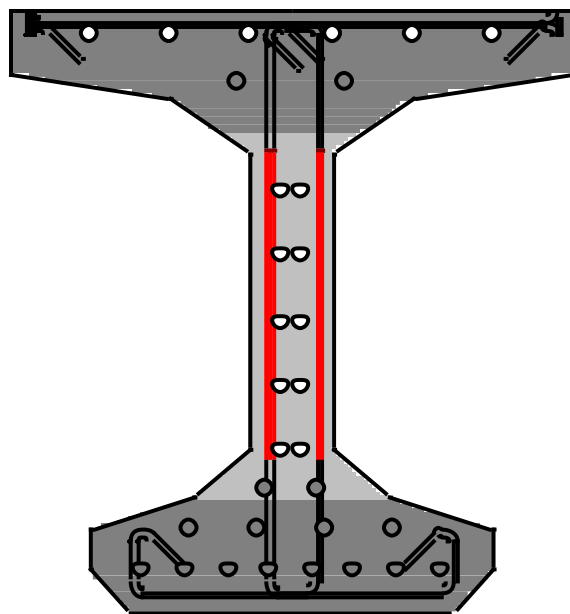


M. C. Vergeer

Shear tension resistance of prestressed concrete beams with shear reinforcement

Based on the MCFT



Shear tension resistance of prestressed concrete beams with shear reinforcement

Based on the MCFT

By

M.C. Vergeer

in partial fulfilment of the requirements for the degree of

Master of Science

in Applied Physics

at the Delft University of Technology,
to be defended publicly on Monday April 8, 2019 at 16:00 PM.

Supervisor:	Dr. Ir. C van der Veen,	TU Delft
Thesis committee:	Ir. M. Roosen,	RWS
	Prof. Dr. ir. J.G. Rots,	TU Delft
	Ir. J.M. Houben,	TU Delft

An electronic version of this thesis is available at <http://repository.tudelft.nl/>

Preface

I have written this thesis report as conclusion of my master Civil Engineering with track structural engineering at the TU Delft. The last 6 years I have learned about structures and other civil engineering topics with great joy and I'm looking forward to bring this into practice. The last 8 months I've been working on my final thesis, which was challenging but I also learned a lot about shear failure.

This thesis is part an ongoing research about the shear tension capacity of prestressed girders by Marco Roosen. This thesis contributed to the insight in the mechanisms of shear tension failure and proposes a model for shear tension failure based on the MCFT.

I would like to thank my graduation committee, and especially my supervisors M.A. Roosen and C. Van der Veen for leading me in the right direction and being enthusiastic about the subject. I also want to thank my parents for supporting me.

Marieke Vergeer

19 March, 2019

Abstract

Old bridges in the Netherlands are reassessed to prove their structural safety because of the increased traffic loads. The Eurocode model for the shear capacity of prestressed concrete beams with sufficient shear reinforcement was found to be very conservative for small amounts of transverse reinforcement, which is typical for old bridges. Code provisions based on the modified compression field theory appear to be much more accurate (Bentz, Vecchio, & Collins, 2006). On the other hand, these models make no distinction between flexural shear and shear tension failure, while 25% of the bridges consists of T-, I-, or box beams which are sensitive to shear tension failure. The aim of this thesis is to present a more accurate prediction for shear tension failure based on the modified compression field theory (MCFT). The report focuses on both the CSA-model and Response-2000. The CSA-model is a simplification of the MCFT for beams under the assumption that $\sigma_z = 0$. The CSA-model shear resistance consists of a concrete and steel part. Response-2000 is a cross-sectional analysis program that works as a non-linear finite element analysis and not only takes into account bending but also shear.

Response analysis of 32 beams (experiments of Xie (Xie, 2009), Choulli (Choulli, 2005), Hanson (Hanson & Hulbos, 1965) and Leonhardt (Leonhardt, Koch, & Rostasy, 1973)) have been made and compared with the experimental observations. The failure load is predicted with a mean ratio of 1.38 and a COV of 19% compared to the experiments. It was found that for small a/d-ratios predictions are more conservative. Failure mechanisms: rupture of the stirrups, crushing of the web concrete and slipping/major crack opening are found in Response. 87% of the failure mechanisms was predicted correctly compared to the experiments. The critical cross-section compared with the experimentally observed failure zone showed that 60% of the beams was predicted in the failure zone. The shear force in the cross section is resisted by reinforcement steel, aggregate interlock and the uncracked concrete, which were found to take up respectively 1/2, 1/6 and 1/3 of the shear force. The steel part is predicted accurately while the aggregate interlock part is underpredicted due to an over prediction of the crack spacing. The uncracked part is overpredicted for small amounts of reinforcement and underpredicted for larger amounts of reinforcement.

The data of the Response analysis have been used to modify the CSA-model to a model solely describing shear tension failure. The comparison showed that the CSA-model underestimates the steel part, overestimates the concrete part, takes a too large cracked height and doesn't take into account the contribution of the uncracked part. From this comparison, modifications for β , θ , V_{max} , h_{crack} and ϵ_x are proposed using Response data and proposals from Esfandiari (Esfandiari & Adebar, 2009). The flanges are taken as uncracked and the contribution of the uncracked part is described with a linear elastic shear stress distribution. This has led to a proposal for a model that solely describes shear tension failure, where the most important addition is the contribution of the uncracked height. Calculations show that the model gives conservative predictions compared to the experiments (mean ratio of 1.36 and a COV 22%) and the predictions are almost the same as for Response. The parameters are predicted conservative compared to the Response-2000 predictions.

For further research, it is recommended to look deeper into the influence of the clamping stress, especially for beams with a small a/d-ratio. It is also recommended doing more analysis of experiments with Response to obtain a more accurate prediction.

Contents

List of Figures	V
List of tables	X
List of symbols	XII
1 Introduction	1
1.1 Research Questions	3
1.2 Thesis outline	4
2 Models based on the MCFT	6
2.1 Modified compression field theory (MCFT)	6
2.1.1 Derivation of the MCFT	7
2.1.2 Calculation procedure	11
2.2 CSA-model	13
2.2.1 Derivation from the MCFT	14
2.2.2 Calculation procedure	20
2.3 Response-2000	22
2.3.1 Model setup	22
2.3.2 Iterative calculation	24
2.3.3 Analysis Results	28
2.3.3.1 Cross-sectional analysis	28
2.3.3.2 Full member Response	32
3 Prediction of shear tension failures with Response-2000	34
3.1 Experiments.....	34
3.2 Comparison Response with experiments	37
3.2.1 General comparison	38
3.2.1.1 Failure Load	38
3.2.1.2 Failure mechanism.....	41
3.2.1.3 Critical location for shear tension failure.....	46
3.2.2 In-depth comparison	51
3.2.2.1 Steel component	52
3.2.2.2 Stress in the steel	53
3.2.2.3 Steel force.....	54
3.2.2.4 Concrete component.....	55
3.2.2.5 Crack width and crack spacing.....	55

3.2.2.6 Uncracked height.....	57
3.2.2.7 Contribution of Parts in Response	58
4 Shear tension model	60
4.1 Failure mechanisms.....	61
4.2 Cracked height.....	63
4.3 Uncracked zone	65
4.4 θ	69
4.4.1 θ -value yielding	72
4.4.2 θ -value crushing	73
4.5 β - value	74
4.5.1 β -value yielding.....	75
4.5.2 β -value crushing.....	75
4.6 V_{max}	77
4.7 ϵ_x	78
4.8 Calculation.....	81
4.8.1 Accuracy	84
5 Conclusions	86
5.1 Response	86
5.2 Modified model.....	89
6 Recommendations.....	91
Bibliography.....	92
Appendix	93
A Planning	94
B Response example input	95
C Example calculation Response values with MCFT	108
D Experiments and Response results	111
D.1 XIE	111
D.2 Choulli	118
D.3 Hanson	126
D.4 Leonhardt.....	142
E shear tension model accuracy	146

List of Figures

- Figure 1.1, Predicted shear failures2
- Figure 1.2, Predicted shear failure Response-2000 (Bentz E. C., Sectional Analysis of Reinforced Concrete Members, 2000)2
- Figure 1.3, Flexural shear (left) and shear tension (right), (Walraven, 2002)3
- Figure 1.4, Relationship between components4
- Figure 1.5, Overview of the content and relations that are treated in each chapter5
- Figure 2.1, Modified compression field theory (Bentz & Collins, Development of the 2004 Canadian standards association (CSA) A23.3 shear provisions for reinforced concrete, 2006)6
- Figure 2.2, Mohr's circle for average strains (Vecchio & Collins, 1985)7
- Figure 2.3, Stress-strain relationships, a. concrete, b. steel (Vecchio F. J., 1990).....8
- Figure 2.4, Local equilibrium between the crack and at the crack (Vecchio & Collins, 1985).....9
- Figure 2.5, CSA-model (Bentz & Collins, Development of the 2004 Canadian standards association (CSA) A23.3 shear provisions for reinforced concrete, 2006).....13
- Figure 2.6, Relationship Beta-values for beams without shear reinforcement (Bentz, Vecchio, & Collins, Simplified Modified Compression Field Theory for Calculating Shear Strength of Reinforced Concrete Elements, 2006)16
- Figure 2.7, Crack width for effective crack spacing of 300 mm (Bentz & Collins, Development of the 2004 Canadian standards association (CSA) A23.3 shear provisions for reinforced concrete, 2006) ...17
- Figure 2.8, Lower and upper limit for theta (Bentz & Collins, Development of the 2004 Canadian standards association (CSA) A23.3 shear provisions for reinforced concrete, 2006)18
- Figure 2.9, Beta and theta for various reinforcement percentages (Bentz, Vecchio, & Collins, Simplified Modified Compression Field Theory for Calculating Shear Strength of Reinforced Concrete Elements, 2006)19
- Figure 2.10, Cross-sectional forces and stiffness relationship (Bentz & Collins, Development of the 2004 Canadian standards association (CSA) A23.3 shear provisions for reinforced concrete, 2006) ...19
- Figure 2.11, Shear force capacity over the beam length for HCP1TW.....21
- Figure 2.12, Input screen Response-200022
- Figure 2.13, Definition of Ramsberg-Osgood parameters (Collins, 1991)23
- Figure 2.14, Loading definition.....24
- Figure 2.15, Nodes on the cross-section25
- Figure 2.16, Initial assumptions.....26
- Figure 2.17, Iteration for Newton-Raphson method (Hendriks & Esposito, 2017)27
- Figure 2.18, Response results general with MCFT formulas.....28
- Figure 2.19, Response results cracking with MCFT formulas.....30
- Figure 2.20, Response results reinforcement with MCFT formulas.....30
- Figure 2.21, Member response results.....32
- Figure 3.1, Cross-section LB2, LB3, LB10 (Xie, 2009)35
- Figure 3.2, Cross-section LB6 to LB8 (Xie, 2009).....35
- Figure 3.3, Cross-section HAP1TW, HAP2TW, HCP1TW, HCP2TW (Choulli, 2005)35
- Figure 3.4, Cross-section HAP1TE, HCP1TE, HCP2TE (Choulli, 2005)35
- Figure 3.5, Cross-section Xie LB2, LB3, LB1035

Figure 3.6, Cross-section Xie LB6 to LB8	36
Figure 3.7, Cross-section Choulli: HAP1TE, HCP1TE, HCP2TE	36
Figure 3.8, Cross-section Choulli: HAP1TW, HAP2TW, HCP1TW, HCP2TW	36
Figure 3.10, Cross-section TP2 (Leonhardt, Koch, & Rostasy, 1973).....	36
Figure 3.11, Cross-section TP4 (Leonhardt, Koch, & Rostasy, 1973).....	36
Figure 3.9, Cross-section Hanson (Hanson & Hulbos, 1965)	36
Figure 3.12, Response cross-section Hanson.....	37
Figure 3.13, Response cross-section TP2.....	37
Figure 3.14, Response cross-section TP4.....	37
Figure 3.15, Failure load	38
Figure 3.16, Failure load prediction as a function of the prestress	39
Figure 3.17, Failure load predictions as a function of the a/d-ratio	40
Figure 3.18, Failure load predictions as a function of the reinforcement ratio	41
Figure 3.19, Stirrup Rupture LB7	42
Figure 3.20, Major crack opening LB3	43
Figure 3.21, Crushing failure HAP1TE	44
Figure 3.22, Crushing failure FX1A	45
Figure 3.23, Crushing failure TP2.....	45
Figure 3.24, Failure location LB3	47
Figure 3.25, Failure location Xie	47
Figure 3.26, Failure location Choulli, * exp. failure zone unknown	48
Figure 3.27, Failure location Hanson, * exp. failure zone unknown	49
Figure 3.28, Failure location Leonhardt.....	50
Figure 3.29, The contribution of the concrete and steel part to the shear stress over the beam	51
Figure 3.30, The relation between the parameters influencing the number of stirrups through the crack.....	53
Figure 3.31, Prediction of the stirrup stress and number of stirrups.....	54
Figure 3.32, The relation between the prediction of the steel force and the prediction of the number of stirrups.....	55
Figure 3.33, Crack width prediction	56
Figure 3.34, Crack width major crack opening (LB3)	56
Figure 3.35, Crack spacing prediction.....	57
Figure 3.36, Prediction uncracked height.....	58
Figure 3.37, Contribution of the different components in Response	59
Figure 4.1, Response (coloured) and CSA (shaded) shear stress HAP1TE	60
Figure 4.2, MCFT load Response different failure mechanisms (Esfandiari & Adebar, 2009).....	63
Figure 4.3, Cross-section HAP1TW (left) and LB3 (right)	64
Figure 4.4, Shear stress HAP1TW (left) and LB3 (right)	64
Figure 4.5, Cracking angle HAP1TW (left) and LB3 (right)	64
Figure 4.6, Shear on the crack HAP1TW (Left) and LB3 (right)	65
Figure 4.7, Shear stress LB2 comparison with the linear elastic calculation.....	66
Figure 4.8, Shear stress LB8 in comparison with the linear elastic calculation	66
Figure 4.9, Tau x b distribution.....	67
Figure 4.10, Comparison shear stress distribution LB2	69

Figure 4.11, Comparison of predicted angle θ with MCFT result at: (a) yielding of transverse reinforcement (b) crushing of concrete for ' c f = 30 MPa, f y = 400 MPa. (Esfandiari & Adebar, 2009)	71
Figure 4.12, Comparison of Theta for LB8: yielding failure, fy= 529, fc= 63.5, rho_z= 1.89e-3	71
Figure 4.13, Comparison of theta for HCP2TW: crushing failure, fy= 525, fc= 90.20, rho_z= 5e-3	72
Figure 4.14, Theta_0	72
Figure 4.15, Accuracy theta yielding	73
Figure 4.16, Accuracy theta crushing	73
Figure 4.17, Comparison of predicted β with MCFT result at: (a) yielding of transverse reinforcement, (b) crushing of concrete for ' c f = 30 MPa, f y = 400 MPa. (Esfandiari & Adebar, 2009)	75
Figure 4.18, Accuracy of beta for yielding failure	75
Figure 4.19, Aggregate size dependency	76
Figure 4.20, Accuracy beta crushing	77
Figure 4.21, Proposed shear stress on Response shear stress	78
Figure 4.22, Longitudinal strain HAP1TW in Response	78
Figure 4.23, Parameters longitudinal strain	80
Figure 4.24, Comparison epsilon_x HAP1TW	81
Figure 4.25, Comparison epsilon_x F4B	81
Figure 4.26, Shear force capacity over beam HCP1TW	83
Figure 4.27, Shear force capacity over beam F4B	83
Figure 4.28, Comparison proposed shear stress distribution and Response for HCP1TW	84
Figure 4.29, Comparison proposed shear stress distribution and Response for F4B	84
Figure 4.30, Accuracy of proposed shear tension model	85
Figure 5.1, Predictions of Response and the variable angle truss model	89
Figure 5.2, Predictions of Response-2000 and the proposed shear tension model	90
Figure B.1, Quick define step 1	95
Figure B.2, Quick define step 2	96
Figure B.3, Quick define step 3	96
Figure B.4, Quick define step 4	97
Figure B.5, Response geometry and material properties	97
Figure B.6, definition concrete cross section	98
Figure B.7, concrete material menu	99
Figure B.8, steel material menu 15M	100
Figure B.9, steel material menu D4	100
Figure B.10, steel material menu duct	101
Figure B.11, longitudinal reinforcement configuration bottom	102
Figure B.12, longitudinal reinforcement configuration top	102
Figure B.13, Longitudinal reinforcement configuration duct bottom	103
Figure B.14, Longitudinal reinforcement configuration duct top	103
Figure B.15, Transverse reinforcement steel menu	104
Figure B.16, Loading menu	104
Figure B.17, Final input overview	105
Figure B.18, Full member properties	105
Figure B.19, Overview of the model data	106
Figure B.20, General output	107
Figure B.21, Full member response output	107

Figure D.1, Load distribution (Xie, 2009)	113
Figure D.2, Contribution of the concrete and steel part to the shear stress over the beam for LB2 ..	114
Figure D.3 Contribution of the concrete and steel part to the shear stress over the beam for LB3 ...	115
Figure D.4, Contribution of the concrete and steel part to the shear stress over the beam for LB6 ..	115
Figure D.26, Contribution of the concrete and steel part to the shear stress over the beam for LB7	116
Figure D.6, Contribution of the concrete and steel part to the shear stress over the beam for LB8 ..	117
Figure D.7, Contribution of the concrete and steel part to the shear stress over the beam for LB10	118
Figure D.8, Cross-section (m) (Choulli, 2005)	118
Figure D.9, Reinforcement configuration (Choulli, 2005)	119
Figure D.10, Prestress configuration, HCP1TE, HCP1TW, HAP1TE, HAP1TW P= 1859, $\epsilon = 6.40 \text{ mm/m}$ (Choulli, 2005)	120
Figure D.11, Prestress configuration HCP2TE, HCP2TW, HAP2TW P= 1225, $\epsilon = 6.67 \text{ mm/m}$ (Choulli, 2005)	120
Figure D.12, Contribution of the concrete and steel part to the shear stress over the beam for HAP1TE	121
Figure D.13, Contribution of the concrete and steel part to the shear stress over the beam for HAP1TW	122
Figure D.14, Contribution of the concrete and steel part to the shear stress over the beam for HAP2TW	122
Figure D.15, Contribution of the concrete and steel part to the shear stress over the beam for HCP1TE	123
Figure D.16, Contribution of the concrete and steel part to the shear stress over the beam for HCP1TW	124
Figure D.17, Contribution of the concrete and steel part to the shear stress over the beam for HCP2TE	125
Figure D.18, Contribution of the concrete and steel part to the shear stress over the beam for HCP2TW	125
Figure D.19, Stress strain diagram transverse reinforcements (Hanson & Hulbos, 1965)	127
Figure D.20, Load-strain curve prestressing strand (Hanson & Hulbos, 1965)	127
Figure D.21, Contribution of the concrete and steel part to the shear stress over the beam for FX1A	129
Figure D.22, Contribution of the concrete and steel part to the shear stress over the beam for FX1B	130
Figure D.23, Contribution of the concrete and steel part to the shear stress over the beam for F1A	131
Figure D.24, Contribution of the concrete and steel part to the shear stress over the beam for F1B.	131
Figure D.25, Contribution of the concrete and steel part to the shear stress over the beam for F2A	132
Figure D.26, Contribution of the concrete and steel part to the shear stress over the beam for F2B	133
Figure D.27, Contribution of the concrete and steel part to the shear stress over the beam for F3A	134
Figure D.28, Contribution of the concrete and steel part to the shear stress over the beam for F3B.	134
Figure D.29, Contribution of the concrete and steel part to the shear stress over the beam for F4A	135
Figure D.30, Contribution of the concrete and steel part to the shear stress over the beam for F4B.	136
Figure D.31, Contribution of the concrete and steel part to the shear stress over the beam for F5A	137
Figure D.32, Contribution of the concrete and steel part to the shear stress over the beam for F5B.	138
Figure D.33, Contribution of the concrete and steel part to the shear stress over the beam for F7A	139

Figure D.34, Contribution of the concrete and steel part to the shear stress over the beam for F10A139

Figure D.35,Contribution of the concrete and steel part to the shear stress over the beam for F11A140

Figure D.36,Contribution of the concrete and steel part to the shear stress over the beam for F19A141

Figure D.37, Contribution of the concrete and steel part to the shear stress over the beam for F19B142

Figure D.38,Contribution of the concrete and steel part to the shear stress over the beam for TP2.144

Figure D.39, Contribution of the concrete and steel part to the shear stress over the beam for TP4 145

List of tables

Table 2.1, Iterative calculation CSA-model HCP1TW	20
Table 2.2, HCP1TW data	21
Table 3.1, Cross-section properties Xie and Choulli	36
Table 3.2, Cross-section properties Hanson and Leonhardt	37
Table 3.3, Failure load prediction accuracy	39
Table 4.1, Division of the failure mechanisms	63
Table 4.2, Accuracy of the uncracked flange contribution	69
Table 4.3, Vmax predictions	78
Table 4.4, Shear tension calculation overview	82
Table 5.1, accuracy failure load	86
Table 5.2, accuracy uncracked height	87
Table 5.3, accuracy cracking angle	87
Table 5.4, accuracy steel stress	87
Table 5.5, accuracy steel component	88
Table 5.6, accuracy crack spacing	88
Table 5.7, contribution parts	88
Table 5.8 Accuracy of uncracked part calculations	89
Table 5.9, Accuracy θ and β	89
Table C.1, Starting values	108
Table C.2, Strains	108
Table C.3, Cracking angle	108
Table C.4, Stress-strain relationship D4	108
Table C.5, Stress in z-direction	108
Table C.6, Crack spacing	109
Table C.7, Diagonal crack spacing	109
Table C.8, Crack width	109
Table C.9, Shear on the crack	110
Table C.10, Principal tensile stress	110
Table C.11, Principal compressive stress	110
Table C.12, Stress on the crack	110
Table D.1, Cross-sectional dimensions	111
Table D.2, Concrete properties	111
Table D.3, Longitudinal reinforcement	111
Table D.4, Transverse reinforcement	112
Table D.5, Reinforcement properties	112
Table D.6, Prestressing properties	112
Table D.7, Concrete properties	118
Table D.8, Longitudinal reinforcement properties	119
Table D.9, Transverse reinforcement configuration	119
Table D.10 Reinforcement properties	119
Table D.11, Prestress properties	120
Table D.12, Concrete cross-section	126
Table D.13, Transverse reinforcement properties	126

Table D.14, Prestress properties	127
Table D.15, Overview properties per beam.....	128
Table D.16, Concrete cross-section	142
Table D.17, Concrete properties	142
Table D.18, Longitudinal reinforcement configuration	143
Table 6.31, Transverse reinforcement configuration	143
Table D.20, Reinforcement properties	143
Table D.21, Prestress properties	143
Table E.1, Shear tension model accuracy overview	146

List of symbols

Used Symbol	Different symbols used in literature	Description
A_c, A_s, A_p		Area of the concrete, reinforcement steel and prestressing in the flexural tension zone
A_{cc}, A_{sc}, A_p		Area of the concrete, reinforcement steel and prestressing of the flexural compression flange
A_{ct}, A_{st}, A_{pt}		Area of the concrete, reinforcement steel and prestressing of the flexural tension flange
A_{sw}		Area of the stirrups
A_{swl}		Area of the longitudinal reinforcement in the web on the flexural compression side
A_{wp}		Area of the prestressing reinforcement in the web on the flexural compression side
a		Shear span
a_g		Aggregate size
b_{top}, b_{bot}		Maximum width of the top or bottom flange
b_w	b	The width of the web
d		Effective depth
d_p		Distance from the web prestressing tendons to the bottom of the flexural tension side
d_s		Distance from the web reinforcement to the bottom of the flexural tension side
E_c, E_s, E_p		Young's modulus of the concrete, reinforcement steel and prestressing steel.
f_c		Cylindrical concrete compressive strength
f_t		Concrete tensile strength
f_u		Ultimate strength
f_y		Yield strength of the steel
h_{bot}		Total height of the bottom flange
h_{crack}		The cracked height of the beam
h_{skew}		The total height of the inclined parts of the flanges
h_{top}		Total height of the top flange
$h_{uncracked}$		Uncracked height of the beam
h_{web}		The height of the web
I		Moment of inertia of the cross-section
M		Bending moment working on the cross-section
N		Normal force working on the cross-section
S		The first moment of area
s		The spacing of the transverse reinforcement
s_x, s_z		Crack spacing in the x- and z-direction
s_{xe}		Effective crack spacing
s_θ		Diagonal crack spacing
V		Shear force working on the cross-section or total shear force resistance
$V_{bottomflange}$		Shear force resisted by the bottom flange
V_c		Shear force resistance of the concrete
V_{crush}		Shear tension resistance at concrete crushing after yielding
V_{exp}		Experimental shear tension resistance

V_{max}		Maximum shear force resistance of the cross-section
V_{prop}		Proposed shear tension resistance
V_r		Shear force resistance of the cross-section
V_s		Shear force resistance of the steel
$V_{topflange}$		Shear force resistance of the top flange
V_{tot}		The total shear force resistance of the cross-section
V_{web}		Shear force resistance of the web
V_{yield}		Shear tension resistance at yielding of the transverse reinforcement
w		Crack width
z	d_v	The internal lever arm of the beam
z_{bot}		Distance from the centre of gravity to the bottom
z_{top}		Distance from the centre of gravity to the top
β		The concrete shear contribution factor
γ_{xz}		Shear strain
γ_{xz0}		Average shear strain
$\Delta\theta$		Predicted rate of change of θ per unit ϵ_x
ϵ_1		Principal tensile strain.
ϵ_2		Principal compressive strain.
ϵ_c		Strain at the flexural compressive side
ϵ_s		Steel strain
ϵ_{sh}		Reinforcement strain at the beginning of strain hardening
ϵ_t		Strain at the flexural tension side
ϵ_u		Strain at ultimate stress
ϵ_x, ϵ_z		Average strains in x- and z- direction
ϵ_{x0}		Longitudinal strain at the middle of the cross-section
ϵ_y		Yield strain of the transverse reinforcement
θ		Cracking angle
θ_0		Predicted value of predicted value of θ at ϵ_x
λ_p		Ratio d_s/d
λ_s		Ratio d_p/d
v_c		Concrete shear stress
ρ_x, ρ_z		Reinforcement percentages in x- and z- direction
σ_1	f_1	Principal tensile stress in the concrete
σ_2	f_2	Principal compressive stress in the concrete
σ_{sx}, σ_{sz}	f_{sx}, f_{sz}	Average steel stress
$\sigma_{sx,cr}, \sigma_{sz,cr}$	$f_{sx,cr}, f_{sz,cr}$	Steel stress on the crack in the x- and z- direction
σ_x, σ_z	f_x, f_z	Applied average stress in x- and z- direction
τ	v	Applied shear stress
$\tau_{ci,max}$	$v_{ci,max}$	The maximum concrete stress transferred by aggregate interlock
τ_{ci}	v_{ci}	Concrete stress transferred by aggregate interlock
$\phi_{uncracked}$		The contribution factor of the uncracked flanges
ϕ		Curvature

1 Introduction

The Netherlands is a country with many rivers and a dense infrastructure network and has, therefore, many bridges. Many of these bridges have been built around 1960-1970 (Rijkswaterstaat), which means that they have now reached an age of 50 years. About 25% of these bridges consist of T-, I- or box-beams. These kinds of beams have a thin web, which makes them sensitive to shear failure of the web.

The increase in traffic and the change of regulations from the '70 to now lead to reassessment of many bridges to prove their structural safety according to the current regulations. For this reassessment, all failure mechanisms of the beam need to be checked individually to obtain the lowest resistance which will be the governing failure mechanism. It is important to have accurate predictions of the resistance to failure mechanisms because based on the predictions a decision is made to either strengthen or replace the bridge.

Until the '70 shear resistance was dealt with differently which has led to less conservative calculations, this means not all beams have sufficient shear reinforcement. Eurocode 2, therefore, predicts the shear failure at instance of diagonal cracking of the beam. However, for beams that have sufficient shear reinforcement this is conservative because the reinforcement takes over the shear force after cracking, resulting in extra capacity. To calculate beams with shear reinforcement Eurocode 2 uses a method based on the variable angle truss model. For 76 experiments on I- and T-beams which all failed in a shear a mean value of 2.02 was found for $V_{R,exp}/V_{R,pred}$ with a coefficient of variation (COV) of 56% (Walraven, 2002). From Figure 1.1 it can be seen that the prediction are very conservative for low percentages of shear reinforcement.

Other models used to describe the shear failure of prestressed beams with shear reinforcement are described in the ACI (American code) and CSA (Canadian code). The ACI model is an empirical model.

The CSA-model is based on the Modified compression field theory (MCFT). The MCFT describes the load response of membrane elements with and without reinforcement and was first presented by Vecchio in 1986. The MCFT model takes cracked concrete as a new material and models it in the principal directions. The reinforcements are modeled in the horizontal and vertical direction. For 102 experiments on membrane elements with various strengths and dimensions, of which 29 had no transverse reinforcement and 22 were tested in axial tension and shear, and which all failed in shear a mean value of 1.01 was found for V_{exp}/V_{mcft} with a coefficient of variation (COV) of 12.2% (Bentz, Vecchio, & Collins, Simplified Modified Compression Field Theory for Calculating Shear Strength of Reinforced Concrete Elements, 2006). The CSA uses a simplified version of this theory for beams. It is presented in simple formulas which take into account contributions of the concrete, stirrups and the prestressing. For 11 experiments on I-beams with varying prestress and flange height which all failed in shear a mean value of 1.11 is found for $V_{R,exp}/V_{R,CSA}$ with a coefficient of variation of 17% (Xie, 2009)

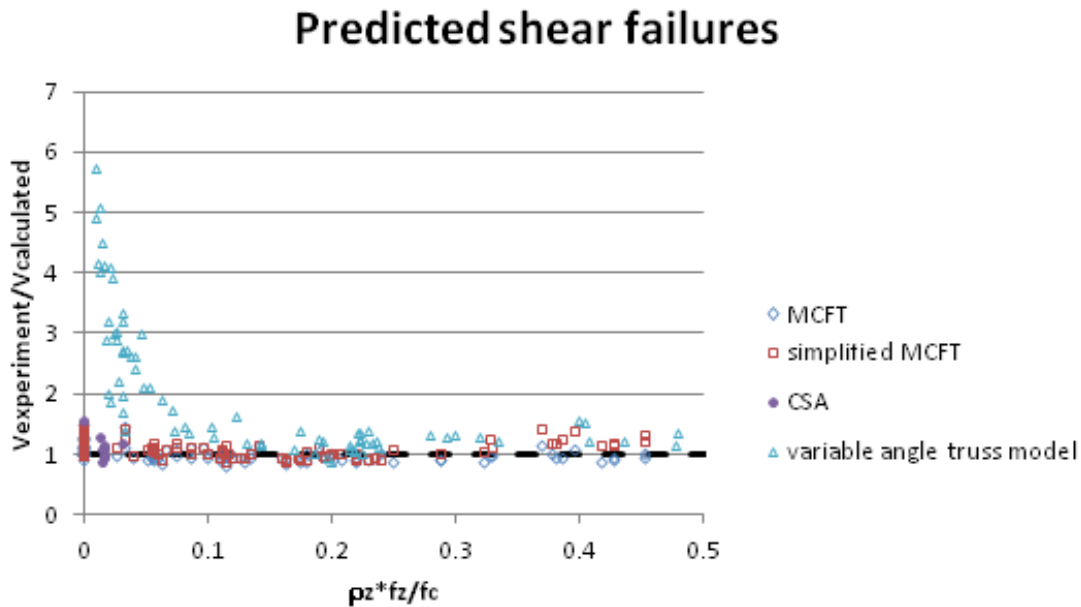


Figure 1.1, Predicted shear failures

Another way to predict shear resistance, based on the MCFT, is with cross-sectional analysis program Response-2000, presented by Bentz (Bentz E. C., Sectional Analysis of Reinforced Concrete Members, 2000). This is a non-linear finite element analysis method, which does not only take bending but also shear into account. This makes the program quite unique in its use. Response-2000 has been compared with a number of experiments which failed in shear. Out of 534 experiments on rectangular beams and columns, round columns, prestressed sections and I-beams which failed in shear a mean value of 1.05 was found for V_{exp}/V_{r2k} with a coefficient of variation of 12% (Bentz E. C., Sectional Analysis of Reinforced Concrete Members, 2000). In Figure 1.2 it can be seen that the predictions of Response-2000 lay close to the experimental values and that Response, therefore, gives a better prediction than the variable angle truss model.

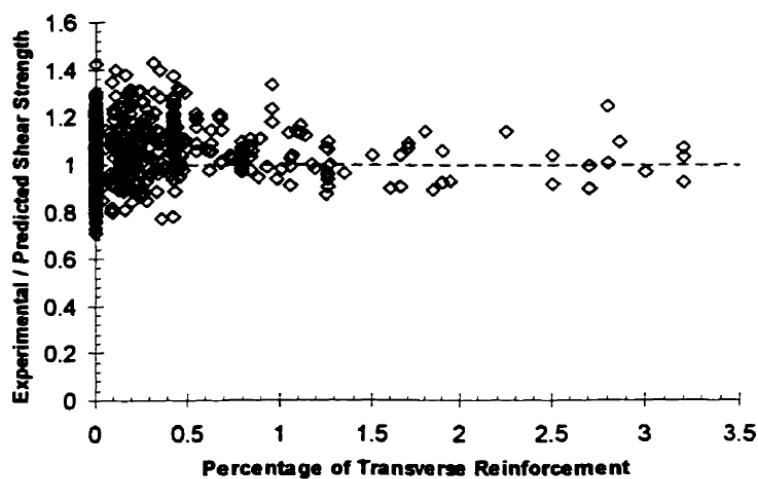


Figure 1.2, Predicted shear failure Response-2000 (Bentz E. C., Sectional Analysis of Reinforced Concrete Members, 2000)

Figure 1.1 and Figure 1.2 show that methods based on the MCFT give results that lay closer to the experimental values than the results based on the variable angle truss model, which is used in the current Eurocode. This means the results are less conservative and therefore predict the real behaviour of the beam better.

Shear failure can be divided into two different modes, namely: flexural shear failure and shear tension failure, see Figure 1.3. According to Xie (Xie, 2009), flexural shear failure is governing for areas with a high moment and shear force. This will lead to flexural cracks which propagate to flexural shear cracks. Shear tension failure, on the other hand, is governing in areas with a low moment and high shear force. Shear tension failure is characterized as a failure that is related to diagonal tension cracks.



Figure 1.3, Flexural shear (left) and shear tension (right), (Walraven, 2002)

As mentioned before 25% of the bridges in the Netherlands are I-, T- or box beams with a thin web. This makes that these beams are especially sensitive to shear tension failure. The methods mentioned above, however, only predict the general shear behaviour and make no distinction between flexural shear failure and shear tension failure, except for the ACI method which specifically predicts shear tension failure. This means not all assumptions made to derive these methods are based solely on shear tension failure, which makes the results for shear tension failure inaccurate. This makes it necessary to investigate if these models can also work to predict shear tension behaviour accurately, so accurate predictions can be made for I-, T- and box beams.

1.1 Research Questions

The aim of this master thesis is to present a more accurate prediction model for shear tension failure based on the modified compression field theory (MCFT).

To complete this, during this thesis the focus is on two practical methods which are based on the MCFT, namely the CSA-model and the cross-section analysis program Response-2000. Response-2000 will be compared with the experiments, while the CSA-model will be compared with Response-2000, which will be used to derive a more accurate model for shear tension failure (Figure 1.4).

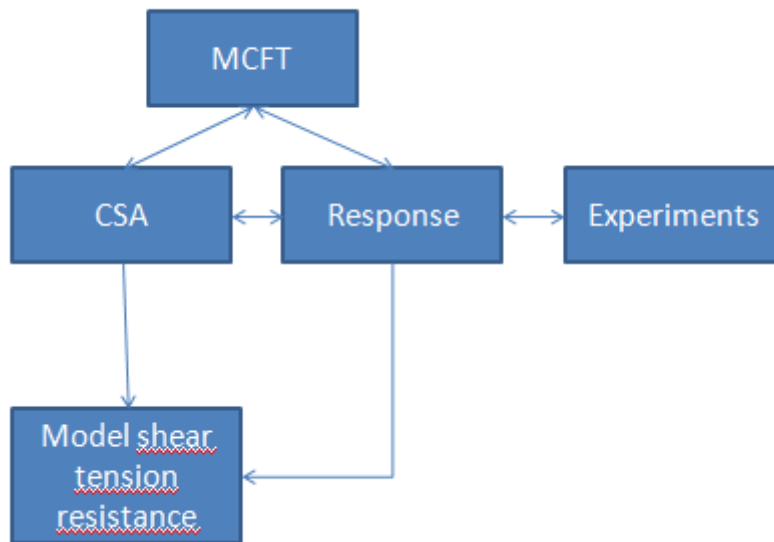


Figure 1.4, Relationship between components

For these two methods the following main questions will be answered during this thesis:

- How can we modify the CSA-model to describe shear tension behaviour more accurate?

- How is the CSA-model derived from the MCFT and which assumptions are made during the simplification?
- Which assumptions focus on flexural shear?
- Which underlying parameters influence the variables of the CSA method and how well are they predicted by the CSA-model compared to Response?

-How accurate is the prediction of shear tension behaviour of Response-2000?

- How does Response work?
- How accurate is the prediction of shear tension failure made by response compared to experiments?
- How well can Response predict several parameters and failure modes of the MCFT compared to experiments?
- What are the different assumptions made by Response-2000 and the CSA-model?

To answer the main questions these are further split up in sub-questions which will be investigated during this thesis. Finally, modifications of the CSA-model will be presented which are believed to apply to shear tension failure specifically.

1.2 Thesis outline

To answer both the main- and sub-questions insight has to be gained in the theory behind the MCFT, CSA-model and Response-2000. Chapter 2 shows an overview of the 3 models. First, in chapter 2.1 the derivation of the MCFT expressions is shown as well as the calculation method. Then in chapter 2.2, it is shown what assumptions are made to derive the CSA-model from the MCFT and an example

calculation with the CSA-model is given. Finally, chapter 2.3 shows how Response-2000 works and how this program is connected to the MCFT. Chapter 3 focuses on the comparison of Response-2000 and the experiments. In this chapter, the Response-2000 analysis of 32 experiments are compared with the experiments on a general and in-depth level. The general level focuses on the comparison of the failure load, failure mechanism, and failure location while the in-depth comparison emphasizes the contribution of the concrete and steel part to the resistance, by comparing parameters that relate to both parts. Chapter 4 focuses on a model for shear tension. The CSA-model is compared with the Response-2000 analysis of the experiments; from this, the parameters of the CSA-model that have to be changed are selected. Subsequently, alternative expressions, based on the Response-2000 results, are proposed for these parameters. This leads to a model for shear tension based on the MCFT. After this, chapters 5 and 6 show the most important conclusions and recommendations. Figure 1.5 shows which relations between the components and models are treated in each chapter. A planning of the research in this thesis can be seen in Appendix A.

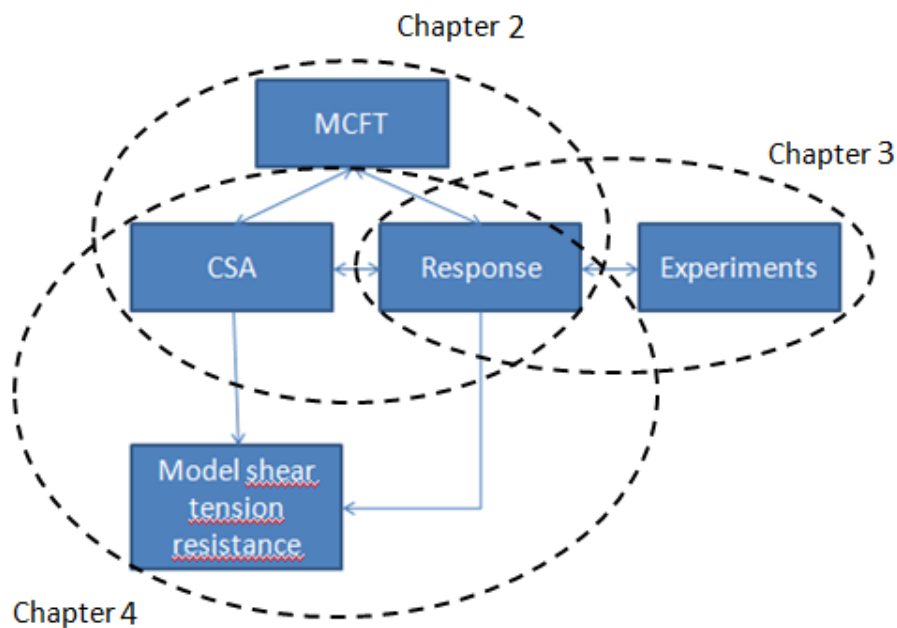


Figure 1.5, Overview of the content and relations that are treated in each chapter

2 Models based on the MCFT

The modified compression field theory (MCFT) was developed by Vecchio and Collins in 1985 (Vecchio & Collins, 1985) and describes the load-deformation response of reinforced concrete membrane elements. Two models that are derived from the MCFT are the CSA-model (Bentz & Collins, Development of the 2004 Canadian standards association (CSA) A23.3 shear provisions for reinforced concrete, 2006) and cross-sectional analysis program Response-2000 presented by Bentz (Bentz E. C., Sectional Analysis of Reinforced Concrete Members, 2000). Both models simplify the expressions of the MCFT so that they can be used to describe beam behaviour. This chapter explains the expressions and calculation method of the MCFT, in paragraph 2.1. After which a deeper look is taken into the CSA-model (paragraph 2.2) and Response-2000 (paragraph 2.3) to see how these methods relate to the MCFT and how these methods calculate the shear resistance of beams.

2.1 Modified compression field theory (MCFT)

The modified compression field theory presents a model for the load-deformation response of reinforced concrete membranes (Vecchio & Collins, 1985). Figure 2.1 presents the MCFT relationships between the average stresses and strains in the concrete and steel. In these equations the cracked on concrete is taken as a new material and models it in the principal stress directions while the reinforcement is modelled in the x- and z-direction.

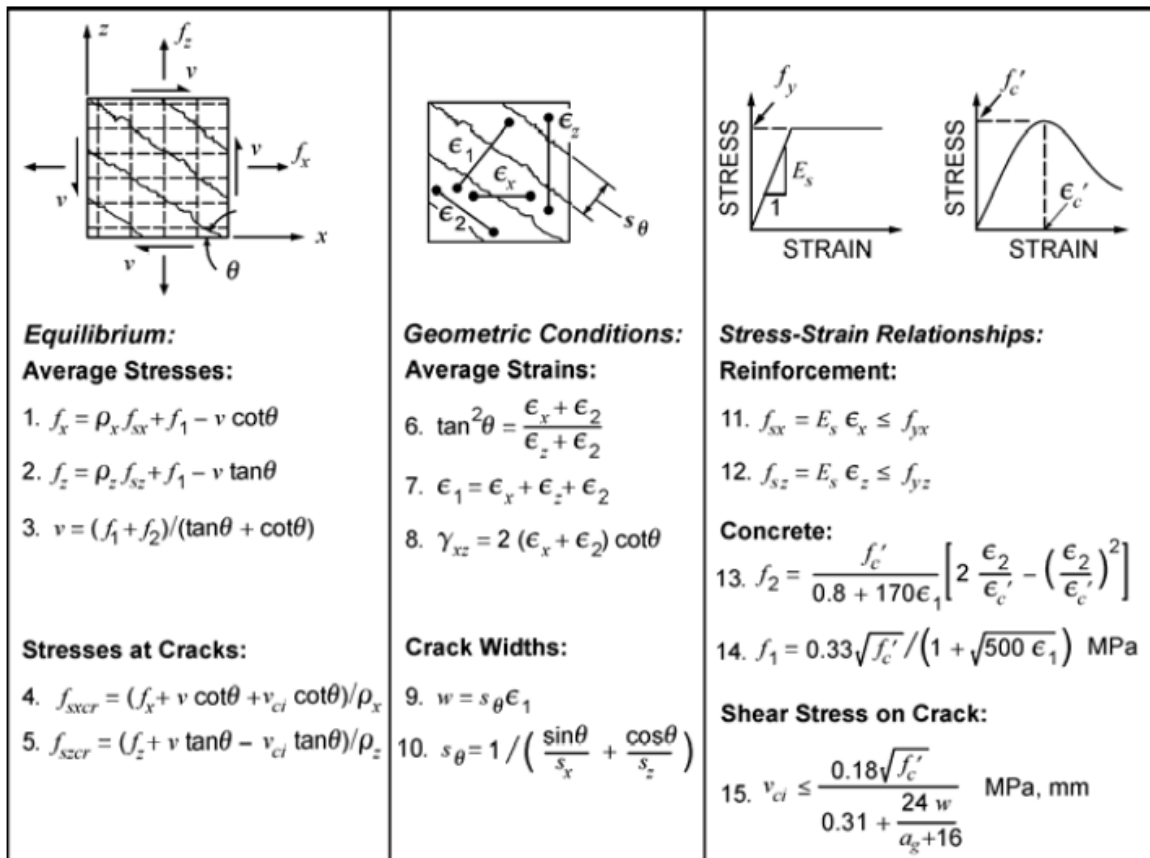


Figure 2.1, Modified compression field theory (Bentz & Collins, Development of the 2004 Canadian standards association (CSA) A23.3 shear provisions for reinforced concrete, 2006)

2.1.1 Derivation of the MCFT

This paragraph describes the MCFT expressions as shown in Figure 2.1 and as derived in (Vecchio & Collins, 1985).

The following assumptions are made to derive the relations of the MCFT:

- Each strain state has only one corresponding stress state (there no influence of the loading history).
- Average stresses and strains are considered (distances over areas that contain multiple cracks).
- Concrete and steel are perfectly bonded ($\epsilon_s = \epsilon_c = \epsilon$).
- The longitudinal and transverse reinforcement bars are uniformly distributed in an orthogonal grid.
- Angle of the principal stresses and principal strains coincide.
- No interaction between the concrete and the steel.

Geometric conditions

The average strains ($\epsilon_x, \epsilon_z, \gamma_{xz}, \epsilon_1$ and ϵ_2) are related to each other by Mohr's circle (Figure 2.2).

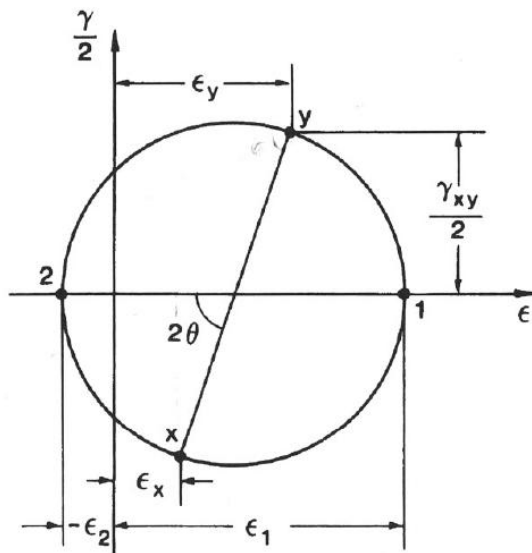


Figure 2.2, Mohr's circle for average strains (Vecchio & Collins, 1985)

The angle of the principal compressive stress (cracking angle) is also derived out of the Mohr's circle. This gives MCFT equations 6 to 8 in Figure 2.1.

Stress-strain relationships

To link the stresses to the strain, stress-strain relationships of the concrete and the steel are needed. It is assumed that there is no interaction between the concrete and the steel.

The stress-strain relationship of the steel is assumed to be depended only on one strain parameter (no shear stress on the plane normal to the reinforcement). As shown in Figure 2.3 b a bilinear stress-strain relationship is used for the reinforcement. This is presented in equations [1] and [2].

$$\sigma_{sx} = E_s \cdot \epsilon_x < f_{yx} \quad [1]$$

$$\sigma_{sz} = E_s \cdot \epsilon_z < f_{yz} \quad [2]$$

The stress-strain relationship of the concrete is defined from the outcomes of 30 membrane shear tests (Vecchio & Collins, 1985). The concrete is modelled in the principal directions and can be in tension and compression, see Figure 2.3 a. The relationship of the principal tensile stress also depends on if the concrete is cracked.

$$\sigma_1 = \frac{0.33\sqrt{f_c}}{1+\sqrt{500}\epsilon_1} \text{ (cracked concrete) }, \sigma_1 = E_c \cdot \epsilon_1 \text{ (uncracked concrete)} \quad [3]$$

$$\sigma_2 = \frac{f_c}{0.8+170\epsilon_1} \left[2 \cdot \left(\frac{\epsilon_2}{\epsilon_c} \right) - \left(\frac{\epsilon_2}{\epsilon_c} \right)^2 \right] \quad [4]$$

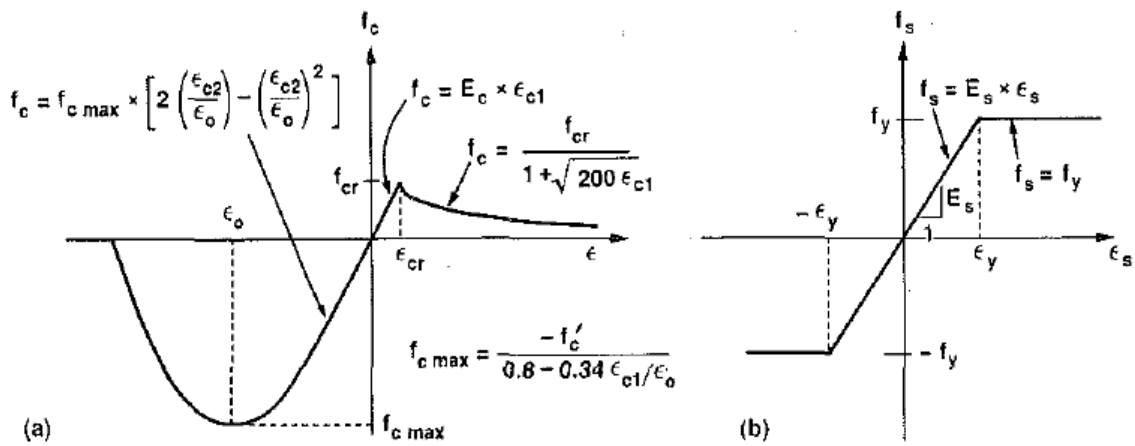


Figure 2.3, Stress-strain relationships, a. concrete, b. steel (Vecchio F. J., 1990)

Shear on the crack

The MCFT assumes the cracked concrete can still transfer forces over the crack due to aggregate interlock; this is presented by $\tau_{ci} \leq \frac{0.18\sqrt{f_c}}{0.31 + \frac{24w}{a_g + 16}}$, based on experiments of Walraven. It can be seen that

this expression depends both on the aggregate size and the crack width. When the crack width becomes larger there is less interlock because the two sides of the crack lay further apart. When the aggregate size becomes larger the interlock becomes larger because there is a bigger area of the aggregate that sticks out of the cracked concrete and provides roughness to the crack.

The average crack width depends on both the diagonal spacing of the cracks and the average principal tensile strain, as presented in equation [5].

$$W = s_\theta \cdot \epsilon_1 \quad [5]$$

where the diagonal crack spacing, $s_\theta = \frac{1}{\frac{\sin \theta}{s_x} + \frac{\cos \theta}{s_z}}$.

Equilibrium conditions

Global equilibrium

The stresses applied on the surface of the membrane element (σ_x, σ_z, τ) have to be resisted by the concrete and the steel. The following equations have been found out of equilibrium:

$$\sigma_x = \sigma_{cx} + \rho_x \cdot \sigma_{sx} \text{ (horizontal equilibrium)} \quad [6]$$

$$\sigma_z = \sigma_{cz} + \rho_z \cdot \sigma_{sz} \text{ (vertical equilibrium)} \quad [7]$$

$$\tau = \tau_{cx} + \rho_x \cdot \tau_{sx} = \tau_{cz} + \rho_z \cdot \tau_{sz} \text{ (shear equilibrium)} \quad [8]$$

It is assumed that the reinforcement has no shear component, so $\tau = \tau_{cx} = \tau_{cz}$.

The concrete carries loads by tension and compression stresses which are not expressed in x- and z-directions but in the principal directions. From Mohr's circle, the relations between the principal concrete stresses and the concrete stresses in x- and z-direction have been found.

$$\sigma_{cx} = \sigma_1 - \tau \cdot \cot \theta \quad [9]$$

$$\sigma_{cz} = \sigma_1 - \tau \cdot \tan \theta \quad [10]$$

$$\sigma_2 = \sigma_1 - \tau \cdot (\tan \theta + \cot \theta) \quad [11]$$

Substitution of equations [9] and [10] in to equilibrium equations [6] and [7] gives MCFT equations 1 and 2 in Figure 2.1. Rearrangement of equation [11] gives equation 3 of the MCFT in Figure 2.1.

Local equilibrium

When the concrete is cracked, there is a local deviation in stresses in the concrete and the steel. The steel stresses are higher than average on a crack, while the concrete stresses are lower than average on a crack. In between the cracks, the steel stress will be lower than average and the concrete stress will be higher than average. To satisfy global equilibrium we need to satisfy equilibrium in the crack (plane 2) as well as between the cracks (plane 1) (see Figure 2.4).

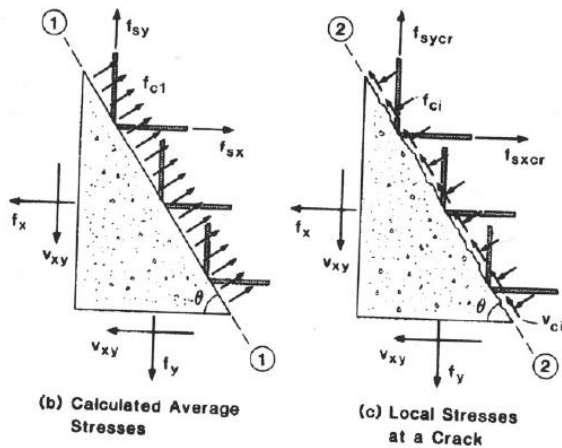


Figure 2.4, Local equilibrium between the crack and at the crack (Vecchio & Collins, 1985)

The following expressions for equilibrium have been found:

Plane 1

$$\sigma_x = \rho_x \cdot \sigma_{sx} \cdot \sin \theta + f_{ci} \sin \theta \quad [12]$$

$$\sigma_y = \rho_z \sigma_{sz} \cdot \cos \theta + \sigma_1 \cos \theta \quad [13]$$

Plane 2

$$\sigma_x = \rho_x \cdot \sigma_{sx,cr} \cdot \sin \theta - f_{ci} \sin \theta - \tau_{ci} \cos \theta \quad [14]$$

$$\sigma_y = \rho_z \sigma_{sz,cr} \cdot \cos \theta - f_{ci} \cos \theta + \tau_{ci} \sin \theta \quad [15]$$

The stresses applied on the edges of the element have to be the same for each plane which means also plane 1 and plane 2 are in equilibrium with each other. By equating plane 1 and plane 2 and assuming that f_{ci} is zero the steel stresses on the crack ($\sigma_{sx,cr}$, $\sigma_{sz,cr}$) can be obtained, as presented in MCFT equations 4 and 5 in Figure 2.1.

Equilibrium of the cracked surface

The local equilibrium as presented by equations [12] to [15] needs to be satisfied at every load stage. There are 3 options to satisfy the local equilibrium on the cracked surface:

1. The reinforcement steel is able to make equilibrium on the crack → there is no shear on the crack required:

$$\sigma_1 = \rho_x (\sigma_{sx,cr} - \sigma_{sx}) = \rho_z (\sigma_{sz,cr} - \sigma_{sz}) \quad [16]$$

2. The reinforcement steel in one of the directions is not able to make equilibrium on the crack → shear on the crack is required:

$$\sigma_1 = \rho_x (\sigma_{sx,cr} - \sigma_{sx}) - \tau_{ci} \cot \theta = \rho_z (\sigma_{sz,cr} - \sigma_{sz}) + \tau_{ci} \tan \theta \quad [17]$$

3. The reinforcement steel in one of the directions is not able to make equilibrium on the crack and the shear on the crack has reached its maximum. To satisfy this condition σ_1 has to be reduced. This situation represents slipping of the cracked surface.

$$\sigma_1 = \rho_x (\sigma_{sx,cr} - \sigma_{sx}) - \tau_{ci,max} \cot \theta = \rho_z (\sigma_{sz,cr} - \sigma_{sz}) + \tau_{ci,max} \tan \theta \quad [18]$$

Which of these options is governing depends on the steel strength and crack width. This method is also called the crack check.

An example of which formula is governing in which situation is given below.

- No yielding: the first equation is governing: $\sigma_1 = \frac{0.33\sqrt{f_c}}{1+\sqrt{500}\epsilon_1}$
- Yielding in 1 direction (weaker reinforcement), shear on the crack is needed:
 - Crack width is small enough: no reduction of σ_1 , τ_{ci} is calculated out of the second equation.
 - Crack width is too big: third equation reduction of σ_1 , τ_{ci} the maximum.
- Yielding in 2 directions: reduction of σ_1 ,
 - $\sigma_1 = \rho_x (\sigma_{sx,cr} - \sigma_{sx}) \cdot \cos^2 \theta + \rho_z (\sigma_{sz,cr} - \sigma_{sz}) \cdot \sin^2 \theta$
 - $\tau_{ci} = (\rho_x (\sigma_{sx,cr} - \sigma_{sx}) - \rho_z (\sigma_{sz,cr} - \sigma_{sz})) \cdot \sin \theta \cdot \cos \theta$

Failure mechanisms

The highest load can be governed by multiple failure mechanisms:

- Slipping of the crack (σ_1 is limited by τ_{ci})

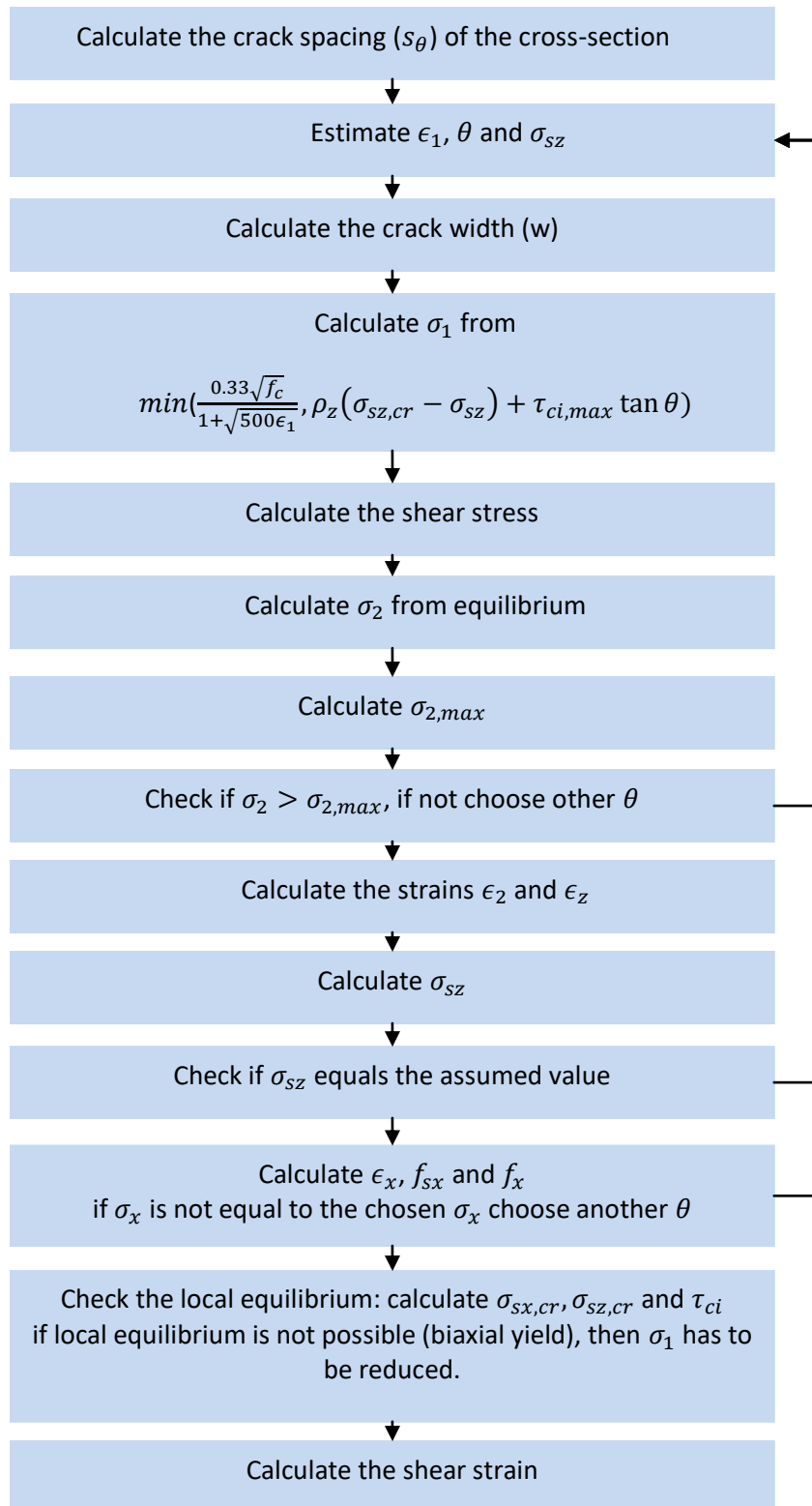
$$\sigma_1 = \rho_x(\sigma_{sx,cr} - \sigma_{sx}) - \tau_{ci,max} \cot \theta = \rho_z(\sigma_{sz,cr} - \sigma_{sz}) + \tau_{ci,max} \tan \theta$$
- Crushing or shear failure (σ_2 is limited by the stress-strain relationship.)

$$\sigma_2 = \sigma_1 - \tau \cdot (\tan \theta + \cot \theta) < \frac{f_c}{0.8+170\epsilon_1} \left[2 \cdot \left(\frac{\epsilon_2}{\epsilon_c} \right) - \left(\frac{\epsilon_2}{\epsilon_c} \right)^2 \right]$$
- Yielding of both the reinforcement directions at the crack (σ_1 is limited by τ_{ci})
 insert $f_{sz,cr} = f_{yz}$ and $f_{sx,cr} = f_{yx}$

These failure mechanisms can occur after each other, slipping at the crack, for instance, reduces the principal tensile stress and has, therefore, influence on the principal compressive stress which has to increase, this can lead to crushing. Also yielding and slipping are interrelated, at least one of the reinforcements has to yield before shear on the crack is needed and therefore slipping can occur. The mechanism which leads to the lowest load is considered as the failure mechanism.

2.1.2 Calculation procedure

The calculation of the shear strength with the MCFT is a complicated iterative procedure. The outcome of this calculation is a relation between the shear stress and shear strain, for a constant σ_x and σ_z . The scheme below shows an overview of the calculation steps that have to be taken to calculate one load step.



This method has to be followed for every load step to get the whole load response and so the actual failure load of the membrane. It is recommended to do this calculation with excel or the program membrane-2000 (Bentz E. C., Sectional Analysis of Reinforced Concrete Members, 2000).

2.2 CSA-model

The Canadian code uses a model for shear resistance that is based on the modified compression field theory (MCFT). The so-called CSA-model (Bentz & Collins, Development of the 2004 Canadian standards association (CSA) A23.3 shear provisions for reinforced concrete, 2006) is presented in equations [19] to [24] and Figure 2.5. The MCFT model is simplified to formulas for the shear resistance, which includes components of the steel as well as the concrete. The CSA-model is used to describe beam behaviour, where the MCFT describes membrane behaviour. The model describes the general shear behaviour of a beam, which means no difference is made between flexural shear failure and shear tension failure. The calculation of the shear resistance with the CSA-model is iterative which means the calculation has to be done till the shear force is converged. This paragraph shows how the CSA-model is derived from the MCFT and how accurate several parameters are compared to the MCFT. In 2.2.2, an example calculation of the shear force capacity with the CSA-model will be given.

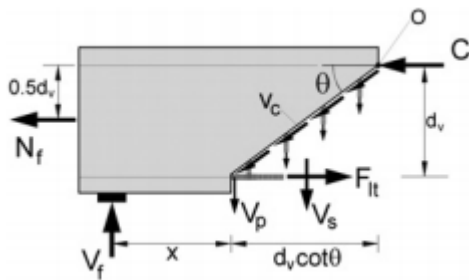


Figure 2.5, CSA-model (Bentz & Collins, Development of the 2004 Canadian standards association (CSA) A23.3 shear provisions for reinforced concrete, 2006)

$$V_R = V_c + V_s < V_{max} \quad [19]$$

$$V_c = \beta \cdot \sqrt{f_c} \cdot b_w \cdot z \quad [20]$$

$$V_s = \frac{A_{sw} \cdot f_y \cdot z}{s} \cdot \cot(\theta) \quad [21]$$

$$\beta = \frac{0.4}{1 + 1500 \cdot \epsilon_x} \quad [22]$$

$$\theta = 29 + 7000 \cdot \epsilon_x \quad [23]$$

$$V_{max} = 0.25 \cdot f_c \cdot b_w \cdot z \quad [24]$$

2.2.1 Derivation from the MCFT

The following assumptions are made to derive the expression [19] to [24] from the MCFT expressions:

- No dowel action (clamping stress), so $\sigma_z = 0$
- The shear force is carried by:
 - Aggregate interlock (τ_{ci}).
 - The transverse reinforcement.
 - Shear stress in the compression zone.
 - The vertical prestressing component.
- Only one biaxial element (membrane element) in the web is taken to represent the whole cross-section:
 - Shear stress is constant over the depth.
 - The Longitudinal strain is constant over the depth.
 - The aggregate interlock of the mid-depth represents the whole cross-section.
- The shear stress resistance of the flexural compression region is larger than of the cracked region: the cracked region is governing for the shear strength.
- The reinforcement yields at failure.
- The cross-section is cracked over the height z .

With the assumptions that $\sigma_z = 0$ equations [25] and [26] for the shear stress have been derived from MCFT equations 2 and 5 (Figure 2.1):

$$\tau = \tau_{ci} + \rho_z f_y \cot \theta \quad [25]$$

$$\tau = f_1 \cot \theta + \rho_z f_y \cot \theta \quad [26]$$

These equations then can be expressed in a concrete component and a steel component:

$$\tau = \tau_c + \tau_s = \beta \sqrt{f_c} + \rho_z f_y \cot \theta \quad [27]$$

Multiplying by $b_w \cdot z$ gives the equations [19] to [21] for shear forces V_R, V_C and V_S .

Equation [19] for the shear force is limited by crushing before yielding of the transverse reinforcement. It is assumed that the transverse- and longitudinal reinforcement both yield at a strain of 0.002 (based on steel with a yield stress of 400 MPa) and that the concrete crushes also at a strain of -0.002. Substituting this value in equations 3, 6, 7, 13 and 14 of the MCFT as shown in Figure 2.1 a shear stress of $0.28 \cdot f_c$ this is rounded to give the following expression for V_{max} :

$$V_{max} = 0.25 \cdot f_c \cdot b_w \cdot z \quad [28]$$

β and θ factor

The variables β en θ as derived in (Bentz, Vecchio, & Collins, Simplified Modified Compression Field Theory for Calculating Shear Strength of Reinforced Concrete Elements, 2006) are assumed to be only depended on the longitudinal strain ϵ_x (measured at mid-depth). β represents the aggregate interlock of the concrete, θ is the angle of the crack. The derivation of the expressions for β and θ from the MCFT for members without stirrups is given below. After that results for beams with stirrups are given.

β

The factor β is derived for members without stirrups; this means only the concrete component is taken into account to calculate the shear stress.

The factor β (concrete aggregate interlock component) can be defined from equations [25] to [27] and the MCFT equations presented in Figure 2.1:

$$\tau_{ci} = \beta \sqrt{f_c} = \frac{0.18 \sqrt{f_c}}{0.31 + \frac{24w}{a_g + 16}} \rightarrow \beta = \frac{0.18}{0.31 + \frac{24w}{a_g + 16}} \quad [29]$$

$$f_1 \cot \theta = \beta \sqrt{f_c} = \frac{0.33 \sqrt{f_c} \cdot \cot \theta}{1 + \sqrt{500} \epsilon_1} \rightarrow \beta = \frac{0.33 \cot \theta}{1 + \sqrt{500} \epsilon_1} \quad [30]$$

$$\text{The MCFT equation for the crack width is: } w = s_\theta \cdot \epsilon_1 \quad [31]$$

There are no stirrups, s_θ is defined as: $\frac{s_x}{\sin \theta}$ (only the spacing between the longitudinal reinforcement)

The effective crack spacing is a combination of s_x and the aggregate size:

$$s_{xe} = \frac{35 \cdot s_x}{16 + a_g} < 0.85 \cdot s_x \quad [32]$$

Substitution of equation [31] and [32] into equation [29] gives:

$$\beta = \frac{0.18}{0.31 + 0.686 \cdot s_{xe} \cdot \epsilon_1 / \sin \theta} \quad [33]$$

It can be seen that the formulas for β (equations [30] and [33]) are depended on both ϵ_1 and θ , while the final formula (equation [22]) only depends on ϵ_x .

To solve ϵ_1 and θ an iterative procedure is followed based on the equations of the MCFT:

- f_c, ϵ_x, s_{xe} are chosen.
- Estimates of ϵ_1 and θ are made.
- ϵ_1 is determined using the relationship between ϵ_1 and ϵ_x and iterating until the value of ϵ_1 is converged:

$$\epsilon_1 = \epsilon_x (1 + \cot^2 \theta) + \epsilon_2 \cot^2 \theta \rightarrow \epsilon_x (1 + \cot^2 \theta) + \frac{\cot^4 \theta}{15000 \cdot (1 + \sqrt{500} \cdot \epsilon_1)}$$

- θ is determined from the equilibrium between the shear stress on the crack and shear stress between the cracks ($\tau = \tau_{ci} = f_1 \cot \theta$) (This gives the highest shear force and β -values) which gives the following formula:

$$\tan \theta = \frac{0.568 + 1.258 \cdot \frac{s_{xe} \cdot \epsilon_1}{\sin \theta}}{1 + \sqrt{500} \cdot \epsilon_1} \quad [34]$$

- The value of θ is iterated until it is converged.
- With this θ value, the β can be calculated.

Results of this calculation of β are presented in Figure 2.6 for various values of s_{xe} , ϵ_1 and ϵ_x

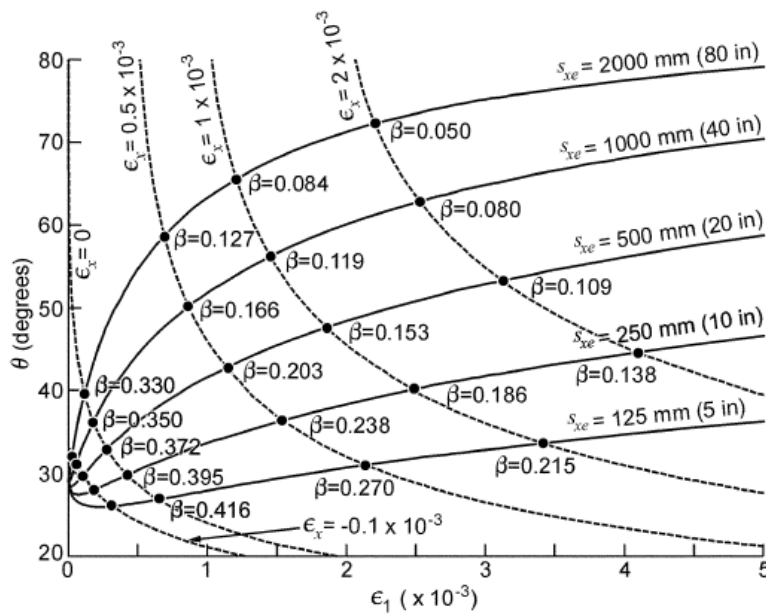


Figure 2.6, Relationship Beta-values for beams without shear reinforcement (Bentz, Vecchio, & Collins, Simplified Modified Compression Field Theory for Calculating Shear Strength of Reinforced Concrete Elements, 2006)

From Figure 2.6 it can be seen that for increasing effective crack spacing the β -value decreases and therefore also the shear strength. The effective crack spacing depends on the size of the member and, therefore, this is also called the size effect.

The values of ϵ_1 and θ implicitly represent the crack width. This means that a relationship between the crack width and the longitudinal strain can be found for specified effective crack spacing. Figure 2.7 shows the crack widths for an effective crack spacing of 300 mm and different concrete compressive strengths in relation to the longitudinal strain. From this an equation for the crack width for members without transverse reinforcement depending on ϵ_x is derived:

$$w = 0.2 + 1000 \cdot \epsilon_x$$

[35]

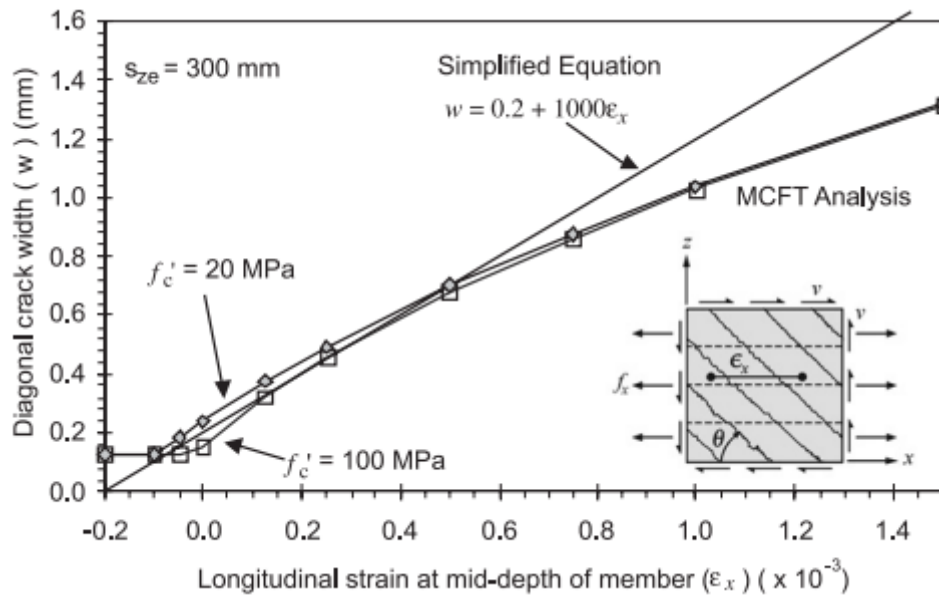


Figure 2.7, Crack width for effective crack spacing of 300 mm (Bentz & Collins, Development of the 2004 Canadian standards association (CSA) A23.3 shear provisions for reinforced concrete, 2006)

Figure 2.7 shows that the crack width increases by increasing strain; this is called the strain effect.

By assuming an effective crack spacing of 300 mm and taking $s_x = 300$ mm the maximum aggregate size is:

$$a_g = 20 \text{ mm}$$

Substitution of the crack width formula (equation [35]) and the standard aggregate size in equation [29] gives the final expression for β :

$$\beta = \frac{0.18}{0.31 + \frac{24 \cdot (0.2 + 1000 \cdot \epsilon_x)}{20 + 16}} \rightarrow \frac{0.4}{1 + 1500 \cdot \epsilon_x} \quad [36]$$

The final expression for β also includes the size effect:

$$\beta = \frac{0.4}{1 + 1500 \cdot \epsilon_x} \cdot \left[\frac{1300}{1000 + s_{xe}} \right] \quad [37]$$

θ

The equation for θ is it derived between the lower and upper limit (Figure 2.8). The upper limit comes from the assumption that the stirrups need to be able to yield before shear failure. The lower limit is reached when the concrete crushes before reaching the desired shear stress ($\tau = 0.25 \cdot f_c$). The θ value is derived for the moment that there is maximum contribution of the aggregate interlock ($\tau_c = \tau_{ci,max}$) this is the point at which the $\tau_{ci,max}$ is governing for the first time (equilibrium situation 3 of the MCFT).

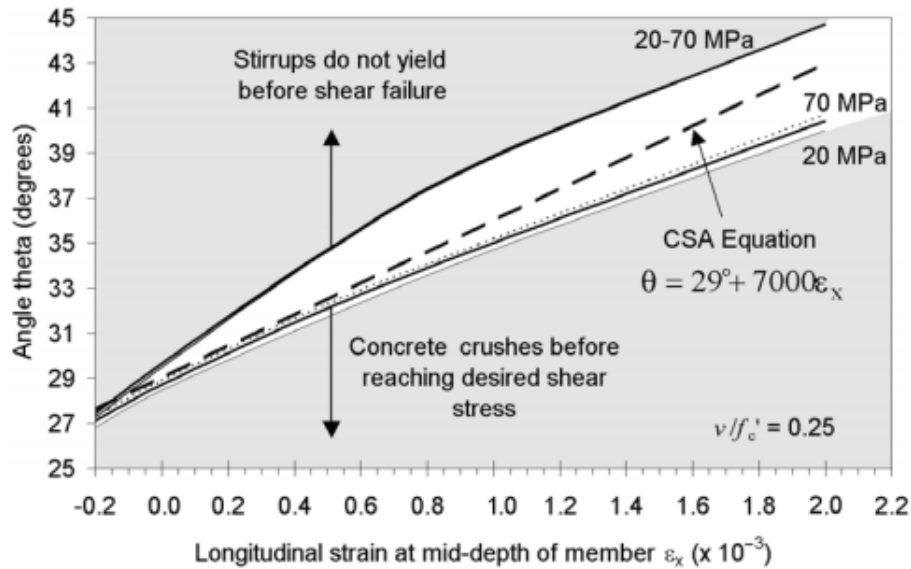


Figure 2.8, Lower and upper limit for theta (Bentz & Collins, Development of the 2004 Canadian standards association (CSA) A23.3 shear provisions for reinforced concrete, 2006)

The expression found for θ , following this approach consists of strain effect factor and a size effect factor.

$$\theta = 29 + 7000 \cdot \epsilon_x \cdot \left(0.88 + \frac{s_{xe}}{2500}\right) \quad [38]$$

Concrete with stirrups

For cross-sections with at least a minimum amount of reinforcement the crack spacing is controlled and therefore the size effect is negligible. This means that the size effect factor equals 1, to achieve this $s_{xe} = 300 \text{ mm}$ shall be taken. This reduces the equations [37] and [38] for β and θ to:

$$\beta = \frac{0.4}{1 + 1500 \cdot \epsilon_x} \quad [39]$$

$$\theta = 29 + 7000 \cdot \epsilon_x \quad [40]$$

Figure 2.9 shows the development of β and θ over ϵ_x and also shows the MCFT predictions of β and θ for various reinforcement ratios. For β it can be seen that the predictions with equation [39] are too big for small values of ϵ_x and too small for higher values of ϵ_x . For θ it can be seen that the predictions with equation [40] are too high for low values of ϵ_x .

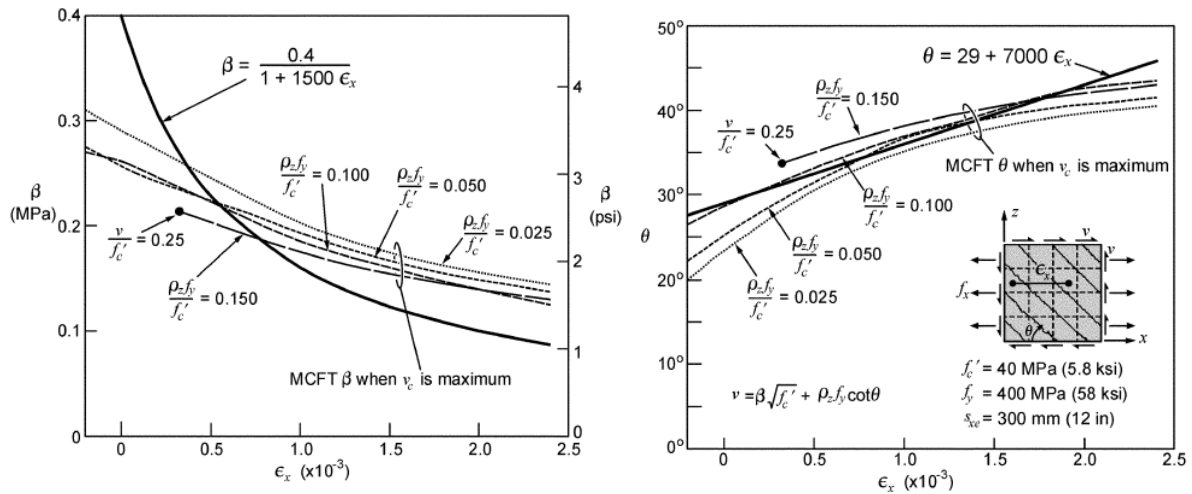


Figure 2.9, Beta and theta for various reinforcement percentages (Bentz, Vecchio, & Collins, Simplified Modified Compression Field Theory for Calculating Shear Strength of Reinforced Concrete Elements, 2006)

Formula for ϵ_x

The CSA-model defines ϵ_x as the strain at mid-depth of the cross-section. The strain at mid-depth then can be defined as the mean value of the strain on the flexural tension side and the flexural compressive side.

$$\epsilon_x = \frac{\epsilon_t + \epsilon_c}{2} \tag{41}$$

Because ϵ_c is considered to be a small negative quantity, the CSA makes the conservative assumption to take the compressive strain not into account which leads to equation [42] for ϵ_x .

$$\epsilon_x = \frac{\epsilon_t}{2} \tag{42}$$

The forces in the concrete on the flexural compressive (C) and flexural tension (T) side have to make moment equilibrium with the sectional force, M, N and V (Figure 2.10). This means that T is defined as follows:

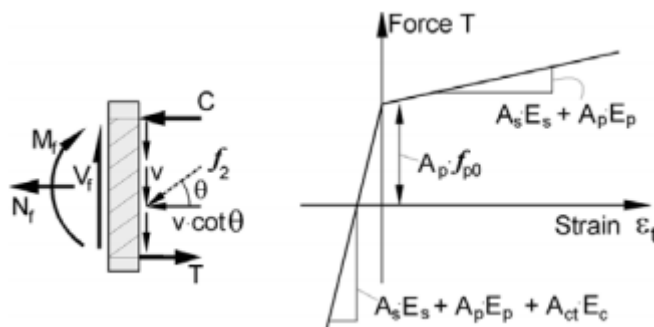


Figure 2.10, Cross-sectional forces and stiffness relationship (Bentz & Collins, Development of the 2004 Canadian standards association (CSA) A23.3 shear provisions for reinforced concrete, 2006)

Moment equilibrium around the compressive force is taken by equation [43] using the assumptions $\sum \tau = V$ and $\frac{1}{2} \cot \theta \approx 1$ this leads to the expression of T in equation [44].

$$\sum C = M_f + N_f \cdot \frac{1}{2}z - T \cdot z + \sum \tau \cdot \cot \theta \cdot \frac{1}{2}z \quad [43]$$

$$T = \frac{M}{z} + V + \frac{N}{2} \quad [44]$$

The general relation to calculate ϵ is:

$$\epsilon = \frac{N}{EA} \quad [45]$$

The cross-section is simplified into a tensile and compressive flange and a web. There is only looked at the tensile force (T), which works on the tensile side of the cross-section. This means that the areas of the reinforcement and prestressing steel only consist of the steel that is within half-depth of the section that is on the flexural tension side. The contribution of the concrete area depends on whether the concrete is cracked at the bottom (Figure 2.10). As long as the longitudinal strain stays below $\frac{1}{2}\epsilon_{crack}$ the concrete is considered uncracked which means the concrete component has to be taken into account when calculating the longitudinal strain. Else only the reinforcement and prestressing steel areas are taken into account.

$$\epsilon_x = \frac{T}{2 \cdot (E_s A_s + E_p A_p + E_c A_c)} \quad [46]$$

The value of ϵ_x is limited by the crack width and flexural failure.

$$-0.2 \cdot 10^{-3} (\text{negative crack width}) < \epsilon_x < 3 \cdot 10^{-3} (\text{flexural failure})$$

If the strain at the compression zone becomes so high that the compression zone cracks then ϵ_x needs to be doubled.

2.2.2 Calculation procedure

To demonstrate the calculation procedure and the influence of the different parameters an example calculation is shown below. The analyzed beam is HCP1TW (properties in Table 2.1) as described by Choulli (Choulli, 2005). The data used for the calculation is presented below.

Geometry			Reinforcement			Prestress			Concrete		
x	1.4	m	f_y	525	N/ mm ²	P	-1859	kN	f_c	81.2	N/ mm ²
L	10	m	E_s	200000	N/ mm ²	e_p	251.75	mm	E_c	41233	N/ mm ²
d	671.4	mm	A_s	772.8	mm ²	E_p	192940	N/ mm ²	A_c	194500	mm ²
z	604	mm	$A_{stensile}$	0	mm ²	$A_{ptensile}$	1386	mm ²	$A_{ctensile}$	75000	mm ²
b_w	100	mm	A_{sw}	100.531	mm				γ_c	25	kN/m ³
			s	200	mm						

Table 2.1, Iterative calculation CSA-model HCP1TW

x	F (kN)	Aload (kN)	Mf (kN/m)	Mtot (kN/m)	Vf (kN)	Vtot (kN)	T (kN)	ex	θ	β	Vrc (kN)	Vrs (kN)	Vtot (kN)	difference
0	845	582.5	0	-452.95	582.5	589.75	-1089.33	-0.00016	27.86	0.52	287.79	301.62	589.41	0.33
0.3	811	559.06	167.71	-285.24	559.06	566.31	-835.21	-0.00012	28.12	0.49	267.72	298.27	566.00	0.30
0.6	782	539.07	323.44	-129.51	539.07	546.32	-597.50	-8.9E-05	28.37	0.46	251.33	295.20	546.53	0.21
0.9	758	522.52	470.27	17.314	522.52	529.77	-371.06	-5.5E-05	28.61	0.43	237.48	292.32	529.80	0.024
1.2	737	508.05	609.66	156.70	508.05	515.30	-154.88	-2.3E-05	28.83	0.41	225.61	289.60	515.21	0.08
1.5	704.5	485.64	728.46	275.51	485.64	492.89	19.32	3.61E-05	29.25	0.37	206.61	284.71	491.32	1.56
1.8	641.5	442.21	795.99	343.03	442.21	449.46	87.63	0.000164	30.14	0.32	174.83	274.57	449.41	0.05
2.1	593	408.78	858.44	405.48	408.78	416.03	157.55	0.000295	31.06	0.27	151.06	264.74	415.80	0.22

Table 2.2, HCP1TW data

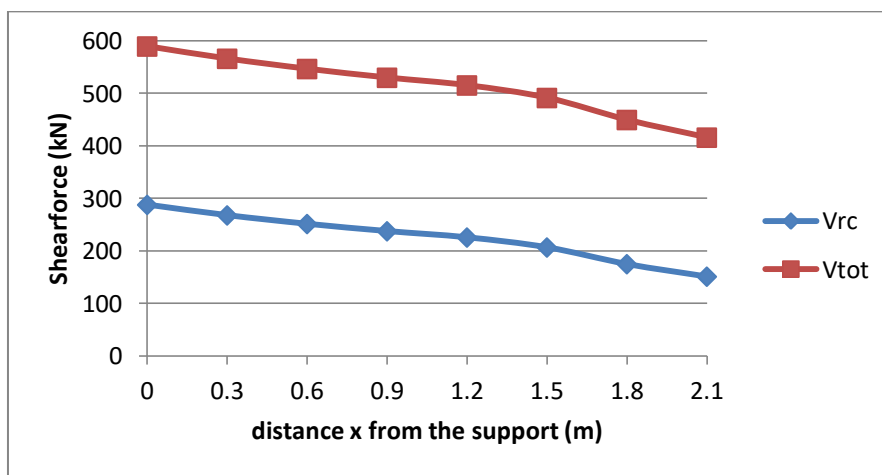


Figure 2.11, Shear force capacity over the beam length for HCP1TW

Figure 2.11 and Table 2.2 show the load and shear forces for different sections of the beam between the support and the load. These values are found by iteration until the shear force coincided. In the graph (Figure 2.11) a clear kink can be seen around 1.5 meter from the support, after this point the beam is cracked. This can be seen through the ϵ_x -values which exceed the tensile strain. Flexural shear failure is defined as shear failure proceeding from flexural cracks. This means that at distances bigger than 1.5 meter from the support the beam will fail due to flexural shear failure. The cracking at longer distances from the support can also be declared by the rise of the moment. It also is observed that the maximum load decreases at a longer distance from the support. The θ increases for longer distances to the support because the mechanism goes more into flexural cracking. On the other hand, the β -factor decreases because when the strain increases there is less interlock between the concrete. This leads to a lower load.

2.3 Response-2000

Response-2000 is a cross-sectional analysis program made by Bentz (Bentz E. C., Sectional Analysis of Reinforced Concrete Members, 2000). The program is based on the MCFT and it is possible to calculate stresses and strains in beams subjected to moments, shear forces and axial forces. This program calculates the shear stress and strain profiles in the cross-section, which makes it useful to analyze shear failure of beams. This paragraph first focus on the model setup of Response-2000 (2.3.1). Paragraph 2.3.2 shows how the program Response calculates the results and how the MCFT is incorporated in that process . In paragraph 2.3.3 an overview of the analysis results and their relationship with the MCFT is shown.

2.3.1 Model setup

To set up a model in Response-2000 the cross-section and material properties have to be entered as well as the loads.

Model input

Response-2000 is an easy to use program which makes it possible to enter every cross-section needed including prestress, longitudinal and transverse reinforcement. The easiest way to define a model is to use the quick define wizard. This wizard guides you through all the parameters needed to set up the model in 4 steps:

1. Material properties.
2. Concrete cross-section.
3. Non-prestressed reinforcement.
4. Transverse steel and prestressing.

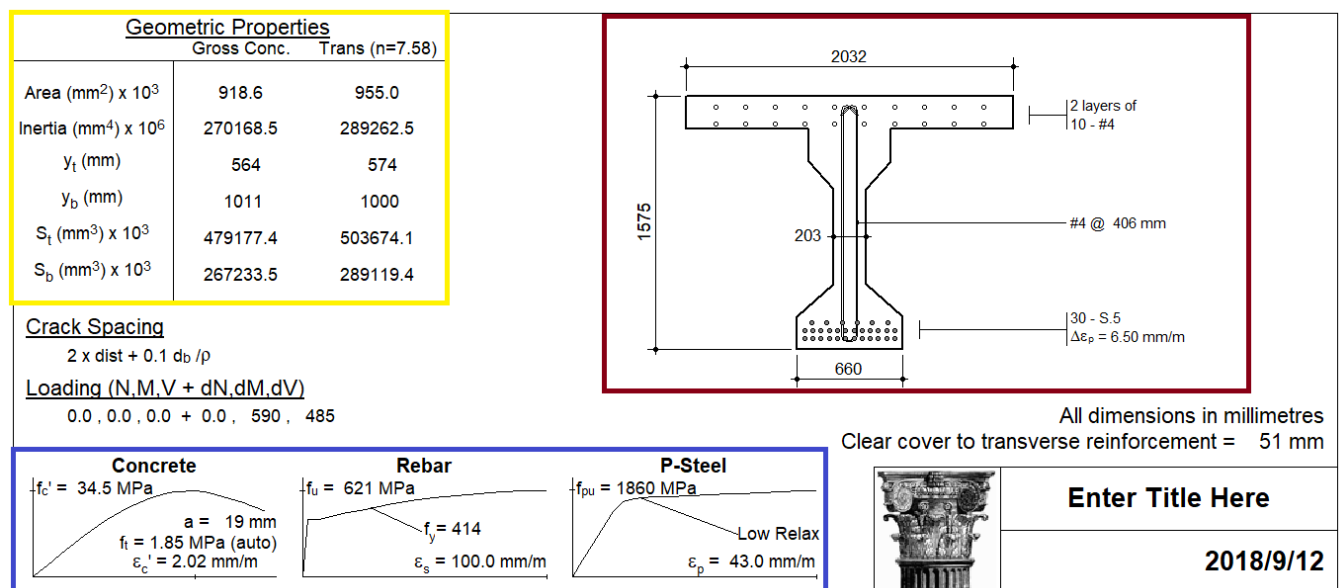


Figure 2.12, Input screen Response-2000

Finishing the wizard leads to the input screen (Figure 2.12). In the yellow, the geometric properties of the cross-section are shown. In the blue, the material properties for the concrete, steel and prestressing steel are summarized in the stress-strain relationships. In the red, the cross-section with the defined reinforcements is shown. It is important to note that the prestress has to be inputted as a pre-strain in the tendons. The quick define gives easy input, where only the most necessary

parameters have to be entered. The other parameters are defined by the programs default. Below some default assumptions are summed up. Changing these default assumptions for, for example, the rebar spacing or concrete material properties, can be done by double-clicking on the properties you want to change. A menu with detailed properties will pop up. After changing click on modify to make the changes permanent. These menus make it possible to define different types of reinforcements and to create multiple materials for the reinforcements. It is also possible to customize the concrete cross-section, to a shape that is not standard given in the quick define, for example, an I-beam with inclined flanges. A detailed example of the input of beam LB3 (Xie, 2009) is given in Appendix B.

Default assumptions for the cross-section (Bentz & Collins, 2001):

- Cover of the longitudinal reinforcement is 40 mm.
- Cover of the prestressing tendons is 50 mm.
- The minimum bar spacing is equal to the bar diameter.
- Concrete:
 - $f_t = 0.45(f_c)^{0.4}$
 - $E_c = 3320 \cdot \sqrt{f_c} + 6900$
 - Maximum aggregate size is 19 mm
 - Base curve: Popovics/Thorenfeldt/ Collins (behaviour of uniform block of concrete subjected to uniform compressive stress).
 - Compression curve:
 - Vecchio-Collins 1986 (for concrete till 90 Mpa)
 - Porasz-Collins 1988 (for concrete above 90 Mpa)
 - Tension stiffening: Bentz 1999
- Steel:
 - $E = 200000$ Mpa
 - $\epsilon_{sh} = 7$ mm/m
 - $\epsilon_u = 10\%$ (strain at f_u)
 - $f_u = 1.5 \cdot f_y$
 - Curve is linear to yield, flat post yield, and quadratic after strain hardening.
- Prestressing steel:
 - Based on Ramberg-Osgood parameters (A, B, C) (Figure 2.13)

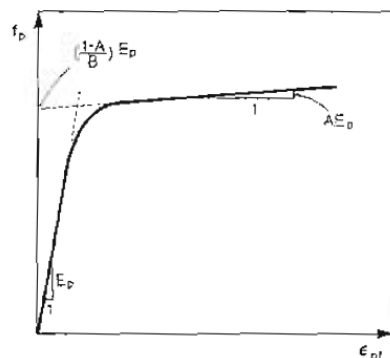


Figure 2.13, Definition of Ramsberg-Osgood parameters (Collins, 1991)

- default values: $A = 0.025, B = 118, C = 10$
- $E = 200000$ Mpa

- $f_u = 1860 \text{ MPa}$
- $\varepsilon_u = 43 \text{ mm/m}$

Loads

The loads are divided into constant loads and increments (see Figure 2.14). The increments are increased during the analysis and therefore it is only necessary to fill in the ratio between the loads. The constant loads are used as a starting value and can, for example, be used to account for self weight or prestressing. The axial load has a positive sign for tension and a negative sign for compression. The moment is positive anti-clockwise (compression on the top side) and the shear force needs to be positive. The load implicitly defines the cross-section looked at in Response-2000 because every beam cross-section has a unique M/V-ratio.

	Constant	+	Increment	
Axial Load	0.00	+	0.00	kN
Moment	0.00	+	589.78	kNm
Shear	0.00	+	484.86	kN

For a "One Load" analysis, only use the left side

OK Cancel Help

Figure 2.14, Loading definition

2.3.2 Iterative calculation

The calculation method of Response is based on the MCFT which is a membrane theory, while Response is used for beams. The following assumptions are made to go from the MCFT to a beam theory:

- Plane cross-sections remain plane.
- There is no transverse clamping stress, $\sigma_z = 0$.

Response divides the cross-section into layers which are represented by a series of biaxial nodes (membrane elements) along the depth of the cross-section (Figure 2.15).

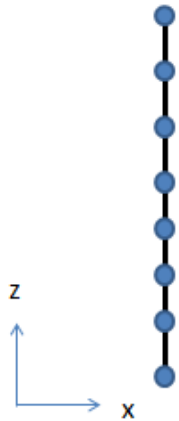


Figure 2.15, Nodes on the cross-section

The strains in the cross-section are defined as the global strain state and each node has a local strain state.

Global strain state is defined as:

- The longitudinal strain at the middle of the cross-section, ϵ_{x0} .
- The curvature, ϕ .
- The average shear strain, γ_{xz0} .

Given for each node the strains are defined from the global strain state as follows:

- The longitudinal strain is linear over the height so $\epsilon_x = \epsilon_{x0} \pm \phi \cdot z$.
- Shear strain at each node is derived using a numerical profile and the average shear strain (γ_{xz0}). The numerical profile relates the average shear strain over the depth of the cross-section. The average value is 1 and the shear strain is zero at top and bottom.
- Transverse strain ϵ_z is derived from $\sigma_z = 0$ and equilibrium. (no clamping stress).

Response-2000 works similar to a finite element program because the cross-section is divided into layers represented by the biaxial nodes. The procedure and numerical techniques that Response uses for every load step are described below.

Initial assumptions (Figure 2.16):

- Estimate the shear strain profile as $\tau = \frac{V \cdot S}{I \cdot b}$ or the profile from the previous load stage.
- Estimate global strain state: ϵ_{x0} , ϕ , γ_{xz0} as 0 or values from previous stages.
- Create a new load stage, values of M, V, N are chosen.
- Choose one variable to be constant during the iteration procedure to have strain controlled behaviour (control plots), generally in our analysis ϵ_{x0} is constant as there is hardly variation in normal force.

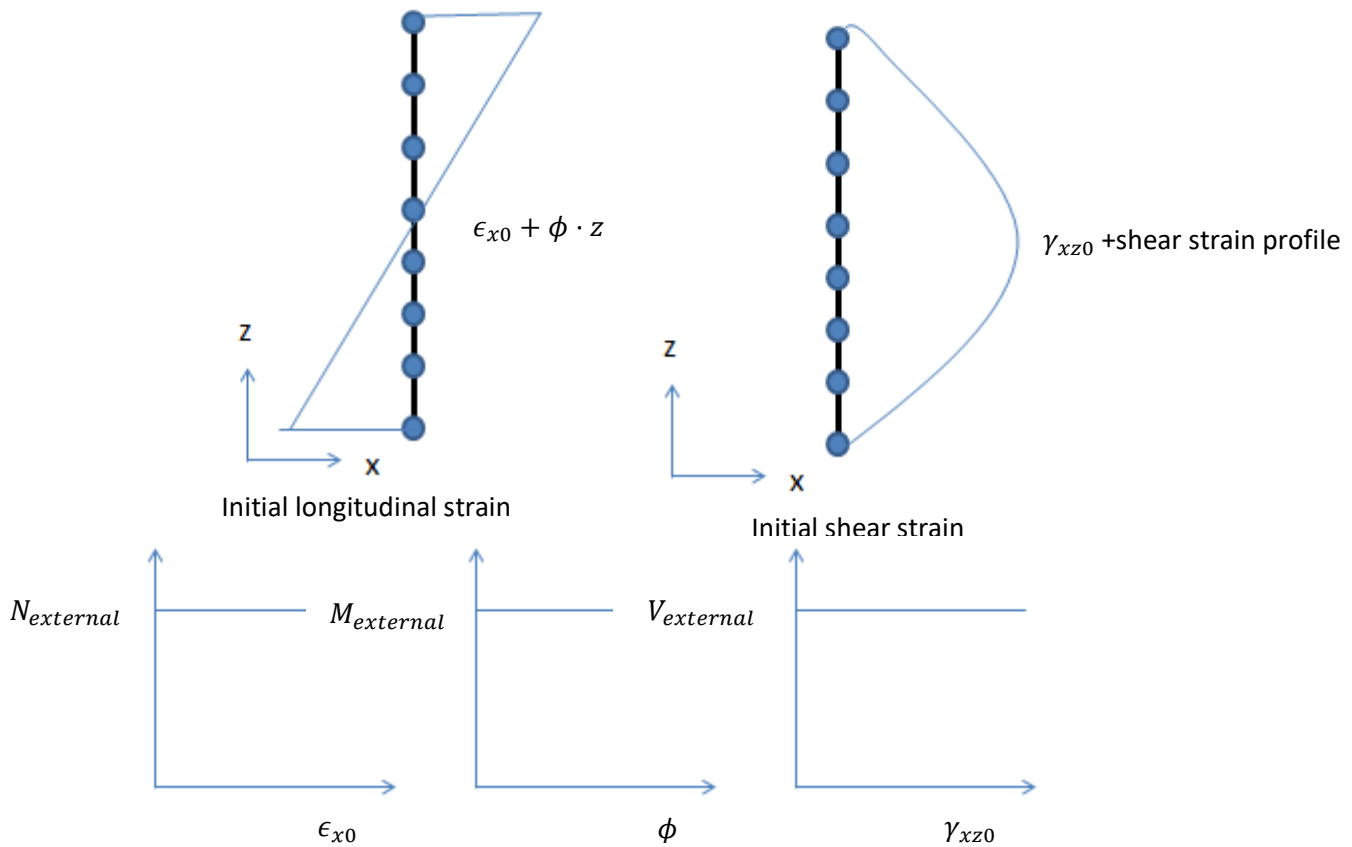


Figure 2.16, Initial assumptions

1. The ϵ_z is calculated in every node from $\sigma = D \cdot \epsilon$

- D is the secant stiffness matrix; build up from concrete and steel stiffnesses. For concrete these are derived from the material behaviour defined in the MCFT (expressions 13 and 14 in Figure 2.1 for σ_1 and σ_2 of cracked concrete) divided by the principal strains and rotated in the x- and z-direction. For the steel, the stiffness is defined as $\frac{\sigma_s}{\epsilon_s}$.
- $\epsilon = \begin{bmatrix} \epsilon_x \\ \epsilon_z \\ \gamma_{xz} \end{bmatrix}$ with $\epsilon_x = \epsilon_{x0} \pm \phi \cdot z$ and γ_{xz} out of the shear strain profile.
- $\sigma = \begin{bmatrix} \sigma_x \\ \sigma_z \\ \tau \end{bmatrix}$ with $\sigma_z = 0$
- Because of the dependency of σ_1 , σ_2 and θ on the strain, ϵ_z has to be solved iteratively.
- σ_1, σ_2 and θ can now be calculated.

2. A tangent stiffness matrix is calculated for every node:

$$K = \begin{bmatrix} \frac{d\sigma_x}{d\epsilon_x} & \frac{d\sigma_x}{d\epsilon_z} & \frac{d\sigma_x}{d\gamma_{xz}} \\ \frac{d\sigma_z}{d\epsilon_x} & \frac{d\sigma_z}{d\epsilon_z} & \frac{d\sigma_z}{d\gamma_{xz}} \\ \frac{d\tau}{d\epsilon_x} & \frac{d\tau}{d\epsilon_z} & \frac{d\tau}{d\gamma_{xz}} \end{bmatrix}$$

If step 3 and 4 do not agree with the assumed values another iteration has to be done, this means the analysis returns to step 1. If the calculated values are close enough to the assumed values the iteration stops.

The outcomes of this iterative method are the global strain profile ($\epsilon_{x0}, \phi, \gamma_{xz}$), transverse strain profile (ϵ_z for every node), the shear stress (τ) and the shear strain profile. There is also an indirect calculation of $\theta, \sigma_1, \sigma_2, \sigma_{sx}, \sigma_{sz}, \epsilon_1$ and ϵ_2 (for every node) because these are inseparable of ϵ_z because they are used to solve for $\sigma_z = 0$.

2.3.3 Analysis Results

2.3.3.1 Cross-sectional analysis

Figure 2.18 to Figure 2.20 show the results of the cross-sectional analysis in Response-2000.

The left-hand side of the output screen (Figure 2.18) shows the control plots. The types of control plots are based on the type of loading, for analysis with shear the control plots are the $V - \gamma_{xz}$ diagram and the $M - \phi$ diagram. The green lines show the load point looked at and by moving these over the graphs the whole load Response can be examined (use Page Up and Page Down). The current loads can be seen on the bottom of the screen.

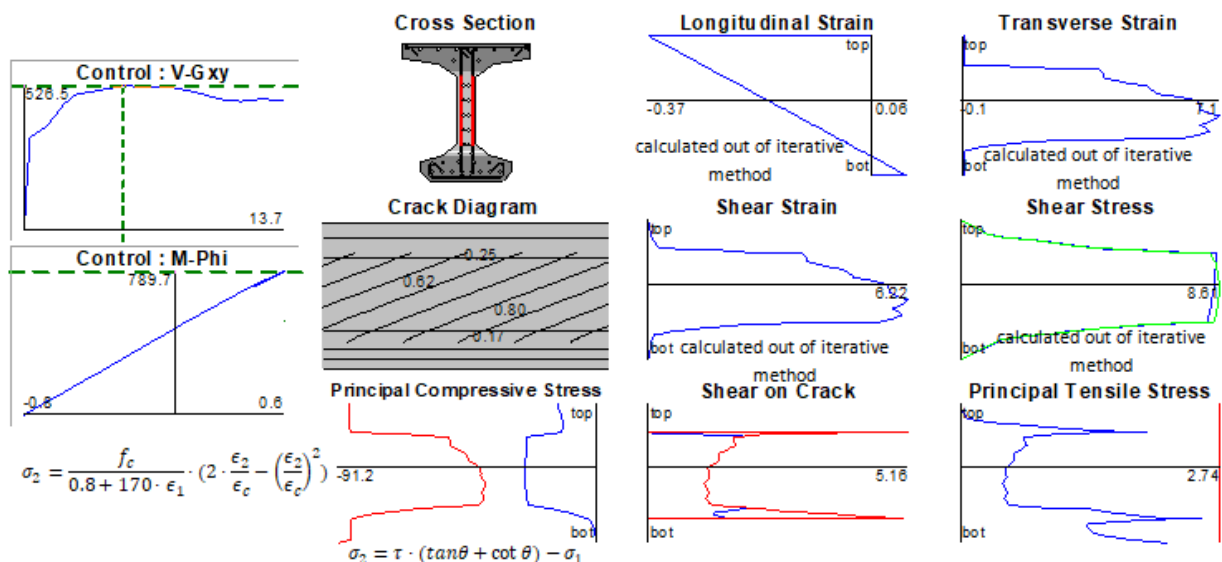


Figure 2.18, Response results general with MCFT formulas

The most important results are the general results shown in Figure 2.18. The meaning of the 9 plots on the right-hand side is declared below (from left to right, top to bottom) (Bentz & Collins, 2001):

1. **Cross-section:** This plot shows the cross-section of the concrete. The light grey regions present the area where the concrete has cracked. The colours of the reinforcements say something about their stress state:

- Dark red: The reinforcement is on the yield plateau.
- Bright red: The reinforcement is in strain hardening stage.
- Dark and bright green: The reinforcement is yielding in compression.

2. **Longitudinal strain**($\times 10^{-3}$): the longitudinal strain (ϵ_x) is plotted over the depth of the cross-section. The assumption plane sections remain plane is valid here.

3. **Transverse strain**($\times 10^{-3}$): the bulging strain (ϵ_z) is plotted over the depth of the cross-section. This strain is dictated by the assumption that $\sigma_z = 0$.

4. **Crack diagram**: Shows the crack pattern over the beam and the crack widths at different heights. It is also possible to plot the principal stress directions here by clicking on the right and then toggle mode. The following colours mean:

- Pink: concrete crushing.
- Purple: failure due to slipping of the reinforcement.

5. **Shear strain** ($\times 10^{-3}$): The distribution of the shear strain (γ_{xz}) over the cross-section. If the section starts to unload a grey envelope presents the maximum value obtained.

6. **Shear stress** (Mpa): the shear stress (τ) over the depth cross-section. There are two lines presented:

- Green: shear stress with longitudinal stiffness method.
- Blue: shear stress from strain state.

Mostly the lines collide when they don't, the load stage should be treated with caution.

7. **Principal compressive stress** (MPa): The principal compressive stress (σ_2) over the depth of the cross-section. Two lines are presented:

- Red: maximum allowable compressive stress (capacity), concrete compression stress is reduced after cracking.
- Blue: actual compressive stress in the cross-section.

If red and blue touch the section is predicted to crush.

8. **Shear on the crack**: Shear stress on the crack (τ_{ci}) over the depth of the cross-section. Two lines are presented:

- Red: maximum allowed shear on the crack.
- Blue: actual shear on the crack.

The blue line is limited by the red line, so the blue cannot become higher than the red.

9. **Principal tensile stress**: the Principal tensile stress (σ_1) over the depth of the cross-section. Two lines are presented:

- Red: maximum allowed principal tensile stress, the tensile strength from the concrete.
- Blue: actual principal tensile stress.

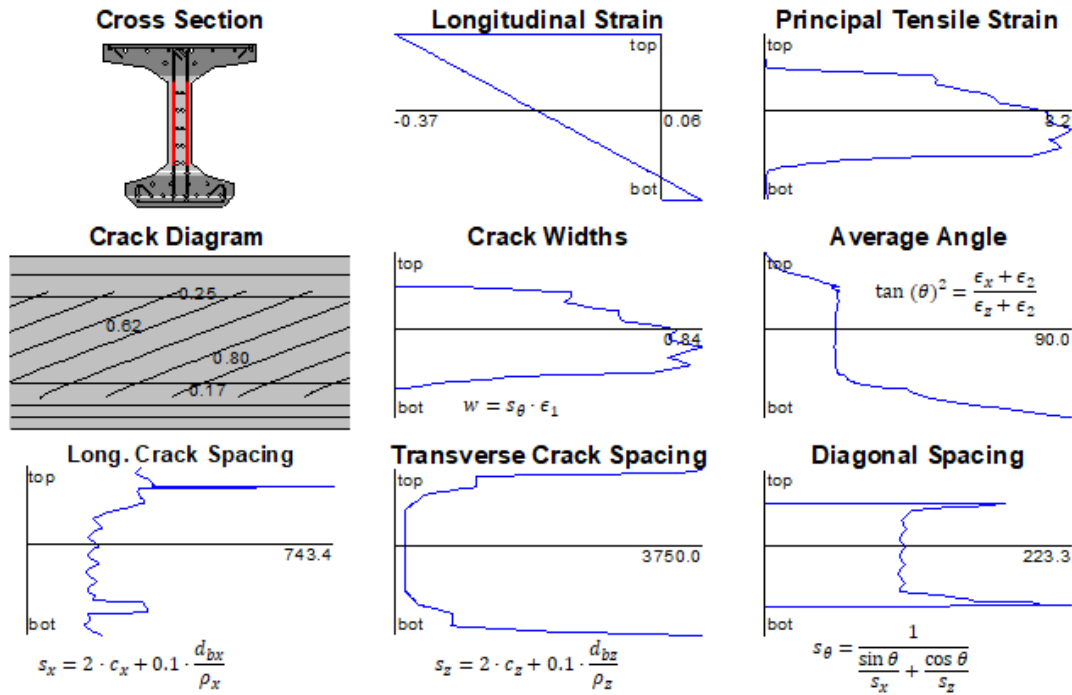


Figure 2.19, Response results cracking with MCFT formulas

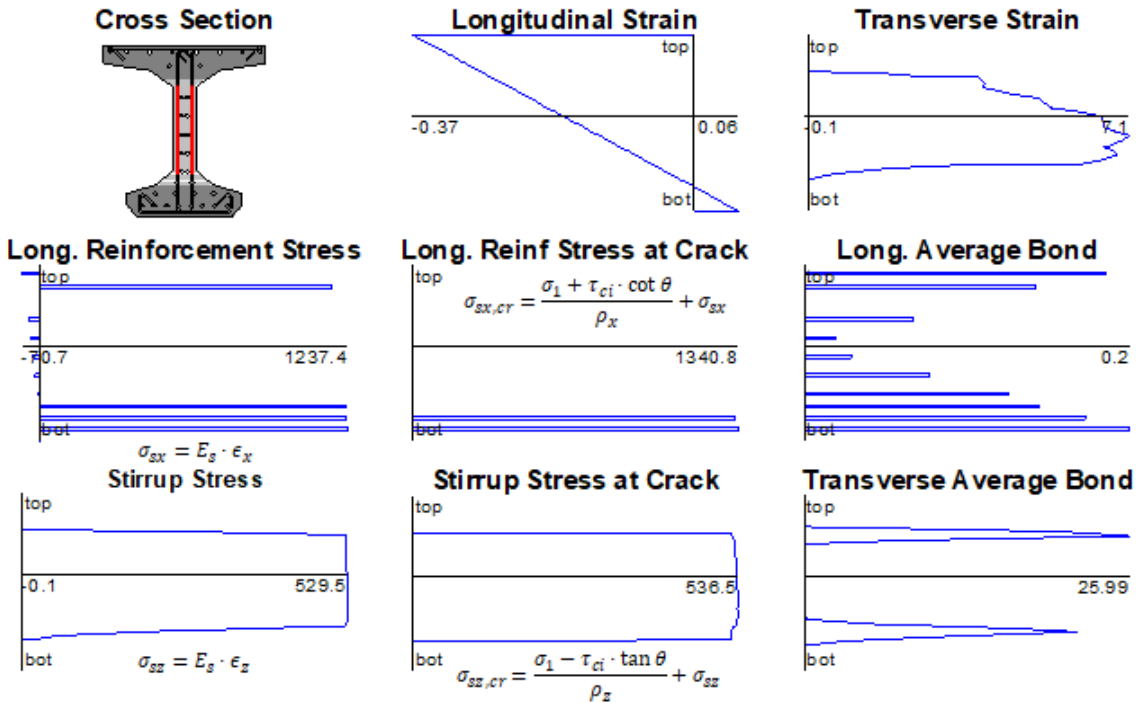


Figure 2.20, Response results reinforcement with MCFT formulas

Not all results shown in Figure 2.18 to Figure 2.20 follow directly out of the iterative calculation most need to be calculated with the MCFT expressions. The MCFT expressions used to calculate the graphs are shown below them, except for the principal tensile stress and the shear on the crack. These parameters need special attention and will be described below. An example of a numerical

calculation of the graphs in Response-2000 with the MCFT formulas is given in the appendix C. This example calculation in Appendix C also shows that a distinct order in calculation needs to be held to be able to calculate all the parameters.

The formulas for the crack spacing as shown in Figure 2.19 need a little bit more explanation. s_x and s_z are the crack spacing in the x- and z-directions and are constant for each load step but vary over the cross-section depth.

In these formulas the parameters are defined as follows:

c_x is the vertical distance from the point calculated to the nearest longitudinal reinforcement.

c_z is the horizontal distance from the point calculated to the nearest transverse reinforcement.

d_{bx} is the diameter of the longitudinal reinforcement.

d_{bz} is the diameter of the vertical reinforcement.

$\rho_z = \frac{A_{s,stirrup}}{b \cdot s}$ where s is the stirrups spacing.

If there is no reinforcement in a direction s is taken as 5h.

Stresses

Special attention has to be given to the stresses in the cross-section, in both the steel and the concrete. The principal tensile stress and the principal compressive stress depend on the state of the concrete.

Before cracking:

$$\tau_{ci} = 0$$

$$\sigma_1 = E_1 \cdot \epsilon_1$$

$$\sigma_2 = E_2 \cdot \epsilon_2$$

$$\sigma_{sx,cr} = 0$$

$$\sigma_{sz,cr} = 0$$

After cracking:

After cracking the MCFT describes 3 options to satisfy equilibrium on the cracked surface (see 2.1.1). Response implements these conditions in the crack check which simultaneously calculates the principal tensile stress and the shear on the crack.

The first step of the crack check is to calculate the ability of the steel to take up the tensile stresses in both directions

$$\Delta f_{c1x} = \sigma_1 - \rho_x (f_{sxy} - \sigma_{sx})$$

$$\Delta f_{c1z} = \sigma_1 - \rho_z (f_{szy} - \sigma_{sz})$$

Four situations are distinguished in the crack-check in Response:

1. The transverse steel has enough capacity to take up all the principal tensile stress (no yielding of the reinforcement) ($\Delta f_{c1z} < 0$):

- $\tau_{ci} = 0$
- $\sigma_1 = \frac{0.33 \cdot \sqrt{f_c}}{1 + \sqrt{3.6m \cdot \epsilon_1}}$ where $m = \frac{A_c}{\sum d_b \cdot \pi}$

2. The transverse steel has not enough capacity to take up all the principal stress but the maximum shear stress on the crack is not required ($\Delta f_{c1z} > 0$):

- $\tau_{ci} = \frac{\Delta f_{c1z}}{\tan \theta}$
- $\sigma_1 = \rho_z(\sigma_{sz,cr} - \sigma_{sz}) + \tau_{ci} \tan \theta$

3. The transverse steel has not enough capacity take up all the principal stress and the shear on the crack has reached its maximum: $\tau_{ci,max}$, σ_1 is reduced, there is slipping of the crack.

- $\tau_{ci} = \tau_{ci,max} = \frac{0.18 \cdot \sqrt{f_c}}{0.31 + \frac{24 \cdot w}{d_{max} + 16}}$
- $\sigma_1 = \rho_z(\sigma_{sz,cr} - \sigma_{sz}) + \tau_{ci,max} \tan \theta$

4. Both the transverse and longitudinal steel are yielding ($\Delta f_{c1z} > 0$ and $\Delta f_{c1x} > 0$):

- $\tau_{ci} = (\rho_x(\sigma_{sx,cr} - \sigma_{sx}) - \rho_z(\sigma_{sz,cr} - \sigma_{sz})) \cdot \sin \theta \cdot \cos \theta$
- $\sigma_1 = \rho_x(\sigma_{sx,cr} - \sigma_{sx}) \cdot \cos^2 \theta + \rho_z(\sigma_{sz,cr} - \sigma_{sz}) \cdot \sin^2 \theta$

The governing situation gives the minimum σ_1 . This calculation of σ_1 is implicitly used in the iterative calculation as σ_1 is used to calculate ϵ_z .

2.3.3.2 Full member Response

Response-2000 has also an option to get the response of a full member instead of one section. For this analysis, Response-2000 divides the beam in at least 20 segments at which a shear force, moment and axial load are determined from the load. The curvature and shear strain are then interpolated from the interaction diagram. To be able to run this analysis the shear length and the loading have to be entered. The results of this analysis are shown in Figure 2.21.

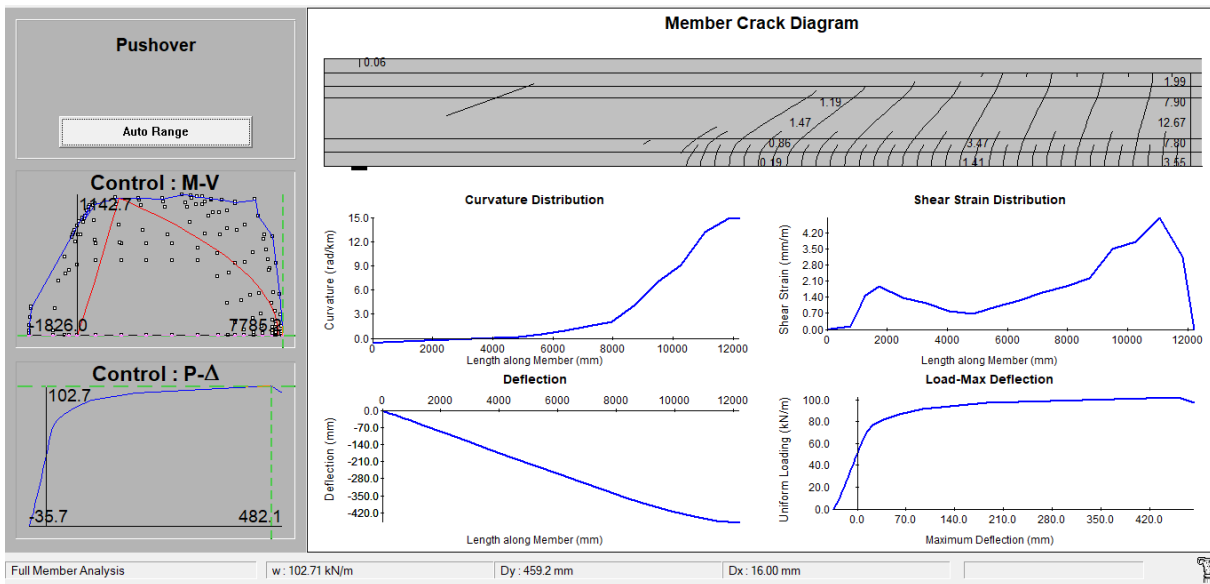


Figure 2.21, Member response results

On the top left of Figure 2.21, the interaction diagram between M and V is shown. In blue, the failure envelope is given and the red line shows the loading envelop. The place where the loading envelope touches the failure envelope says something about the failure mechanism. When the envelopes touch on top ($V > M$) this means shear tension failure and when they touch on the right ($M > V$) this

means flexural failure. The loading envelope is linear on the right and parabolic on the left because the active shear is trimmed at the supports over a distance d . The shear diagrams are trimmed at a distance d from the support and the point load to satisfy the assumption that there are no stresses in the transverse direction. The squares on the control plot represent a solved combination of moment, shear and axial load, and can be examined by clicking on it. On the right, the curvature, deflection, shear strain distribution and load deflection diagram are presented for the case of failure. It is possible to view these plots for every load step up to failure by using the load deflection control plot on the left.

3 Prediction of shear tension failures with Response-2000

To investigate how accurate Response predicts shear tension failures, the results of Response analysis are compared with experiments that fail in shear tension. For this investigation test series of Xie (Xie, 2009), Choulli (Choulli, 2005), Hanson (Hanson & Hulbos, 1965) and Leonhardt (Leonhardt, Koch, & Rostasy, 1973) have been analyzed with Response. To obtain consistent results the following starting points are taken for analysis of shear tension failure with Response:

- Automatic crack spacing is used.
- Material properties determined out of test results are used as much as possible.
- If ϵ_c and f_t are not defined by the experiments automatic calculation by Response is used.
- The aggregate size is linearly decreased to 0 for concrete strengths between 60-80 Mpa.
- Popovics/Thorenfeld is used for the compression curve.
- Vecchio-Collins compression softening is used for normal strength concrete and Porasz-Collins is used for concretes with strengths higher than 90 MPa.
- The critical cross-section for shear tension failure is defined as the cross-section with the lowest shear strength which has no bending cracks on the ultimate fibre of the flanges.

3.1 Experiments

A totality of 32 beams has been analyzed with Response. All of these beams are I-beams with a certain amount of shear reinforcement and prestressing. All beams have straight prestressing tendons, but beams from Xie (Xie, 2009) have unbonded tendons while the other experiments all have bonded tendons. The beams of Choulli (Choulli, 2005) and Leonhardt (Leonhardt, Koch, & Rostasy, 1973) have longitudinal reinforcement in the web while Xie only has longitudinal reinforcement in the flanges and Hanson has no extra longitudinal reinforcement other than the prestressing tendons. Table 3.1 and Table 3.2 show the most important characteristics of each experiment, in appendix D a detailed description of each beam and its characteristics can be found.

	Xie (Xie, 2009)	Choulli (Choulli, 2005)
Cross-section	<p style="text-align: center;">A-A</p>	
	<p>Figure 3.1, Cross-section LB2, LB3, LB10 (Xie, 2009)</p>	<p>Figure 3.3, Cross-section HAP1TW, HAP2TW, HCP1TW, HCP2TW (Choulli, 2005)</p>
	<p style="text-align: center;">A-A</p>	
	<p>Figure 3.2, Cross-section LB6 to LB8 (Xie, 2009)</p>	<p>Figure 3.4, Cross-section HAP1TE, HCP1TE, HCP2TE (Choulli, 2005)</p>
Number of experiments	6 experiments: LB2, LB3, LB6, LB7, LB8, LB10	7 experiments: HAP1TE, HAP1TW, HAP2TW, HCP1TE, HCP1TE, HCP2TE, HCP2TW
Static scheme	Statically indeterminate	Statically determinate
a/d-ratios	5.1	3 or 3.1
Transverse reinforcement ratio	$\rho_z = 0.187\%$ (0.37% for LB10)	$\rho_z = 0.50\%$
Prestress	Variable between 4.34 and 11.16 MPa	9.56 MPa for HAP1TE, HAP1TW, HCP1TE, HCP1TE 6.30 MPa for HCP2TE, HCP2TW, HAP2TW
Concrete strength (MPa)	63.2 MPa for LB2 and LB3 63.5 MPa for LB6, LB7 and LB8 63.3 MPa for LB10	90.2 MPa for HCP2TE, HCP2TW 96 MPa for HAP2TW 81.2 MPa for HCP1TE, HCP1TW 91.2 MPa for HAP1TE, HAP1TW
Response cross-section		
	<p>Figure 3.5, Cross-section Xie LB2, LB3, LB10</p>	

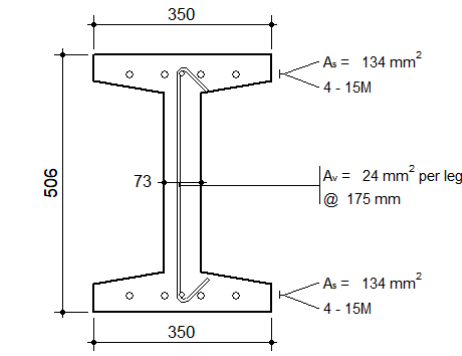


Figure 3.6, Cross-section Xie LB6 to LB8

Figure 3.7, Cross-section Choulli: HAP1TE, HCP1TE, HCP2TE

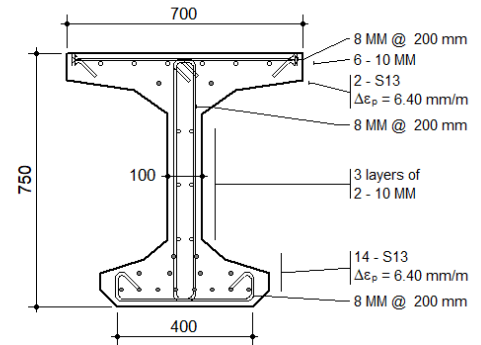


Figure 3.8, Cross-section Choulli: HAP1TW, HAP2TW, HCP1TW, HCP2TW

Table 3.1, Cross-section properties Xie and Choulli

	Hanson (Hanson & Hulbos, 1965)	Leonhardt (Leonhardt, Koch, & Rostasy, 1973)
Cross-section	<p>Figure 3.9, Cross-section Hanson (Hanson & Hulbos, 1965)</p>	<p>Figure 3.10, Cross-section TP2 (Leonhardt, Koch, & Rostasy, 1973)</p>
Number of experiments	17 experiments	2 experiments: TP2 and TP4
Static scheme	Statically determinate	Statically determinate
a/d-ratios	Between 1.9 and 4.4	3.9
Transverse reinforcement ratio	Between: 0.19% and 0.74%	TP2: $\rho_z = 0.70\%$ TP4: $\rho_z = 2.31\%$
Prestress	Variable between 5.85 and 6.40	TP2: 5.50 MPa

Figure 3.10, Cross-section TP2 (Leonhardt, Koch, & Rostasy, 1973)

Figure 3.11, Cross-section TP4 (Leonhardt, Koch, & Rostasy, 1973)

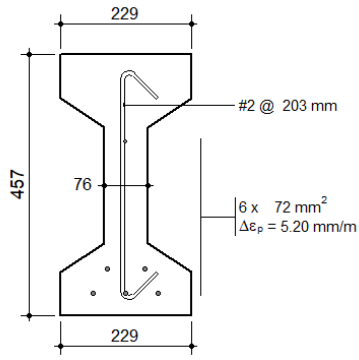
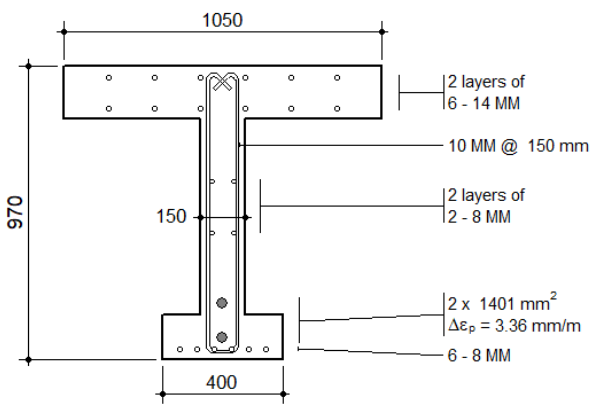
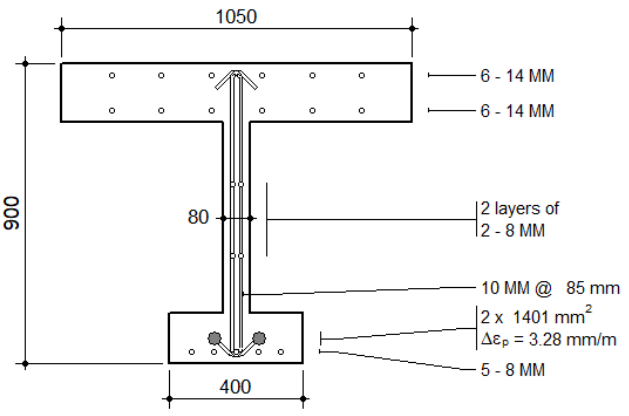
	MPa	TP4: 6.32 MPa
Concrete strength (MPa)	Variable between: 51.1 MPa and 43.5 MPa.	TP2: 22.8 MPa TP4: 46.6 MPa
Response cross-section	 <p>Figure 3.12, Response cross-section Hanson</p>	 <p>Figure 3.13, Response cross-section TP2</p>
		 <p>Figure 3.14, Response cross-section TP4</p>

Table 3.2, Cross-section properties Hanson and Leonhardt

3.2 Comparison Response with experiments

To determine the accuracy of Response-2000 for beams failing in shear tension, a comparison between the results of Response and several experiments is made. For this comparison, the series of experiments from Xie (Xie, 2009), Choulli (Choulli, 2005), Hanson (Hanson & Hulbos, 1965) and Leonard (Leonhardt, Koch, & Rostasy, 1973) are used. To get a fair comparison, between Response and the experiments, several parameters are compared. This gives insight in where Response differs from the experiments and what parameters are predicted correctly.

The comparison will be divided in a general comparison, which consists of a comparison of the failure load, failure mechanism and failure location, and a more in-depth comparison of the components that resist the load. The load can be resisted by the concrete (both cracked and uncracked) and the reinforcement steel. The steel part of the resistance is determined by the cracking angle and the steel stress. The contribution of the concrete depends on the height over which the concrete is cracked. For the cracked concrete the aggregate interlock is the most important parameter and this is characterized by the crack width and the crack spacing.

The behaviour of the beams largely depends on its characteristics such as: a/d-ratio, amount of reinforcement and amount of prestress. When the predictions are plotted against the parameters the dependency of the predictions on the parameters can be seen. This gives us the ability to relate the accuracy to different parameters and gain insight for predictions of shear tension failure.

3.2.1 General comparison

The general comparison of the beams consists of an analysis of the failure load, failure mechanism and failure location. The failure load is the most important of these parameters because it gives the capacity of the beam and if this is predicted correctly. Both the failure mechanism and the failure location are vital to get a good prediction of the failure load. The critical cross-section gives the M/V-ratio. The failure mechanism provides insight in the cause of failure at that certain location and the lead up to the failure load. Below an analysis of these parameters is given, for this analysis a conclusion about the quality of the prediction will be drawn.

3.2.1.1 Failure Load

The failure load is one of the most important parameters to compare because it demonstrates the capacity of the beam in shear tension and therefore it shows that the beam is able to carry the load. In both Response and the experiments, the failure load is defined as the maximum load the beam is able to resist.^a

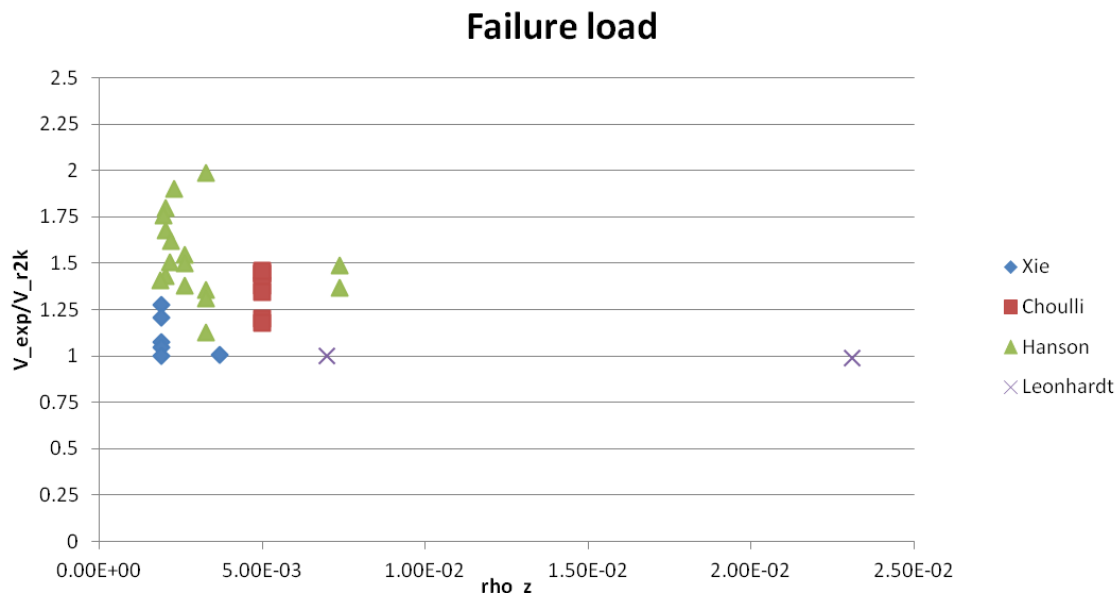


Figure 3.15, Failure load

The above graph (Figure 3.15) shows the ratio between experimental and predicted shear failure loads, grouped by their experimental series. It can be seen that the experiments of Choulli and Hanson are predicted quite conservative because most of the experiments lay above the 1.25 line.

^a The self weight is not taken into account in the Response analysis and this can cause a small inaccuracy for beams with significant self weight. However, the experimental failure loads of Xie (Xie, 2009) and Hanson (Hanson & Hulbos, 1965) do also not take into account self weight in the failure load. The influence of the self weight decreases for higher variable loads. Choulli and Leonhardt have significant self weight and this is also taken into account in the experimental failure load.

The predictions of Xie and Leonhardt lay close to one, this makes them very accurate. The predicted accuracy of the experimental series is shown in Table 3.3.

	Mean	COV	Number of specimens
Xie	1.098	10%	6
Choulli	1.33	8%	7
Hanson	1.54	15 %	17
Leonhardt	0.99	0.89%	2
Total	1.38	19 %	32

Table 3.3, Failure load prediction accuracy

Hanson has the highest mean and variability. This can be caused by variability in the test results, for example, FX1A and FX1B have the same properties but FX1A has a 17% higher failure load.

Prestress

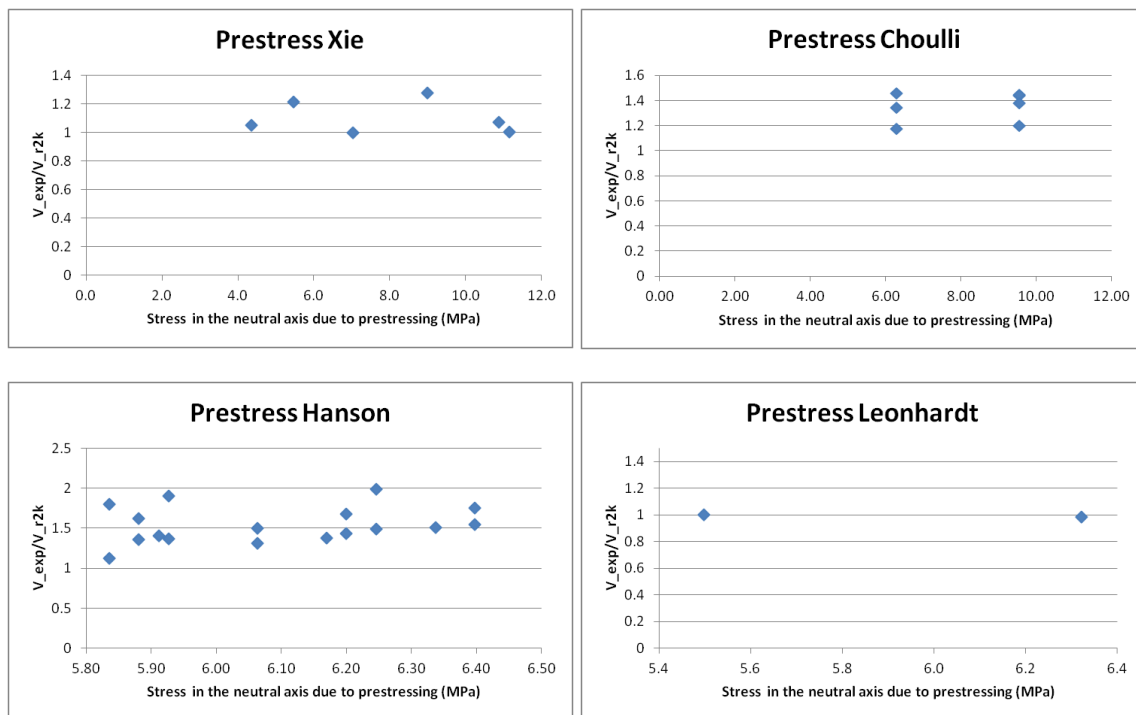


Figure 3.16, Failure load prediction as a function of the prestress

Higher prestress causes higher compressive stress in the cross-section; these compressive stresses carry a part of the load due to transverse clamping. The clamping stresses are neglected in Response ($\sigma_z = 0$) so this part of the load carrying mechanism is not taken into account and therefore the prediction of beams with high prestress are more conservative than beams with lower prestress. In Figure 3.16 the ratio of the failure load is plotted against the compressive stress in the neutral line of the cross-section caused by prestressing. For Xie and Leonhardt no clear increase in the ratio of the failure load can be seen. For Xie, the beams with high prestress (LB6 and LB10) lay closer to 1 than beams with lower prestress. For Choulli and Hanson, the effect of higher prestress can be seen as for higher prestress the results are slightly more conservative. Xie has a high a/d -ratio (5.1) which means that in the critical cross-section the influence of the prestress is lower than for beams with smaller

a/d-ratios such as Hanson (between 1.9 and 4.53) and Choulli (3.1) which give more conservative values for higher prestress.

a/d-ratio

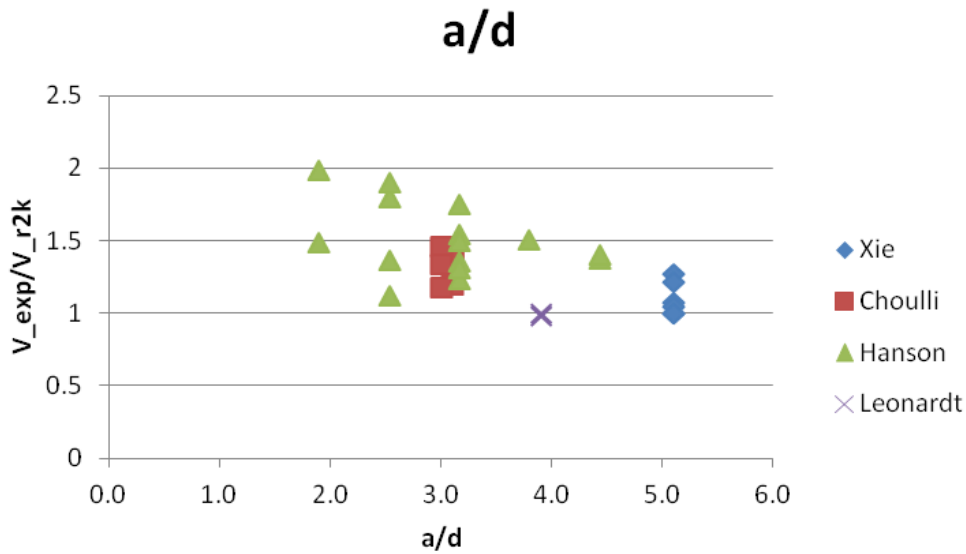


Figure 3.17, Failure load predictions as a function of the a/d-ratio

The influence of the clamping stress can also be recognized when the ratio of the failure load is plotted against the a/d-ratio (Figure 3.17). It can be seen that the predicted failure load of the beams with lower a/d-ratio are more conservative, their load carrying capacity is underestimated by Response because the force resisted by the clamping stresses is not taken into account. It can be seen that especially the experiments of Hanson and Choulli have small a/d-ratios and are therefore quite conservative.

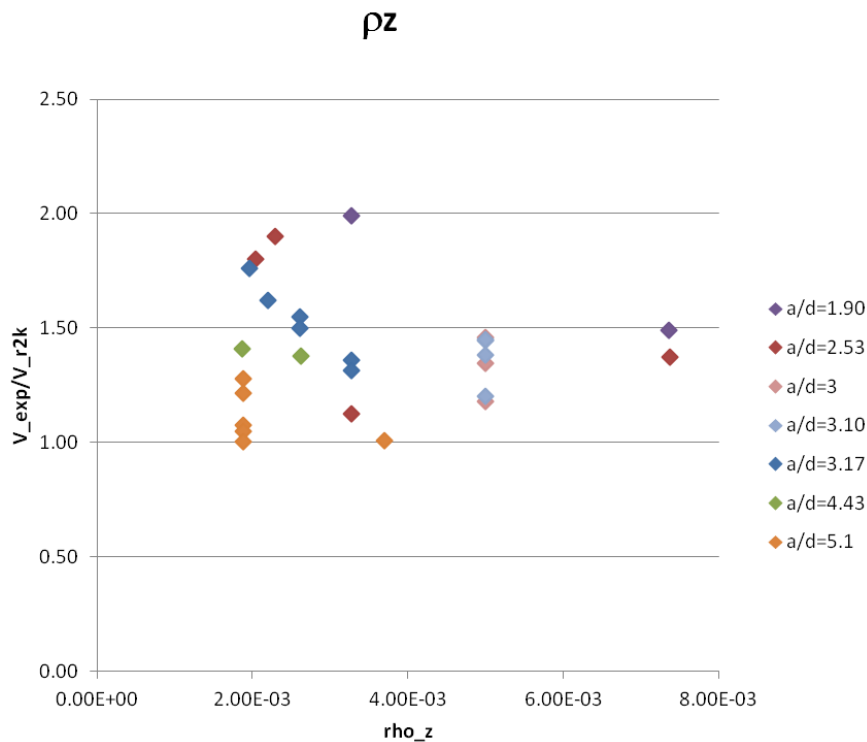


Figure 3.18, Failure load predictions as a function of the reinforcement ratio

The scatter observed in the predictions in Figure 3.17 can be explained by combining the a/d -ratio and the transverse reinforcement ratio, as showed in Figure 3.18. The beams are divided based on their a/d -ratio to show the relation between the failure load, the reinforcement ratio and the a/d -ratio. It can be seen that beams with a higher reinforcement ratio but the same a/d -ratio are predicted less conservative. It can also be seen that beams with a higher a/d -ratio have less conservative predictions than beams with a low a/d -ratio for the same reinforcement ratio, which is explained by not taking into account the clamping stresses ($\sigma_z = 0$).

3.2.1.2 Failure mechanism

Within the experimentally observed shear tension failure of the beams multiple failure mechanisms are distinguished:

- Rupture of the stirrups
- Major crack opening/ slipping of the crack
- Crushing of the web concrete
- Buckling of the flanges
- Shear compression failure

It is possible that a beam fails in a combination of multiple failure mechanisms, in that case, the mechanism that is dominant will be indicated as the failure mechanism. The failure mechanisms are collected from the experimental data and from the results of Response. The comparison of the failure mechanisms is important because it gives a direct indication of the behaviour of the beam. If the predictions of Response result in a correct failure mechanism the results will be more reliable because the beams behave in a similar way.

The failure of the beams, as predicted in Response, is described in more detail in Appendix D for every beam. Below an overview for each failure mechanism will be given:

- **Rupture of the stirrups:**

The failure mechanism "rupture of the stirrups" is correctly predicted for LB2, LB7 and F10A. Rupture of the stirrups was also observed in Response for beams F3B and F5B.

- After diagonal tension cracking the shear force continues to increase because the average stirrup stress and the shear on the crack are still able to make equilibrium and the cracking angle decreases. The shear reinforcement on the crack already yielded and the maximum shear on the crack decreases. When the crack slips ($\tau_{ci} = \tau_{ci,max}$) the principal compressive capacity starts to decrease and the stirrup stress in the crack increases. When the steel stress in the stirrup reaches its maximum stress the maximum load is calculated while the principal concrete strain is still below the crushing strain. This results in the failure "Rupture of the stirrups" shown in Figure 3.19.

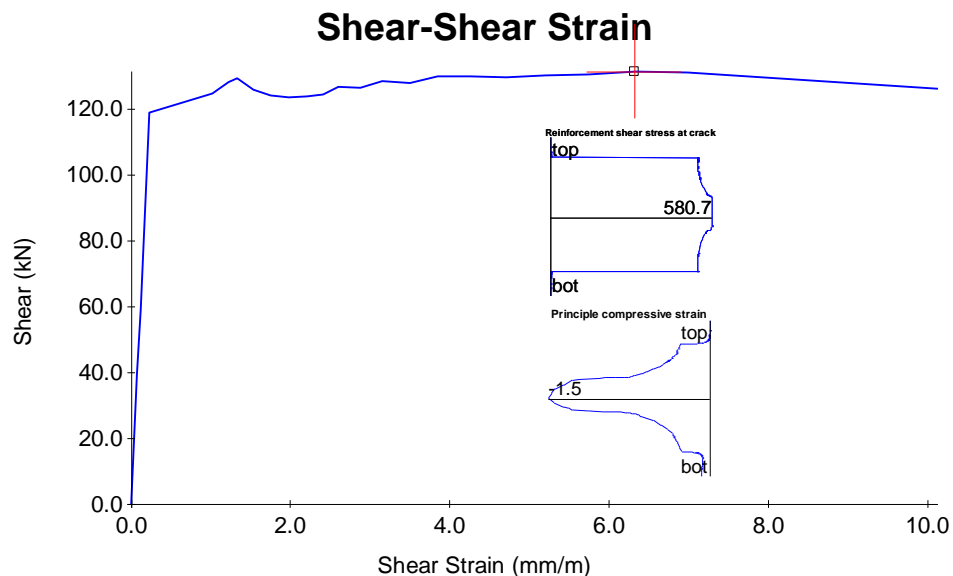


Figure 3.19, Stirrup Rupture LB7

- **Major crack opening/slipping:**

Major crack opening is correctly predicted for LB3 and LB8.

- After diagonal tension cracking the stirrup on the crack yields. The shear force keeps increasing because the average steel stress and the shear on the crack are still able to make equilibrium, meanwhile, the angle of the crack is decreasing. On the same moment, the maximum shear on the crack decreases. The maximum load is calculated just after the instant that the crack slips ($\tau_{ci} = \tau_{ci,max}$). After this the stress in the stirrups on the crack increases and the principal compressive stress capacity decreases and the flange cracks. The crack width increases rapidly after the maximum load. The reinforcement does not rupture at the last load stage nor does the concrete crush. The shear-shear strain diagram of this failure is shown in Figure 3.20.

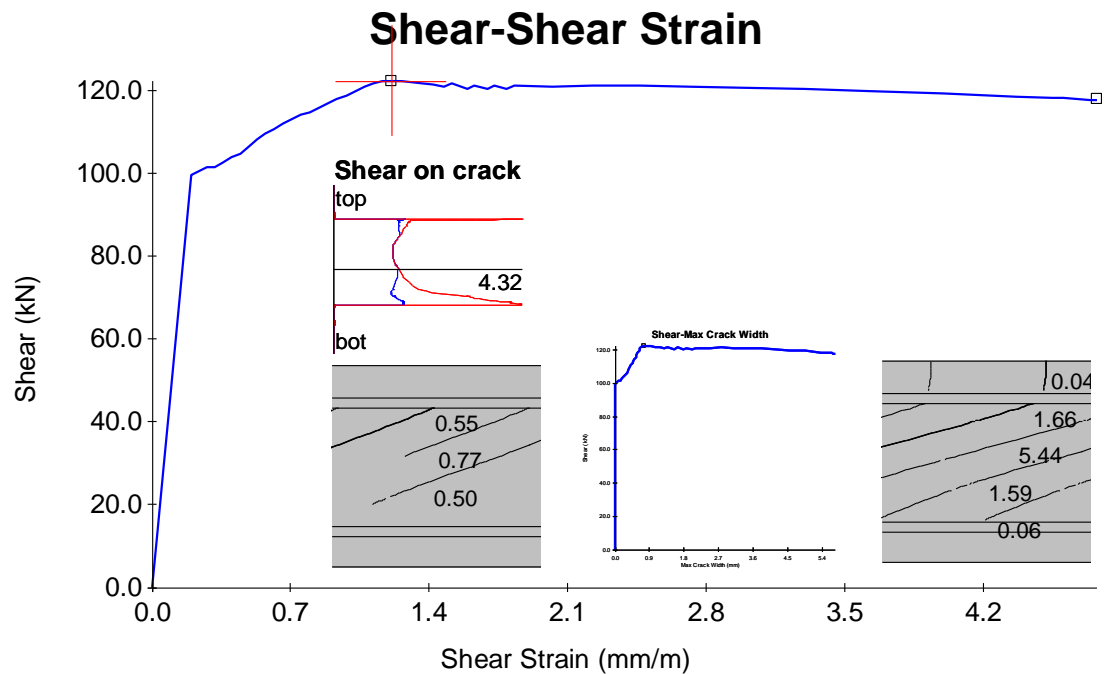


Figure 3.20, Major crack opening LB3

- **Crushing of the web concrete:**

Crushing of the web concrete is correctly predicted for: HAP1TE, HAP1TW, HAP2TW, HCP1TE, HCP1TW, HCP2TE, FX1A, FX1B, F1A, F1B, F2B, F3A, F4A, F7A, F19A, TP2, and TP4. Crushing of the web concrete is also predicted for: LB6, LB10, HCP2TW, F2A, F4B, F5A, F11A, and F19B.

- After diagonal tension cracking the load increases, because the average steel stress and the shear on the crack are still able to make equilibrium, meanwhile, the angle of the crack is decreasing. At the moment of diagonal tension cracking the stirrup on the crack yields and the maximum shear on the crack starts decreasing. The angle of the crack is decreasing when the forces increases. When the crack slips ($\tau_{ci} = \tau_{ci,max}$) the stirrup stress at the crack starts increasing while the principal compressive capacity decreases. When the maximum load is reached the principal compressive stress does not reach its capacity nor does the stirrup. After this, the shear force decreases and the principal compressive stress soon reaches its capacity while the stirrup stress at the crack does not reach its maximum stress. The shear-shear strain diagram of this failure is shown in Figure 3.21.

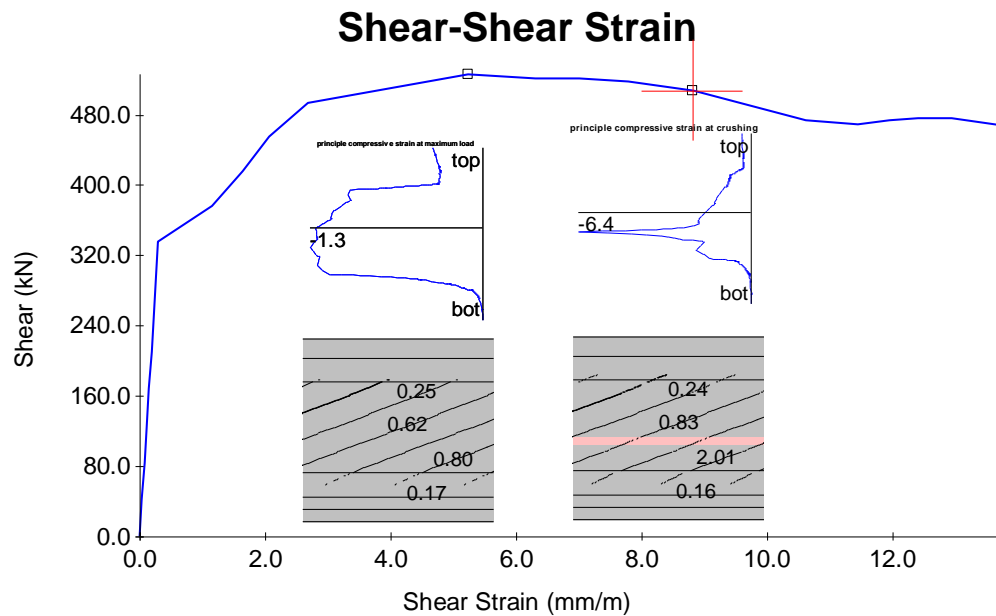


Figure 3.21, Crushing failure HAP1TE

- HCP1TE fails as the above description with the exception that crushing happens at maximum load.
- F2A, F3A and F4A fail similarly as the above description with the exception that the maximum load is reached when the crack slips for the first time.
- For beams FX1A, FX1B, F1B, F2B, F4B, F7A, F11A and F19B the failure mechanism is described as follows: After diagonal tension cracking the load drops a bit and the reinforcement on the crack yields immediately. Then the load increases, because the average steel stress and the shear on the crack are still able to make equilibrium, meanwhile, the angle of the crack is decreasing. At the same moment, the maximum shear on the crack decreases and also the principal compressive capacity starts decreasing. The maximum shear force is reached at the first instant of slipping of the crack ($\tau_{ci} = \tau_{ci,max}$). After this the shear force decreases, as well as the principal compressive capacity. The principal compressive capacity is reached soon after the maximum load while the stirrup stress does not reach its maximum. The shear-shear strain diagram of this failure is shown in Figure 3.22.

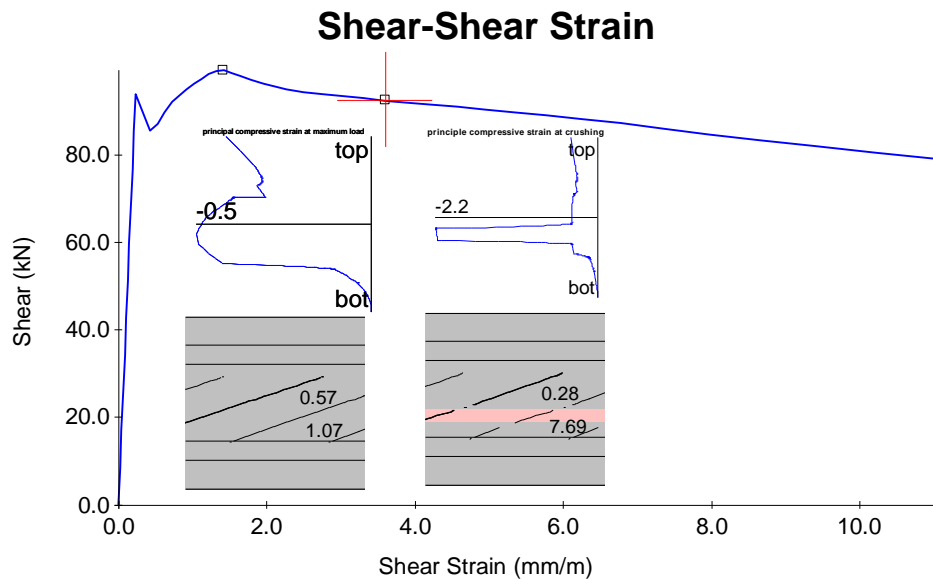


Figure 3.22, Crushing failure FX1A

- For beams TP2 and TP4 the failure mechanism is described as follows: After diagonal tension cracking the force increases because the average steel stress and the shear on the crack are still able to make equilibrium. The stirrup at the crack does not yield immediately. The maximum shear on the crack decreases. The crack does not slip when the maximum load is reached. The principal compressive stress reaches the principal compressive capacity at the maximum load ($\epsilon_c = -2.261 > -2.20$), while the stirrup stress at the crack does not reach its maximum. The stirrup stress at the crack is only at yielding ($426.9 < 545$). The shear-shear strain diagram of this failure is shown in Figure 3.23.

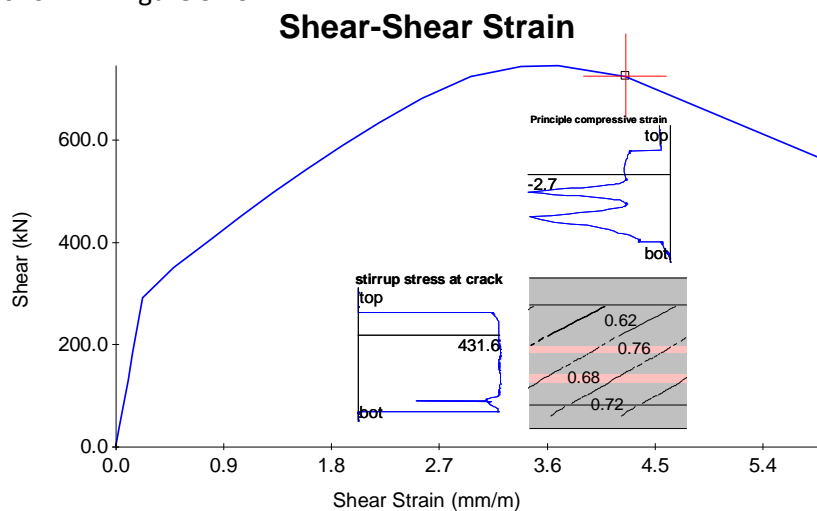


Figure 3.23, Crushing failure TP2

From the analysis, it is obtained that the failure mechanism is predicted correctly for 87% of the analysis.

Rupture of the stirrups was predicted by Response incorrectly for 2 beams, F3B en F5B, in the experiments these beams failed due to crushing. Both of these beams have 3/16 reinforcement which is not very ductile, and the steel is defined to break at the strain corresponding to the maximum stress instead of after necking of the steel. This makes that the capacity of the

reinforcement is reached quicker than the capacity of the concrete however the concrete is near crushing.

Crushing of the web concrete was predicted incorrectly for LB10, LB6, HCP2TW, F2A, F4B, F5A, F11A, and F19B. LB10 and LB6 were observed failing due to buckling of the flanges and opening of a major crack; because it is not possible for Response to predict buckling this failure mechanism is wrongly predicted. For F2A, F4B, F11A and F19B the experimental failure mode was rupture of the stirrups. These beams have a small a/d -ratio (which means a large part of the force is carried by transverse clamping (stress in the transverse direction). In Response this stress is zero causing less stress in the stirrups, therefore the crushing becomes governing instead of rupture of the stirrups. Another reason for the wrong prediction could be that for these beams the Response predicts not much load increase after diagonal tension cracking (Figure 3.22) and in combination with the large yield plateau of the reinforcement (Appendix D figure D.19) this means that the reinforcement stress is not able to increase till the rupture stress before crushing occurs. F5A was observed failing due to shear compression failure because it is not possible to predict this failure with Response this failure mechanism was wrongly predicted.

It can be concluded that the failure mechanism is predicted with an accuracy of 86.75% in Response. It can also be concluded that there is a distinct load response for each failure mechanism, except for crushing where deviation has been found for a couple of beams experimented on by Hanson. This is explained by the low reinforcement ratios of these beams. For incorrectly predicted failure mechanisms crushing and rupture of the stirrups are interchanged, this can be explained by the ductility of the stirrups.

3.2.1.3 Critical location for shear tension failure

Response-2000 is a cross-sectional program, which means a critical cross-section has to be chosen. Codes such as the CSA define the cross-section at a distance d from the support or the load as the critical cross-section for shear failure. For the Response analysis, the critical cross-section for shear tension failure is chosen as: The cross-section that has the lowest capacity when failing in shear tension (no cracks at the bottom/top).^b This decision is based on the definition of shear tension failure which states that it is shear failure without bending cracks. All investigated experiments are selected to fail in shear tension which makes it likely that the defined section really is the failure section. An example of the chosen failure location can be seen in Figure 3.24 where the critical shear force per cross-section as found in Response is shown for beam LB3 of Xie (Xie, 2009). The green dot is the defined failure location while the red dots present flexural shear failure. The cross-section is related to the ratio between M/V which follows from choosing V as 1 in the analysis.

^b This is not totally correct as it is also possible to have shear tension cracks at first and after that cracks at the top and the bottom, which will still be characterized as shear tension failure. For this analysis this is however ignored which makes it possible the failure location is at a higher M/V -ratio then predicted.

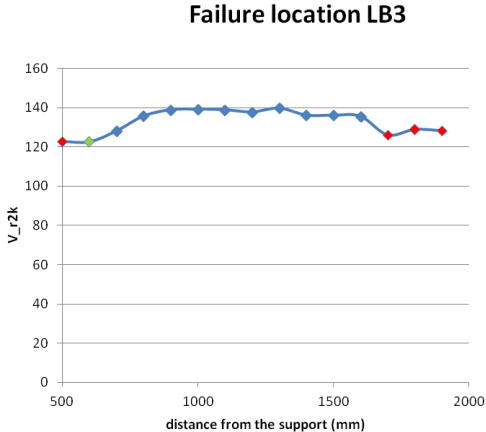


Figure 3.24, Failure location LB3

To determine if the cross-section in Response is in agreement with the failure location observed in the experiment, the failure location in the experiment is obtained in various ways depending on the available information. Below the failure locations will be compared for all the experimental series separately.

Xie:

The failure location is obtained out of the stirrup strains (figure 4.61 and 4.62 of (Xie, 2009)), because Xie (Xie, 2009) states that the maximum stirrup strain corresponds with the maximum crack width. However, the strain was not measured in all stirrups, only the even-numbered stirrups where measured. This leads to an uncertainty in the location of 175 mm (stirrups spacing) on both sides of the maximum stirrup strain (except LB10 s= 87.5 mm).

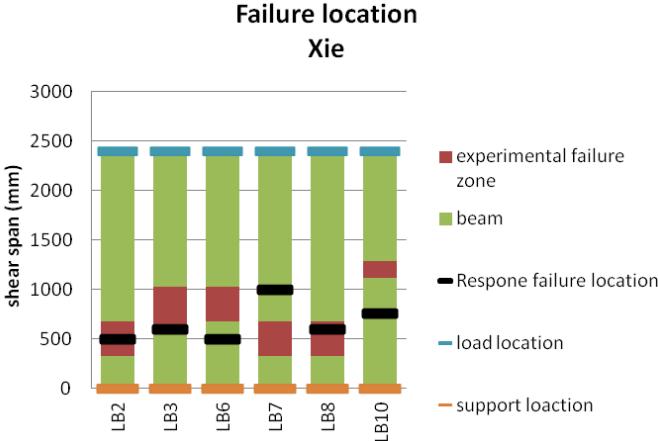


Figure 3.25, Failure location Xie

For the beams experimented on by Xie (Xie, 2009) the failure location and prediction of Response is close to the support. This is because the beam is continuous so also close to the support the moment is high. The failures are reported at a minimum of d from the support. Failures closer to the support are not considered because the beam is designed with extra shear reinforcement in the d region to prevent failures in this region. Variation in the failure location can be explained by the amount of prestressing. Beams with the highest prestress (LB2, LB6) fail at a higher M/V-ratio (closer to the

support) then beams with lower prestress (LB7). It can be seen that 3 of the 6 failures predicted by Response are within the failure region of the experiment. For LB6, LB7 and LB10 the prediction is, however, not completely wrong because the crack is spread over a large part of the beam and the failure region is only determined from the maximum stirrup strain.

Choulli:

Because of the failure mechanism (crushing), no primary cracks can be obtained nor is it possible to determine the maximum stirrup stress (only a few measurement locations). The failure location is taken within the region with the biggest damage determined from inspection of the pictures ((Choulli, 2005) figures A.33, A.44, A.65, A.76, A.87, A.98 and A.109). These pictures are shot under an angle and do not depict the whole beam, this means the values obtained are not very accurate, which leads to an uncertainty in the failure zone. HCP2TW has a very large failure zone (consisting of almost the whole shear span) because a large crack is formed over this region.

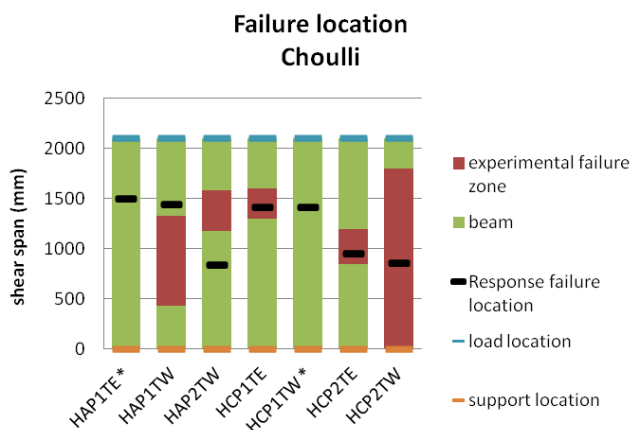


Figure 3.26, Failure location Choulli, * exp. failure zone unknown

Figure 3.26 shows that the predicted failure location is much closer to the location of the load than for the beams of Xie. Especially for beams with high prestress (HAP1TE, HAP1TW, HCP1TE and HCP1TW), the failure is predicted close to the load location. This means that the M/V-ratio is much higher than for beams with lower prestress. These beams fail around d from the load while the beams with the lower prestress are predicted to fail in shear tension at the middle of the beam. No difference in failure location can be seen between the east and west side of the beams, this means the amount of longitudinal reinforcement has no influence on the failure location. It can be seen that 3 of the 7 failure locations are predicted correctly. For 2 beams, however, it was not possible to determine the experimental failure location. The prediction of the failure location of HAP1TW is close to the failure zone obtained from the experiments, while the failure location of HAP2TW differs significantly from the observed failure location.

Hanson:

The failure location is determined from available pictures ((Hanson & Hulbos, 1965) figures 14 to 17, 20 and 21) and for the beams failing due to stirrup fracture the region is determined by the location of the stirrup fracture. The failure locations from the pictures are not very accurate because the location of the crushing failure is characterised from the biggest damage in the picture. Not all beams had a picture available so the experimental failure zone is not obtained for these beams.

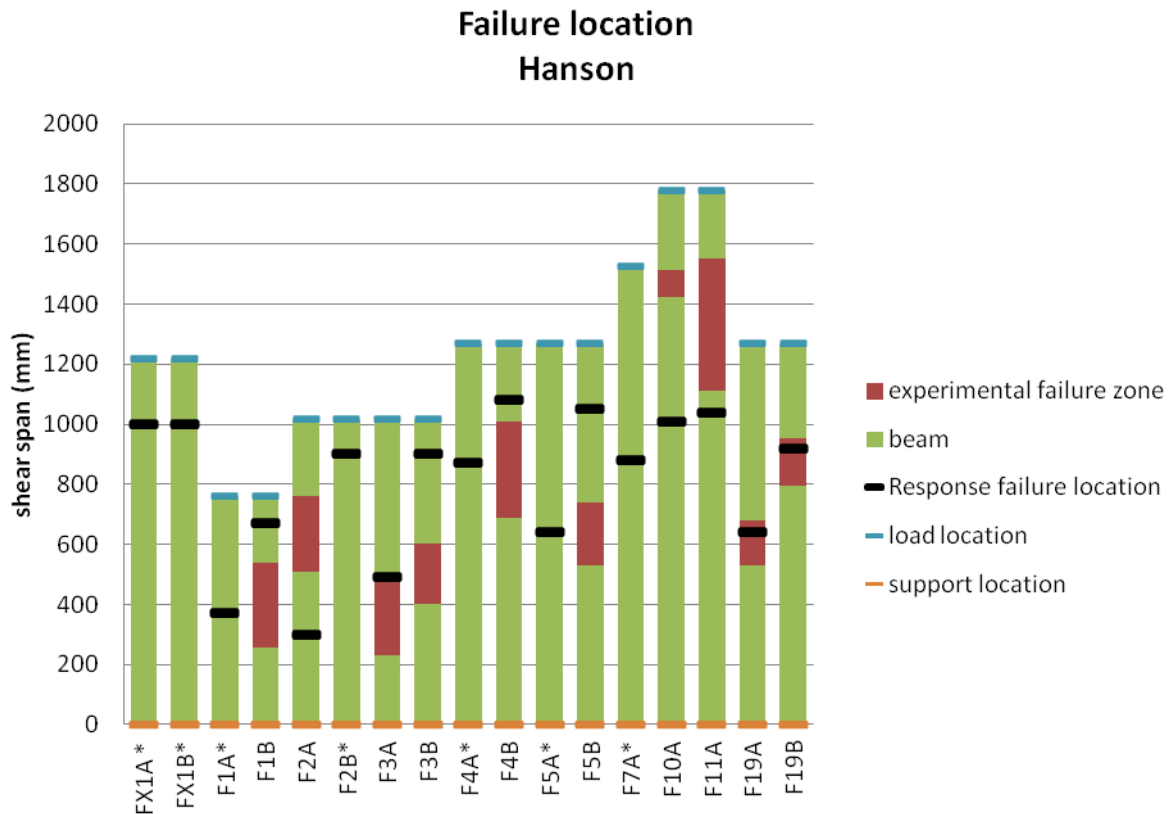


Figure 3.27, Failure location Hanson, * exp. failure zone unknown

Hanson (Hanson & Hulbos, 1965) tested beams with various shear span lengths which makes it difficult to compare them all. Therefore, the results will be compared for beams which have the same shear span. When beams F2A, F2B, F3A and F3B are compared it can be seen that Response predicts the failure location of F2B and F3B close to the load (within a distance d) and that F2A and F3A are predicted closer to the middle of the shear span. The difference between the A- and the B-side of the beam is the reinforcement percentage. F2B has a lower reinforcement percentage than F2A. The same holds for F3B and F3A. The difference in the location critical cross-section is explained by the definition of the critical cross-section. Both sides of the beam have the same properties and need, therefore, the same moment to crack the ultimate fibre. A lower reinforcement percentage, however, means that the capacity of the steel to resist the load is less thus the ultimate shear resistance is less. A lower shear force with the same moment means a higher M/V -ratio is needed which leads to a failure location closer to the load location. This phenomenon can also be observed for other A and B beams from different shear spans. The experimentally predicted failure location is closer to the middle section. It can be seen that only 3 out of 17 beams are predicted to fail within the observed failure zone. However, it is not possible to obtain the experimental failure location for 7 of the beams. The predicted failure zone of F11A and F4B are very close to the observed failure zone. The difference in experimentally predicted failure zone and the failure zone in Response can also be explained by the small a/d -ratios of the beams, the beams have a relatively small shear span and a large part of the force is transferred by clamping stresses. Response-2000 does not take into account these clamping stresses ($\sigma_z = 0$). These clamping stresses are the largest under the support and the load and give therefore extra capacity that is not taken into account here. It is, therefore, more likely that the beams fail in the middle.

Leonhardt:

The failure region is determined from available sketches (Leonhardt, Koch, & Rostasy, 1973) figure 8.5 and 8.6). It was possible to quite accurately determine the failure location from the sketches because the locations of crushing were highlighted.

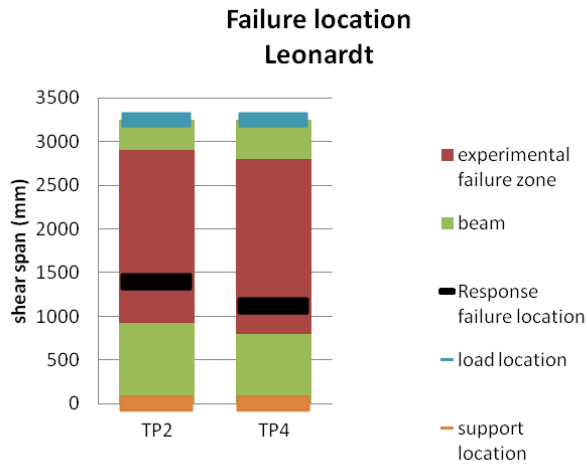


Figure 3.28, Failure location Leonhardt

The beams tested experimentally by Leonhardt (Leonhardt, Koch, & Rostasy, 1973) have a very large shear span. The failure locations predicted by Response lie towards the support but fall in the predicted failure range. The predicted failure location of TP4 lays closer to the support than that of TP2; this can be explained by the prestress which is higher for TP2 than for TP4.

From this, it can be concluded that the cross-section that gives the lowest capacity in shear tension in Response corresponds to the location where the beam fails for 61% of the analysed beams (beams, where the failure location cannot be determined, are not taken into account and LB6, LB7 and LB10 as correct).

Conclusion

When the analysis of the failure load, failure mechanism and failure location are combined it can be concluded that:

- Using the above-described definition of the critical failure location in Response the location is predicted within the experimental failure zone with an accuracy of 61%. The failure location varies over the shear span for the Response predictions as well as the experimental predictions. Most failures are predicted between d from the support/load and the middle of the shear span. It has been found that the failure location in Response is influenced by the amount of transverse reinforcement (especially low amounts) and the level of prestressing; both contribute to a higher M/V -ratio. This is explained by the definition of the failure mechanism which is defined as the cross-section with the lowest load just before cracking of the ultimate fibre.
- The failure mechanisms Rupture, major crack opening/slipping and crushing can be distinguished in Response. The failure mechanisms were predicted correctly for 87% of the

beams and an incorrect prediction was mainly an interchange of rupture of the stirrups and crushing of the concrete due to the ductility of the reinforcement. For crushing failure, multiple ways of failing were predicted in Response. For the beams of Hanson which had a low reinforcement ratio and a/d-ratio, there was not much load increase after diagonal tension cracking. While this was not the case for the other beams failing in crushing. The beams of Leonhardt are observed to be crushing before yielding of the reinforcement.

- The failure load was predicted with an average accuracy of 1.38 and a variation of 19.15%. It can be concluded that the predictions of Hanson and Choulli are most conservative (highest mean values). It can be concluded that the a/d-ratio has influence on the accuracy of the predictions as well as the reinforcement ratio. Especially, the combination of low a/d-ratio and low reinforcement ratios give conservative predictions. There is no visible influence of the prestressing force on the prediction of the shear force however, from theory beams with more prestressing should be a bit more conservative.

From this all it can be concluded that Response predicts the behaviour of beams in shear tension quite well but that for beams with a small a/d-ratio and small transverse reinforcement ratio the results are less accurate because the critical failure location is influenced as well as the failure mechanism and this gives a relative conservative failure load prediction.

3.2.2 In-depth comparison

For the in-depth comparison, the cross-section is divided into a reinforcement part and a concrete part. The concrete part consists of the cracked concrete as well as the uncracked concrete while the steel part consists of the stirrups. The graph in Figure 3.29 gives the contributions of each part from the Response analysis at the maximum shear force (V) that the beam is able to resist. The diagram for each beam can be seen in the appendix D. The blue surface shows the uncracked part, the green surface shows the reinforcement part and the red surface shows the force carried by the shear on the crack. The contribution of the flanges and web is given outside the graph. The force carried by the reinforcement and shear on the crack is given inside the graph. The shear force is defined as the area under the shear stress diagram multiplied with the width. The reinforcement shear stress is calculated with the following formula: $\tau = \frac{\sigma_{sz,cr} \cdot \rho_z}{\tan \theta}$. The concrete shear stress in the cracked zone is equal to τ_{ci} .

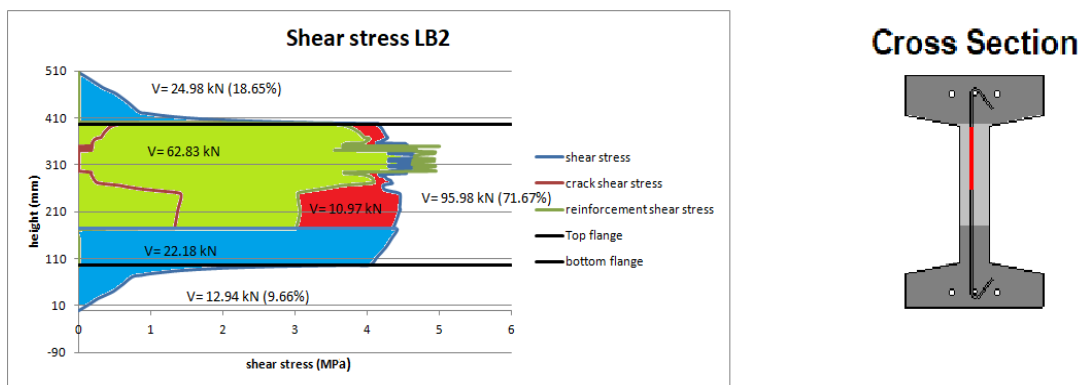


Figure 3.29, The contribution of the concrete and steel part to the shear stress over the beam

It is unfortunately not possible to determine the contributions of the steel and the concrete directly out of the experiments. This is why a comparison is made between several parameters that define

these parts. For the steel part, the most important parameters are the cracking angle, the stress in the steel and the height of the crack (uncracked height). For the concrete part, important parameters are the crack spacing and crack width for the cracked concrete and the uncracked height for the uncracked concrete. Below the comparison of these parameters is given for the beams in which these parameters are available from the experiments.

3.2.2.1 Steel component

The steel component is influenced by the angle of the crack, the stress in the steel and the height of the crack.

$$V_s = \frac{A_{sw} \cdot f_s \cdot h_{crack}}{s} \cdot \cot \theta \quad [47]$$

The cracking angle and height of the crack are connected closely and decide how many stirrups pass through the crack.

Below the predictions of Response for these parameters will be compared as well as the force in the steel calculated from Response as shown in Figure 3.29 and calculated from the experiment using equation [47].

The angle of the crack and cracking height

The angle of the crack and the height over which the crack propagates in the beam determines how many stirrups cross the crack and, therefore, how large the steel capacity is in the crack. A larger predicted cracking angle means fewer stirrups passing the crack and, therefore, less possibility to resist the shear forces (ratio <1). A smaller predicted cracking angle, on the other hand, means that there are more stirrups present in the crack and, therefore, more possibility to take up shear forces (ratio >1). But the number of stirrups in the crack also closely depends on the height of the crack. When there is a larger angle predicted but also a larger height then still the same number of stirrups crosses the crack, and so the effect of the larger angle is evened out. The same holds for a smaller angle and smaller cracking height. This is shown in Figure 3.30 where the ratio of the uncracked height and the ratio of cracking angle are plotted against each other. For every analysis, the ratio of the number of stirrups/ predicted number of stirrups is shown. It has to be noted that Response calculates the number of stirrups continuously which makes it possible to have a non-integer value. Each quadrant, separated by the 1.0 ratio line, has a different combination of the crack height and angle causing more or fewer stirrups passing the cracks, as shown in the figures at each quadrant.

The cracking angle in Response is taken as the mean angle over the entire cracked height at the shear force V . The experimental values of the angle are reported in the reports (Xie, 2009) paragraph 4.6, (Leonhardt, Koch, & Rostasy, 1973) paragraph 8.3.1) or are measured in the pictures of the crack pattern (Choulli, 2005) figures A.33, A.44, A.65, A.76, A.87, A.98 and A.109, (Hanson & Hulbos, 1965) figures 14 to 17, 20 and 21).

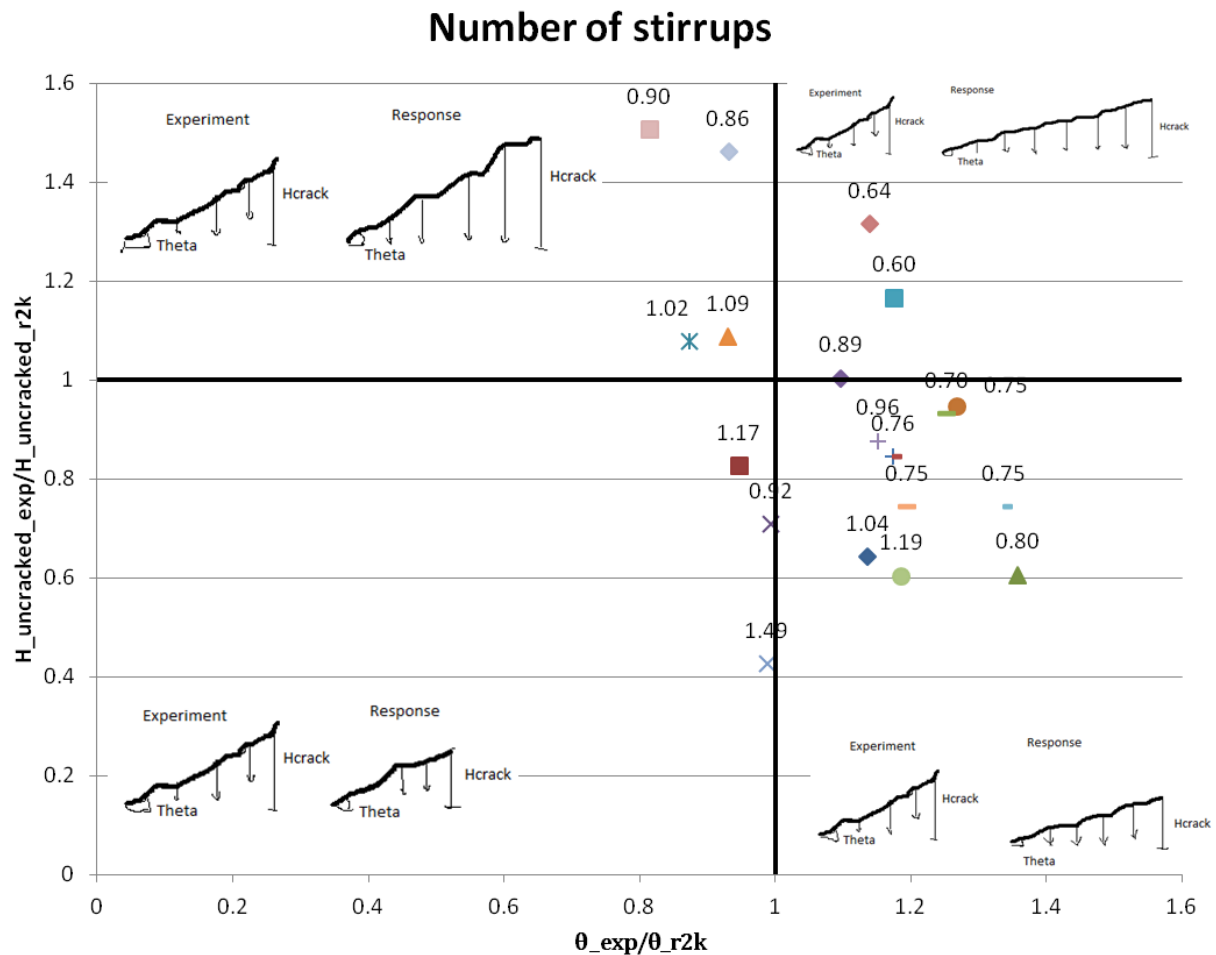


Figure 3.30, The relation between the parameters influencing the number of stirrups through the crack

From Figure 3.30 it can be seen that for the most beams the ratio of $\theta_{exp}/\theta_{r2k}$ is bigger than 1 (mean of 1.08 and COV of 14%). The ratio of $H_{uncracked,exp}/H_{uncracked,r2k}$ for most beams is smaller than 1 (mean of 0.95 COV of 31%). This causes most predictions to lie in the 4th quadrant meaning Response predicts a smaller cracked height and a smaller angle causing more stirrups to be effective in the crack.

3.2.2.2 Stress in the steel

The predicted stress in the steel is in direct relation with the predicted number of stirrups through the crack. When more stirrups go through the crack the stress in the stirrups will be smaller for the same load and vice versa. From the previous paragraph, it is concluded that Response predicts generally more stirrups in the crack due to smaller angle and lower cracked height.

For Response-2000 the maximum value of the stirrup stress on the crack ($\sigma_{sz,cr}$) is taken, because this is governing for deformation and failure. For the experiments, it was only possible to determine the stirrup stress for Xie and Leonhardt. This is done in the following ways:

Xie: the maximum stirrup strain is obtained from the diagrams in figure 4.61 and 4.62 of (Xie, 2009) (this strain is measured in the middle of the cross-section height) and calculated into stress using the stress-strain diagram of the stirrups. The strain is measured at the load stage just before failure and

then linearly interpolated to the failure load. For beams where rupture of the stirrups was reported the stress is taken as f_u .

Leonhardt: The stirrup stresses are defined as the maximum stirrup stress in the beam, reported in the diagrams in figures 8.14 and 8.16 of (Leonhardt, Koch, & Rostasy, 1973).

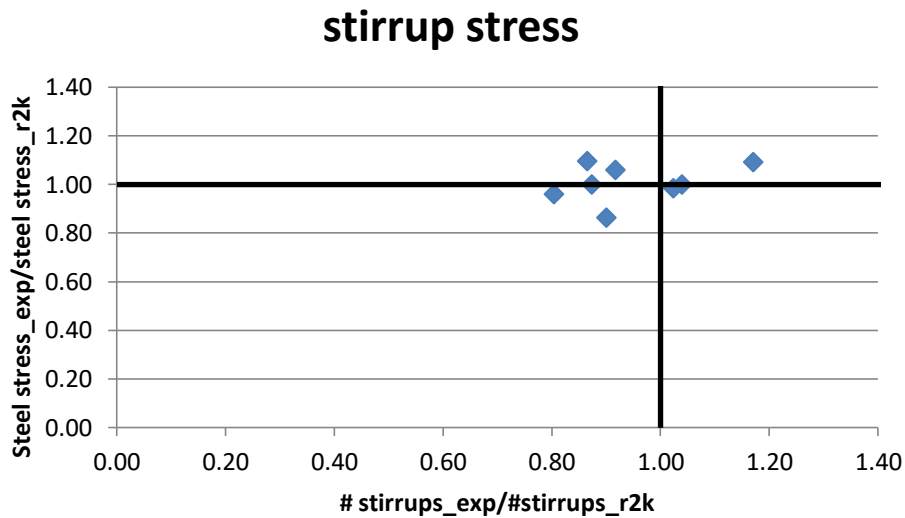


Figure 3.31, Prediction of the stirrup stress and number of stirrups

Figure 3.31 shows that the stress in the steel is predicted with high accuracy (mean of 1.01 with an accuracy of 8%). It can be seen that if the number of stirrups is overpredicted the steel stress in a few cases is lower, as expected because there are more stirrups to take up the force. This is, however, not the case for all predictions which has an influence on the overall prediction of the force in the steel, which will be slightly higher than in the experiments.

3.2.2.3 Steel force

The prediction of the steel force (only calculated for Xie and Leonhardt) which is depended on the parameters above has a mean ratio of 0.996 with a variability of 15%. This is a very good prediction and the variability can mainly be declared by the overprediction of the number of stirrups in the crack caused by the prediction of a too small angle in combination with a small crack height (big uncracked height) and the underprediction of the steel stress.

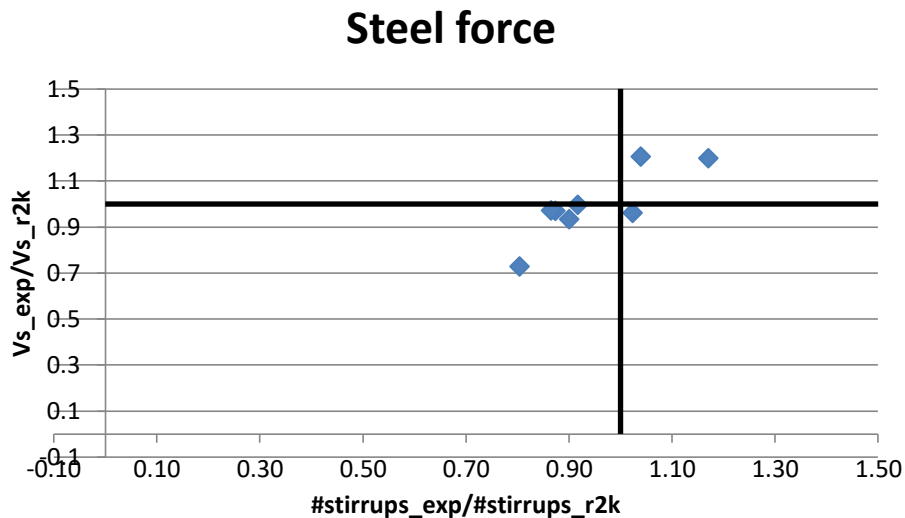


Figure 3.32, The relation between the prediction of the steel force and the prediction of the number of stirrups

3.2.2.4 Concrete component

The concrete component consists of the force carried by the uncracked concrete and the force carried by the shear on the crack (due to aggregate interlock). Both of these forces are not directly measurable in an experiment and can, therefore, not be compared. It is, however, possible to compare parameters that relate to the forces. The aggregate interlock component is dependent on the crack width. Larger cracks widths mean less force transmission in the cracks. The crack width is influenced by the crack spacing so it is useful to compare this. The uncracked height gives information about which part of the cross-section is not cracked and therefore is able to resist more shear.

3.2.2.5 Crack width and crack spacing

The crack width has a direct influence on the shear on the crack as a bigger crack width causes less aggregate interlock (if the maximum shear on the crack is already governing) and therefore the shear stress that can be transferred by the crack is less than for a smaller crack width.

The crack width in Response is taken as the average crack width over the height of the crack at the maximum load (V). From Response, it appears that there is much variation in the crack width which means that generally there is more force taken by the shear on the crack than suggested by the average crack width over the height of the crack. For the experiments also the average crack width over the height of the governing is taken ((Xie, 2009) figures 4.35, 4.36, 4.39 to 4.41 and 4.43, (Leonhardt, Koch, & Rostasy, 1973) table 8.3). It is unfortunately only possible to obtain the crack widths for the experiments of Xie and Leonhardt. Therefore, the crack spacing which indirectly can be related to the crack width is also compared. When the crack spacing is small there will be more cracks which lead to smaller crack widths because the deformation is divided over multiple cracks and therefore there is more aggregate interlock. While at a large crack spacing there are fewer cracks and the deformation localizes in the cracks causing larger crack widths and less aggregate interlock.

The crack spacing is taken as the mean value of the diagonal crack spacing at the maximum shear force in Response. For the experiments the diagonal crack spacing is measured from the available figures ((Xie, 2009) figures 4.35, 4.36, 4.39 to 4.41 and 4.43, (Choulli, 2005) figures A.33, A.44, A.65,

A.76, A.87, A.98 and A.109), (Hanson & Hulbos, 1965) figures 14 to 17, 20 and 21, (Leonhardt, Koch, & Rostasy, 1973) figure 8.5 and 8.6). The average values are taken as the crack spacing.

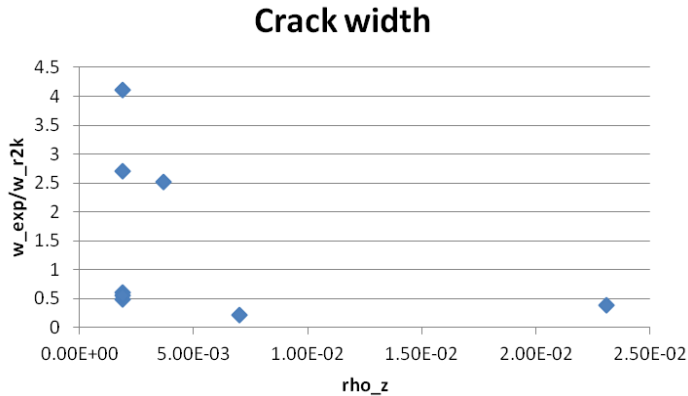


Figure 3.33, Crack width prediction

In Figure 3.33 it can be seen that for a few beams the crack width is underestimated (ratio>1), these are beams LB3, LB6 and LB10, while for the other beams the crack width is overestimated. The underestimation can be explained by the failure mechanism major crack opening. The maximum load is reached at a small crack width and after this, the crack width increases rapidly while the force stays approximately the same (Figure 3.34). During the experiment, the crack width at the end is measured which makes the crack width prediction at the maximum load conservative. When compared with the load stage before failure these crack widths the crack widths already are less conservative.

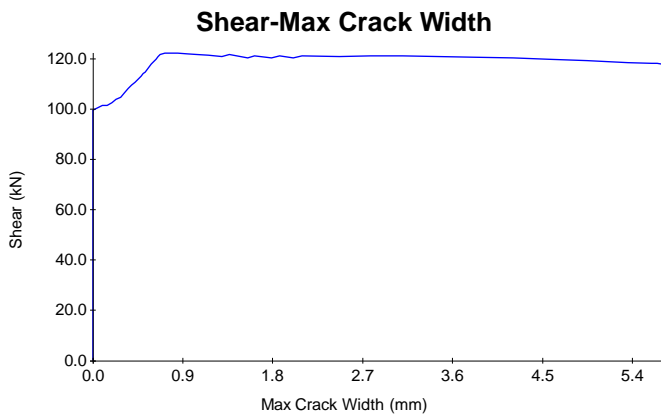


Figure 3.34, Crack width major crack opening (LB3)

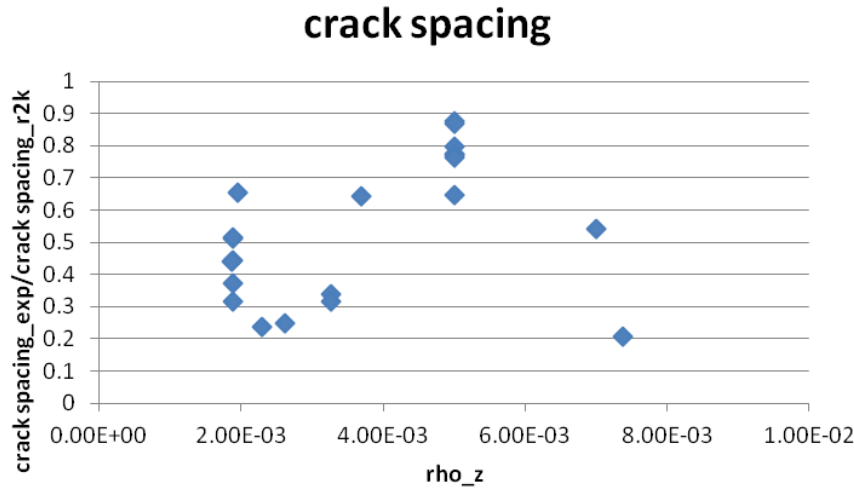


Figure 3.35, Crack spacing prediction

Figure 3.35 shows that the crack spacing is overestimated in Response (mean ratio of 0.53 with a COV of 42%). It shows, however, that for larger reinforcement ratios the results become closer to one. This can be explained by the crack spacing formulas which depend on the ρ_z . The prediction of a larger crack spacing means a larger crack width. This was also observed from Figure 3.33 with exception of LB3, LB6 and LB10 which are conservative and therefore contradict with the conclusion of the crack spacing which predicts larger crack widths. As the cause of these conservative predictions is shown in Figure 3.34, the predictions of the aggregate interlock are conservative based on the crack spacing because larger crack widths mean less aggregate interlock and therefore less shear force carried by the interlock in the crack.

3.2.2.6 Uncracked height

The uncracked concrete carries also a part of the load. For failures in shear tension, the flanges are uncracked and sometimes also a part of the web is uncracked. The ratio of uncracked height is an important parameter to compare because it explains how the forces are divided between concrete and steel. When the ratio is below 1 the experiment has a smaller uncracked part and therefore a larger cracked part which means the steel component has to resist more force.

To be able to compare the uncracked height of the cross-section for various heights, the percentage of the cross-section that is uncracked will be compared. This is obtained in response as the height where the crack width is zero. For the experiments the uncracked height is measured in the figures with the crack patterns ((Xie, 2009) figures 4.35, 4.36, 4.39 to 4.41 and 4.43, (Choulli, 2005) figures A.33, A.44, A.65, A.76, A.87, A.98 and A.109), (Hanson & Hulbos, 1965) figures 14 to 17, 20 and 21, (Leonhardt, Koch, & Rostasy, 1973) figure 8.5 and 8.6).

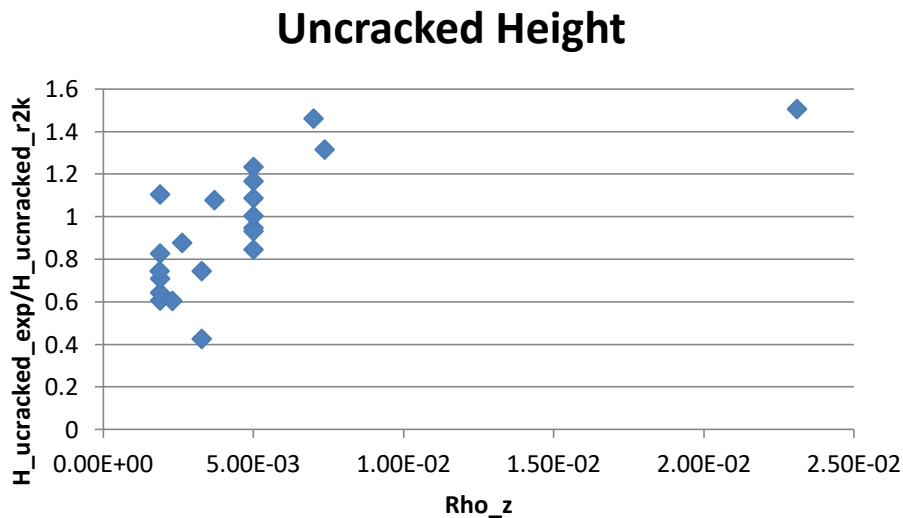


Figure 3.36, Prediction uncracked height

It is shown in Figure 3.36 that the uncracked height is overestimated for low transverse reinforcement ratios while it is underestimated for higher reinforcement ratios. Low reinforcement ratios mean that the steel has a small capacity so in these beams will reach the capacity before the cross-section is cracked over the whole web, causing large uncracked heights. In the experiments, the crack almost immediately propagates over the whole height of the web. This leads to an overestimation of the uncracked height for low reinforcement ratios. As mentioned before the uncracked height is predicted with a mean value is mean of 0.95 and a COV of 31%. An overestimation of the uncracked height means that the uncracked concrete takes up more force than in the experiment and that less force is taken up by the aggregate interlock. An underestimation of the uncracked height for higher reinforcement ratios means that more force is taken up by the aggregate interlock in the crack and less by the uncracked zone.

Conclusion

It can be concluded that the concrete aggregate interlock component is underestimated in Response for low reinforcement percentages due to overestimation of the crack spacing and, therefore, the crack width and due to underestimation of the crack height (overestimation of the uncracked height). For higher reinforcement percentages the overestimation of the crack spacing is smaller and the uncracked height is underestimated, this leads to a slight overestimation of the aggregate interlock. The contribution of the uncracked height is overestimated by Response for low transverse reinforcement percentages due to an overestimation of the uncracked height while for higher reinforcement percentages the uncracked height is underestimated which leads to an underestimation of the contribution of the uncracked height.

3.2.2.7 Contribution of Parts in Response

From the graphs in appendix D, the contribution of the steel and concrete part to the shear force in Response can be determined. This is shown in Figure 3.37.

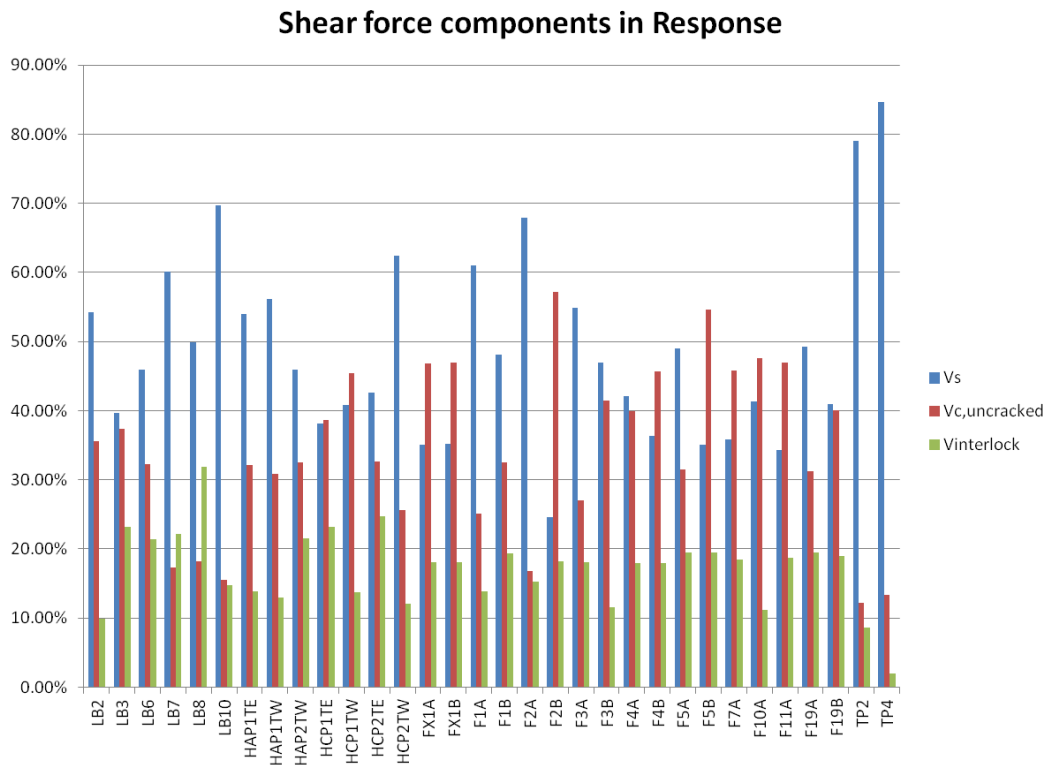


Figure 3.37, Contribution of the different components in Response

Figure 3.37 shows that the steel component takes up the most shear force for most beams (mean of 48.79%) It can also be seen that the interlock component is mostly the smallest component (mean of 17.19%). The remaining shear force is taken up by the uncracked concrete (mean of 34.29%). For TP2 and TP4 the contribution of the steel component is very high. This is because the uncracked height is very small and the stirrups have enough capacity to take up most of the shear force in the crack. For beams HCP1TE, HCP1TW, FX1A, FX1B, F2B, F4B, F7A, F10A and F11A the uncracked concrete has the largest contribution. This can be explained by the very large uncracked height which is nearly 60% for all these beams.

Conclusion

From the in-depth analysis of the beams was found that the steel component is predicted with an average accuracy of 0.996 with a variation of 15%. Response predicts generally more stirrups to be activated through the crack caused by a small underestimation of the angle and an overestimation of the uncracked height (lower cracked height). The steel stress is in direct relation with the number of stirrups and is predicted with an average accuracy of 1.01 and a variation of 7%. The concrete aggregate interlock in the crack is underestimated due to an overestimation of the crack spacing causing fewer cracks and larger crack widths. Also, the overestimation of the uncracked height causes the aggregate interlock component to be underestimated and the shear force taken up by the uncracked part to be overestimated compared to the experiments. From the division of the contributions in Response-2000, it can be concluded that the steel component takes up the greater part of the in the critical cross-section. For beams that were concluded to be predicted very conservative in the general analysis (small ρ_z and small a/d -ratio) the largest part of the force will be taken up by the uncracked concrete because of the low cracked height.

4 Shear tension model

To derive an accurate model for shear tension failure based on the MCFT both the CSA-model and Response are used. The CSA-model is a simplified version of the MCFT and describes general shear behaviour instead of making a difference between flexural shear and shear tension failure. This model gives a solid basis for an analytical shear tension model but has to be modified to make it suitable for solely shear tension. Response-2000, on the other hand, gives a deeper insight into the different parameters of the MCFT and their profile over the cross-section. With the result from the Response-2000 analysis for experiments failing in shear tension enough information about the parameters of the MCFT in shear tension failure is gained. Response-2000 will, therefore, be used as a basis to modify the CSA-model into a model for shear tension failure.

It appears that Response (mean of 1.38 with COV of 19%) is a bit more conservative than the current CSA-model (mean 1.30 with COV of 17%). However, it is still opted to use Response to modify the CSA-model because Response gives a good insight in all parameters and is more sophisticated in comparison to the CSA-model. To identify the parameters which have to be modified for shear tension failure the results of both the CSA-model and Response are compared.

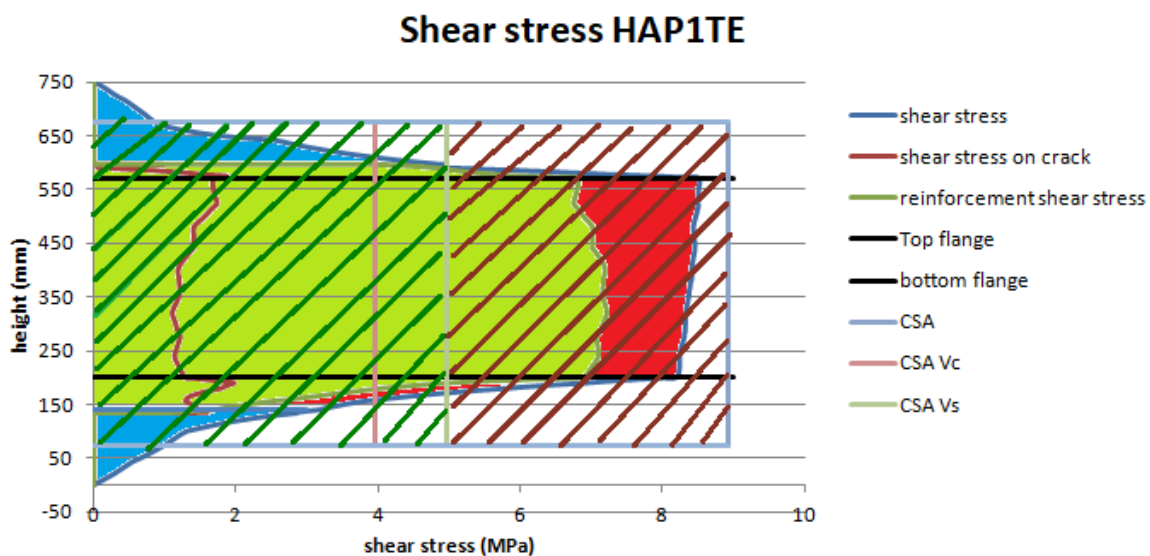


Figure 4.1, Response (coloured) and CSA (shaded) shear stress HAP1TE

When laying the results of both models (Response and CSA) over each other, see Figure 4.1, it is shown that:

- The contribution of the concrete aggregate interlock component is bigger than that of the aggregate interlock component in Response. This can be caused by the following factors:
 - The β -value in the CSA-model is overestimated for low values of ϵ_x (see Figure 2.9, presenting the beta in the CSA-model)
 - In the CSA-model a constant aggregate interlock is taken over a depth z , the cracked height is generally lower.

- The aggregate interlock in the CSA-model is always taken as the maximum V_c (Bentz, Vecchio, & Collins, Simplified Modified Compression Field Theory for Calculating Shear Strength of Reinforced Concrete Elements, 2006) while in Response the V_c will be lower for crushing failure because of the extra rotation of the cracking angle.
- The contribution of the steel component in the CSA-model is smaller than in Response. This can be caused by the following factors:
 - The θ -value is overestimated for low values of ϵ_x (see Figure 2.9, presenting the theta in the CSA-model).
 - The contribution is taken over the whole height z which is larger than the cracked height, causing another number of stirrups to pass through the crack. This leads to a different steel component contribution.

Other differences between Response and the CSA-model are:

- The longitudinal strain in the CSA-model is taken as $\frac{\epsilon_t}{2}$, while from the Response results it turns out that most of the cross-section is in compression and that for the governing cross-section the strain on the tensile side is close to zero because the cross-section is not cracked in the flanges. This means the longitudinal strain at mid-depth is a small negative value for shear tension failure.
- The CSA-model only distinguishes yielding of the stirrups and crushing before yielding as the failure mechanisms while Response distinguishes more mechanisms for shear tension failure.
- The CSA-model assumes no influence of the aggregate size and the crack spacing on the interlock. The aggregate size is always chosen as 20 mm and the cracks spacing is 300 mm. Response, however, has variable crack spacing and takes the aggregate size into account.
- Response takes into account the contribution of the uncracked parts, while the CSA-model only takes the cracked parts into account.

From this comparison it can be concluded that the following parameters need to be analyzed to come to an appropriate model for shear tension failure:

- Failure mechanisms.
- Cracked height.
- Contribution of the uncracked zone.
- β -value for small values of longitudinal strain.
- θ -value for small values of longitudinal strain.
- Longitudinal strain.

Next, these parameters will be analyzed based on the Response results and an alternative for shear tension will be proposed. This leads to a model for shear tension failure.

4.1 Failure mechanisms

The current CSA-model distinguishes only two failure mechanisms namely:

- Failure at yielding of the transverse reinforcement.
- Crushing of the web concrete before yielding of the transverse reinforcement.

However, from the Response data, other failure mechanisms have been distinguished. As described in chapter 3.2.1.2, the following failure mechanisms have been found:

- Crushing after yielding
- Rupture of the stirrups
- Slipping/major crack opening
- Crushing before yielding

Esfandiari presents the following division in failure mechanisms in the paper shear strength evaluation of concrete bridge girders (Esfandiari & Adebar, 2009):

- Yielding of the transverse reinforcement.
- Crushing of the web concrete after yielding of the transverse reinforcement.
- Crushing of the web concrete before yielding of the transverse reinforcement.

In the Response analysis yielding of the transverse reinforcement (average steel stress equals the yielding stress) is not considered a failure mechanism, because as opposed to the CSA-model the reinforcement is able to take up force after yielding. In the experiments yielding of the reinforcement will also not be distinguished as a failure mechanism because this is not visible in the experiment unless the strain in the reinforcement is measured and the yielding will trigger another failure mechanism which occurs soon after. So when the maximum load is reached at yielding in Response the strains increase quickly and just after the maximum load the beam fails in either crushing or rupture of the transverse reinforcement, which is then taken as the failure mechanism.

However, the failure mechanisms defined in Response differ from the division made by (Esfandiari & Adebar, 2009). The division of Esfandiari is appropriate because two distinct load responses can be defined in Response independent of the defined failure mechanism. The first has its maximum capacity at first yielding of the transverse reinforcement. The second is able to increase after yielding of the transverse reinforcement. This is in agreement with the proposed division and leads to more rotation of the cracking angle and opening of the cracks (smaller θ and smaller β) for beams where the capacity is not reached at reinforcement yielding. Figure 4.2 gives examples of the MCFT stress-strain diagram for various reinforcement ratios. The failure mechanisms: yielding of the transverse reinforcement and crushing after yielding can clearly be distinguished. Figure 4.2 also gives a third failure mechanism namely yielding of both the transverse and longitudinal reinforcement, this failure mechanism is not taken into account for shear tension failure because the longitudinal strains in the reinforcement stay small because the flanges are uncracked. This makes yielding of the longitudinal reinforcement unlikely for this kind of failure.

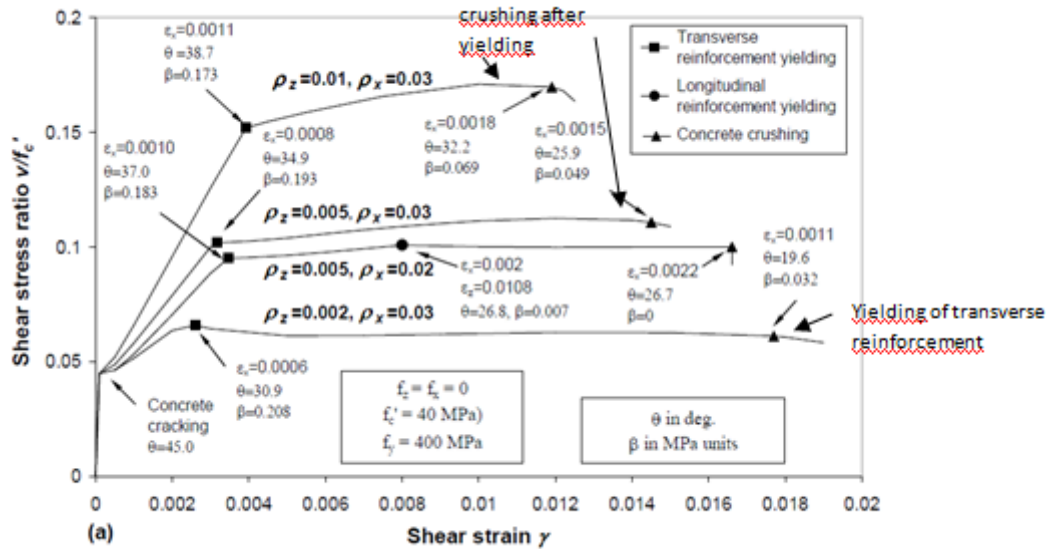


Figure 4.2, MCFT load Response different failure mechanisms (Esfandiari & Adebar, 2009)

Table 4.1 shows the division of failure mechanisms made based on the Response results. This division depends on the $\frac{\rho_z f_y}{f_c}$ of the beams. Beams with a low $\frac{\rho_z f_y}{f_c}$ values are sorted at yielding of the transverse reinforcement, while beams with higher $\frac{\rho_z f_y}{f_c}$ values are sorted as crushing after yielding.

Failure mechanism	Experiments
Yielding of the transverse reinforcement	LB3, LB8, HAP1TE, HCP2TE, F1A, F3A, F4B, F11A
Crushing after yielding	LB2, LB6, LB7, LB10, HAP1TW, HAP2TW, HCP1TE, HCP1TW, HCP2TW, FX1A, FX1B, F1B, F2A, F2B, F3B, F4A, F5A, F5B, F7A, F10A, 19A, 19B
Crushing before yielding	TP2, TP4

Table 4.1, Division of the failure mechanisms

4.2 Cracked height

In the CSA-model the shear stress, aggregate interlock and cracking angle are considered to be constant over a depth z because only one biaxial element is taken over the depth z and it is assumed that these values are represented by the mid-depth of the cross-section. This is a good approximation for flexural shear failure because a large part of the flange is cracked. For shear tension however, the flanges are mostly uncracked meaning the depth z would be too large. From Response it can be seen that there is a considerable variation over depth z for multiple parameters:

- The width is not constant over the whole z, because the height z covers the part of the flanges and the web (Figure 4.3).

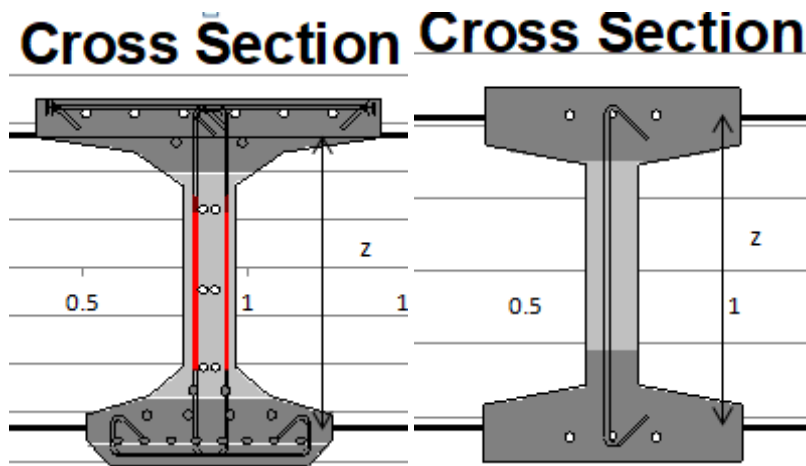


Figure 4.3, Cross-section HAP1TW (left) and LB3 (right)

- The cross-section is not cracked over the whole z (Figure 4.3).
- The shear stress is not constant over the whole z , in the flanges the stress goes to zero (Figure 4.4).

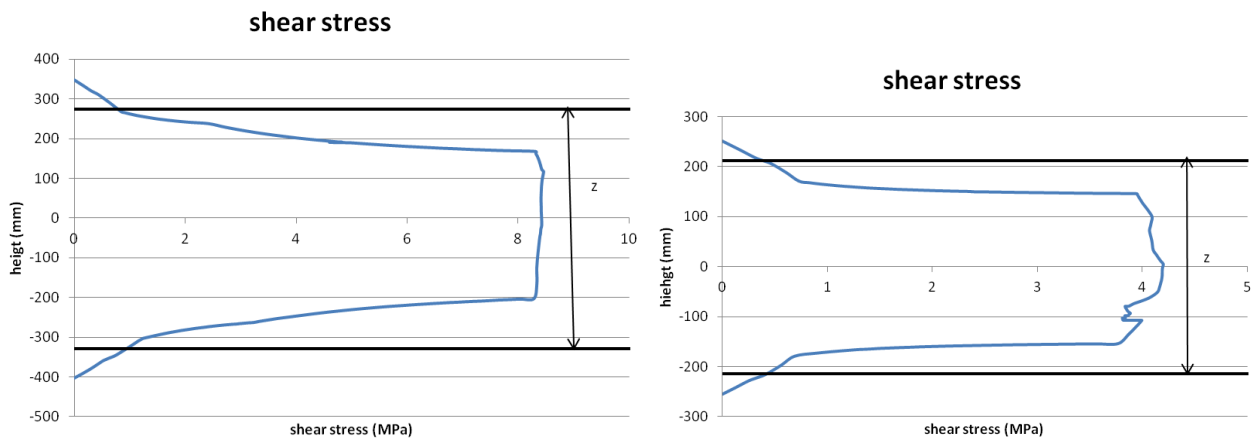


Figure 4.4, Shear stress HAP1TW (left) and LB3 (right)

- The cracking angle deviates over the z (Figure 4.5).

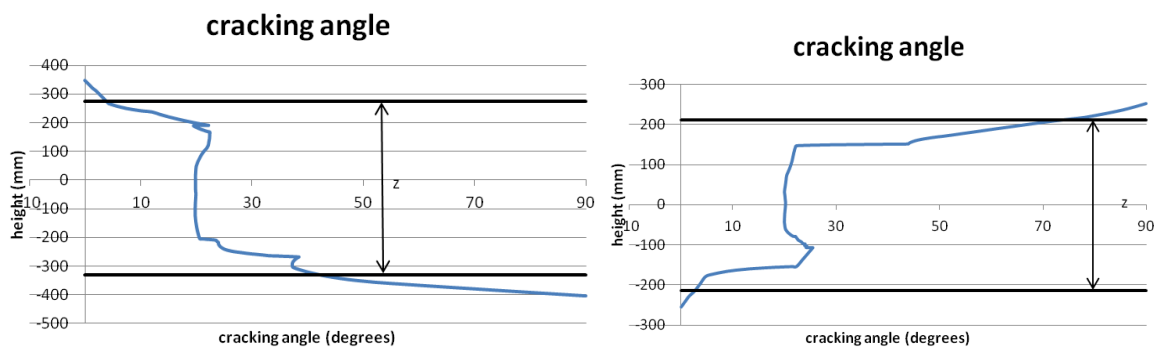


Figure 4.5, Cracking angle HAP1TW (left) and LB3 (right)

- The shear on the crack deviates over the z , for the parts where the cross-section is not cracked it is zero (Figure 4.6).

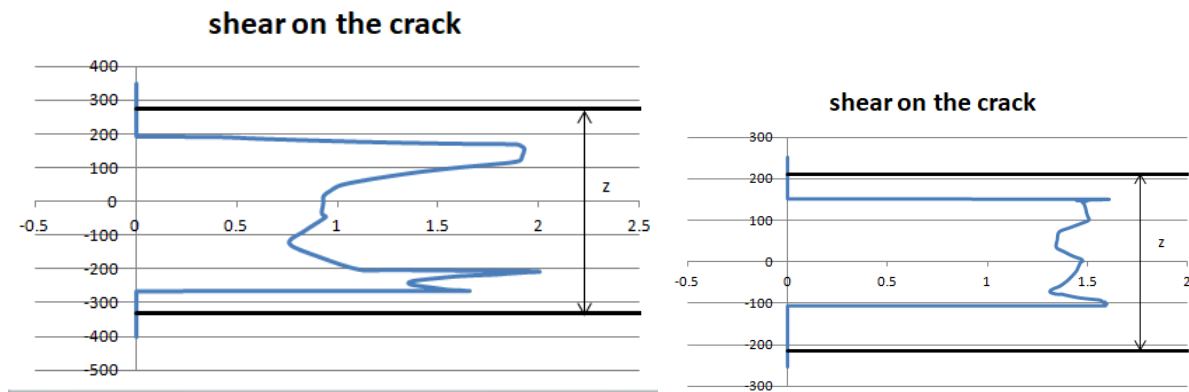


Figure 4.6, Shear on the crack HAP1TW (Left) and LB3 (right)

Considering the deviations over z for the above-stated parameters presenting the whole height z by the mid-depth value will lead to:

- To large shear stresses at the upper and lower part of z (due to a too small width, Figure 4.3 and Figure 4.4).
- Too small or too large angles in the upper and lower parts of z (Figure 4.5).
- An overestimation of the shear on the crack because part of the height z is not cracked (Figure 4.3 and Figure 4.6).
- An overestimation of the cracked part (Figure 4.3).

From Figure 4.3 to Figure 4.6 it is concluded that:

- The cracked part is mainly in the web (flanges are mainly uncracked).
- The value at mid depth is representative for the values over the web height (b_w , shear stress, angle).
- For the shear on the crack the mean value over the web height has to be taken at mid-depth.

This leads to the conclusion that h_{web} is a good height for the cracked zone and that the value at mid-depth is representative over this height. For cross-sections with a smaller cracking height in Response the values of the shear stress will be a bit overestimated while for cross-sections with a higher cracking height the values will be a bit underestimated. However, all values of h_{crack} in Response are smaller than z .

4.3 Uncracked zone

The CSA-model takes only the contribution of the cracked part into account by taking the contribution of the steel and the aggregate interlock of the cracked concrete. This is a good approximation for beams failing in flexural shear because most of the cross-section is cracked. From the Response results, it can, however, be concluded that for shear tension failure a large part of the cross-section is uncracked at failure. These uncracked parts of the cross-section are able to resist part of the shear force. From the Response analysis, it is obtained that the uncracked parts resist about 1/3 of the ultimate shear force. This is a significant amount of extra capacity which is currently not included in the CSA-model. As pointed out above a good approximation of the cracked zone is the height of the web, this means a good approximation of the uncracked part, are the flanges. It is, therefore, proposed to include the contribution of the uncracked flanges in the new expression for shear tension.

The contribution of the uncracked flanges is determined with the help of Response. As a first approximation, it is chosen to use the linear elastic shear stress distribution, defined by $\tau = \frac{V \cdot S}{I \cdot b}$, to calculate the shear stress in the points where the width in the cross-section changes. Combined with a linear gradient between these points the linear elastic shear stress distribution is found. In Figure 4.7 and Figure 4.8 this distribution is plotted over the shear stress distribution obtained from Response. It can be seen that for both cases the linear approximation of the shear stress in the flanges is very close to that of Response. This means that the linear elastic shear stress distribution is suitable to describe the shear stress in the flanges.

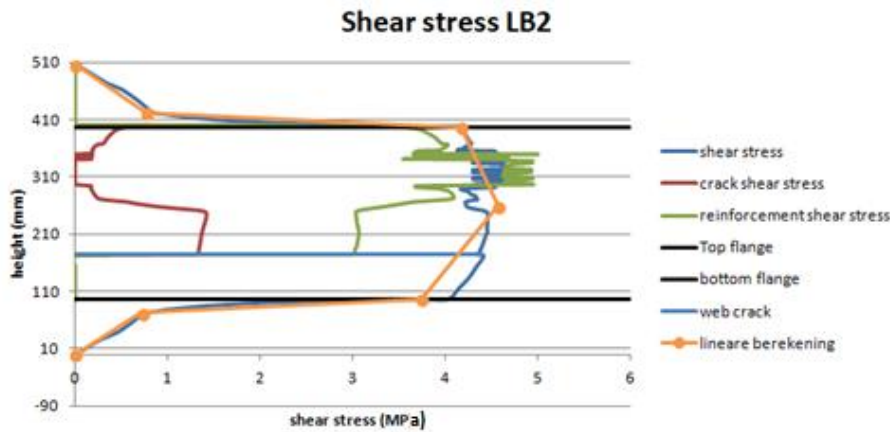


Figure 4.7, Shear stress LB2 comparison with the linear elastic calculation

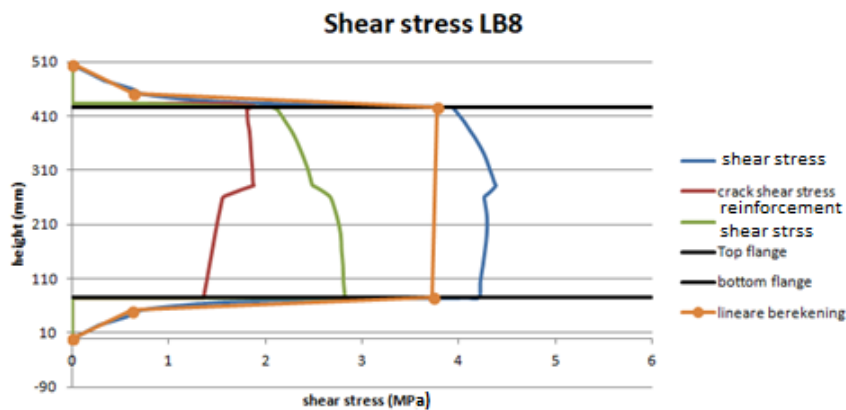


Figure 4.8, Shear stress LB8 in comparison with the linear elastic calculation

The contributions of the flanges as part of the total shear force ($\phi_{uncracked}$) can be calculated with formula [48].

$$\phi_{uncracked} = \frac{V_{topflange} + V_{bottomflange}}{V_{tot}} \quad [48]$$

The shear forces needed for this ($V_{topflange}$, $V_{bottomflange}$, V_{tot}) are calculated from the linear distribution calculated with $\tau = \frac{V \cdot S}{I \cdot b}$. This expression can be rearranged to $\tau \cdot b = S \cdot \left(\frac{V}{I}\right)$. $\frac{V}{I}$ is constant over the whole cross-section and will therefore not influence the ratio of the shear force in the flanges and the web. Calculating the first moment of area (S), at the points of the cross-

section where the width changes, gives the distribution of $\tau \times b$ over the height of the cross-section as shown in Figure 4.9. Integrating this distribution over the height gives the shear force (stress times area), as expressed in expression [49].

$$V = \sum \left(\frac{\tau_i \cdot b_i + \tau_{i+1} \cdot b_{i+1}}{2} \cdot \Delta h \right) \quad [49]$$

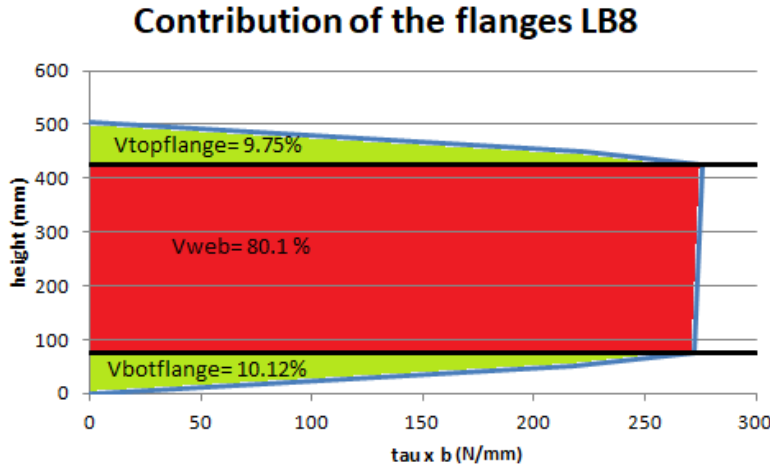


Figure 4.9, Tau x b distribution

With this shear forces, the factor $\phi_{uncracked}$ can be calculated. The total shear force is then the shear force in the web, a combination of the steel (V_s) and aggregate interlock (V_c), increased with a percentage to cover the contribution of the flanges.

$$V = \frac{1}{1 - \phi_{uncracked}} \cdot (V_c + V_s) \quad [50]$$

It is recommended to calculate $\phi_{uncracked}$ using excel because of the variations in width and the differences in every cross-section.

Analytical expression

An analytical expression to calculate $\phi_{uncracked}$ is derived based on a cross-section with straight flanges. This means the shear force of the top flange, bottom flange and web are able to be expressed in a single expression. $c = \frac{V}{I}$

$$V_{topflange} = h_{top} \cdot \frac{S_{top}}{2} \cdot c \quad [51]$$

$$V_{bottomflange} = h_{bot} \cdot \frac{S_{bot}}{2} \cdot c \quad [52]$$

$$V_{web} = h_{web} \cdot \frac{S_{bot} + S_{top}}{2} \cdot c \quad [53]$$

$$\phi_{uncracked} = \frac{V_{topflange} + V_{bottomflange}}{V_{tot}} \quad [54]$$

When simplifying these expressions the following formula for $\phi_{uncracked}$ is found:

$$\phi_{uncracked} = \frac{h_{bot} \cdot A + h_{top} \cdot B}{A \cdot (h_{bot} + h_{web}) + B \cdot (h_{top} + h_{web})} \quad [55]$$

$$A = h_{bot} \cdot b_{bot} \cdot (h_{bot} - 2 \cdot z_{bot})$$

$$B = h_{top} \cdot b_{top} \cdot (h_{top} - 2 \cdot z_{top})$$

For beams that have sloped flanges with variable width, this formula, which only takes the S at the flange-web junction, is less appropriate. Figure 4.10 shows the shear stress distribution for LB2, which has inclined flanges, for the excel calculation and the analytical formula. Using the analytical formula for beams with sloped flanges, the height of the flange (h_{top} , h_{bot}) is taken as the total height of the flange including the sloped height. The width (b_{top} , b_{bot}) is taken as the maximum width of the flange. This approximation leads to a higher value of $\tau \times b$ at the flange-web junction (see Figure 4.10), due to a bigger area and a shift of the centre of gravity of the flange. This compensates for the lost area caused by calculating the shear force as a triangle and not considering the change in slope due to the change in width. This means the shear force taken up by the flanges is approximately the same as calculated by Excel. However, the overestimation of $\tau \times b$ at the flange-web junction causes the shear force of the web to be larger (area under the graph is bigger than for the excel calculation). This means the ratio between the shear force in the flanges and the web is altered. To compensate for the overestimation of $\tau \times b$ at the flange-web junction the height of the web needs to be modified to get the same shear force (area) as for the excel calculation. It is proposed to lower the web height with 1/3 of the total height in which the width in the flanges deviates (both top and bottom flange).

$$h_{web} = h_{web} - \frac{1}{3} \cdot h_{skew} \quad [56]$$

Analytical shear stress distribution

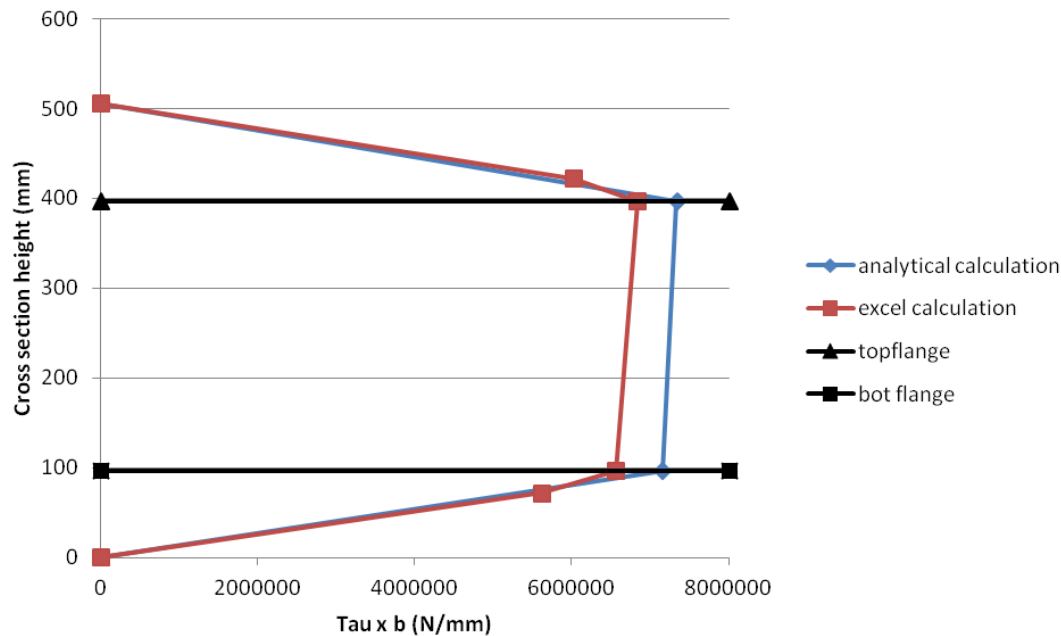


Figure 4.10, Comparison shear stress distribution LB2

Table 4.2 shows the percentages of the total shear force that are taken up by the uncracked flanges, for Response-2000, the excel calculation and the analytical expression. It can be seen that the excel calculations of the contribution of the uncracked flange resemble the contribution of the flanges in Response (mean ratio of 1.03 with COV of 3%). The analytical formula lies also close to the Response-2000 values but slightly underestimates the contribution of the uncracked parts which makes the formula conservative (mean ratio of 1.05 with a COV of 2%).

	Response-2000	Excel	Analytical
Xie LB2-LB3	27.89%	27%	26.7%
Xie LB6-LB7-LB10	20.18%	20%	18.96%
Xie LB8	19.43 %	19.88%	18.76%
Choulli	41.31%	39.6%	38.79%
Hanson	44.46%	42%	43%
Leonhardt TP2	20.65%	20%	20%
Leonhardt TP4	23.78%	22%	22%

Table 4.2, Accuracy of the uncracked flange contribution

4.4 θ

The θ in the CSA-model is defined as $\theta = 29 + 7000\epsilon_x$. As shown in Figure 2.9 this expression gives too high values for θ for low values of ϵ_x and low transverse reinforcement percentages. This makes for an overestimation of θ compared to Response (average ratio of 0.69 and COV 11.26%). In the paper shear strength evaluation of concrete bridge girders (Esfandiari & Adebar, 2009) an alternative formula for θ is presented namely:

$$\theta = \theta_0 + \Delta\theta \cdot \epsilon_x \quad [57]$$

Where at yielding of the transverse reinforcement:

$$\theta_0 = \left(85 \cdot \frac{\rho_z \cdot f_y}{f_c} + 19.3 \right) (-50\epsilon_y + 1.1) \quad [58]$$

$$\Delta\theta = 1000[37.5(-200\epsilon_y + 1.4) - \theta_0] \quad [59]$$

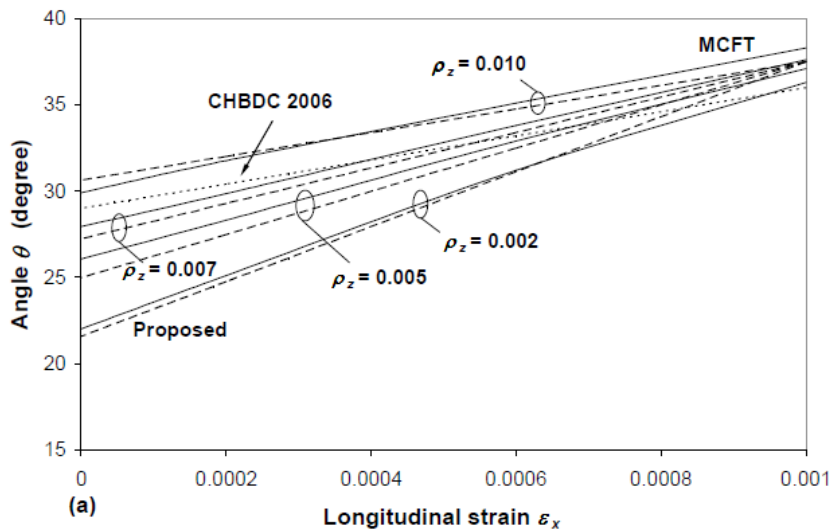
$$\epsilon_y \leq 0.002 \quad [60]$$

and at crushing of the web concrete:

$$\theta_0 = 119 \cdot \frac{\rho_z \cdot f_y}{f_c} + 15.6 \quad [61]$$

$$\Delta\theta = 15000 \cdot \frac{\rho_z \cdot f_y}{f_c} + 2000 \quad [62]$$

Opposed to the CSA expressions these formulas depend not only on the longitudinal strain but also on the reinforcement and concrete strength. As shown in Figure 4.11 these expressions lie much closer to the MCFT predictions than that of the CSA-model, however, they still deviate a bit for low values of ϵ_x and higher reinforcement ratios. These formulas compared with the theta found in Response gives a mean ratio of 1.05 with a COV of 7% for transverse reinforcement yielding and a mean ratio of 1.05 with a COV of 6% for concrete crushing after yielding.



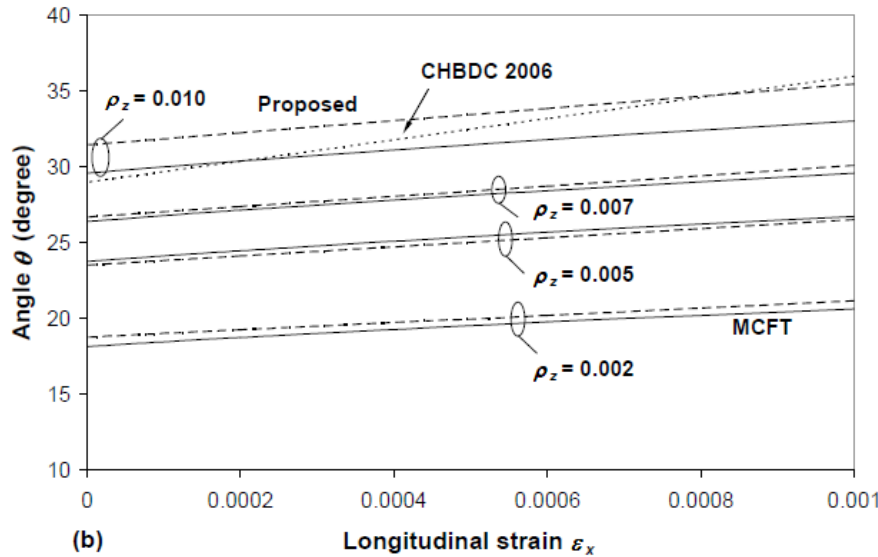


Figure 4.11, Comparison of predicted angle θ with MCFT result at: (a) yielding of transverse reinforcement (b) crushing of concrete for $f_c = 30$ MPa, $f_y = 400$ MPa. (Esfandiari & Adebar, 2009)

Figure 4.12 and Figure 4.13 show a comparison between the angle predicted by Response, the angle predicted by the expression proposed by Esfandiari (Esfandiari & Adebar, 2009) and the angle predicted by the CSA-model. It can be seen that the angles predicted by Esfandiari and Response are very close however the angle of the paper is a bit underestimated for these cases which results in an overestimation of the force carried by the reinforcement. The CSA-model is not close to the Response values and overestimates the angle.

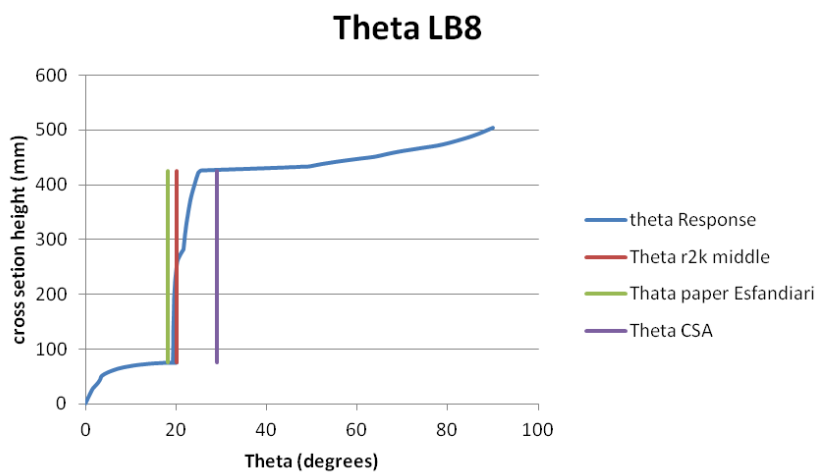


Figure 4.12, Comparison of Theta for LB8: yielding failure, $f_y = 529$, $f_c = 63.5$, $\rho_z = 1.89e-3$

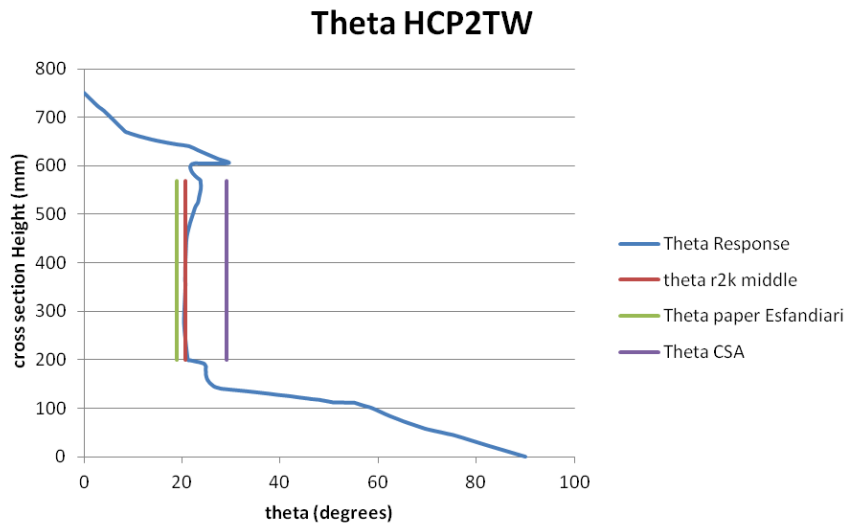


Figure 4.13, Comparison of theta for HCP2TW: crushing failure, $f_y= 525$, $f_c= 90.20$, $\rho_z= 5e-3$

4.4.1 θ -value yielding

Figure 4.11A shows that the value for θ_0 for yielding (θ at $\epsilon_x = 0$) is overestimated especially for the higher values of ρ_z . The current relationship between ρ_z and θ_0 is linear namely: $85 \cdot \frac{\rho_z f_y}{f_c} + 19.3$

To calculate the θ_0 from the θ found in Response the following expression is used, based equations [57] and [59] assuming the gradient is correct, and based on beams without the influence of ϵ_y .

$$\theta_{0,r2k} = \frac{\theta_{r2k} - 37500 \cdot \epsilon_x}{1 - 1000 \cdot \epsilon_x} \quad [63]$$

The outcomes are plotted against $\frac{\rho_z f_y}{f_c}$ in Figure 4.14, it can be seen that a parabolic relation between $\frac{\rho_z f_y}{f_c}$ and θ_0 fits the Response results the best. This parabolic relationship has its maximum at $\frac{\rho_z f_y}{f_c} = 0.05$. For higher values of $\frac{\rho_z f_y}{f_c}$ the θ_0 -value will increase linearly and the formula proposed by Esfandiari (Esfandiari & Adebar, 2009), expression [58], can be used.

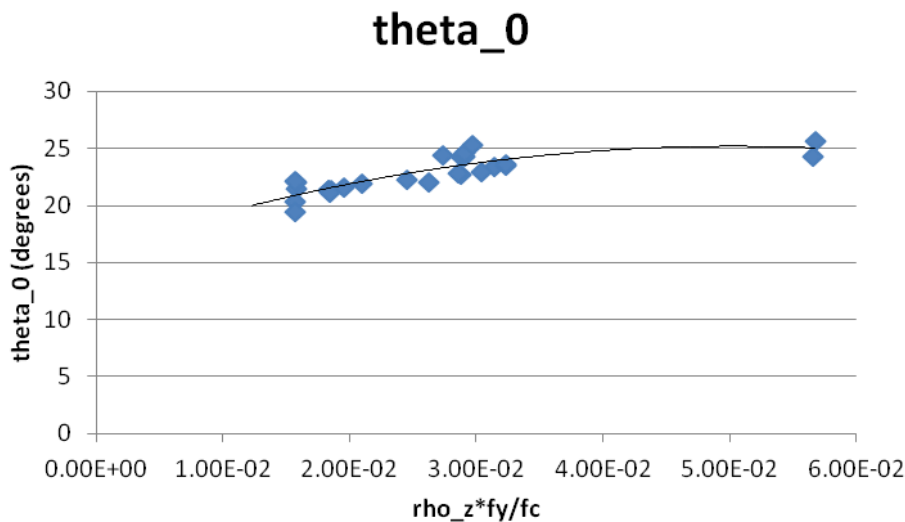


Figure 4.14, Theta_0

The proposed formula for θ_0 in case of yielding of the transverse reinforcement therefore becomes:

$$\theta_0 = \left(-3913 \cdot \left(\frac{\rho_z f_y}{f_c}\right)^2 + 393 \cdot \frac{\rho_z f_y}{f_c} + 15.3\right) \cdot (-50 \cdot \epsilon_y + 1.1) \text{ for } \frac{\rho_z f_y}{f_c} < 0.05 \quad [64]$$

$$\theta_0 = \left(85 \cdot \frac{\rho_z f_y}{f_c} + 19.3\right) (-50 \epsilon_y + 1.1) \text{ for } \frac{\rho_z f_y}{f_c} > 0.05 \quad [65]$$

The $\Delta\theta$ part of the formula stays unchanged.

This leads to an increase in the accuracy of θ to a mean ratio of 1.007 and a COV of 4.09% (Figure 4.15).

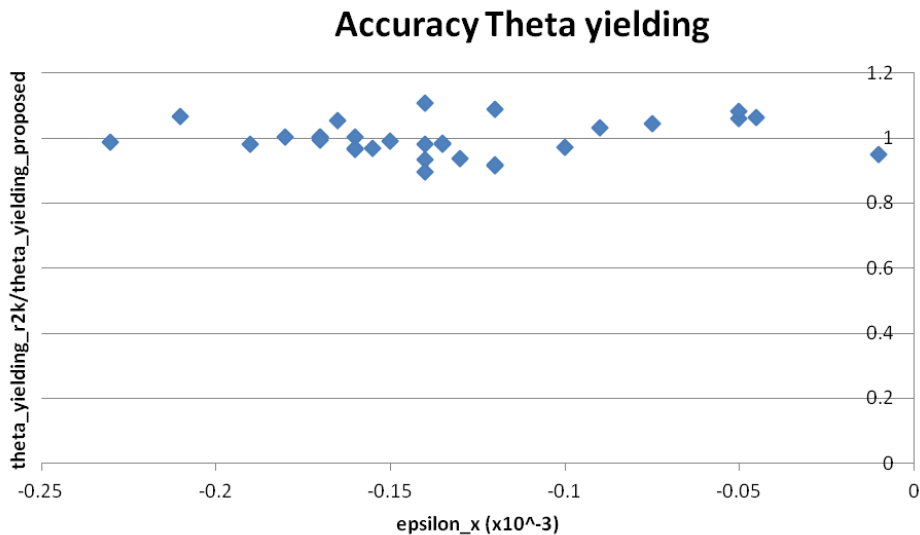


Figure 4.15, Accuracy theta yielding

4.4.2 θ -value crushing

For the θ at crushing failure, the θ proposed by (Esfandiari & Adebar, 2009) will be used because this prediction is quite good. There could be a bit of improvement for lower reinforcement ratios, it is however not easy to do this without influencing the results for other reinforcement ratios. The accuracy is shown in Figure 4.16 and it can be seen that it is equally accurate over the whole ϵ_x range implying that the relation between θ and ϵ_x is described well.

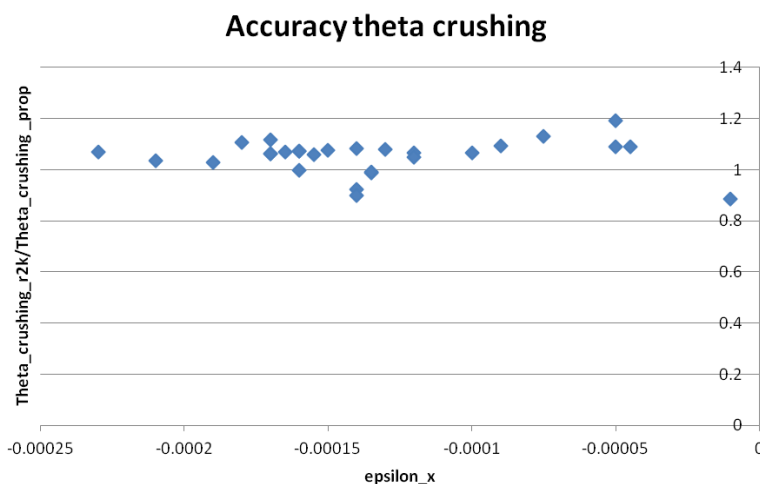


Figure 4.16, Accuracy theta crushing

4.5 β - value

In the CSA-model the β is defined as $\beta = \frac{0.4}{1+1500\epsilon_x}$, this formula, however, is unconservative for low values of ϵ_x . This makes it less suitable for the description of shear tension failure because shear tension failure occurs at a small longitudinal strain. This expression of β also is independent of the aggregate size because it is derived at a constant aggregate size of 20 mm and a constant crack spacing of 300 mm. In the paper shear strength evaluation of concrete bridge girders (Esfandiari & Adebar, 2009) expressions [66] and [67] are proposed for β .

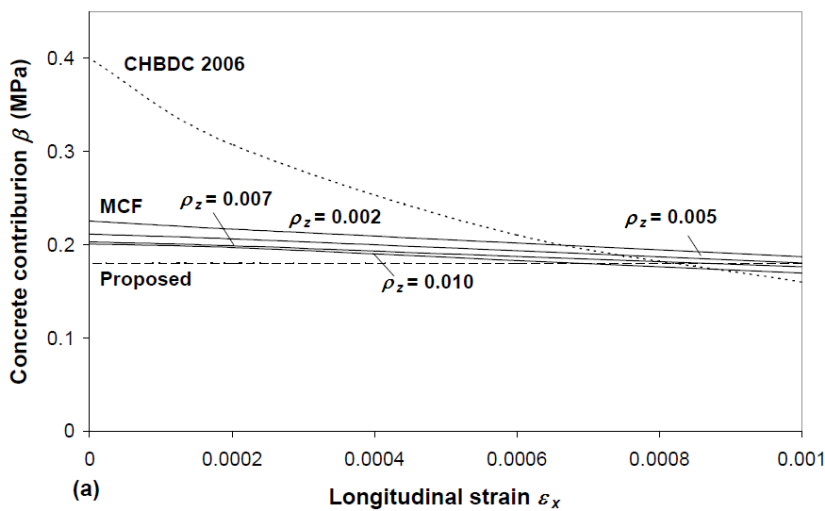
Yielding of the transverse reinforcement:

$$\beta = 0.18 \cdot (-300 \cdot \epsilon_y + 1.6) > 0.18 \quad [66]$$

Crushing of the web concrete:

$$\beta = 0.65 \cdot \frac{\rho_z f_y}{f_c} + 0.03 \quad [67]$$

As shown in Figure 4.17 the proposed values lie much closer to the MCFT values for small longitudinal strain but that most of the proposed values are a bit conservative.



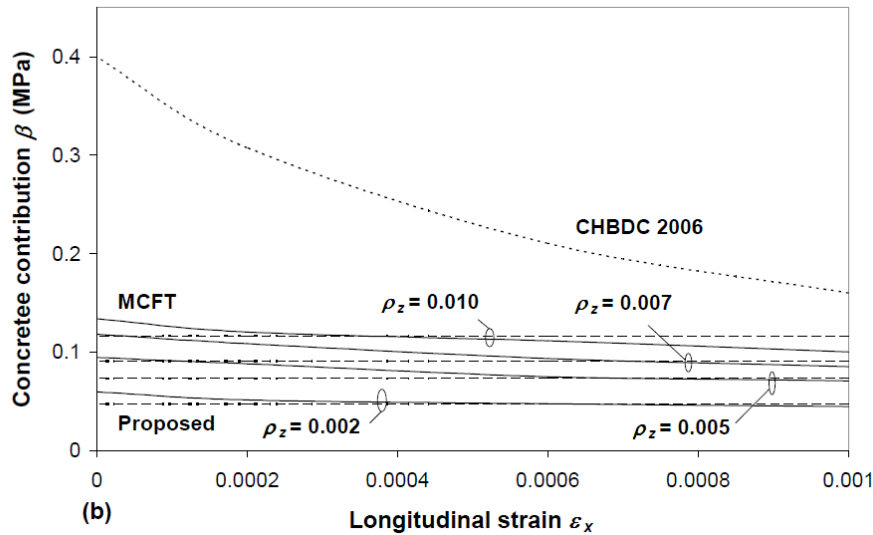


Figure 4.17, Comparison of predicted β with MCFT result at: (a) yielding of transverse reinforcement, (b) crushing of concrete for $f_c = 30$ MPa, $f_y = 400$ MPa. (Esfandiari & Adebar, 2009)

4.5.1 β -value yielding

The β expression for yielding of the stirrups gives a constant value and doesn't depend on material properties or loading. Compared to the Response results of β this gives a mean ratio of 1.01 with a COV of 9%. In Figure 4.18 it can be seen that for beams with lower longitudinal strain the predictions are a little bit unconservative while for beams with higher longitudinal strain they are a bit conservative which makes the prediction of a constant value very good.

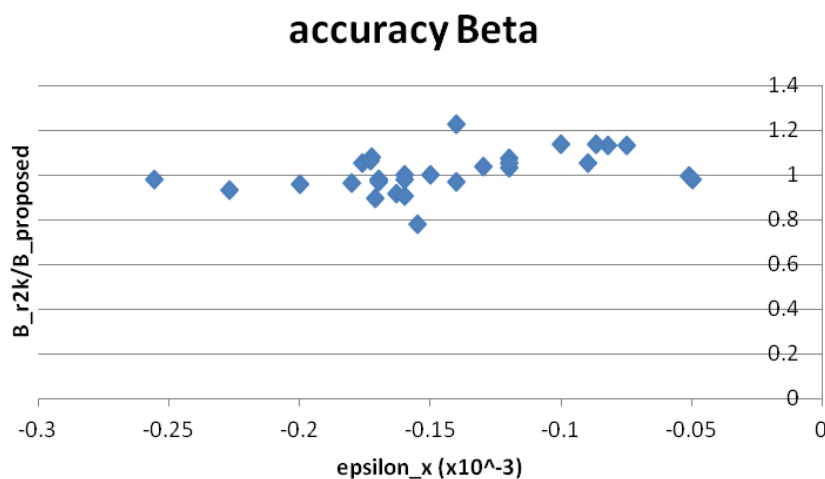


Figure 4.18, Accuracy of beta for yielding failure

4.5.2 β -value crushing

The β expression for crushing failure depends on $\frac{\rho_z f_y}{f_c}$. Compared to the Response results for β a means ratio of 2.9 with a COV of 40% is found. This means that this expression underestimates the contribution of the aggregate interlock vastly. An alternative expression is proposed which not only depends on $\frac{\rho_z f_y}{f_c}$, but also on the aggregate size. The aggregate size becomes more important for

beams failing in crushing because the interlock decreases rapidly after yielding due to an increasing crack width, at bigger aggregate sizes however more interlock is still possible.

The β -values found in Response for various aggregate sizes are plotted in Figure 4.19 for a number of beams. A clear relation between the β and the aggregate size can be seen. Also, the influence of $\frac{\rho_z f_y}{f_c}$, is visible in Figure 4.19 as the beams with lower $\frac{\rho_z f_y}{f_c}$ have lower β values. For instance, F3B has a value of 0.0123 while beams HCP1TE, HAP1TW and LB10 have a much higher value of 0.0324, 0.288 and 0.0314 respectively.

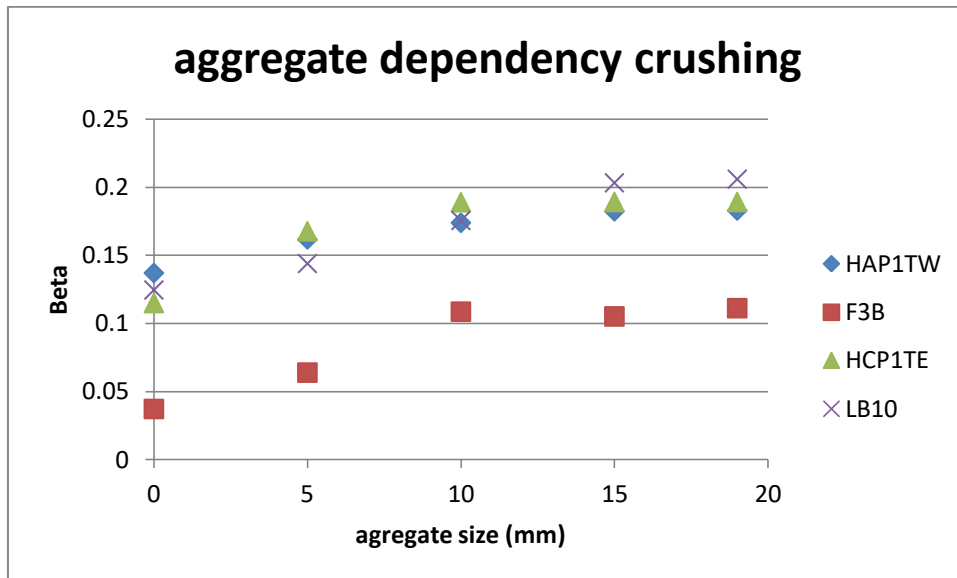


Figure 4.19, Aggregate size dependency

The relationship between β and the aggregate size can be described by the expression:

$$-0.0002 \cdot a_g^2 + 0.0078 \cdot a_g + \text{starting value}$$

The starting value depends on $\frac{\rho_z f_y}{f_c}$, and is proposed as:

$$3.8 \cdot \frac{\rho_z f_y}{f_c}$$

This gives the total expression for beta in crushing:

$$\beta = 3.8 \cdot \frac{\rho_z f_y}{f_c} - 0.0002 \cdot a_g^2 + 0.0078 \cdot a_g^c \quad [68]$$

There is, however, a restriction to this expression. The aggregate interlock decreases after yielding due to the increasing crack width. For the failure mechanism crushing after yielding this means that

^c This formula is verified to an aggregate size of 20 mm and has its maximum at 19.5 mm. For larger aggregate sizes 19.5 has to be used to get an appropriate interlock because using the formula with actual aggregate size will give a too small value for higher aggregate sizes (parabola goes downwards again).

the aggregate interlock can never be higher than the aggregate interlock at the point of yielding. Therefore the β value shall not be bigger than that of the yielding failure.

This expression gives a mean ratio of 1.03 with a COV of 21% compared to Response. As shown in Figure 4.20 the proposed expression overestimates the contribution of the aggregate interlock a bit.

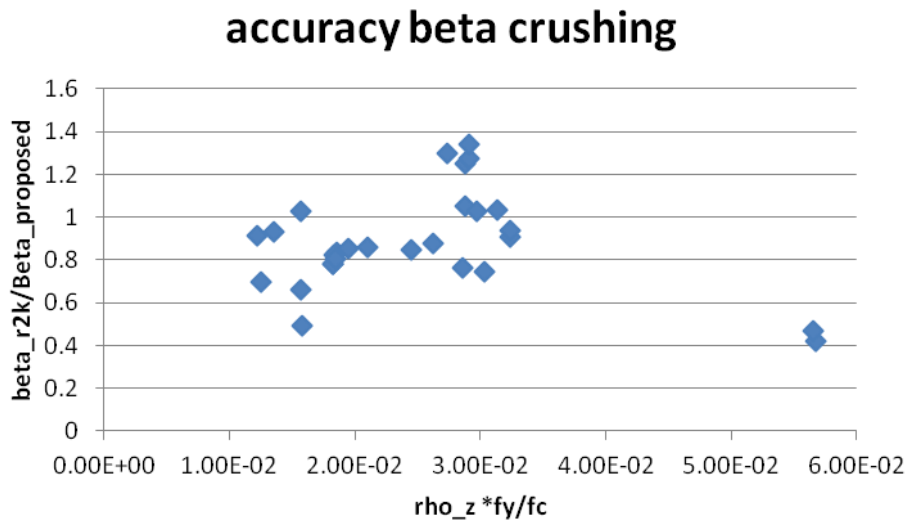


Figure 4.20, Accuracy beta crushing

To sum up the proposed expressions for β are:

$$\beta = 0.18 \cdot (-300 \cdot \epsilon_y + 1.6) \text{ for yielding of the reinforcement, } \epsilon_y \leq 0.002. \quad [69]$$

$$\beta = 3.8 \cdot \frac{\rho_z f_y}{f_c} - 0.0002 \cdot a_g^2 + 0.0078 \cdot a_g < 0.18 \cdot (-300 \cdot \epsilon_y + 1.6) \text{ for crushing of the concrete.} \quad [70]$$

4.6 V_{max}

The CSA-model describes the maximum shear force as $V_{max} = 0.25 \cdot f_c \cdot b_w \cdot z$. As explained in chapter 2.2.1, the shear stress of $0.25 \cdot f_c$ comes from yielding and crushing the same time. The chosen ϵ_x value for this calculation is 0.002 mm/mm, however for shear tension failure the longitudinal strain values are zero or smaller. As mentioned in (Bentz, Vecchio, & Collins, Simplified Modified Compression Field Theory for Calculating Shear Strength of Reinforced Concrete Elements, 2006) this gives a shear stress of approximately $0.32 \cdot f_c$ which should be more appropriate for shear tension failure. In Response-2000, it was found that V_{max} was governing for beam TP4. As can be seen in Figure 4.21 the proposed shear stress of $0.32 \cdot f_c$ is a good approximation of the web shear stress, however, as seen before, the shear stress in the flanges is much smaller. From Table 4.2 it can be seen that the contribution of the uncracked zone is predicted well by the contribution factor and therefore this factor will also be used in V_{max} to contribute for the uncracked flanges.

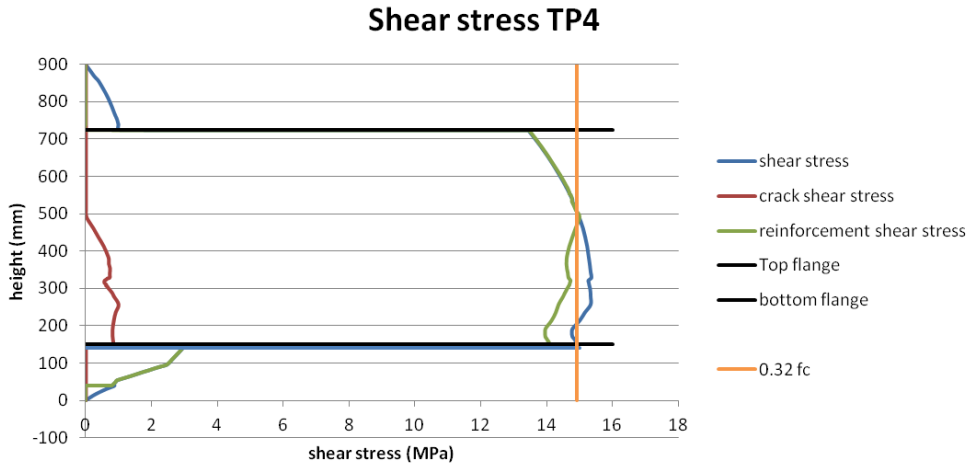


Figure 4.21, Proposed shear stress on Response shear stress

With the proposed adjustments the formula for V_{max} becomes:

$$V_{max} = 0.32 \cdot f_c \cdot b_w \cdot h_{web} \cdot \frac{1}{1 - \phi_{uncracked}} \quad [71]$$

Table 4.3 shows the prediction of TP4:

	Vmax	Ratio V_{exp}/V_{max}
TP4	879.42	1.00

Table 4.3, Vmax predictions

4.7 ϵ_x

The longitudinal strain in the CSA-model is defined as half of the strain of the flexural tension side where it is assumed that the strain on the flexural compression side is small and therefore neglected. The Response results (Figure 4.22), show that in the governing cross-section for shear tension, the strain on the flexural tension side is close to zero because the governing cross-section is taken just before cracking of the tensile zone. The longitudinal strain on the compression side is also small but not zero. The expression for the longitudinal strain defined in the CSA-model is not appropriate to describe the longitudinal strain in the case of shear tension failure because the strain in the middle would be given as a tensile strain instead of a compressive strain.

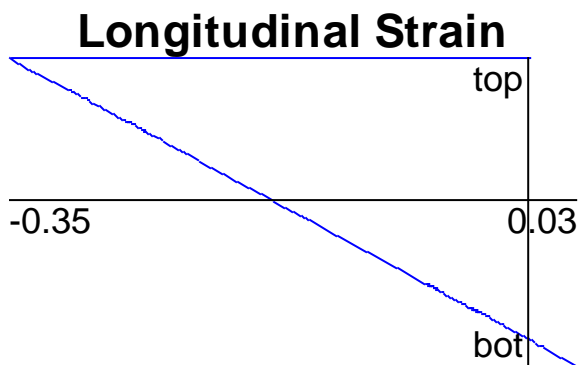


Figure 4.22, Longitudinal strain HAP1TW in Response (mm/m)

However, the strain is small, it is not appropriate to take the longitudinal strain at mid height as zero because this inaccuracy would result in an overestimation of the cracking angle. Especially for beams failing due to yielding this would lead to an overestimation of the cracking angle because the gradient is quite steep (Figure 4.11A). An overestimation of the angle then leads to an underestimation of the steel component leading to more conservative results.

For the governing cross-section, it would be appropriate to define the strain at mid-height as half of the strain on the flexural compression side. However, for other cross-sections, it is possible that the strain on the flexural tension side is also compressive which makes this definition not suitable for all sections along the beam. Therefore, it is proposed to take:

$$\epsilon_x = \frac{\epsilon_c + \epsilon_t}{2} \quad [72]$$

ϵ_c is:

$$\epsilon_c = \frac{-\frac{M}{z} + V + \frac{N}{2} + A_{pw} \cdot f_{pw} \cdot \lambda_p}{2 \cdot (E_c A_{cc} + E_s (A_{sc} + A_{sw} \cdot \lambda_s^2) + E_p (A_{pc} + A_{wp} \cdot \lambda_p^2))} \quad [73]$$

where:

A_{cc} is the area of the flexural compressive flange.

A_{sc} is the area of the reinforcement in the flexural compressive flange.

A_{sw} is the area of longitudinal reinforcement in the compressive zone of the web.

A_{pc} is the area of the prestress tendons in the flexural compressive flange.

A_{pw} is the area of the prestress tendons in the compressive zone of the web.

$$\lambda_s = \frac{d_s}{d}$$

$$\lambda_p = \frac{d_p}{d}$$

ϵ_t is:

$$\epsilon_t = \frac{\frac{M}{z} + V + \frac{N}{2}}{2 \cdot (E_c A_{ct} + E_s A_{st} + E_p A_{pt})} \quad [74]$$

Where:

A_{ct} is the area of the flexural tension flange.

A_{st} is the area of the reinforcement in the flexural tension flange.

A_{pt} is the area of the prestressing tendons in the flexural tension flange.

For the expression of the strain on the flexural compression side (expression [73]), the place of the reinforcement and prestressing tendons in the web is taken into account to acquire additional accuracy. This refinement will not be used in the expression of the strain on the flexural tension side (expression [74]) because the strain generally is very small so it will not lead to additional accuracy. The area of the concrete is taken as the area of the flange because the cross-section is considered to be cracked in the web, which means this part loses stiffness. Cracking of the flanges is not taken into account in this model, because this is not typical for shear tension failures. When the longitudinal strain on the flexural tension or flexural compression side exceeds the cracking strain, it is likely that another failure mechanism is governing and will give lower capacity. The parameters needed to calculate the longitudinal strain are shown in Figure 4.23.

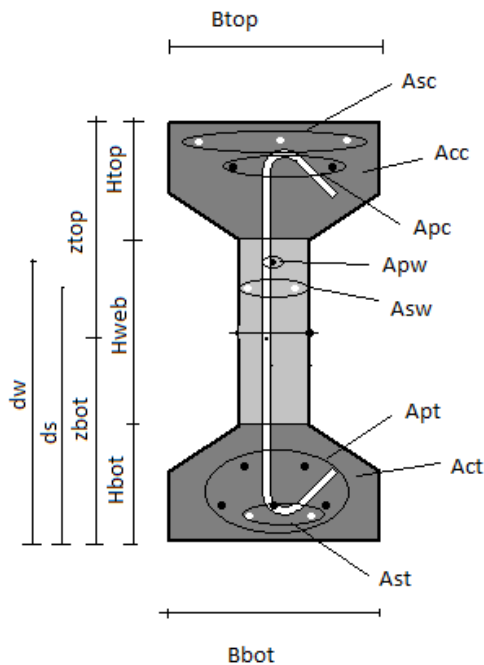


Figure 4.23, Parameters longitudinal strain

The proposed values for the longitudinal strain lay close to the Response values although there is some difference due to the calculation of the concrete stiffness (Figure 4.24 and 4.25). In Response-2000 the cracked area is accurately calculated for every cross-section, while in the analytical model the cracked area is constant. This leads to a difference in stiffness.

Another cause of the difference in stiffness is the expression for the E-modulus used in Response which differs from the Eurocode 2 expression, $E_c = 28053$ in Response-2000 compared to $E_c = 34242$ in the Eurocode. In Figure 4.24 and 4.25, it can be seen that for the analytical calculation with the same E-modulus as used in Response there is a smaller difference than for calculations with the Eurocode 2 E-modulus. The accuracy of $\epsilon_{x_{r2k}}/\epsilon_{x_{proposed}}$ for the Response E-modulus has a mean ratio of 1.09 with a COV of 34%. The Eurocode 2 E-modulus is higher and therefore leads to a bit bigger strain (less negative). The accuracy of $\epsilon_{x_{r2k}}/\epsilon_{x_{proposed}}$ for the Eurocode E-modulus has a mean ratio of 1.29 with a COV of 32%. The E-modulus of the Eurocode 2 is 20% higher than the one used in Response, this is also visible in the accuracy as the difference in accuracy is 20%.

The difference in stiffness influences the capacity as the cracking angle is predicted to big for both yielding and crushing failure. This leads to a too small capacity for yielding compared to Response and a too high capacity for crushing after yielding compared to Response.

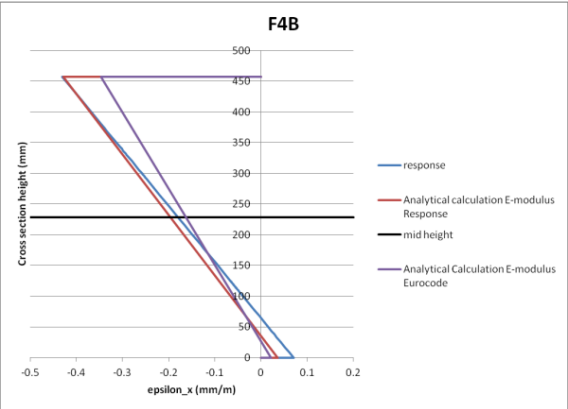
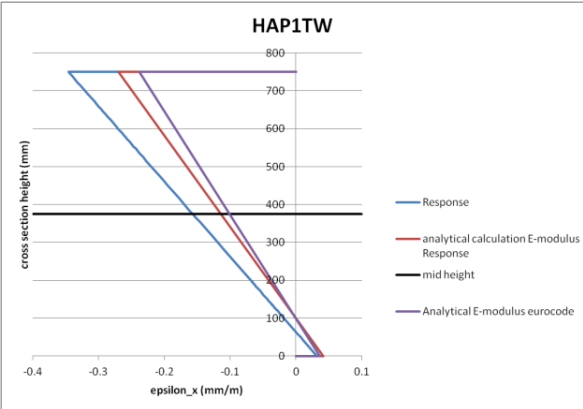


Figure 4.24, Comparison epsilon_x HAP1TW

Figure 4.25, Comparison epsilon_x F4B

4.8 Calculation

The total proposed method to calculate the shear tension capacity of a beam is shown in Table 4.4. This is an iterative method and, therefore, it is recommended calculating this with the use of excel.

Shear tension capacity	
$V = \max(V_{yield}, V_{crush}) < V_{max} = \frac{1}{1 - \phi_{uncracked}} (0.32 \cdot f_c \cdot b_w \cdot h_{web})$ $V_{yield/crush} = \frac{1}{1 - \phi_{uncracked}} (V_c + V_s)$ $V_c = \beta \cdot \sqrt{f_c} \cdot b_w \cdot h_{web}$ $V_s = \frac{A_{sw} f_y h_{web}}{s} \cot \theta$	
<p style="text-align: center;">Yielding of the transverse reinforcement</p> $\theta = \theta_0 + \Delta\theta \cdot \epsilon_x$ $\theta_0 = (-3913 \cdot \left(\frac{\rho_z f_y}{f_c}\right)^2 + 393 \cdot \frac{\rho_z f_y}{f_c} + 15.3) \cdot (-50 \cdot \epsilon_y + 1.1) \text{ for } \rho_z f_y f_c < 0.05$ $\theta_0 = \left(85 \cdot \frac{\rho_z f_y}{f_c} + 19.3\right) (-50 \epsilon_y + 1.1) \text{ for } \frac{\rho_z f_y}{f_c} > 0.05$ $\Delta\theta = 1000 [37.5(-200 \epsilon_y + 1.4) - \epsilon_0]$ $\beta = 0.18 \cdot (-300 \cdot \epsilon_y + 1.6) \geq 0.18$ $\epsilon_y \leq 0.002$	<p style="text-align: center;">Crushing of the web concrete</p> $\theta = \theta_0 + \Delta\theta \cdot \epsilon_x$ $\theta_0 = 119 \cdot \frac{\rho_z \cdot f_y}{f_c} + 15.6$ $\Delta\theta = 15000 \cdot \frac{\rho_z \cdot f_y}{f_c} + 2000$ $\beta = 3.8 \cdot \frac{\rho_z f_y}{f_c} - 0.0002 \cdot a_g^2 + 0.0078 \cdot a_g$ ≤ 0.18 $a_g \leq 19.5$
<p style="text-align: center;">Contribution of the uncracked zone</p> $\phi_{uncracked} = \frac{h_{bot} \cdot A + h_{top} \cdot B}{A \cdot (h_{bot} + h_{web,red}) + B \cdot (h_{top} + h_{web,red})}$ $A = h_{bot} \cdot b_{bot} \cdot (h_{bot} - 2 \cdot z_{bot})$ $B = h_{top} \cdot b_{top} \cdot (h_{top} - 2 \cdot z_{top})$ $h_{web,red} = h_{web} - \frac{1}{3} \cdot h_{skew}$	<p style="text-align: center;">$\lambda_s = \frac{d_s}{d}$</p> <p style="text-align: center;">$\lambda_p = \frac{d_p}{d}$</p>
<p style="text-align: center;">Longitudinal strain</p> $\epsilon_x = \frac{\epsilon_c + \epsilon_t}{2}$ $\epsilon_c = \frac{-\frac{M}{Z} + V + \frac{N}{2} + A_{pw} \cdot f_{pw} \cdot \lambda_p}{2 \cdot (E_c A_{cc} + E_s (A_{sc} + A_{swl} \cdot \lambda_s^2) + E_p (A_{pc} + A_{wp} \cdot \lambda_p^2))}$ $\epsilon_t = \frac{\frac{M}{Z} + V + \frac{N}{2}}{2 \cdot (E_c A_{ct} + E_s A_{st} + E_p A_{pt})}$	

Table 4.4, Shear tension calculation overview

Figure 4.26 and Figure 4.27 show only a small difference in capacity between the various cross-sections calculated by the proposed method, while in Response there is a notable difference. This is caused by the assumption that the height of the cracked zone is always equal while for the Response there the cracked zone varies and so does the stiffness. This influences the longitudinal strain and therefore the capacity. In Figure 4.26 and Figure 4.27, the shear stress from Response lies a bit higher at the cross-sections that are not governing for shear tension, because of the different stiffness. The cross-sections where the Response value lies significantly lower are identified as the cross-sections where the tensile strain exceeds the cracking strain meaning the flanges are cracked. This is not considered in the proposed calculation causing the capacity to be higher. The distance where the Response line crosses the predicted capacity for the second time equals the critical cross-section in Response.

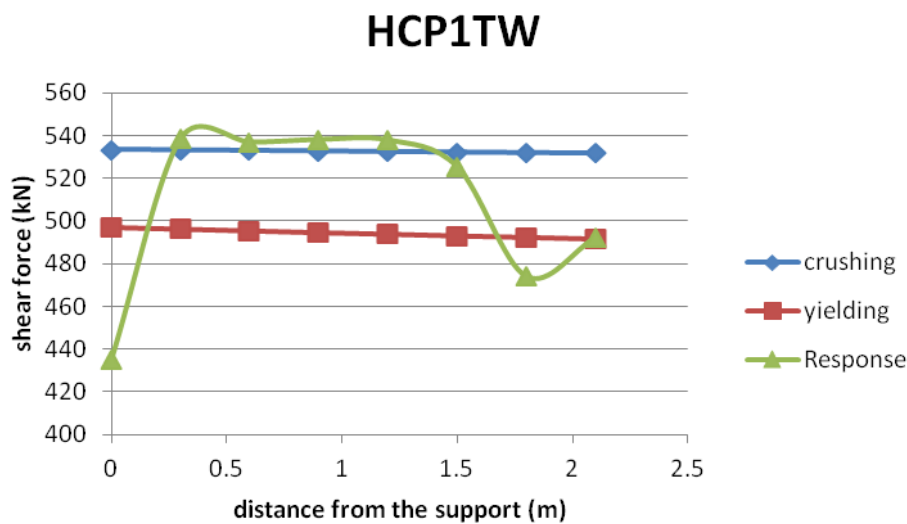


Figure 4.26, Shear force capacity over beam HCP1TW

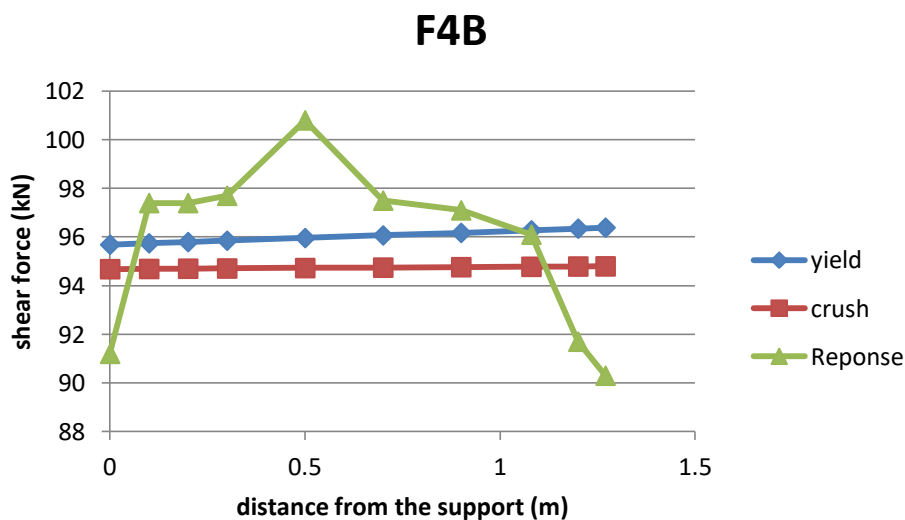


Figure 4.27, Shear force capacity over beam F4B

When the proposed shear stress of the governing cross-section is plotted over the shear stress distribution found in Response (Figure 4.28 and Figure 4.29) it can be seen that the contribution of the steel, aggregate interlock and uncracked components are predicted very well. It can be seen that the distribution of the parts differs a bit because of the different cracked height. This means a part that in response is resisted by the reinforcement is now resisted by the uncracked flange and vice versa.

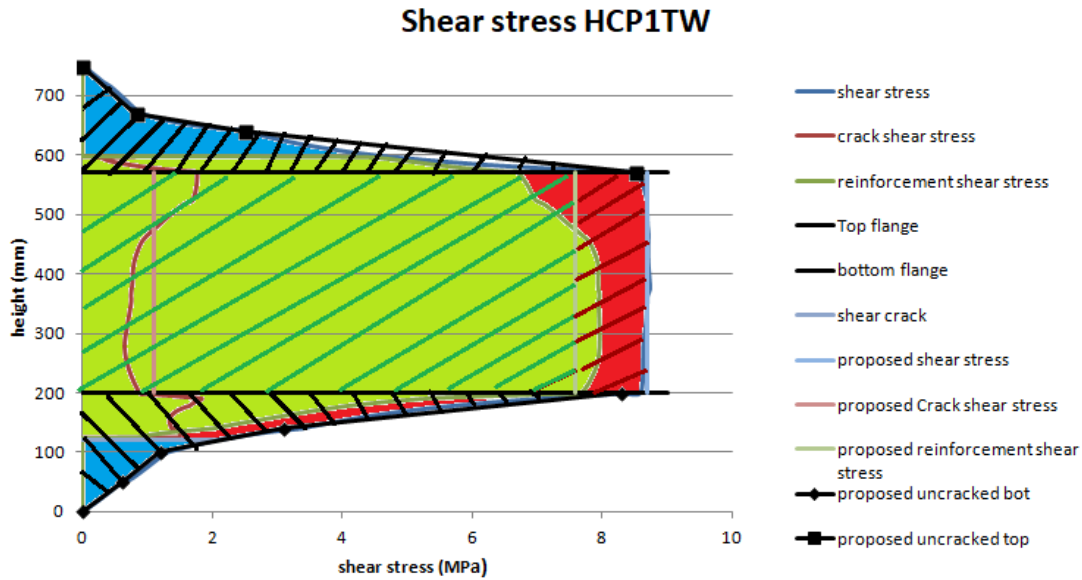


Figure 4.28, Comparison proposed shear stress distribution and Response for HCP1TW

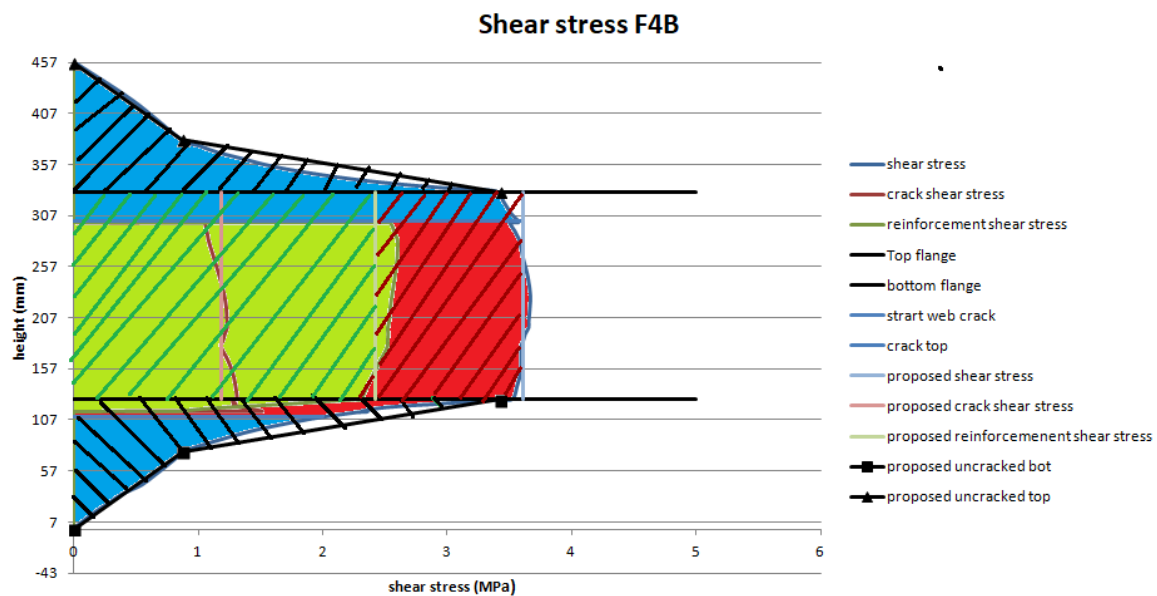


Figure 4.29, Comparison proposed shear stress distribution and Response for F4B

4.8.1 Accuracy

The accuracy of the proposed method compared to the experiments gives a mean value of $V_{exp}/V_{prop} = 1.36$ with a variation of 22%, and is shown in Figure 4.30. This is a bit less conservative than Response which gave a mean of $V_{exp}/V_{prop} = 1.38$, however, the variation which was 19%, is a

bit bigger. An overview of the results of the iterative calculation and its accuracy is given in Appendix E.

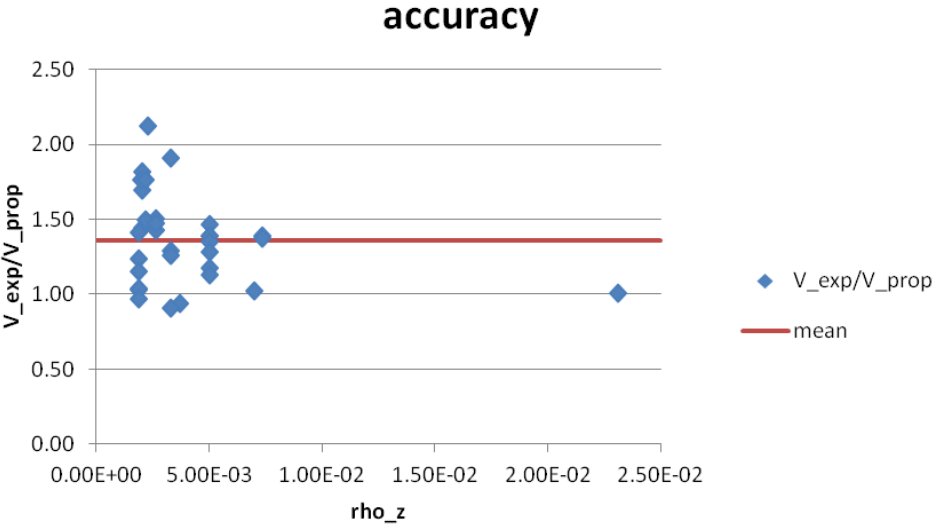


Figure 4.30, Accuracy of proposed shear tension model

The combination of the conservative ϵ_x that causes bigger θ and the slightly unconservative expressions for θ cause that the overall prediction of θ for the failure mechanism yielding is quite good. This makes that the proposed shear force is a bit higher than the values found in Response, however, the predictions compared to the experimental values are still conservative.

It can be concluded that the model as presented in Table 4.4 gives a prediction of shear tension failure with a mean ratio of $V_{exp}/V_{prop} = 1.36$ and a variation of 21.86%. The proposed model for shear tension gives more accurate predictions for the aggregate interlock and cracking angle than the CSA-model. The proposed model for shear tension failure also gives more insight into the force distribution within the cross-section and the failure mechanism causing shear tension failure.

5 Conclusions

The aim of this thesis was to find a more accurate prediction model for shear tension failure based on the MCFT. The focus was on two practical methods: the CSA-model and Response-2000. The two main questions for these methods were:

- How accurate is the prediction of shear tension behaviour of Response-2000?
- How can we modify the CSA-model to describe shear tension behaviour more accurately?

5.1 Response

To answer the first main question Response-2000 analysis of 32 beams failing in shear tension were compared to the experimental results. From the use of Response-2000 and the comparison the following conclusions can be drawn:

From the use of Response-2000, it can be concluded that:

- Response-2000 is an easy to use program which can be used to predict shear tension failure because shear is taken into account in the calculation.
- Response-2000 gives elaborate insight into the distribution of stresses and strains in the reinforcement and concrete for every load step which makes it possible to compare the results with the experiments.

From the general comparison of Response and the experiments, it can be concluded that:

- The shear tension capacity of 32 beams failing in shear tension is predicted conservative (see Table 5.1) The predictions of the beams from Hanson and Choulli are the most conservative (see Table 5.1) because the beams have the smallest a/d-ratios.

	Mean ratio	COV	Number of specimens
Xie	1.098	10%	6
Choulli	1.33	8%	7
Hanson	1.54	15 %	17
Leonhardt	0.99	0.89%	2
Total	1.38	19 %	32

Table 5.1, Accuracy failure load

- Beams with small a/d-ratios give more conservative results because the effect of clamping stresses is not taken into account in Response ($\sigma_z = 0$).
- For beams with higher prestress and a small a/d-ratio predictions become more conservative because the prestress adds to the clamping stress.
- The combination of a small a/d-ratio and a small transverse reinforcement ratio leads to more conservative results.

- The failure mechanisms are predicted correctly in 87% of the analysis. The following failure mechanisms can be distinguished in Response:
 - Rupture of the stirrups.
 - Crushing of the web concrete.
 - Slipping/major crack opening.

Incorrect prediction is caused mainly by the interchange of failure mechanisms crushing of the web concrete and Rupture of the stirrups or due to failure mechanisms as buckling of the flanges or shear compression failure which cannot be predicted by Response-2000.

- The critical cross-section for shear tension failure is predicted within the experimental failure zone in 61% of the analysis. Opposed to many shear codes, Response-2000 predicts variation of the critical cross-section over the shear span, where, in other codes, the critical cross-section is taken a distance d from the support or load. It is, however, observed that the definition used to find the critical cross-section for shear tension failure causes the failure location to be influenced by the amount of prestress and the amount of transverse reinforcement. Both cause the cross-section to fail at higher M/V -ratios because there is a higher moment needed to crack the ultimate fibre.

From the in-depth comparison of Response and the experiments, it can be concluded that:

- The height of the uncracked zone in Response is a bit over predicted compared to the experiments (Table 5.2).

	Mean ratio	COV
Uncracked height	0.95	31%

Table 5.2, Accuracy uncracked height

- The contribution of the uncracked height is overestimated for low transverse reinforcement percentages and underestimated for higher reinforcement percentages. Because beams with low reinforcement percentages reach the steel capacity earlier. Causing less stress development in the cross section making the cross-section cracked over a smaller height. This means a bigger uncracked height, while the experiments crack immediately over the whole web height.
- The cracking angle (θ) in Response is a bit under predicted compared to the experiments (Table 5.3)

	Mean ratio	COV
Cracking angle (θ)	1.08	14%

Table 5.3, Accuracy cracking angle

- A small underestimation of the cracking angle (θ) and an overestimation of the uncracked height leads to the prediction of more stirrups through the crack in Response compared to the experiments.
- The steel stress in Response is predicted very accurate compared to the experiments (Table 5.4).

	Mean ratio	COV
Steel stress	1.01	8%

Table 5.4, Accuracy steel stress

- The predictions of the number of stirrups and steel stress lead to an accurate prediction of the steel component with Response (see Table 5.5)

	Mean ratio	COV
Steel component	0.996	15%

Table 5.5, Accuracy steel component

- The crack spacing is overestimated (see Table 5.6) especially for low amounts for transverse reinforcement (see Figure 3.18). This leads to an overestimation of the crack width.

	Mean ratio	COV
Crack spacing	0.53	42%

Table 5.6, Accuracy crack spacing

- The concrete aggregate interlock component is underestimated because of a too large crack width prediction and an overestimation of the uncracked height.
- The shear force in the cross section is resisted by the uncracked part, steel component and aggregate interlock component with the following distribution (Table 5.7)

Part	Mean	Minimum	Maximum
Uncracked part	1/3	12%	57%
Steel part	1/2	25%	84%
Aggregate interlock	1/6	2%	31%

Table 5.7, Contribution parts

These conclusions about Response-2000 lead to the general conclusion that the predictions of Response-2000 for shear tension failure are conservative but much more accurate than the variable angle truss model for small relative reinforcement ratios, see **Fout! Verwijzingsbron niet gevonden.** The Response analysis gives insight in not only the capacity of the beam but also the failure mechanism and failure location. The failure mechanism is predicted correctly in most cases which makes the prediction reliable. It is also concluded that Response gives insight into how the shear force is resisted by the cross-section, namely the distribution between the steel component, the concrete aggregate interlock component and the shear force resisted by the uncracked zone. It is concluded that the steel component is predicted very accurate while the concrete component is a bit underestimated. It is also concluded that the uncracked part of the cross-section resists a significant part of the shear force.

Predicted shear failures

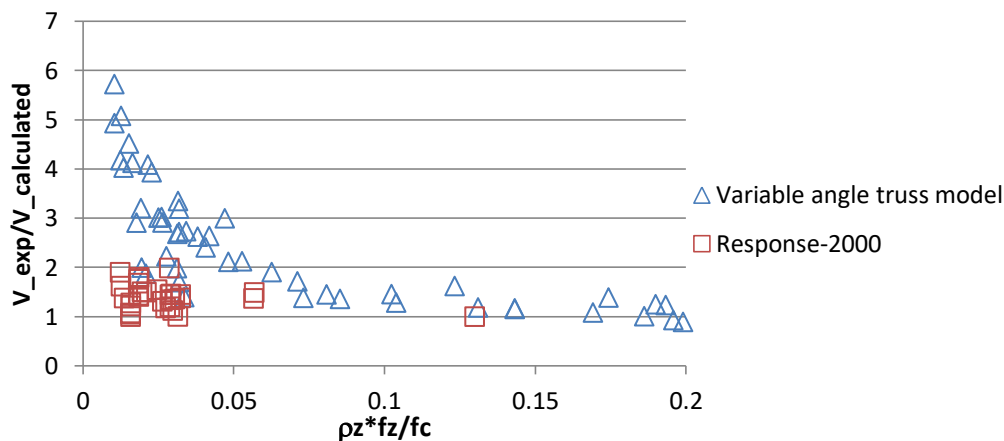


Figure 5.1, Predictions of Response and the variable angle truss model

5.2 Modified model

To answer the second main question the CSA-model is compared to the Response-2000 results for shear tension failure, to identify the parameters that are more appropriate for flexural shear failure instead of shear tension failure. From the comparison it can be concluded that the following parameters of the CSA need to be modified to come to a model for shear tension:

- The depth of the cracked zone.
- The contribution of the cracked height.
- The failure mechanism.
- The distribution of the longitudinal strain.
- The accuracy of the β -value for low longitudinal strain.
- The accuracy of the θ -value for low longitudinal strain.

From the analysis of Response-2000 and the CSA-model, the model in Table 4.4 is presented. The following can be concluded about the proposed model:

- The failure mechanisms:
 - Yielding of the transverse reinforcement.
 - Crushing of the web concrete after yielding.
 - Crushing before yielding.
 need to be taken into account.
- h_{web} is a good approximation for the height of the cracked zone because the cracked part is mainly in the web and the mid-depth is representative for the value over h_{web} .
- The uncracked flanges are described by a linear elastic distribution. The accuracy of the proposed calculation methods for the contribution of the uncracked zone is shown in Table 5.8. It can be concluded that both methods are very accurate and conservative.

	Mean ratio	COV
Excel calculation	1.03	3%
Analytical calculation	1.06	2%

Table 5.8 Accuracy of uncracked part calculations

- The proposed expressions for the cracking angle (θ) and aggregate interlock component (β) have an accuracy compared to Response, as shown in Table 5.9. It can be concluded that both expressions for θ are very accurate but a bit unconservative (lower cracking angle more contribution of the steel) and that both expressions for β are accurate and conservative.

	θ		β	
	Mean ratio	COV	Mean ratio	COV
Yielding	1.01	4%	1.01	9%
Crushing	1.05	6%	1.03	21%

Table 5.9, Accuracy θ and β

- The proposed shear stress of $0.32 \cdot f_c$ for V_{max} gives accurate results for beam TP4 (Leonhardt, Koch, & Rostasy, 1973).
- The predictions of the longitudinal strain have an accuracy of 1.09 with a COV of 34% for the same E-modulus as Response. This means a less negative prediction of the longitudinal strain leading to a too large prediction of the cracking angle for both crushing and yielding failure.

This is caused by the difference in stiffness due to another cracked height and E-modulus. The difference in E-modulus of Response and the Eurocode leads to a 20% more conservative prediction of the longitudinal strain compared to Response.

- There is not much variation in capacity over the beam length because the cracked height is taken constant.

From the conclusions about the proposed model, it can be concluded that the proposed model for shear tension as presented in Table 4.4 is able to conservatively describe shear tension failure (mean ratio of 1.36 with a COV of 22% compared to the experiments) and that its predictions lie very close to Response-2000 (mean of 1.38 with a COV of 19%), see Figure 5.2 . It can be concluded that this model gives inside into the governing failure mechanism and the distribution of the shear force by the steel, interlock and uncracked parts. With this model, it is possible to find predictions solely for shear tension behaviour which are more accurate than the variable angle truss model for small relative reinforcement ratios. In practice, this means when we reassess old bridges we can make predictions of the strength that lie closer to the actual strength for shear tension failure. This means less need for strengthening or replacement to prevent shear tension failure which can save a lot of money.

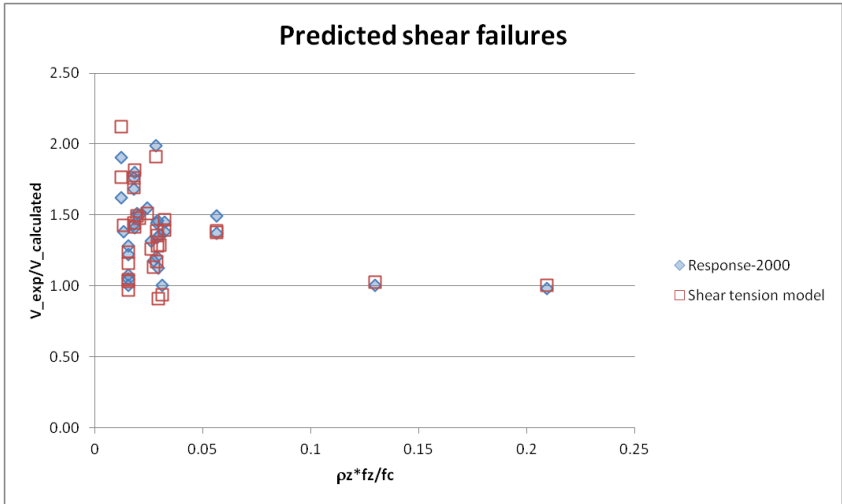


Figure 5.2, Predictions of Response-2000 and the proposed shear tension model

6 Recommendations

Based on the conclusions some recommendations for further research can be made to further improve the prediction of shear tension failure for beams:

- The accuracy of Response in this report is based on the analysis of 32 experiments to get a more accurate and trustworthy overview of Response it is recommended to analyze more experiments with Response.
- The used and proposed methods for the analysis of shear tension failure ignore the influence of the clamping stresses by taking $\sigma_z = 0$. This leads to an underestimation of the strength for beams with a small a/d-ratio. It is therefore recommended to do further research on the contribution of the clamping stresses to the capacity. Especially for beams with small a/d-ratios. This will lead to less variability in the shear force prediction.
- During the analysis in this thesis self weight was not taken into account. It is however recommended, to take self weight into account in the analysis because it leads to a more precise prediction especially for beams with significant self weight and for cross-sections with small bending moments (close to the support). The inclusion of self weight will also influence the critical cross-section. It is however only beneficial when the reported experimental shear resistances also take the self weight into account.
- The critical cross-section in this report is defined as the cross-section with the lowest capacity where the ultimate fibre is not yet cracked. This definition is a practical application and is found to be influenced by the prestress and amount of transverse reinforcement. It is, therefore, recommended to also look at cross-sections at which the flanges crack after diagonal tension cracking but not cause flexural tension failure.
- The proposed formula for ϵ_x has a high coefficient of variation and it is, therefore, recommended to do more research to decrease the variation of ϵ_x . This will lead to more accurate predictions of ϵ_x and therefore more accurate predictions of shear tension failure.
- The proposed shear tension model in this thesis is derived from the CSA-model and Response analysis. However not all parameters of Response are correctly predicted. It is, therefore, recommended to also compare the shear tension model with the experiments to get more accurate expressions for, for example, the crack spacing.

Bibliography

- Bentz, E. C. (2000). *Sectional Analysis of Reinforced Concrete Members*. Toronto.
- Bentz, E. C., & Collins, M. P. (2006). *Development of the 2004 Canadian standards association (CSA) A23.3 shear provisions for reinforced concrete*. Toronto.
- Bentz, E. C., Vecchio, F. J., & Collins, M. P. (2006). Simplified Modified Compression Field Theory for Calculating Shear Strength of Reinforced Concrete Elements. *ACI Structural Journal*.
- Bentz, E., & Collins, M. P. (2001, September). Response-2000 User Manual.
- Choulli, Y. (2005). *shear behaviour of Prestressed I-beams made with High-strength self compacting Concrete*. Barcelona.
- Collins, M. a. (1991). *Prestressed Concrete Structures*. Toronto: Response Publications.
- Esfandiari, A., & Adebar, P. (2009). Shear Strength Evaluation of Concrete Bridge Girders. *ACI Structural Journal*.
- Hanson, J., & Hulbos, C. (1965). *Ultimate shear strength of prestressed concrete beams with web reinforcement, April 1965*. Fritz Laboratory reports. Paper 52.
- Hendriks, M., & Esposito, R. (2017, October). CIE5148 Lecture 4 introduction to NLFEA.
- Leonhardt, F., Koch, R., & Rostasy, F. S. (1973). *Schubversuche an Spanetoträgern*. Berlin.
- Rijkswaterstaat. (sd). *Bruggen*. Opgeroepen op 10 15, 2018, van Rijkswaterstaat.nl: <https://www.rijkswaterstaat.nl/wegen/wegbeheer/bruggen/index.aspx>
- Vecchio, F. J. (1990). *Reinforced concrete membrane element formulation*. Journal of Structural Engineering, Vol. 116, No 3.
- Vecchio, F. J., & Collins, M. P. (1985). The modified compression-Field Theory for Reinforced Concrete Element Subjected to Shear.
- Walraven, P. d. (2002). *Background document for prENV 1992-1-1:2002* .
- Xie, L. (2009). *The influence of Axial Load and prestress on the shear strength of web-shear critica reinforced concrete elements*. Toronto.

Appendix

A Planning

Maand	Week	To do	Beschrijving
September	36	Onderwerp kiezen en doorlezen	
September	37	Starten met berekening CSA	HCP1TW beam berekening
September	38	Response berekening	Elzanaty
September	39	Response berekening en beschrijving	Xie/elzanty/vertrouwen krijgen
Oktober	40	Response theorie en vergelijking	Xie /vertrouwen krijgen
Oktober	41	Dieper ingaan op de theorie van Response	Xie
Oktober	42	Theory CSA en Theory Response	Papers en berekening
Oktober	43	Theory CSA en Theory Response	Papers en berekening
Oktober/November	44	Evaluatie MCFT/theory CSA en Response	Papers en berekening
November	45	Start bespreking/Evaluatie MCFT/ alle theory op orde	Papers en berekening
November	46	Evaluatie MCFT/invoeren experimenten	
November	47	Invoeren en evaluatie experimenten	Response
November/December	48	Invoeren en evaluatie experimenten	Response experimenten
December	49	Invoeren en evaluatie experimenten	Response experimenten
December	50	Invoeren en evaluatie experimenten	Response experimenten
December	51	Response en CSA	Vergelijken van aannamen
December	52	Vakantie	
Januari	1	Vakantie	
Januari	2	Response en CSA	Vergelijken van aannamen
Januari	3	Parameters focused on flexural shear	Vinden van aannamen die focussen op flexural shear
Januari	4	Parameters focused on flexural shear	Vinden van aannamen die focussen op flexural shear
Januari/februari	5	Aanpassingen in parameters CSA	Het vinden van meer accurate waarden voor de parameters die focussen op flexural shear
Februari	6	Aanpassingen in parameters CSA	Het vinden van meer accurate waarden voor de parameters die focussen op flexural shear
Februari	7	Aanpassingen in parameters CSA	Het vinden van meer accurate waarden voor de parameters die focussen op flexural shear
Februari	8	Aanpassingen in parameters CSA	Andere aanpassingen die de formules accurater maken
Februari/Maart	9	Aanpassingen in parameters CSA	Andere aanpassingen die de formules accurater maken
Maart	10	Conclusie/aanbevelingen	
Maart	11	schrijven eerste versie	
Maart	12	Schrijven eerste versie	
Maart	13	Schrijven eerste versie	
April	14	Inleveren eerste versie/Groenlicht	
April	15	verbeteringen/Presentatie	
April	16	verbeteringen/Presentatie	
April	17	Afstuderen	

B Response example input

The following steps give a detailed description of how to input the parameters of beam LB3 experimented on by Xie (Xie, 2009) in Response-2000.

1. Open Response-2000.
2. Go to the define tab and click quick-define.
3. Material properties.

Quick Define - Step 1 of 4

General Information

Title: Enter Title Here

Analysis By:

Material Properties

Concrete Cylinder Strength: 63.2 MPa

Long. Steel Yield Strength: 409 MPa

Transverse Steel Yield: 529 MPa

Prestressed Steel Type: None

< Vorige Volgende > Annuleren

Figure B.1, Quick define step 1

Fill in the strengths of the concrete, longitudinal reinforcement (15M), and Transverse reinforcement (D4). No prestress reinforcement type is filled in because we have unbonded tendons.

4. Cross-section.

Quick Define - Step 2 of 4

Title

- Rectangle Section
- Circular Section
- T-Beam Section
- I-Beam Section**
- General hollow core slab

btop: 348 mm

h: 506 mm

bweb: 73 mm

ttop: 80 mm

tbot: 76 mm

bbot: 351 mm

Bottom flange width

< Vorige Volgende > Annuleren

Figure B.2, Quick define step 2

Choose the I-beam section and fill in the required dimensions, as given above.

5. Top and bottom reinforcement

Quick Define - Step 3 of 4

Top Non-Prestressed Reinforcement

Number of Bars: 2 (e.g. 4)

Select bar by area

Bar Designation: 15M (eg: 25M)

Bottom Non-Prestressed Reinforcement

Number of Bars: 2 (e.g. 4)

Select bar by area

Bar Designation: 15M (eg: 25M)

< Vorige Volgende > Annuleren

Figure B.3, Quick define step 3

Enter the number of bars for the top and bottom reinforcement (2) and type (15M)

6. Stirrups

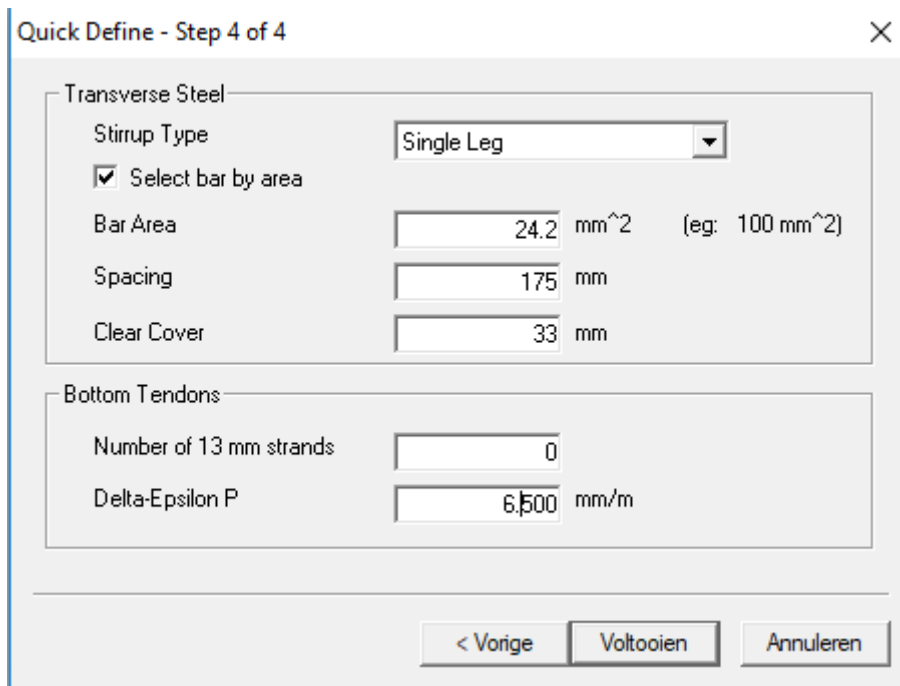


Figure B.4, Quick define step 4

We choose single leg stirrups. The D4 reinforcement type is not known in the program so we use the Select bar by area option to enter the area. No Tendons are selected.

7. Finished quick-define.

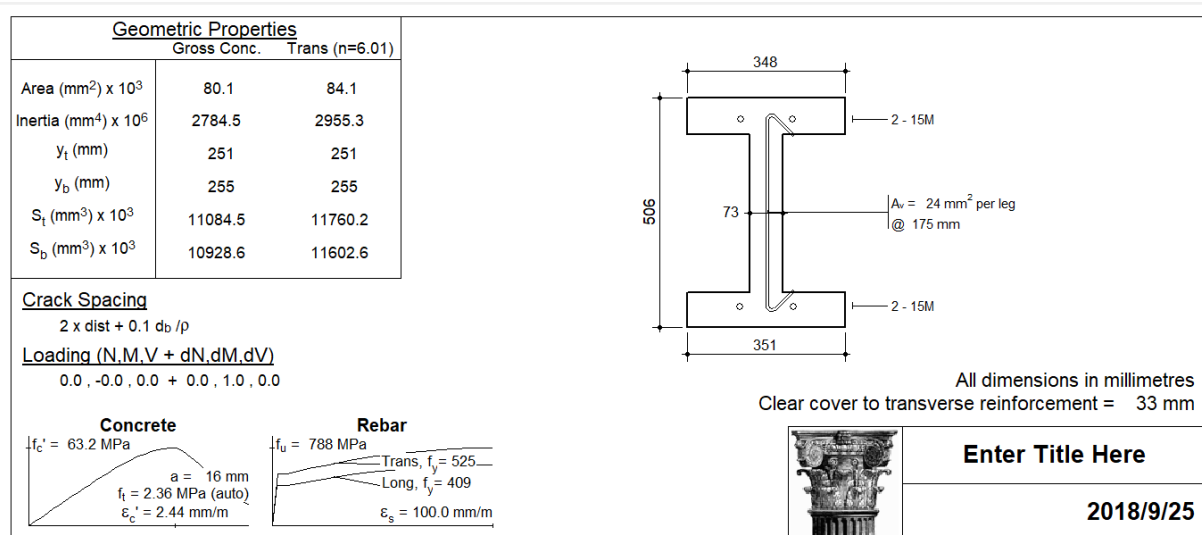


Figure B.5, Response geometry and material properties

After the quick-define is finished the geometry and material properties are defined as shown in Figure B.5. These are made up from the values of the quick-define and the default values. It can be seen that some properties are missing or that the default value disagrees with the wanted value. So we have to modify the default properties to the wanted properties.

8. Concrete cross section

To modify the concrete cross section, double click on the concrete cross section to open the menu and go to the tab user defined.

Now we are able to fill in the sloped sides of the flanges by changing 426 73 to 401 73 and 76 73 to 101 73, as shown in Figure B.6

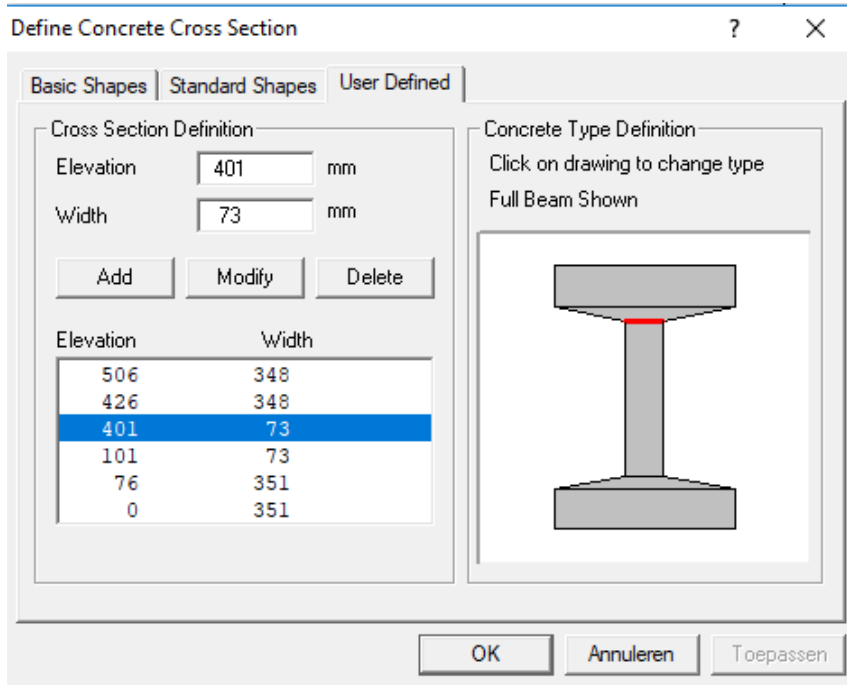


Figure B.6, definition concrete cross section

9. Concrete properties

Open the concrete material menu by double clicking on the concrete curve.

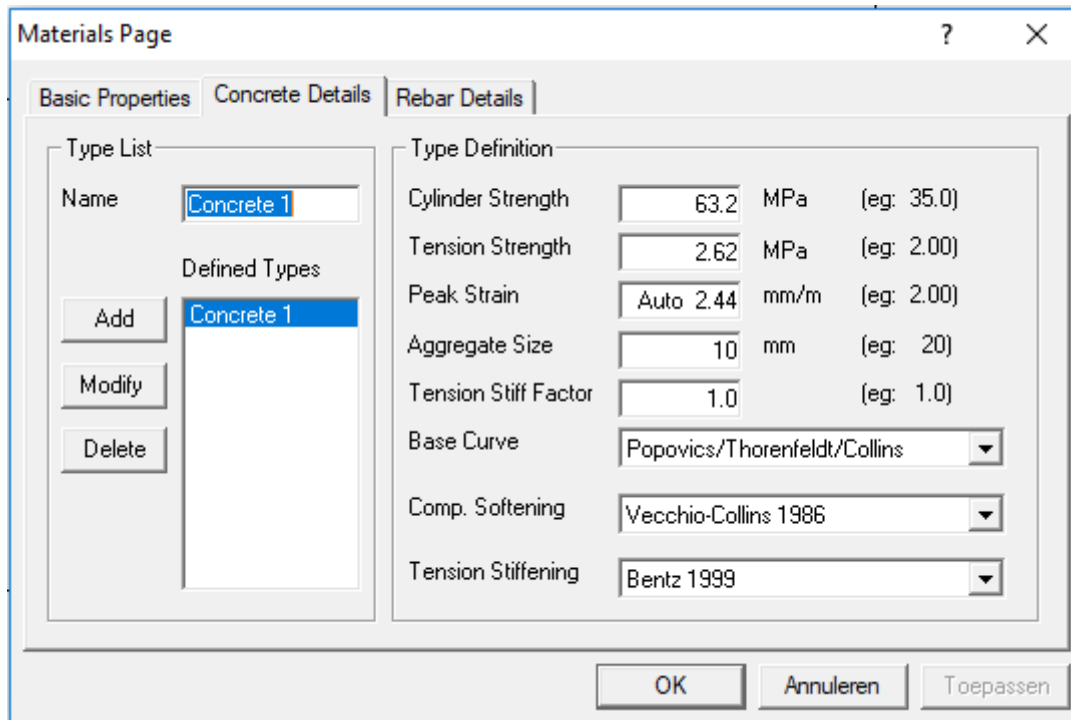


Figure B.7, concrete material menu

Change the aggregate size into 10 mm and leave the rest unchanged. Press modify after so all changes are permanent. The peak strain is taken as the automatic value because this is close to the measured value.

10. Steel properties

Open the steel material menu by double clicking on the steel stress strain curve.

Materials Page

Basic Properties | Concrete Details | Rebar Details

Type List

Name: 15M

Defined Types

Add: 15M, D4, D6, prestress bar

Modify

Delete

Type Definition

Elastic Modulus: 200000 MPa (eg: 200000)

Yield Strength: 409 MPa (eg: 400)

e-Strain Hardening: 12.1 mm/m (eg: 20.0)

Rupture Strain: 130 mm/m (eg: 100)

Ultimate Strength: 671 MPa (eg: 600)

Predefined Type: Custom type

OK Annuleren Toepassen

Figure B.8, steel material menu 15M

Enter the required values for the rupture strain, e-strain hardening en ultimate strength for the longitudinal reinforcement and change its name to 15M. Do the same for the transverse reinforcement and change its name to D4.

Materials Page

Basic Properties | Concrete Details | Rebar Details

Type List

Name: D4

Defined Types

Add: 15M, D4, D6, prestress bar

Modify

Delete

Type Definition

Elastic Modulus: 200000 MPa (eg: 200000)

Yield Strength: 529 MPa (eg: 400)

e-Strain Hardening: 2.6 mm/m (eg: 20.0)

Rupture Strain: 40 mm/m (eg: 100)

Ultimate Strength: 581 MPa (eg: 600)

Predefined Type: Custom type

OK Annuleren Toepassen

Figure B.9, steel material menu D4

We also need to add material for the ducts, this can be done by filling in the properties and then click add.

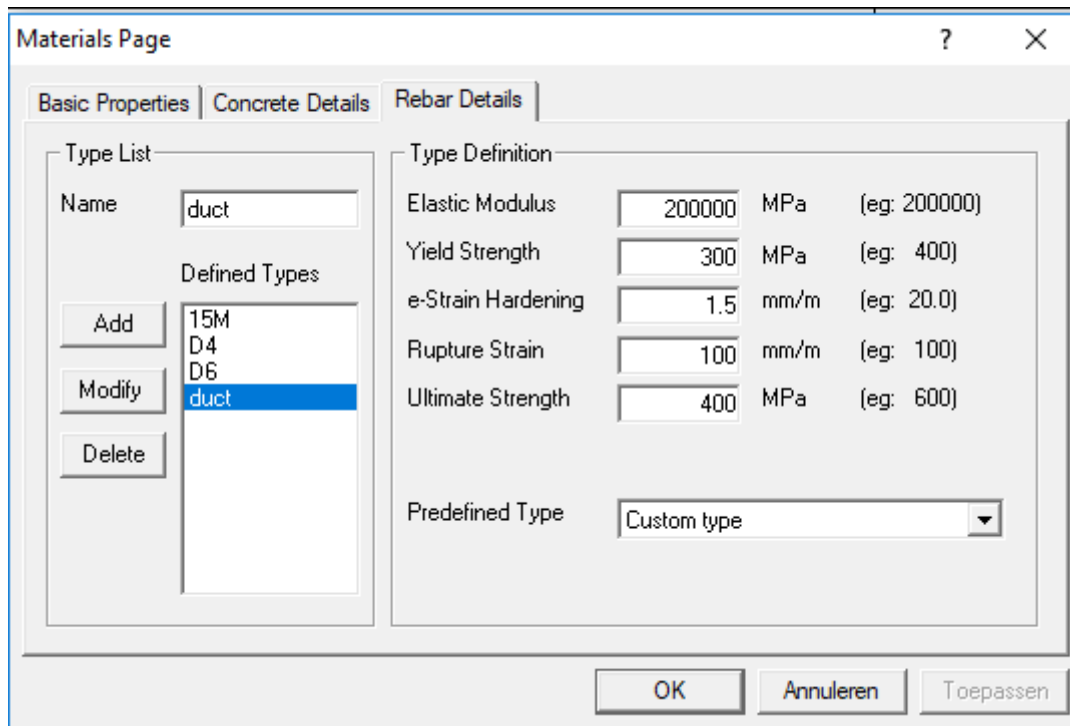


Figure B.10, steel material menu duct

11. Longitudinal reinforcement

Open the menu for longitudinal reinforcement configuration by double clicking on the reinforcement area.

Change the distance from the bottom for the top and bottom reinforcement and make sure that the rebar type is 15M.

The dialog box 'Define Longitudinal Reinforcement' is shown with the 'Individual Layers' tab selected. The 'Layer List' on the left contains a table with the following entries:

Name	Defined Types
bot	bot
	duct bot
	duct top
	top

The 'Layer Definition' section on the right is configured as follows:

- Number of Bars: 2 (eg: 4)
- Selection Type: Select bar by area
- Bar Designation: 15M (eg: 25M)
- Dist. from Bottom: 33 mm (eg: 75)
- Rebar Type: 15M

Buttons at the bottom include 'OK', 'Annuleren', and 'Toepassen'.

Figure B.11, longitudinal reinforcement configuration bottom

The dialog box 'Define Longitudinal Reinforcement' is shown with the 'Individual Layers' tab selected. The 'Layer List' on the left contains a table with the following entries:

Name	Defined Types
top	bot
	duct bot
	duct top
	top

The 'Layer Definition' section on the right is configured as follows:

- Number of Bars: 2 (eg: 4)
- Selection Type: Select bar by area
- Bar Designation: 15M (eg: 25M)
- Dist. from Bottom: 467 mm (eg: 75)
- Rebar Type: 15M

Buttons at the bottom include 'OK', 'Annuleren', and 'Toepassen'.

Figure B.12, longitudinal reinforcement configuration top

Also, the ducts can be added to the cross-section, make new reinforcement layers for the bottom ducts and the ducts on top. Fill in the number of ducts in the layer, the area and distance from the bottom. For the rebar type, it can be chosen between 15M (as assumed by Xie) or real duct material as defined above.

The dialog box 'Define Longitudinal Reinforcement' is shown with the 'Individual Layers' tab selected. The 'Layer List' on the left shows 'duct bot' as the selected layer. The 'Layer Definition' on the right is configured as follows:

Parameter	Value	Unit	Example
Number of Bars	1		(eg: 4)
Selection Type	<input checked="" type="checkbox"/> Select bar by area		
Bar Area	134	mm ²	(eg: 500 mm ²)
Dist. from Bottom	33	mm	(eg: 75)
Rebar Type	duct		

Buttons at the bottom: OK, Annuleren, Toepassen.

Figure B.13, Longitudinal reinforcement configuration duct bottom

The dialog box 'Define Longitudinal Reinforcement' is shown with the 'Individual Layers' tab selected. The 'Layer List' on the left shows 'duct top' as the selected layer. The 'Layer Definition' on the right is configured as follows:

Parameter	Value	Unit	Example
Number of Bars	1		(eg: 4)
Selection Type	<input checked="" type="checkbox"/> Select bar by area		
Bar Area	134	mm ²	(eg: 500 mm ²)
Dist. from Bottom	467	mm	(eg: 75)
Rebar Type	duct		

Buttons at the bottom: OK, Annuleren, Toepassen.

Figure B.14, Longitudinal reinforcement configuration duct top

12. Transverse reinforcement

Open the transverse reinforcement steel menu by double-clicking on the transverse reinforcement.

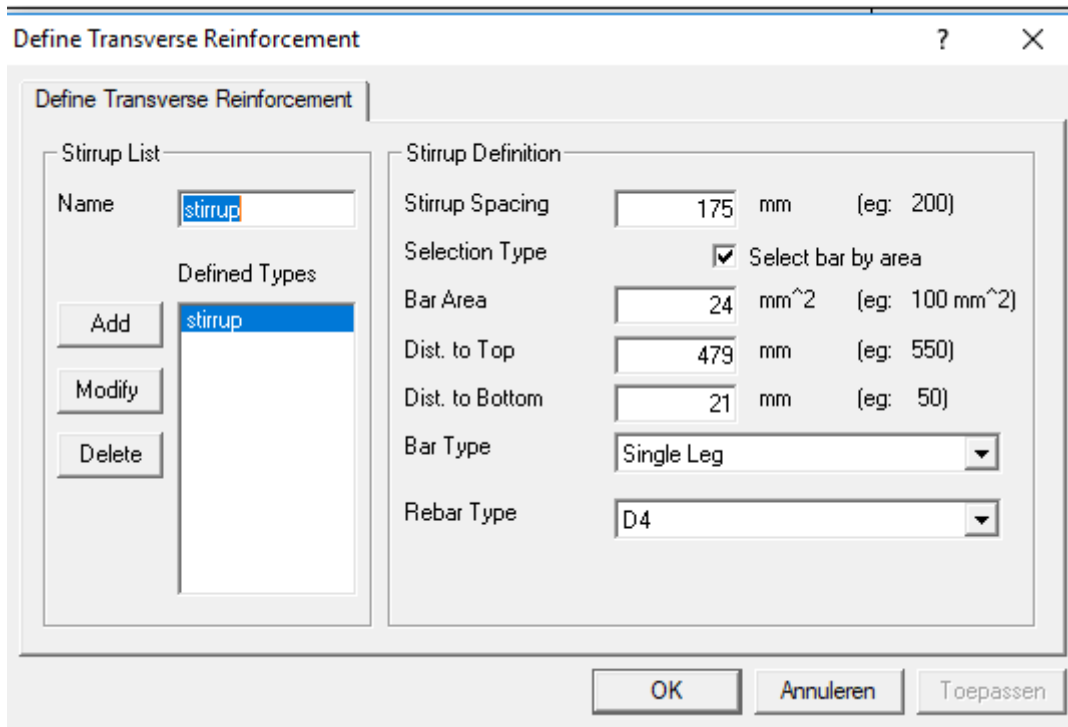


Figure B.15, Transverse reinforcement steel menu

Make sure the right distances to the top and bottom are taken into account and that the rebar type is correct. It is only possible to enter the web stirrups, so the horizontal stirrups are ignored.

13. Load

Open the loading menu, by double-clicking on the loading. For the axial load fill in the prestressing load (unbonded tendons) in the constant part and for the moment and shear fill in the increment, start at 0.7 1.

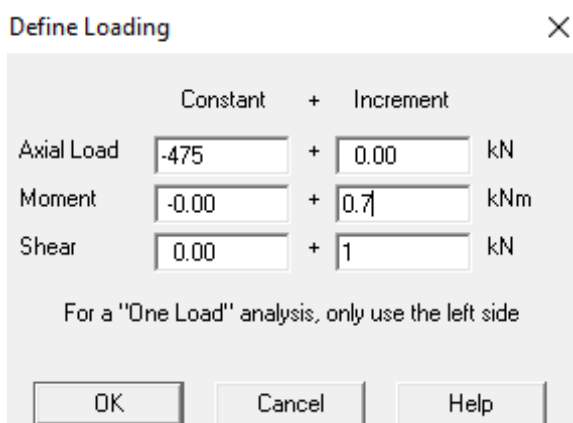


Figure B.16, Loading menu

An overview of the final input is given in Figure B.17

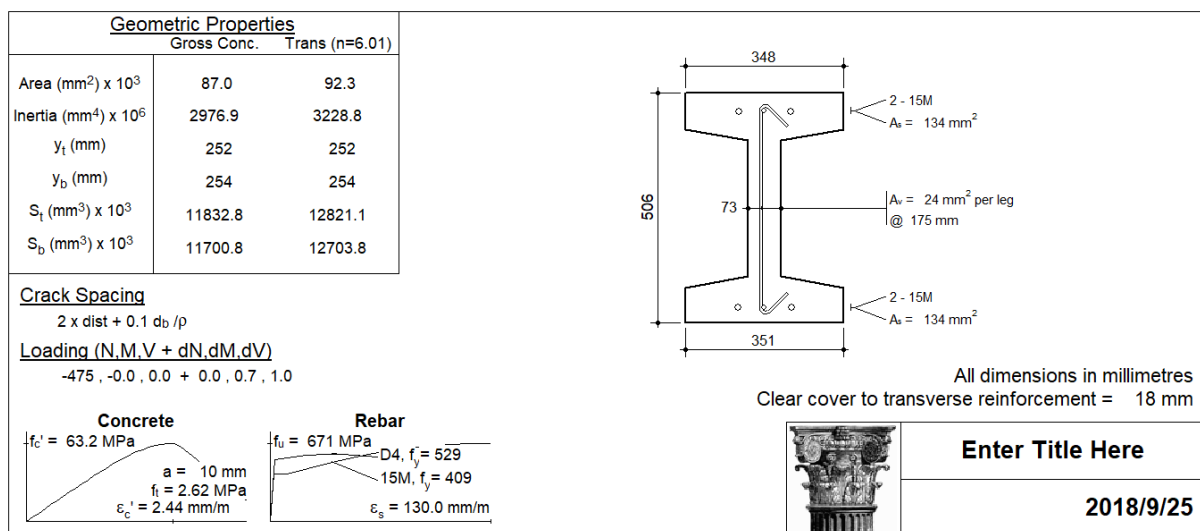


Figure B.17, Final input overview

Full member analysis input.

Click loads in the main menu and then full member properties.

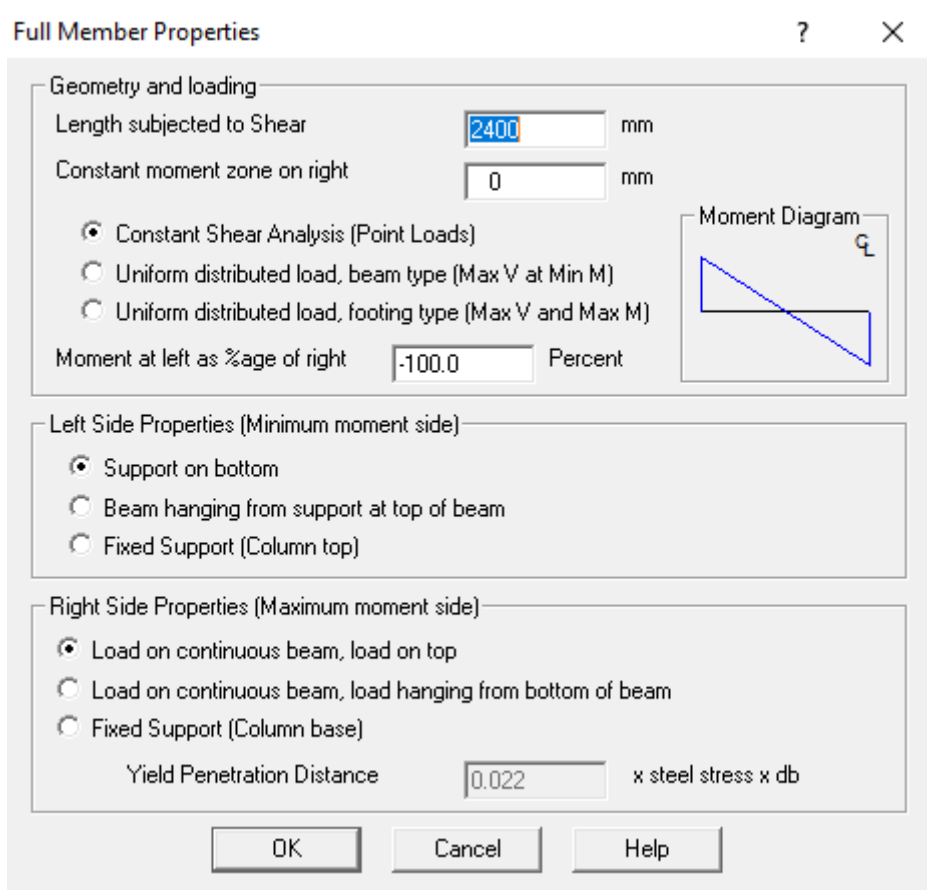


Figure B.18, Full member properties

For the length subjected to shear we enter the length between the support and the load (2400 mm). We do the analysis for a point load, so constant shear analysis is chosen. Because it is a continuous

beam there is a moment on both sides. To achieve this the left moment is taken as -100% of the right moment (equal sized but with an opposite sign). The left side is the support and the right side is the load on a continuous beam.

Checks:

General checks can be carried out to see if the input is correct:

- Check the concrete area, to see if the dimensions are correct.
- Double click in the middle of the final input screen and menu with the section information will pop up. From this the d value, the reinforcement area and reinforcement steel percentages can be checked.

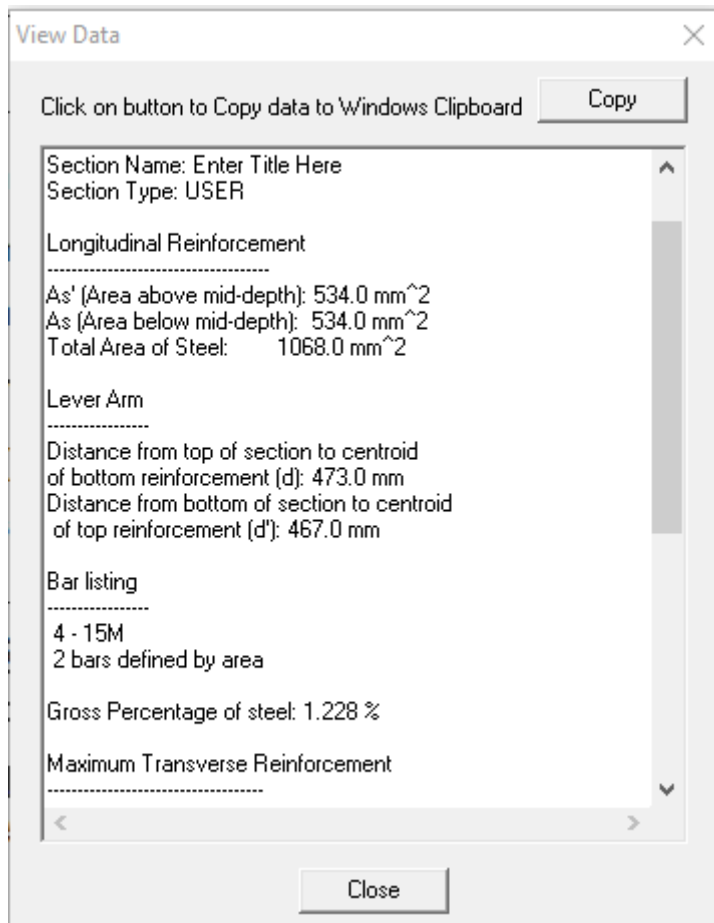


Figure B.19, Overview of the model data

- From the internal forces graph at the starting point the prestress input can be checked, extra check concrete stress distribution.

14. Run the analysis

Go to solve in the menu and choose Sectional Response, now an analysis with shear will be run. Also, a full member analysis can be run by choosing Member Response.

Results:

The results for the Sectional response consist of 9 plots for each load stage (Figure B.20). There are 4 possible sets of 9 graphs available: General (shear), no shear (internal forces), reinforcement (reinforcement stresses), cracking (crack widths, angle). It is possible to scroll through the results for the load stages by making use of PageUp and PageDown.

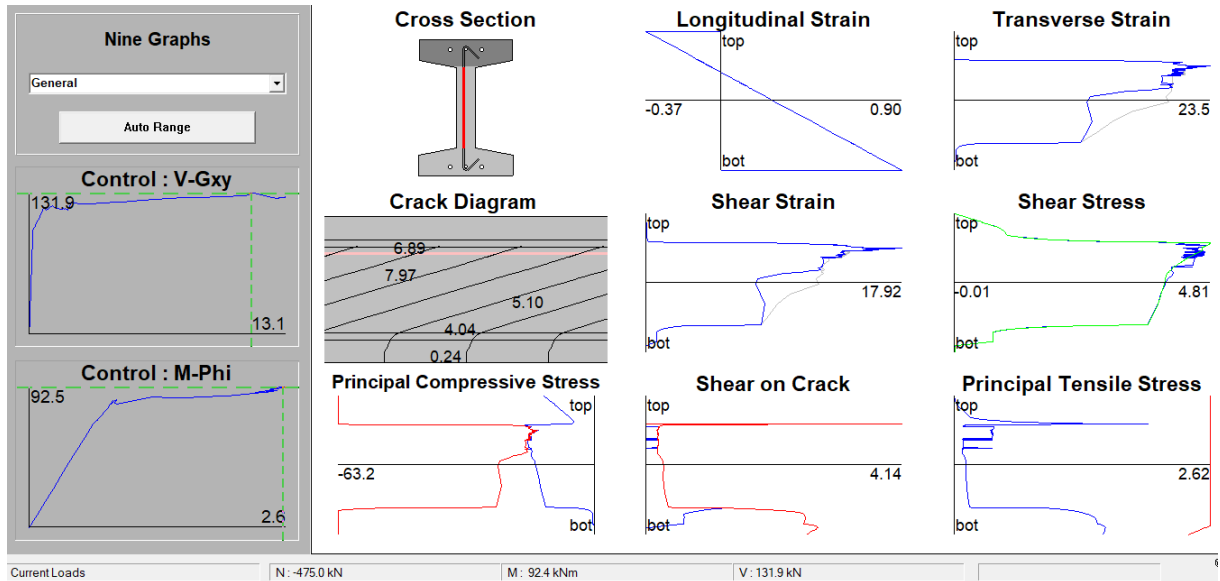



Figure B.20, General output

The full member response gives an overview of the results for the whole beam (Figure B.21). For the points on the M-V control graph, the sectional response can be seen by clicking on it. You go back to the nine graphs by clicking on the icon 

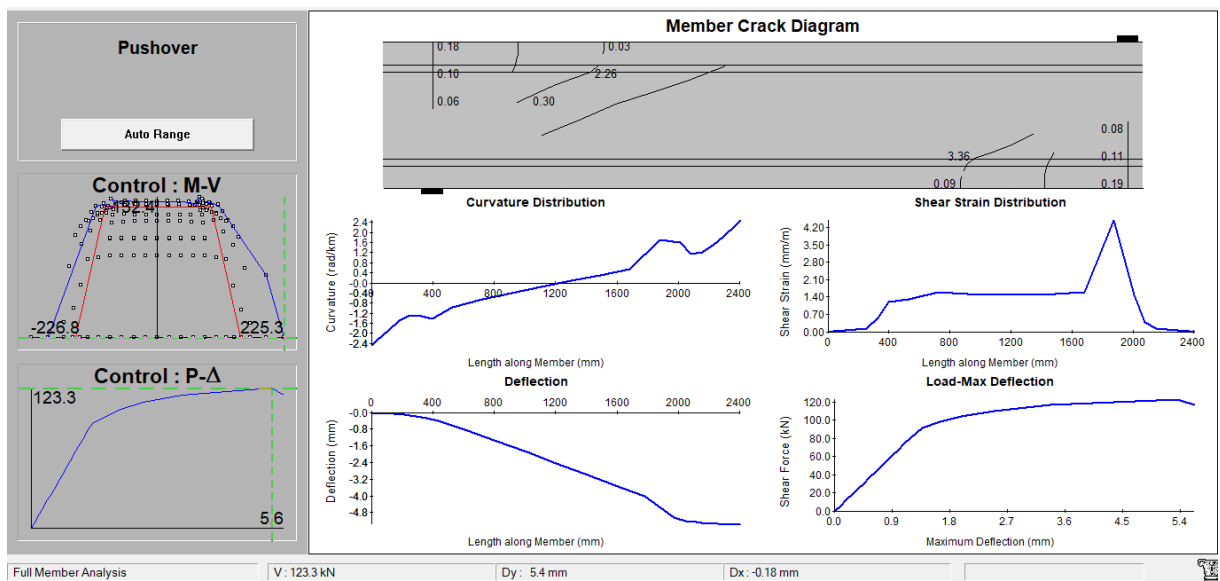


Figure B.21, Full member response output

C Example calculation Response values with MCFT

To demonstrate the relationship between the MCFT equations and the figures in Response an example calculation for one point in the cross-section of Lb2 (Xie, 2009) is made. The calculated values with the MCFT expressions, as presented below the graphs in Figure 2.18 to Figure 2.20, are compared with the actual outcomes of Response. A point at the middle of the cross-section is chosen (coordinate = -0.439) and the starting values (the values that are found from the iterative procedure) are shown in Table C.1.

ϵ_x	-0.2059 mm/m
ϵ_z	12.701 mm/m
γ_{xz}	7.2717 mm/m
τ	4.3464 MPa

Table C.1, Starting values

First, the principal strains are calculated from Mohr's circle:

	Calculated	R2k	
ϵ_1	13.655	13.655	mm/m
ϵ_2	-1.159		mm/m

Table C.2, Strains

The angle of the principal stresses is calculated:

$$\tan(\theta)^2 = \frac{-0.2059 + 1.159}{12.701 + 1.159}$$

	Calculated	R2k
θ	14.694	14.698

Table C.3, Cracking angle

Reinforcement stress:

There is no longitudinal reinforcement at this point of the cross-section so $\sigma_{sx} = 0$

The σ_{sz} is calculated from the stress-strain relationship of the reinforcement steel D4 (Table C.4) and the known ϵ_z .

Strain (ϵ_z)	Stress (σ_{sz})
10.116	547.72 MPa
13.8515	555.52 MPa

Table C.4, Stress-strain relationship D4

	Calculated	R2k
σ_{sz}	553.1177 MPa	553.229 MPa

Table C.5, Stress in z-direction

Crack spacing:

orthogonal crack spacings:

$$s_x = 2 \cdot 225.361 + 0.1 \cdot \frac{16}{0.023122}$$

$$\rho_z = \frac{24.2}{74.175} = 1.868 \cdot 10^{-3}$$

$$s_z = 2 \cdot 87.5 + 0.1 \cdot \frac{5.55}{1.868 \cdot 10^{-3}}$$

	Calculation	R2k
Sx	519.92 mm	506 mm
Sz	471.99 mm	473.962 mm

Table C.6, Crack spacing

Diagonal crack spacing:

$$s_\theta = \frac{1}{\frac{\sin 14.698}{506} + \frac{\cos 14.698}{473.962}}$$

	Calculation	R2k
s_θ	393.3652 mm	393.35 mm

Table C.7, Diagonal crack spacing

Crack width:

$$w = 393.3652 \cdot 13.655 \cdot 10^{-3}$$

	Calculation	R2k
w	5.371402 mm	5.3712 mm

Table C.8, Crack width

Stresses:

$$\Delta f_{c1} = f_1 - \rho_z (f_{yy} - f_{sy}) = 0.1084 - 0.187 \cdot 10^{-2} \cdot (529 - 553.229) = 0.15086$$

$\Delta f_{c1} > 0$ and there is no longitudinal reinforcement at the chosen point which means only options 2 or 3 of the crack check are left.

This means the shear on the crack is the minimum of the following:

$$\tau_{ci} = \frac{\Delta f_{c1}}{\tan \theta} = 0.5751$$

Shear stress on the crack:

$$\tau_{ci,max} = \frac{0.18 \cdot \sqrt{63.2}}{0.31 + \frac{24 \cdot 5.3712}{10+16}} = 0.2716 \text{ MPa}$$

The shear stress on the crack is governed by $\tau_{ci,max}$ this means there is slipping on the crack.

	Calculation	R2k
τ_{ci}	0.2716 MPa	0.2721 MPa

Table C.9, Shear on the crack

σ_1 is calculated out of MCFT equation 2 (Figure 2.1) with $\sigma_z = 0$. This is equivalent to the proposed equation at option 3 in the crack check.

$$\sigma_1 = 4.3464 \tan 14.698 - 0.187 \cdot 10^{-2} \cdot 553.229 = 0.1055$$

	Calculation	R2k
σ_1	0.1055 MPa	0.1084 MPa

Table C.10, Principal tensile stress

Principal compressive stress:

$$\sigma_2 = 4.3464 \cdot (\tan 14.698 + \cot 14.698) - 0.1084$$

Principle compressive capacity:

$$\sigma_2 = \frac{63.2}{0.8 + 170 \cdot 15.655 \cdot 10^{-3}} \cdot \left(2 \cdot \frac{-1.159 \cdot 10^{-3}}{2.44 \cdot 10^{-3}} - \left(\frac{-1.159 \cdot 10^{-3}}{2.44 \cdot 10^{-3}} \right)^2 \right)$$

	Calculation	R2k
σ_2	17.60154 MPa	-17.601 MPa
σ_2 capacity	-23.8036 Mpa	-23.65 MPa

Table C.11, Principal compressive stress

Steel stress at the cracks:

There is no longitudinal steel at this cross-section so the steel stress $\sigma_{sx,cr} = 0$.

$$\sigma_{sz,cr} = \frac{0.1084 - 0.2721 \cdot \tan 14.698}{0.187 \cdot 10^{-2}} + 553.229 = 573.029$$

	Calculation	R2k
$\sigma_{sz,cr}$	573.029 MPa	573.06 MPa

Table C.12, Stress on the crack

D Experiments and Response results

This appendix gives a description of the experimental properties entered in Response-2000 and their outcomes used for comparison. For every experiment a description of the failure, an overview of the parameters and 2 figures showing the load deformation response and the division of the parameters are given.

D.1 XIE

The beams LB2, LB3, LB6, LB8 and LB10 experimented on by Xie (Xie, 2009) are entered into Response.

Properties

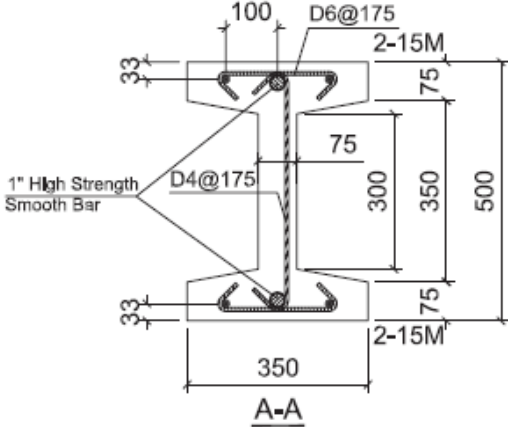
The input for the response calculation is gathered from Xie 2009

Concrete

cross-section

	Dimension (As build table 4.2 Xie 2009)(mm)
h	506
$h_{f_{top}}$	80
$h_{f_{bot}}$	76
$b_{f_{top}}$	348
$b_{f_{bot}}$	351
b_{web}	73
h_1 & h_2	25

Table D.1, Cross-sectional dimensions



Concrete properties (table 4.3 (Xie, 2009))

f_{cm} (MPa)	E_c (MPa)	f_t (Mpa)	ϵ_c' (mm/m)	a (p. 123)
63.2	39600	2.62	2.10	10

Table D.2, Concrete properties

Reinforcement

Longitudinal reinforcement

Place	kind	Cover (mm)	d (mm)	Distance from the bottom (mm)
Top	2-15M			467 mm ($c_{longitudinal} + d_v + \frac{\phi}{2}$)
Bottom	2-15M	33	473	33 mm

Table D.3, Longitudinal reinforcement

Stirrups

Place	kind	Distance from the bottom (mm)	Distance from the top (mm)
Top	D6@175	33	33
Bottom	D6@175	33	33
Web	D4@175	$21 (c_{longitudinal} - \frac{\phi}{2})$	$479 (\text{top reinforcement} + \frac{\phi_{longitudinal}}{2} + \frac{\phi_{stirrups}}{2})$

Table D.4, Transverse reinforcement

Reinforcement properties (table 4.6 (Xie, 2009))

	f_y (MPa)	f_u (MPa)	ϵ_y (mm/m)	ϵ_u (mm/m)	E_s (MPa)
15M	409	671	2.05	130	201100
D4	529	581	2.65	40	195800
D6	609	657	3.05	45	200330

Table D.5, Reinforcement properties

Prestress

kind	A_p (p. 126) (mm ²)	d(table 4.2 Xie) (mm)	Cover (mm)	f_y (MPa) (table 4.6 Xie)	f_u (MPa) (Table 4.6 Xie)	P (kN) (Table 4.2 Xie)
2x 1" smooth bar (unbonded)	507	473	33	972	1074	-475
ducts	134	473	33	300	400	

Table D.6, Prestressing properties

Load

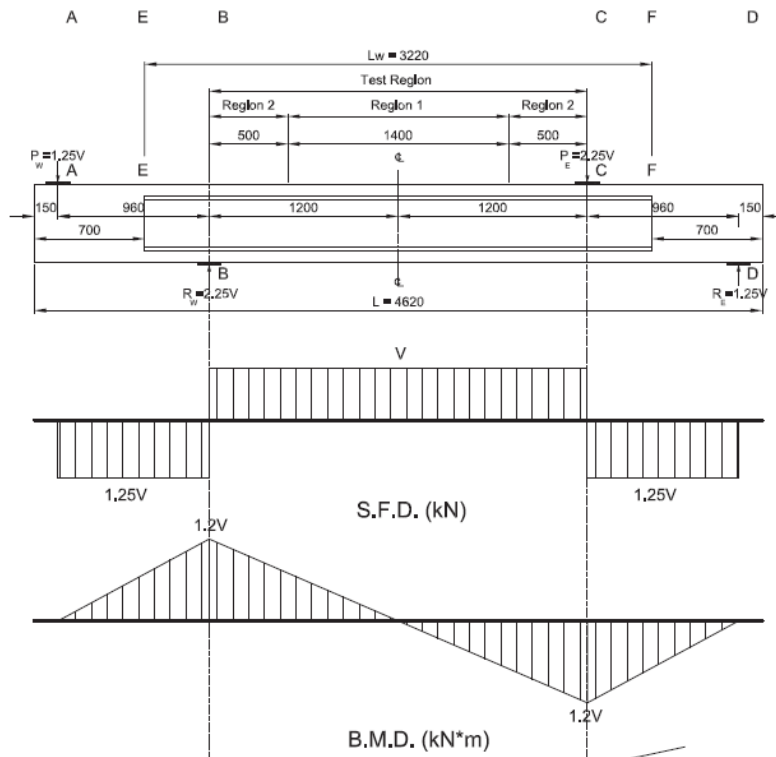


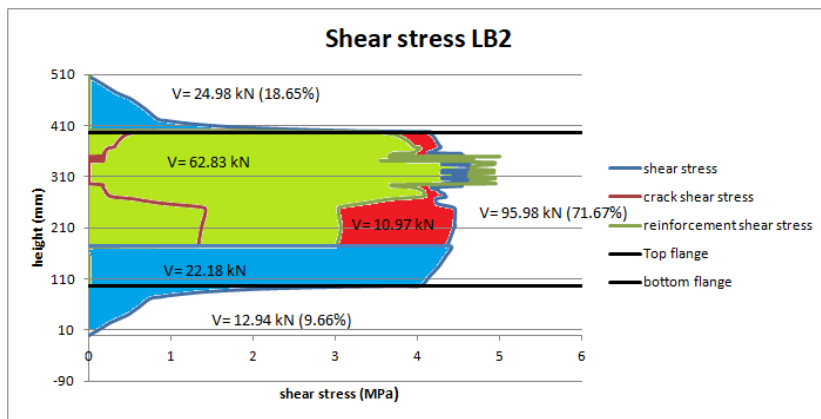
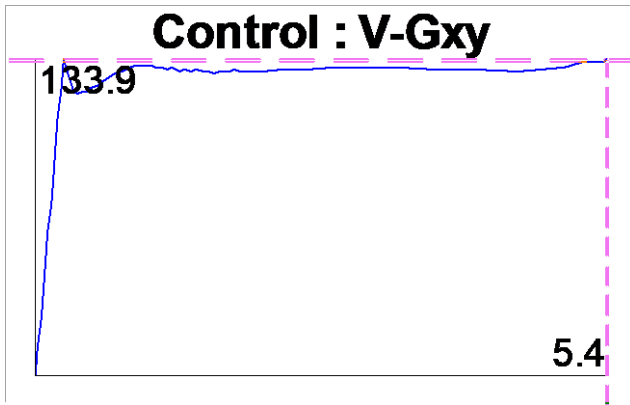
Figure D.1, Load distribution (Xie, 2009)

Figure D. shows the used combination of moment and shear (Figure 4.1 (Xie, 2009)). The beam must fail in Region 1, due to the chosen transverse reinforcement (Xie, 2009), P. 111). The following combinations will be calculated within region 1.

Results

LB2

After diagonal tension web shear cracking the shear resistance drops a bit and then starts increasing again. The reinforcement is yielding and the maximum shear on the crack becomes smaller. After the crack slips ($\tau_{ci} = \tau_{ci,max}$) the stirrups stress at the crack starts increasing and the principal compressive capacity starts decreasing. At the maximum load the stirrups rupture (stress is higher than rupture stress) while the concrete is near crushing ($\epsilon_c = -2.3 < -2.44$). So the failure mechanism is Rupture of the stirrups this is in agreement with the experimental failure mechanism as described by Xie (Xie, 2009) in paragraph 4.6.



Cross Section

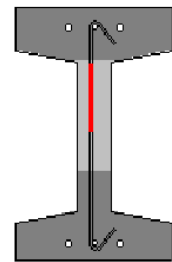
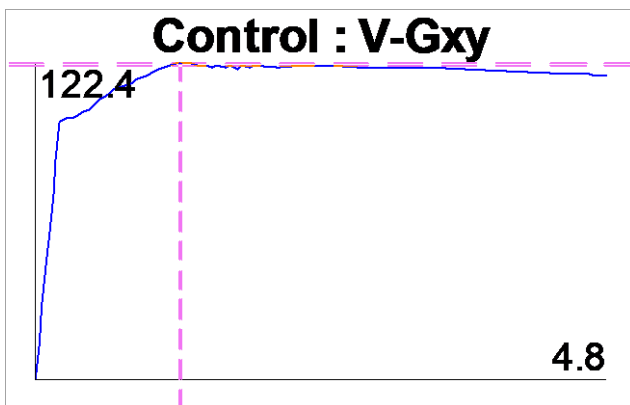


Figure D.2, Contribution of the concrete and steel part to the shear stress over the beam for LB2

LB3

After diagonal tension cracking the stirrup on the crack is yielding, the shear resistance keeps increasing while the maximum shear on the crack decreases. The maximum load is reached just after the moment that the crack slips. After this the stress in the stirrups on the crack increases and the principal compressive stress capacity decreases and the top flange cracks. The crack width increases rapidly after the maximum load. The reinforcement does not rupture at the last load stage nor does the concrete crush. The failure mechanism is slipping of the crack and major cack opening this is in agreement with the experimental failure mechanism as described by Xie (Xie, 2009) in paragraph 4.6.



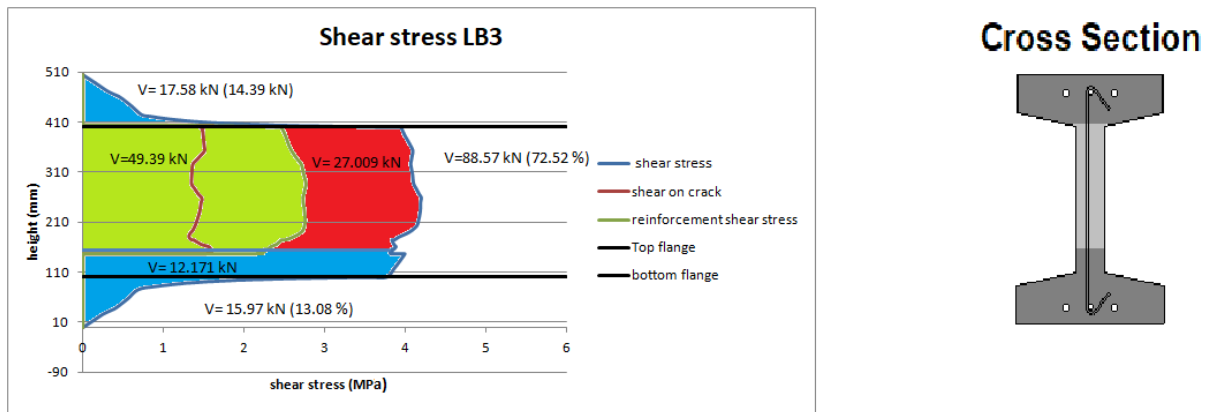


Figure D.3 Contribution of the concrete and steel part to the shear stress over the beam for LB3

LB6

After diagonal tension cracking the shear resistance drops a bit and then starts increasing again. The reinforcement yields and the maximum shear on the crack start decreasing. After slipping of the crack the stirrup stress at the crack increases and the principal compressive capacity decreases. When the maximum load is reached the web concrete crushes ($\epsilon_c = -2.56 > -2.44$). The stirrup stress is 568 N/mm^2 at this moment. After the maximum load the strain increases and the stirrups rupture. The failure mechanism is crushing and rupture of the stirrups this is not in agreement with the experimental failure mechanism which is major crack opening and buckling of the flanges as described by Xie (Xie, 2009) in paragraph 4.6.

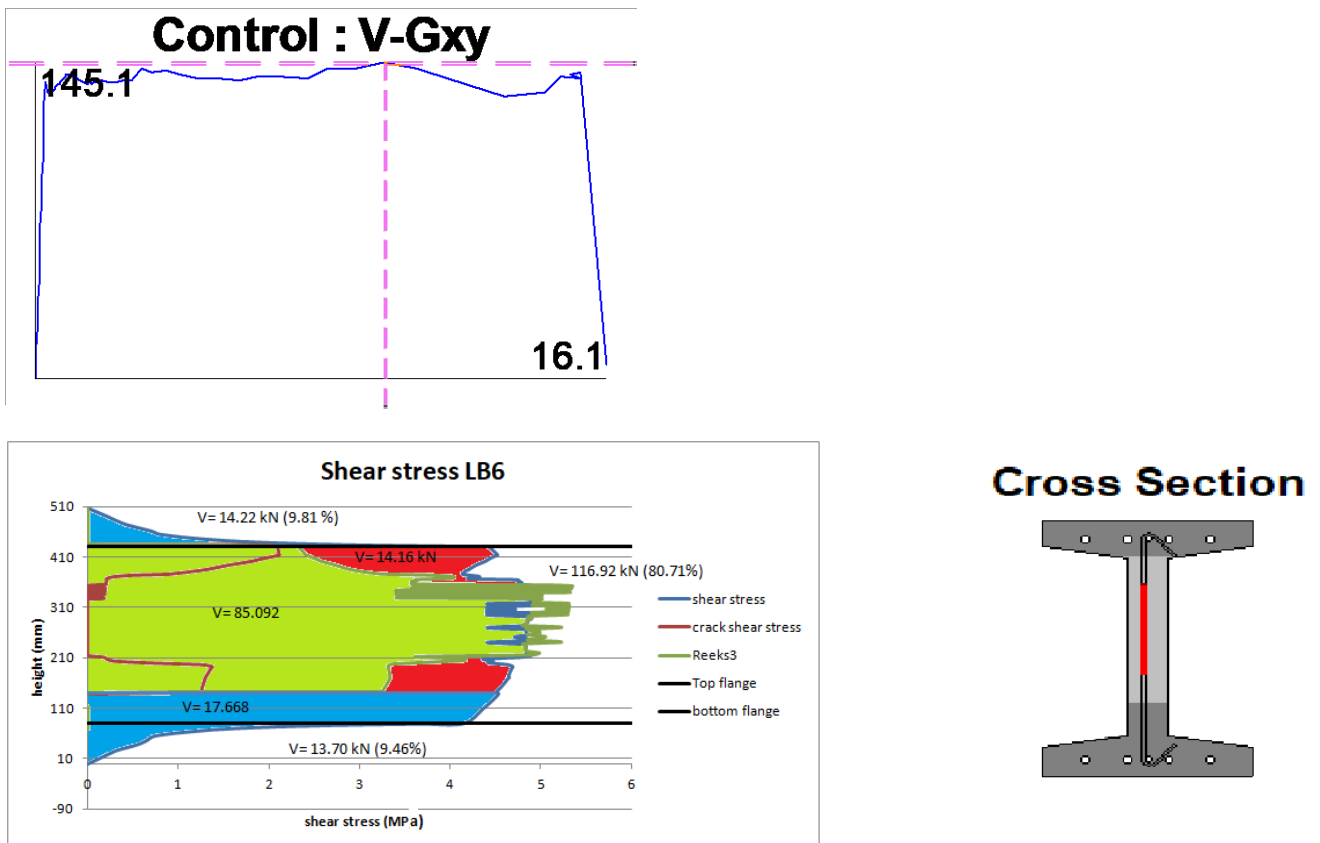


Figure D.4, Contribution of the concrete and steel part to the shear stress over the beam for LB6

LB7

After diagonal tension cracking the shear resistance increases, the reinforcement on the crack yields and the maximum shear on the crack decreases. After the crack slips the load decreases again and while the stirrup stress on the crack increases and the principal compressive capacity decreases the shear resistance increases again. The maximum load is reached at the point where the stirrup stress at the crack reaches its rupture stress, the principal compressive stress does not reach the capacity. After this, the reinforcement fails. The failure mechanism is rupture of the stirrups this is in agreement with the experimental failure mechanism as described by Xie (Xie, 2009) in paragraph 4.6.

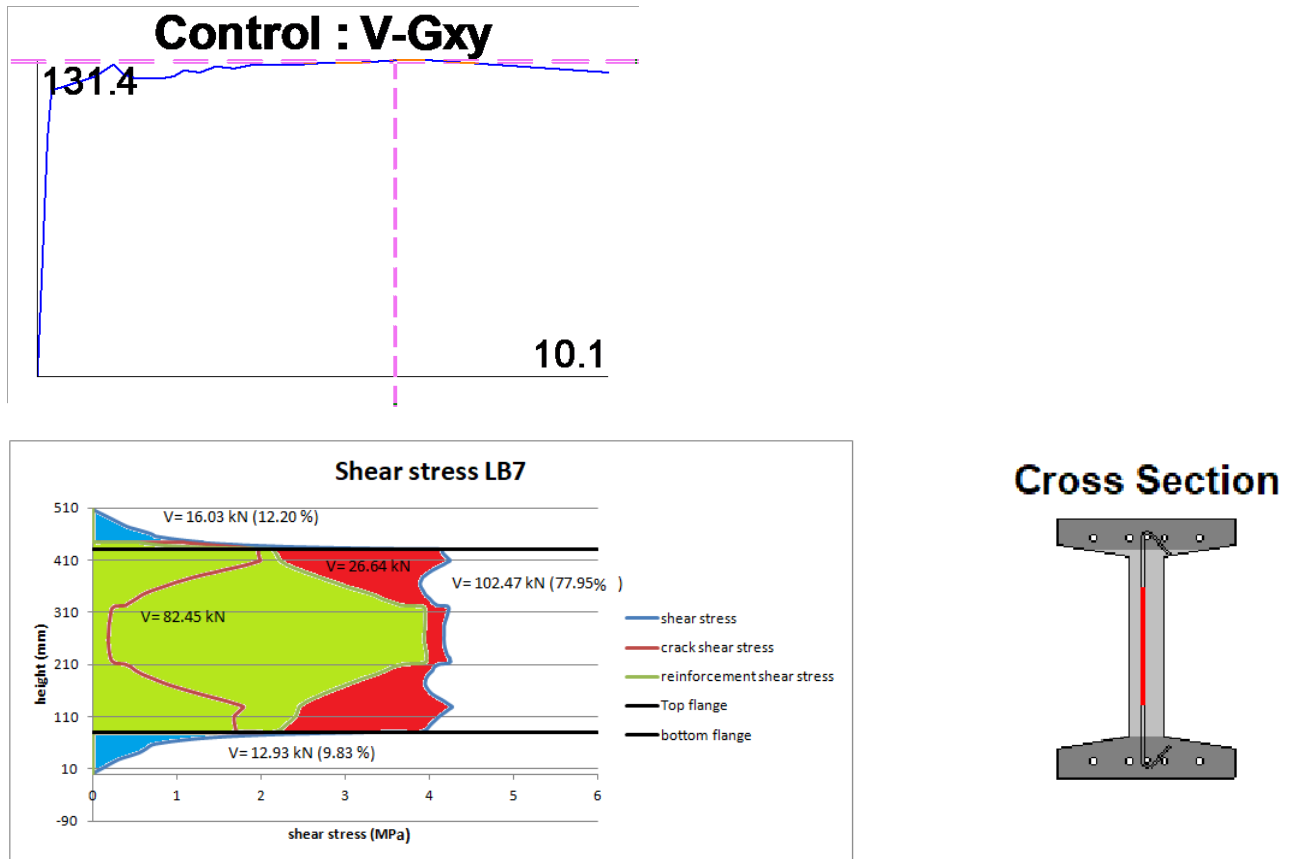


Figure D.5, Contribution of the concrete and steel part to the shear stress over the beam for LB7

LB8

After diagonal tension cracking the load increases, the stirrups at the crack yields and the maximum shear on the crack decreases. The maximum load is reached just before the shear on the crack reaches the maximum shear on the crack. After this the shear resistance drops and the top flange crack, the crack width increases enormously. The failure mechanism is slipping of the crack and major crack opening this is in agreement with the experimental failure mechanism as described by Xie (Xie, 2009) in paragraph 4.6.

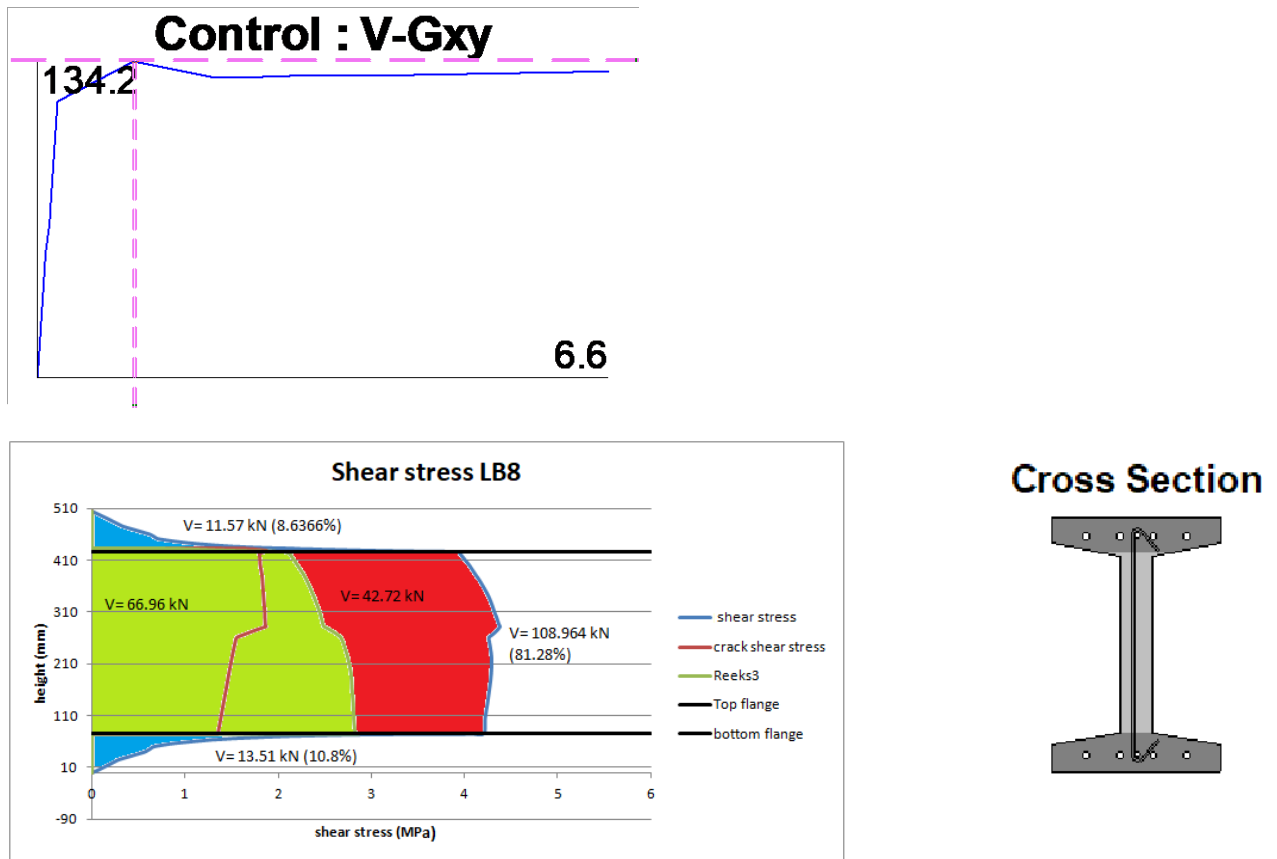
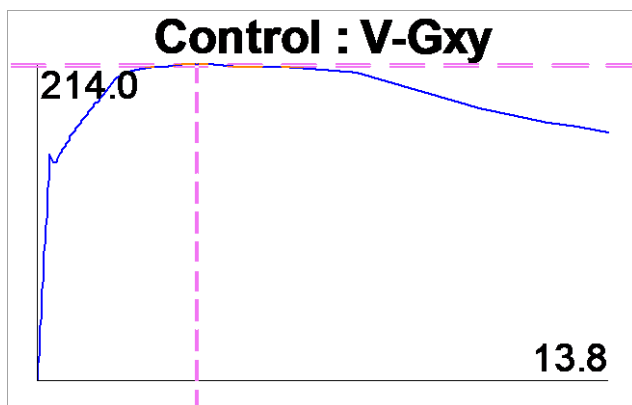


Figure D.6, Contribution of the concrete and steel part to the shear stress over the beam for LB8

LB10

After diagonal tension cracking the load increases, the stirrup on the crack yields and the maximum shear on the crack decreases. When the crack slips the stirrups stress at the crack starts increasing while the principal compressive capacity decreases. When the maximum load is reached the principal compressive stress does not reach its capacity nor does the stirrup. After the maximum load the concrete crushes in the web ($\epsilon_c = -3.5 > -2.44$), while the stirrups stress is just below rupture stress (579.8 kN). The failure mechanism is crushing of the web concrete this is not in agreement with the experimental failure mechanism which is major crack opening and buckling of the flanges as described by Xie (Xie, 2009) in paragraph 4.6.



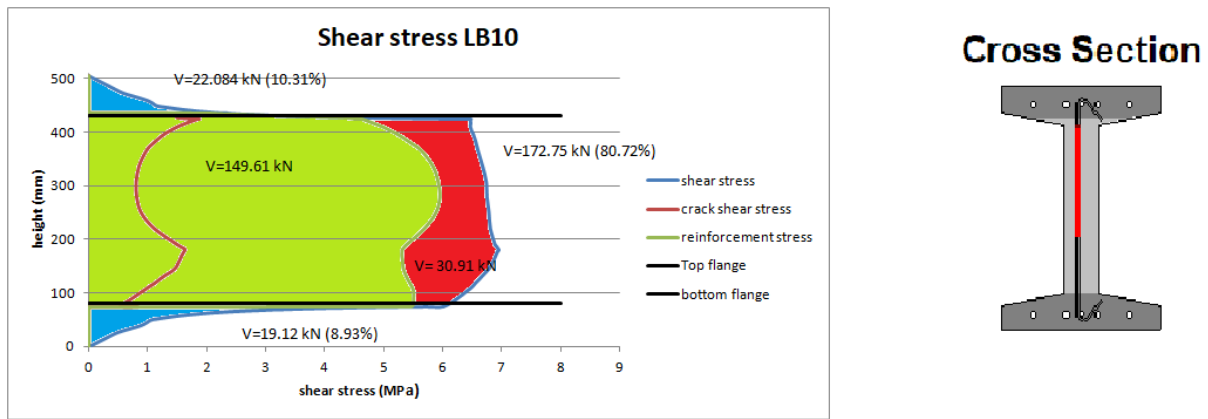


Figure D.7, Contribution of the concrete and steel part to the shear stress over the beam for LB10

D.2 Choulli

Beams HAP1TE, HAP1TW, HAP2TW, HCP1TE, HCP1TW, HCP2TE and HCP2TW described in Choulli (Choulli, 2005) are modelled in Response as follows:

Cross-section

All beams have the same cross-section.

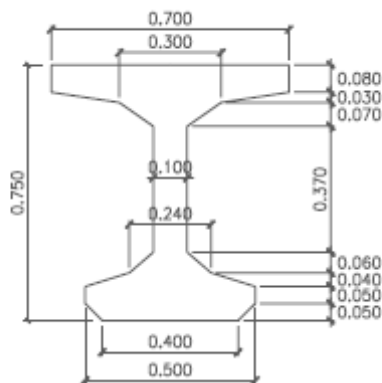


Figure D.8, Cross-section (m) (Choulli, 2005)

Concrete properties (Annex A, table 3 (Choulli, 2005))

	f_{cm} (MPa)	E_c (MPa)	f_t (Mpa)	$\epsilon_c'^*$ (mm/m)	a_g^{**} (mm)
HAP1TE	91.23	39855	5.05	2.82	0
HAP1TW	91.23	39855	5.05	2.82	0
HAP2TW	95.97	39569	5.20	2.88	0
HCP1TE	81.17	33675	5.86	2.69	0
HCP1TW	81.17	33675	5.86	2.69	0
HCP2TE	90.24	39788	5.20	2.81	0
HCP2TW	90.24	39788	5.20	2.81	0

Table D.7, Concrete properties

* automatic calculated

** high strength concrete

Reinforcement

The reinforcement configuration depends on if it is a east or a west side beam. East: beam names ending on E and west beam names ending on a W.

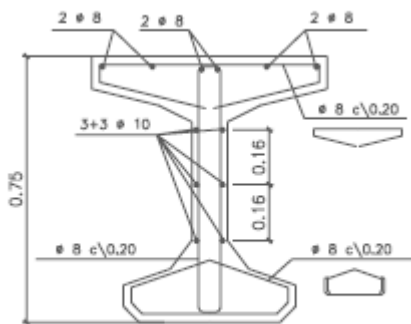


Fig 3.2(a): Transversal reinf. of the west side

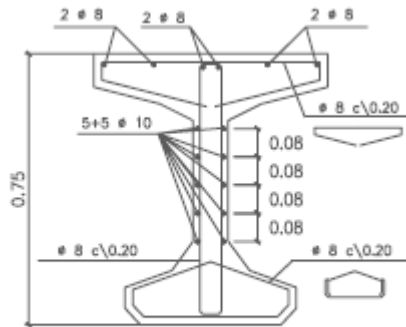


Fig 3.2(b): Transversal reinf. of the east side

Figure D.9, Reinforcement configuration (Choulli, 2005)

Longitudinal reinforcement

Place	kind	Distance from the bottom (mm)
Top	6 \emptyset 10	718
Web west	3 · 2 \emptyset 10	200, 360 and 520
Web east	5 · 2 \emptyset 10	200, 280, 360, 440, 520

Table D.8, Longitudinal reinforcement properties

Stirrups

Place	kind	Distance from bottom to bottom of the reinforcement (mm)	Distance from bottom to top of the reinforcement (mm)
Top	\emptyset 8 – 200 open stirrup	730	731
Bottom	\emptyset 8 – 200 Open stirrup	20	100
Web	\emptyset 8 – 200 Closed stirrup	20	730

Table D.9, Transverse reinforcement configuration

Reinforcement properties (Annex B)

	f_y (MPa)	f_u (MPa)	ϵ_{sh} (mm/m)	ϵ_u (mm/m)	E_s (MPa)
\emptyset 8- B500S	525.38	660.63	2.6	269	200000
\emptyset 10- B400SD	581	691	2.9	240	200000

Table D.10 Reinforcement properties

Prestress

There are two prestress configurations one with high prestress (16 tendons) and one with lower prestress (10 tendons)

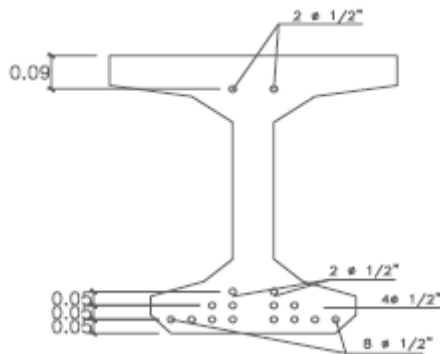


Figure D.10, Prestress configuration, HCP1TE, HCP1TW, HAP1TE, HAP1TW $P=1859$, $\epsilon = 6.40 \text{ mm/m}$ (Choulli, 2005)

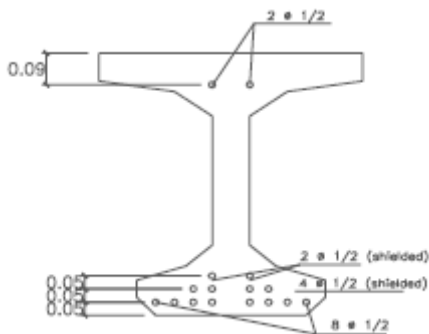


Figure D.11, Prestress configuration HCP2TE, HCP2TW, HAP2TW $P=1225$, $\epsilon = 6.67 \text{ mm/m}$ (Choulli, 2005)

kind	A_p (mm^2)	ϵ_u (%)	f_y (MPa)	f_u (MPa)	A	B	C
Y1860 S7 13		5.17	1776	1941.4	0.02	108.65	10

Table D.11, Prestress properties

Results

HAP1TE

After diagonal tension cracking the force increases, the stirrup at the crack yields and the maximum shear on the crack decreases. Also, the principal compressive stress starts decreasing. The maximum load is reached when the crack slips for the first time. The principal compressive stress and the stirrup stress at the crack do not reach their capacity. After this, the shear resistance decreases and the principal compressive stress reaches its capacity ($\epsilon_c = -6.36 > -2.74$), while the stirrup stress at the crack does not reach its maximum ($556.8 < 661$). The failure mechanism is crushing of the web concrete this is in agreement with the experimental failure mechanism as described in (Choulli, 2005) Annex A.74.

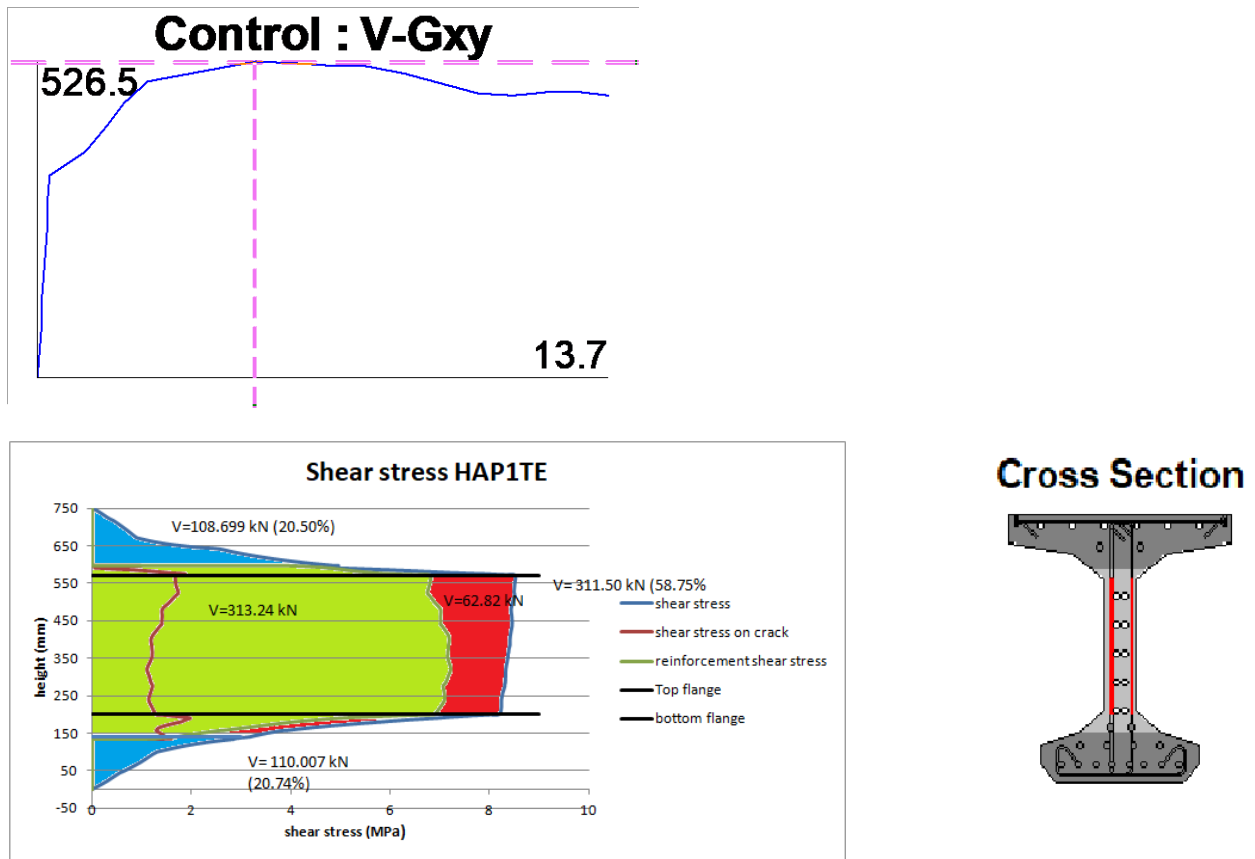
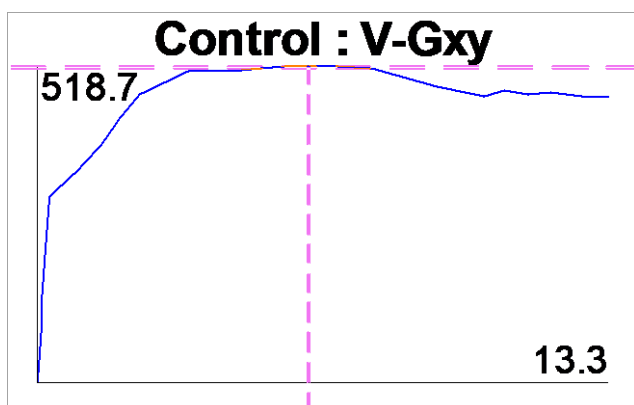
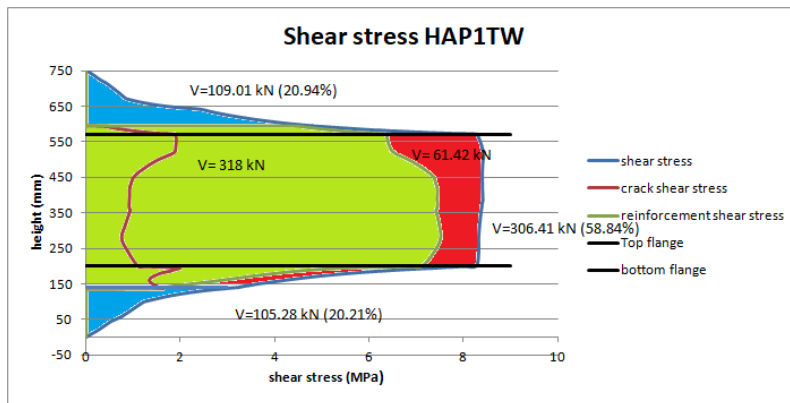


Figure D.12, Contribution of the concrete and steel part to the shear stress over the beam for HAP1TE

HAP1TW

After diagonal tension cracking the force increases, the stirrup at the crack yields and the maximum shear on the crack decreases. Also, the principal compressive stress starts decreasing. When the maximum load is reached (already after the crack has slipped), the principal compressive stress and the stirrup stress at the crack do not reach their capacity. After this, the shear resistance decreases and the principal compressive stress reaches its capacity ($\epsilon_c = -16.870 > -2.82$), while the stirrup stress at the crack does not reach its maximum ($556.9 < 661$). The failure mechanism is crushing of the web concrete, this is in agreement with the experimental failure mechanism as described in (Choulli, 2005) Annex A.83.





Cross Section

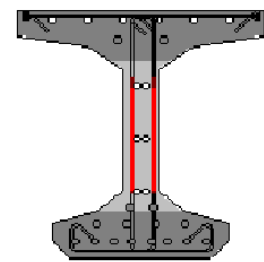
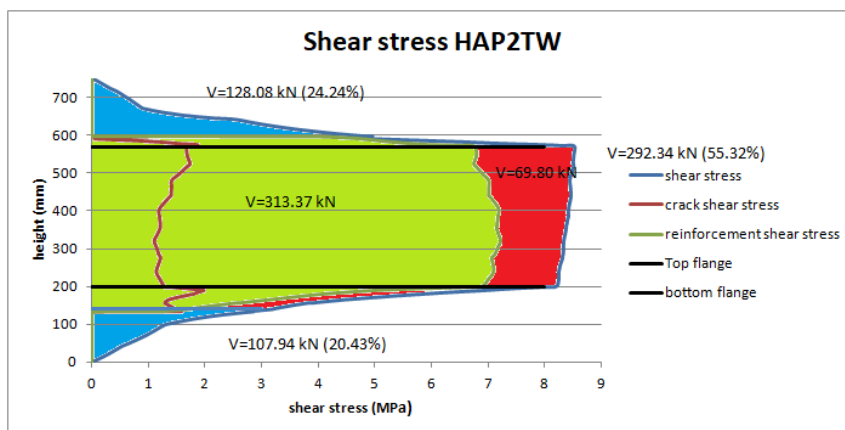
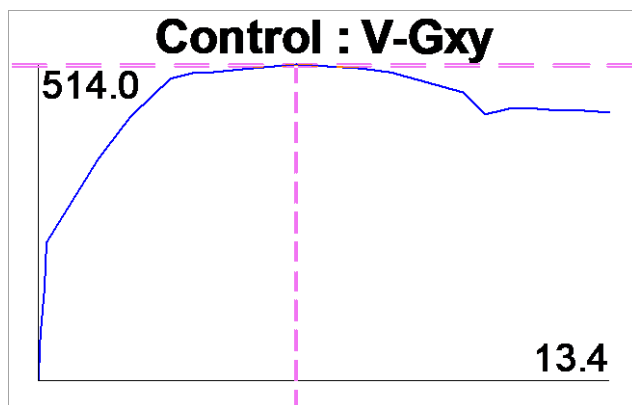


Figure D.13, Contribution of the concrete and steel part to the shear stress over the beam for HAP1TW

HAP2TW

After diagonal tension cracking the force increases, the stirrup at the crack yields and the maximum shear on the crack decreases. Also the principal compressive stress starts decreasing. When the maximum load is reached (already after the crack has slipped), the principal compressive stress and the stirrup stress at the crack do not reach their capacity. After this the shear resistance decreases and the principal compressive stress reaches its capacity ($\epsilon_c = -4.213 > -2.82$), while the stirrup stress at the crack does not reach its maximum ($558.3 < 661$). The failure mechanism is crushing of the web concrete this is in agreement with the experimental failure mechanism as described in (Choulli, 2005) Annex A.63.



Cross Section

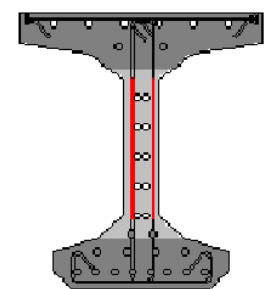
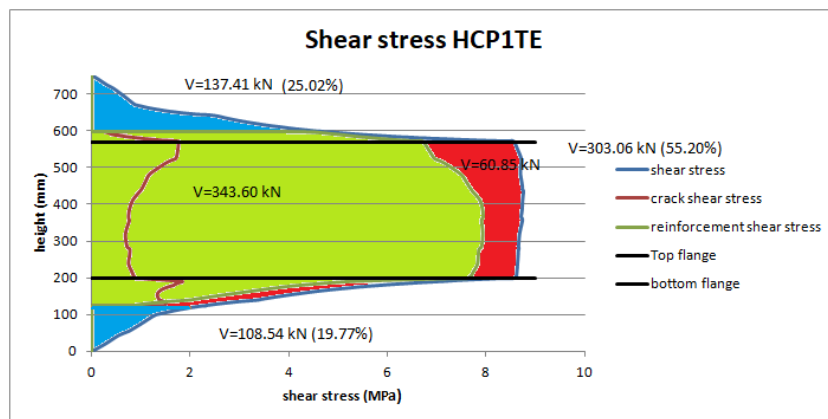
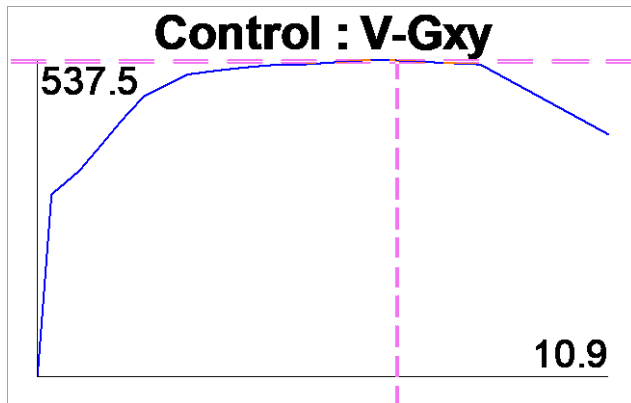


Figure D.14, Contribution of the concrete and steel part to the shear stress over the beam for HAP2TW

HCP1TE

After diagonal tension cracking the force increases, the stirrup at the crack yields and the maximum shear on the crack decreases. Halfway the first increasing branch the principal compressive capacity starts to decrease. After slipping of the crack the slope of the branch decreases. At maximum load, the principal compressive stress has reached the principal compressive capacity ($\epsilon_c = -3.093 > -2.69$), while the stirrup stress has not reached its capacity ($556.2 < 661$). The failure mechanism is crushing of the web concrete this is in agreement with the experimental failure mechanism as described in (Choulli, 2005) Annex A.95.



Cross Section

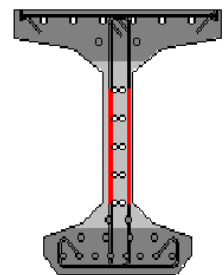


Figure D.15, Contribution of the concrete and steel part to the shear stress over the beam for HCP1TE

HCP1TW

After diagonal tension cracking the force increases, the stirrup at the crack yields and the maximum shear on the crack decreases. Halfway the first increasing branch the principal compressive capacity starts to decrease. After slipping of the crack the slope of the branch decreases. When the maximum load is reached the principal compressive stress and the stirrup stress at the crack do not reach their capacity. After this, the shear resistance decreases and the principal compressive stress reaches its capacity ($\epsilon_c = -18.732 > -2.61$), while the stirrup stress at the crack does not reach its maximum ($558.3 < 661$). The failure mechanism is crushing of the web concrete this is in agreement with the experimental failure mechanism as described in (Choulli, 2005) Annex A.105.

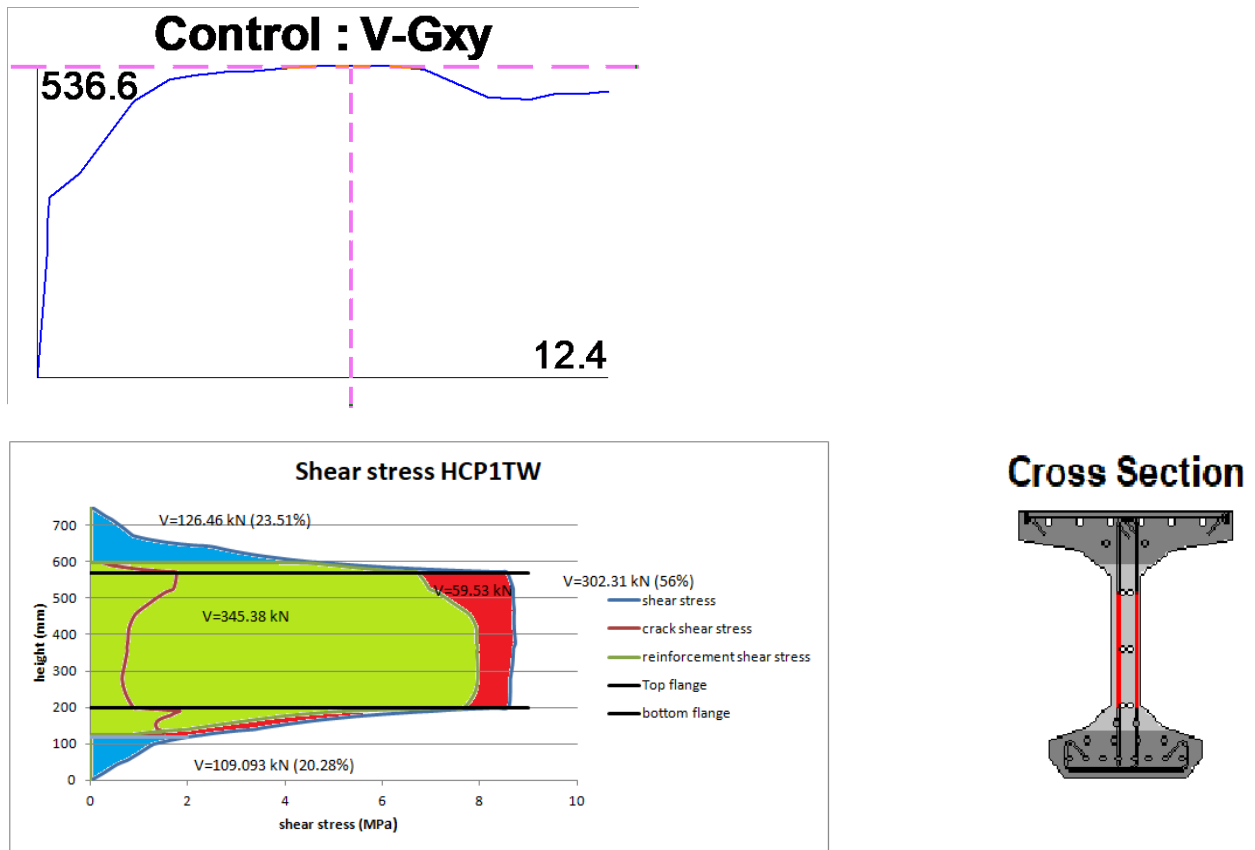
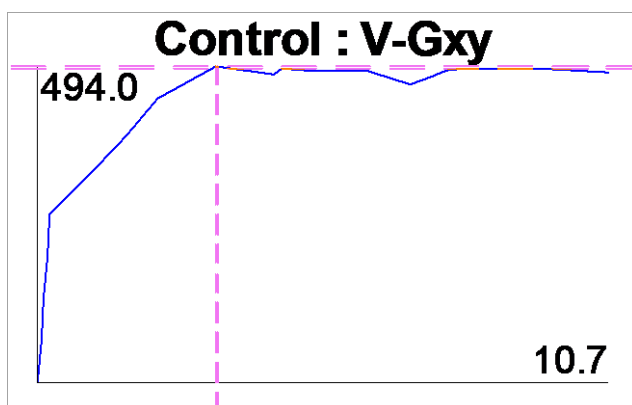


Figure D.16, Contribution of the concrete and steel part to the shear stress over the beam for HCP1TW

HCP2TE

After diagonal tension cracking the force increases, the stirrup at the crack yields and the maximum shear on the crack decreases. Also, the principal compressive stress starts decreasing. The maximum load is reached when the crack slips for the first time. The principal compressive stress and the stirrup stress at the crack do not reach their capacity. After this, the shear resistance decreases and the principal compressive stress reaches its capacity ($\epsilon_c = -3.038 > -2.72.$), while the stirrup stress at the crack does not reach its maximum ($554.0 < 661$). The failure mechanism is crushing of the web concrete this is in agreement with the experimental failure mechanism as described in (Choulli, 2005) Annex A.35.



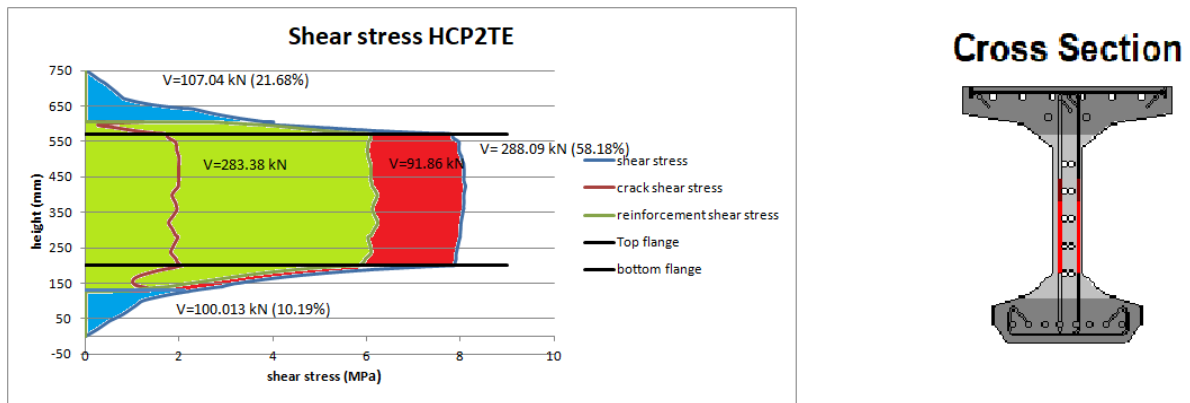


Figure D.17, Contribution of the concrete and steel part to the shear stress over the beam for HCP2TE

HCP2TW

After diagonal tension cracking the force increases, the stirrup at the crack yields and the maximum shear on the crack decreases. Also the principal compressive stress starts decreasing. When the maximum load is reached (already after the reinforcement has slipped), the principal compressive stress and the stirrup stress at the crack do not reach their capacity. After this the shear resistance decreases and the principal compressive stress reaches its capacity ($\epsilon_c = -3.005 > -2.82$), while the stirrup stress at the crack does not reach its maximum ($553.8 < 661$). The failure mechanism is crushing of the web concrete this is in agreement with the experimental failure mechanism as described in (Choulli, 2005) Annex A.44.

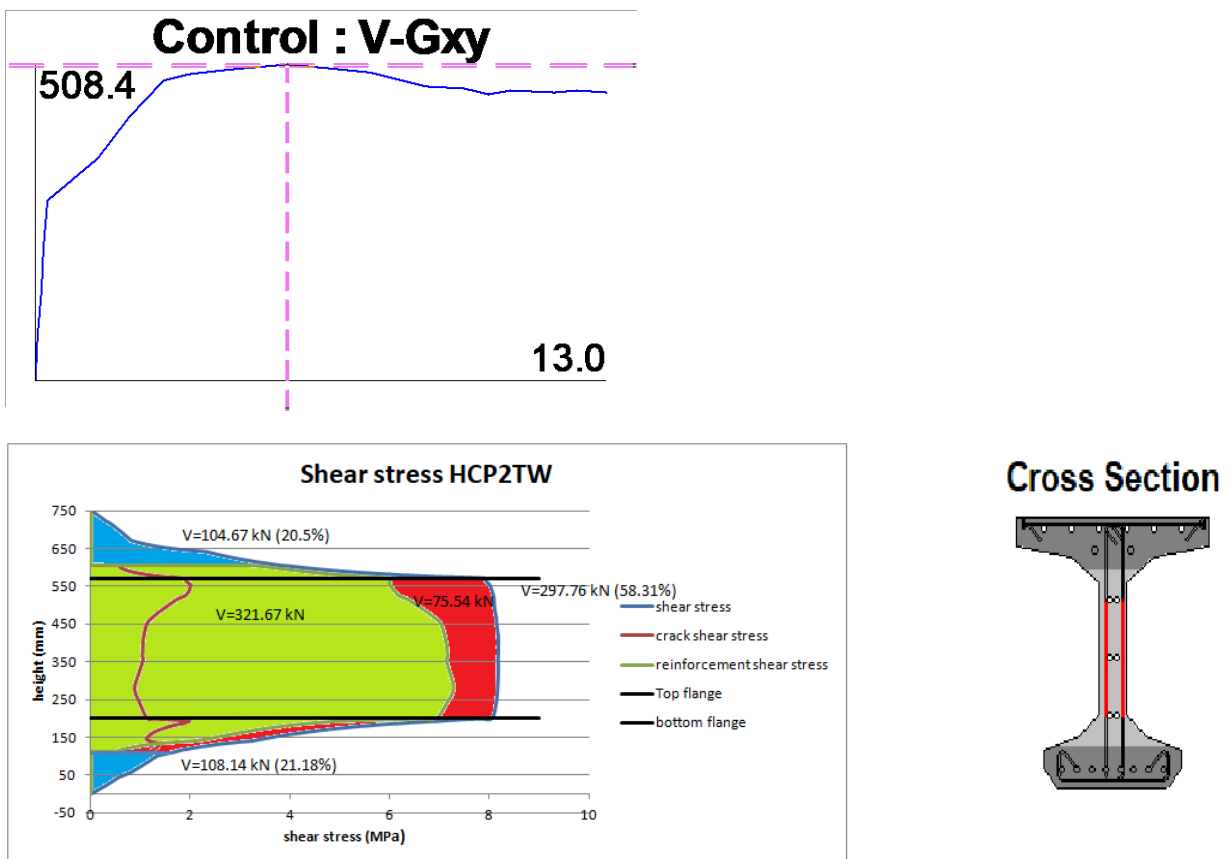


Figure D.18, Contribution of the concrete and steel part to the shear stress over the beam for HCP2TW

D.3 Hanson

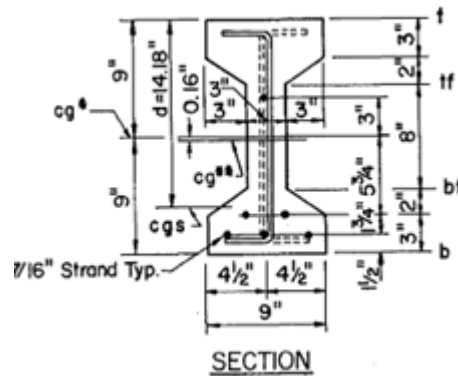
For beams FX1A, FX1B, F1A, F1B, F2A, F2B, F3A, F3B, F4A, F4B, F5A, F5B, F7A, F10A, F11A, F19A, F19B as experimented on by Hanson (Hanson & Hulbos, 1965), the following properties are entered into Response.

Concrete

cross-section

	Dimension (mm)
h	457.2
$h_{f_{top}}$	76.2
$h_{f_{bot}}$	76.2
$b_{f_{top}}$	229
$b_{f_{bot}}$	229
b_{web}	76
h_1 & h_2	50.8

Table D.12, Concrete cross-section



Reinforcement ((Hanson & Hulbos, 1965)fig. 5.)

Reinforcement properties

	f_y (MPa)	f_u (MPa)	ϵ_{sh} (mm/m)	ϵ_u (mm/m)	E_s (MPa)
#2	410	591	19.3	210	164095
#3	360	540	22.9	70	168177
3/16	298	386	20	34	166799

Table D.13, Transverse reinforcement properties

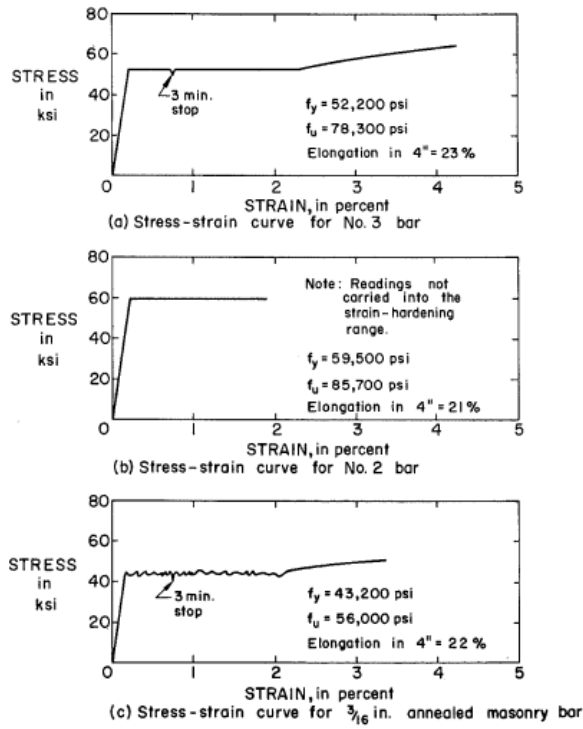


Figure D.19, Stress strain diagram transverse reinforcements (Hanson & Hulbos, 1965)

Prestress ((Hanson & Hulbos, 1965)fig. 4.)

kind	A_p (p. 126) (mm ²)	f_u (MPa)	ϵ_u	A	B	C	Dist bottom 1 (mm)	Dist bottom 2 (mm)	Dist bottom 3 (mm)
7/16"	6x 72	1875	23	0.040	102.207	10	305	81	38

Table D.14, Prestress properties

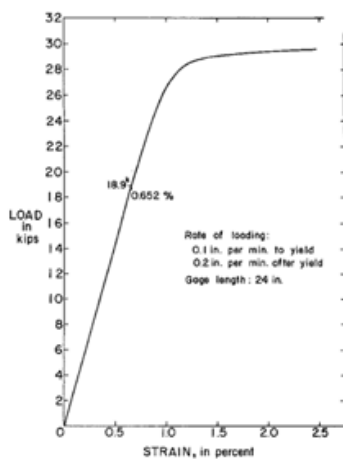


Figure D.20, Load-strain curve prestressing strand (Hanson & Hulbos, 1965)

Beam	F _{cm} (MPa) (Hanson table 2)	F _t (MPa) (automatic)	ε _c (automatic)	Stirrups (Hanson table 1)	Strain in tendons % (Hanson table 4)			P (kN)	A (mm)
					ε ₁	ε ₂	ε ₃		
FX1A	45.9	2.19	2.19	#2@203	0.520	0.520	0.520	408	1219
FX1B	45.9	2.19	2.19	#2@203	0.520	0.520	0.520	408	1219
F1A	47		2.20	#3@127	0.589	0.524	0.511	411	762
F1B	47		2.20	#2@127	0.589	0.524	0.511	411	762
F2A	45.2	2.07	2.18	#3@127	0.561	0.490	0.476	384	1016
F2B	45.2	2.07	2.18	#2@203	0.561	0.490	0.476	385	1016
F3A	47.2	2.10	2.20	#3@169	0.568	0.497	0.483	390	1016
F3B	47.2	2.10	2.20	3/16@102	0.568	0.497	0.483	390	1016
F4A	43.7	2.04	2.15	#2@159	0.537	0.537	0.537	421	1270
F4B	43.7	2.04	2.15	#2@212	0.537	0.537	0.537	421	1270
F5A	44.2	2.05	2.16	#2@127	0.564	0.492	0.492	387	1270
F5B	44.2	2.05	2.16	3/16@106	0.564	0.492	0.492	387	1270
F7A	45.6	2.07	2.18	#2@190	0.593	0.533	0.521	417	1524
F10A	48.6	2.13	2.23	3/16@89	0.583	0.520	0.507	406	1778
F11A	41.6	2.00	2.12	#2@222	0.570	0.496	0.481	389	1778
F19A	51.1	2.17	2.26	#2@127	0.575	0.510	0.497	399	1270
F19B	51.1	2.17	2.26	#2@159	0.575	0.510	0.497	399	1270

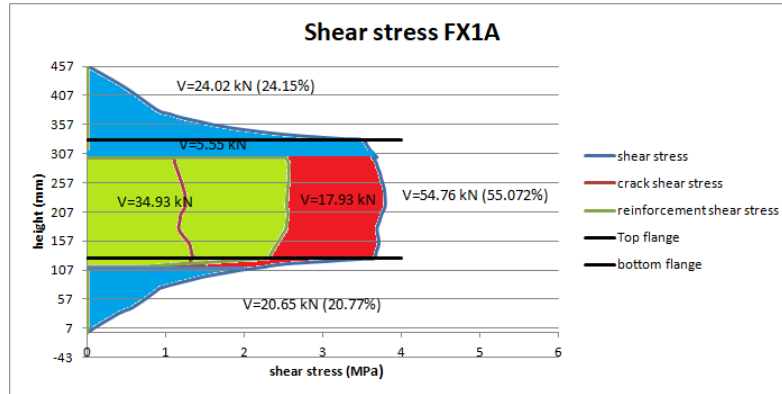
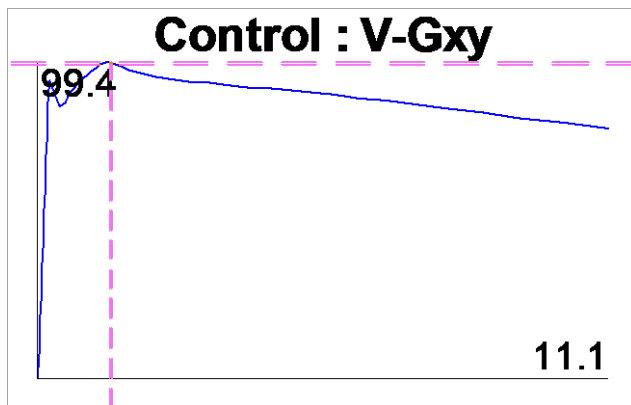
Table D.15, Overview properties per beam

The aggregate size for all beams is 19 mm.

Results

FX1A

After diagonal tension cracking the load drops a bit and the reinforcement on the crack yield immediately. Then the load increases while the maximum shear on the crack decreases and also the principal compressive capacity starts decreasing. The maximum shear resistance is reached at the first moment of slipping of the crack. After this the shear resistance decrease, as well as the principal compressive capacity. The principal compressive capacity ($\epsilon_c = -2.221 > -2.19$), while the stirrup stress no reaches its maximum. The failure mechanism is crushing of the web concrete this is in agreement with the experimental failure mechanism as described in table 6 of (Hanson & Hulbos, 1965).



Cross Section

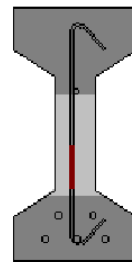
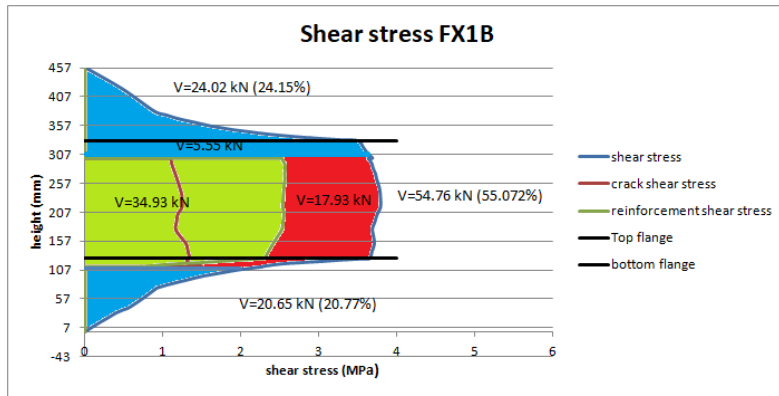
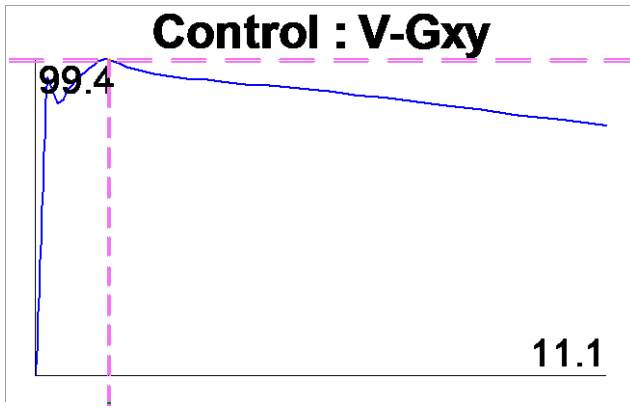


Figure D.21, Contribution of the concrete and steel part to the shear stress over the beam for FX1A

FX1B

After diagonal tension cracking the load drops a bit and the reinforcement on the crack yields immediately. Then the load increases while the maximum shear on the crack decreases and also the principal compressive capacity starts decreasing. The maximum shear resistance is reached at the first moment of slipping of the crack. After this the shear resistance decrease, as well as the principal compressive capacity. The principal compressive capacity ($\epsilon_c = -2.221 > -2.19$), while the stirrup stress no reaches its maximum. The failure mechanism is crushing of the web concrete this is in agreement with the experimental failure mechanism as described in table 5 of (Hanson & Hulbos, 1965).



Cross Section

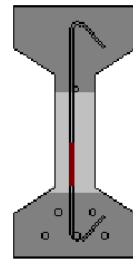
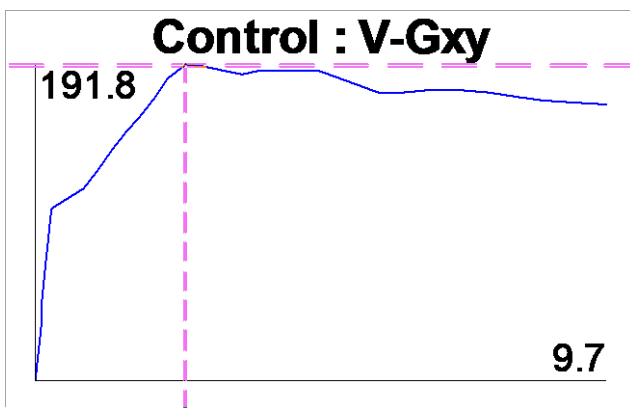


Figure D.22, Contribution of the concrete and steel part to the shear stress over the beam for FX1B

F1A

The load increases after diagonal tension cracking, the reinforcement on the crack yields not directly after cracking but halfway the increasing branch. The maximum shear on the crack decreases after cracking. Also the principal compressive stress capacity decreases. When the maximum load is reached at the moment of first slipping of the crack, the principal compressive stress and the stirrup stress at the crack do not reach their capacity. After this the shear resistance decreases and the principal compressive stress reaches its capacity ($\epsilon_c = -3.126 > -2.20$), while the stirrup stress at the crack does not reach its maximum ($359.9 < 540$). The failure mechanism is crushing of the web concrete this is in agreement with the experimental failure mechanism as described in table 6 of (Hanson & Hulbos, 1965).



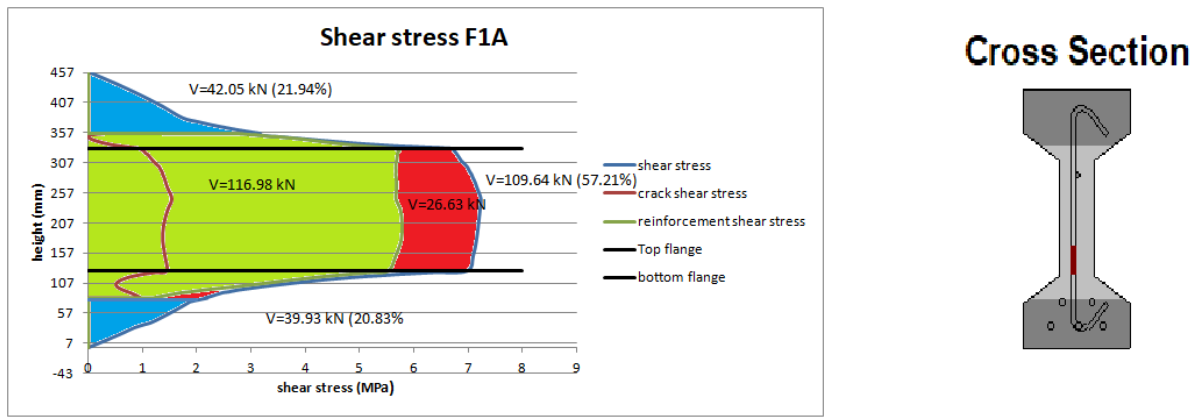


Figure D.23, Contribution of the concrete and steel part to the shear stress over the beam for F1A

F1B

The load increases after diagonal tension cracking, the reinforcement on the crack yields and the maximum shear on the crack and the principal compressive capacity decrease. The maximum load is reached at the moment of first slipping of the crack. At this moment the principal compressive stress and the stirrup stress at the crack do not reach their capacity. After this the shear resistance decreases and the principal compressive stress reaches its capacity ($\epsilon_c = -3.952 > -2.20$), while the stirrup stress at the crack does not reach its maximum ($440.8 < 540$). The failure mechanism is crushing of the web concrete this is in agreement with the experimental failure mechanism as described in table 5 of (Hanson & Hulbos, 1965).

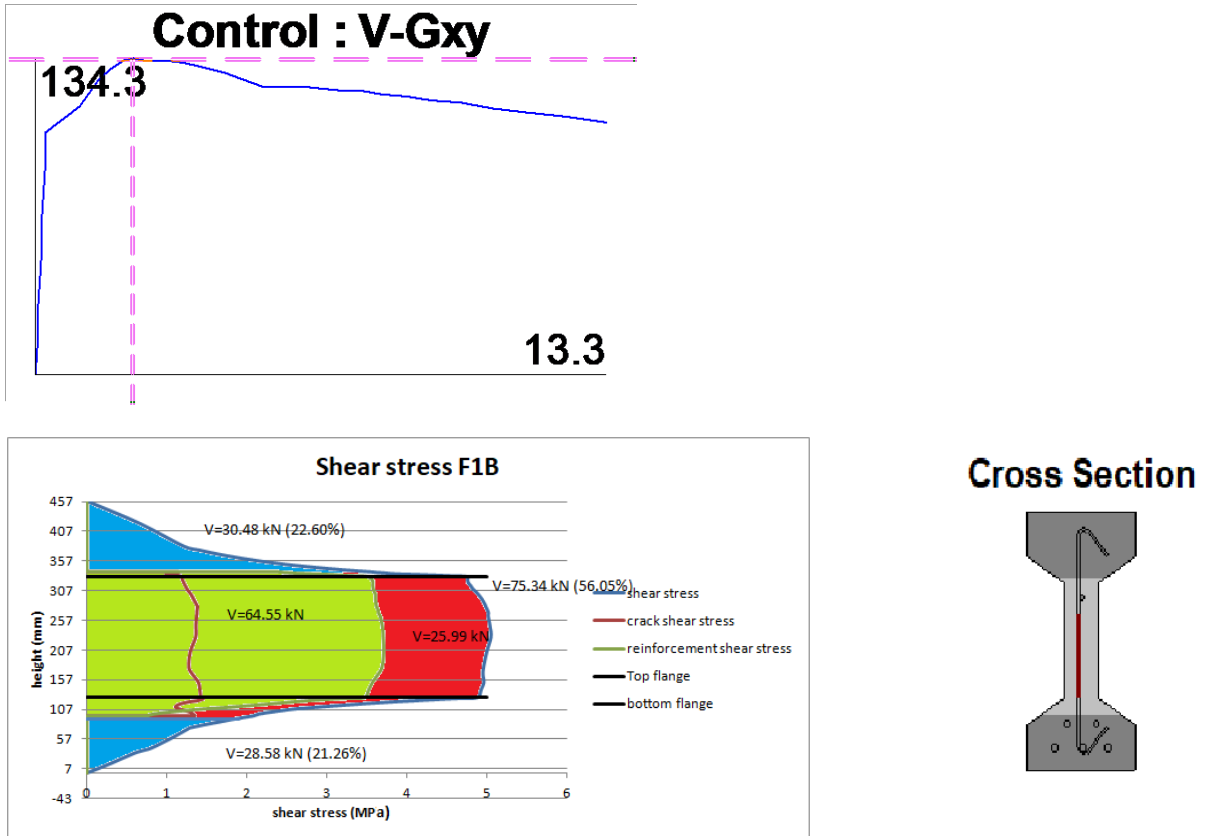
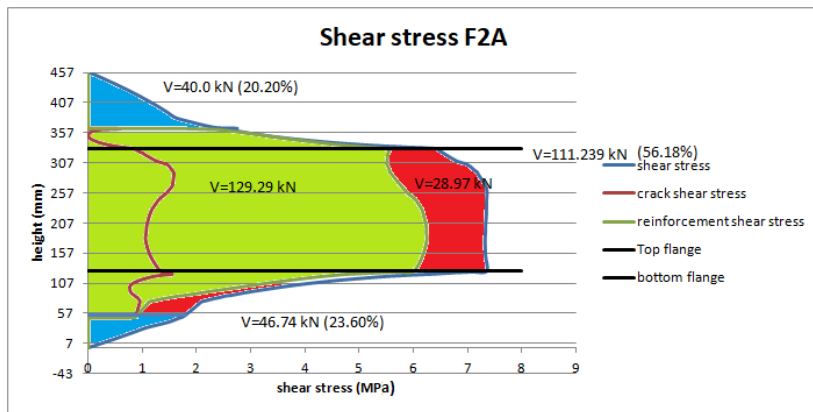
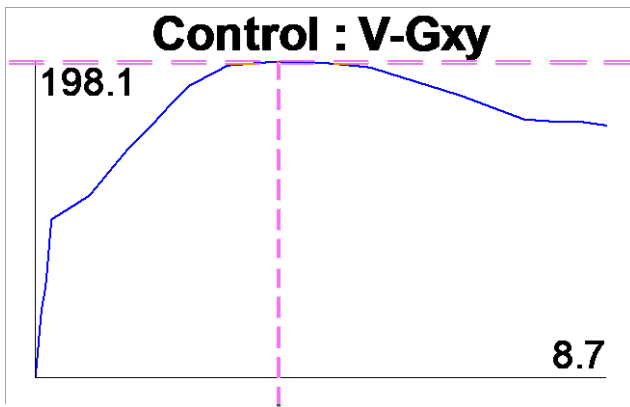


Figure D.24, Contribution of the concrete and steel part to the shear stress over the beam for F1B

F2A

Maximum load increases after diagonal tension cracking, the reinforcement on the crack yields not directly after cracking but halfway the increasing branch. The maximum shear on the crack decreases after cracking. Also the principal compressive stress capacity decreases. The maximum load is reached at the moment slipping of the crack occurs ($\tau_{ci} = \tau_{ci,max}$). The principal compressive stress and the reinforcement stress do not reach their capacity. After this the shear resistance decreases and the principal compressive stress reaches its capacity ($\epsilon_c = -3.097 > -2.18$), while the stirrup stress at the crack not is still at yielding value ($359.9 < 540$). The failure mechanism is crushing of the web concrete this is not in agreement with the experimental failure mechanism which is Rupture of the stirrups as described in table 6 of (Hanson & Hulbos, 1965).



Cross Section

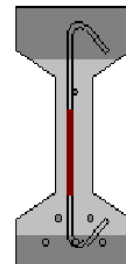


Figure D.25, Contribution of the concrete and steel part to the shear stress over the beam for F2A

F2B

After diagonal tension cracking the load drops a bit and the reinforcement on the crack yields immediately. Then the load increases while the maximum shear on the crack decreases and also the principal compressive capacity starts decreasing. The maximum shear resistance is reached at the first moment of slipping of the crack. After this the shear resistance decrease, as well as the principal compressive capacity. The principal compressive stress reaches its capacity ($\epsilon_c = -2.18 \geq -2.18$), while the stirrup stress does not reach its maximum. The failure mechanism is crushing of the web concrete this is in agreement with the experimental failure mechanism as described in table 5 of (Hanson & Hulbos, 1965).

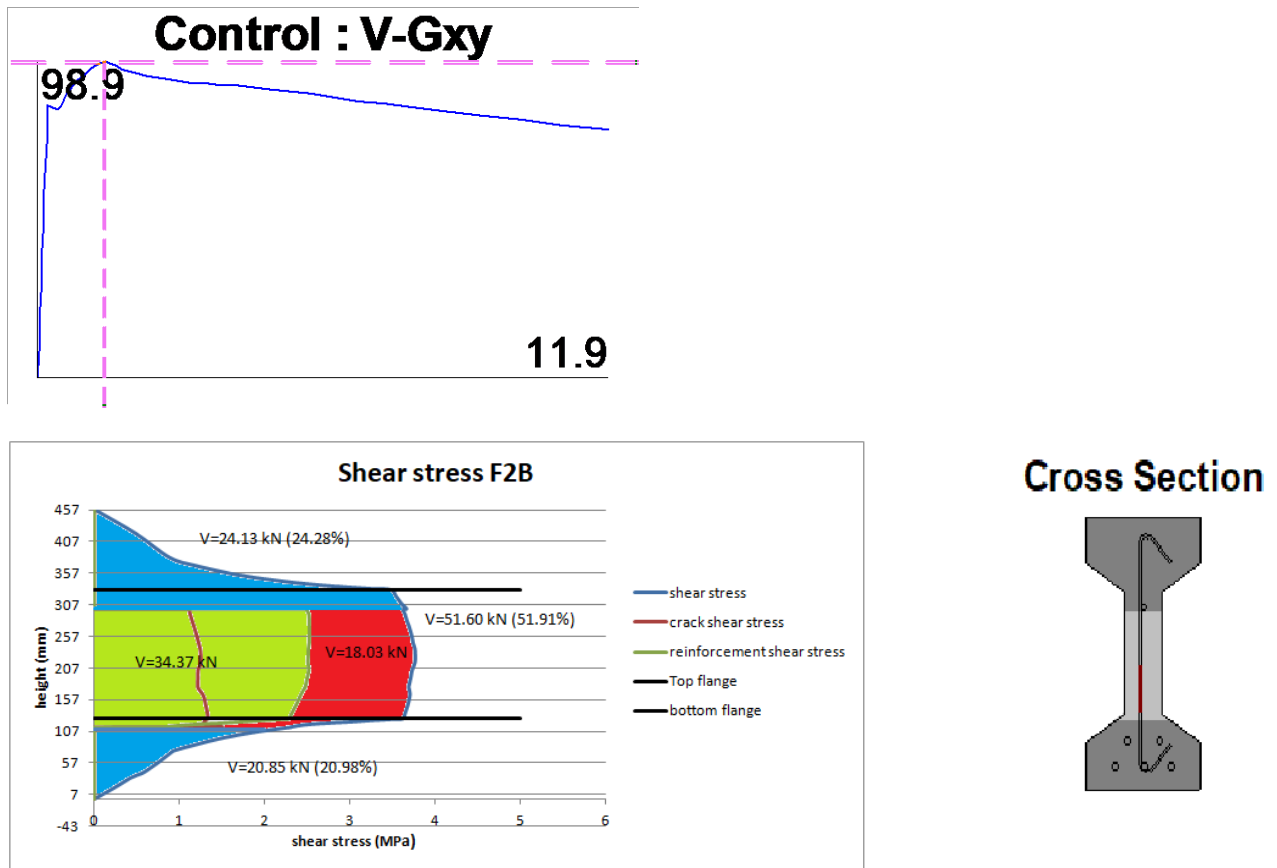
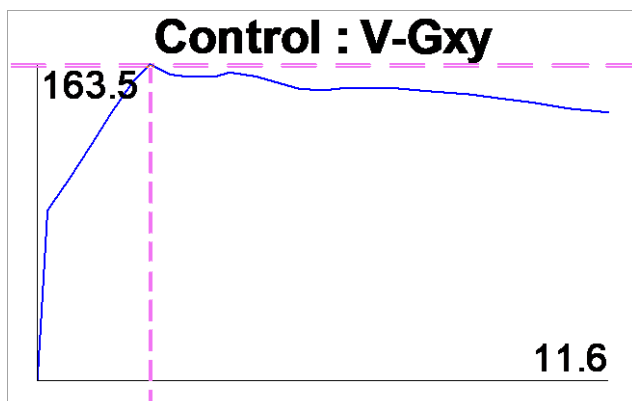


Figure D.26, Contribution of the concrete and steel part to the shear stress over the beam for F2B

F3A

Maximum load increases after diagonal tension cracking, the reinforcement on the crack yields not directly after cracking but halfway the increasing branch. The maximum shear on the crack decreases after cracking. Also the principal compressive stress capacity decreases. The maximum load is reached at the moment slipping of the crack occurs ($\tau_{ci} = \tau_{ci,max}$). The principal compressive stress and the reinforcement stress do not reach their capacity at that moment. After this the shear resistance decreases and the principal compressive stress reaches its capacity ($\epsilon_c = -2.759 > -2.21$), while the stirrup stress at the crack not is still at yielding value ($376.3 < 540$). The failure mechanism is crushing of the web concrete this is in agreement with the experimental failure mechanism as described in table 6 of (Hanson & Hulbos, 1965).



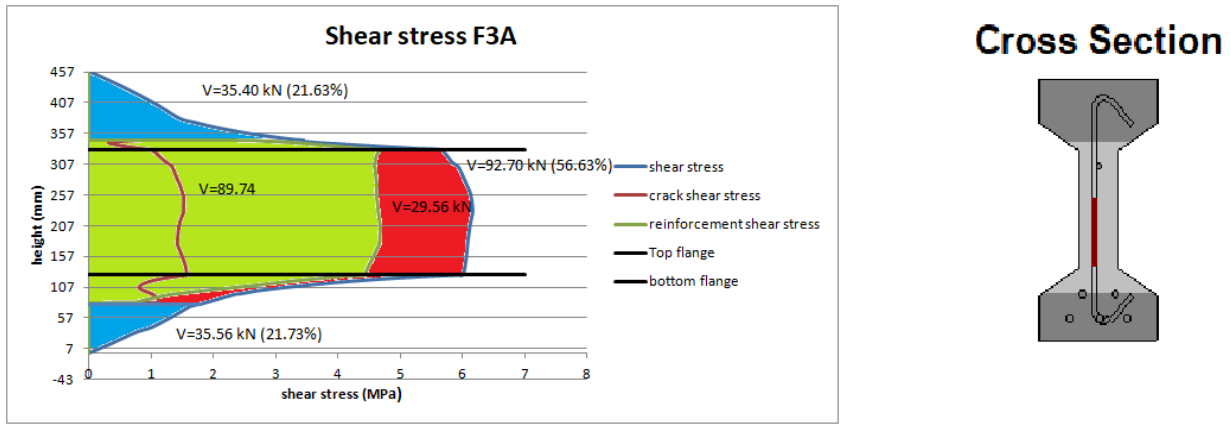


Figure D.27, Contribution of the concrete and steel part to the shear stress over the beam for F3A

F3B

After diagonal tension cracking the load drops a bit, the reinforcement on the crack yields. When the shear resistance starts to increase again the maximum shear on the crack starts decreasing as well as the principal compressive capacity. When the crack slips the stirrup stress at the crack also starts to increase. The maximum shear resistance is reached when the reinforcement stress on the crack reaches the ultimate strength of the reinforcement, the concrete is near crushing at that moment ($\epsilon_c = -1.753 > -2.21$). The failure mechanism is rupture of the stirrups this is not in agreement with the experimental failure mechanism which is crushing of the web concrete as described in table 5 of (Hanson & Hulbos, 1965).

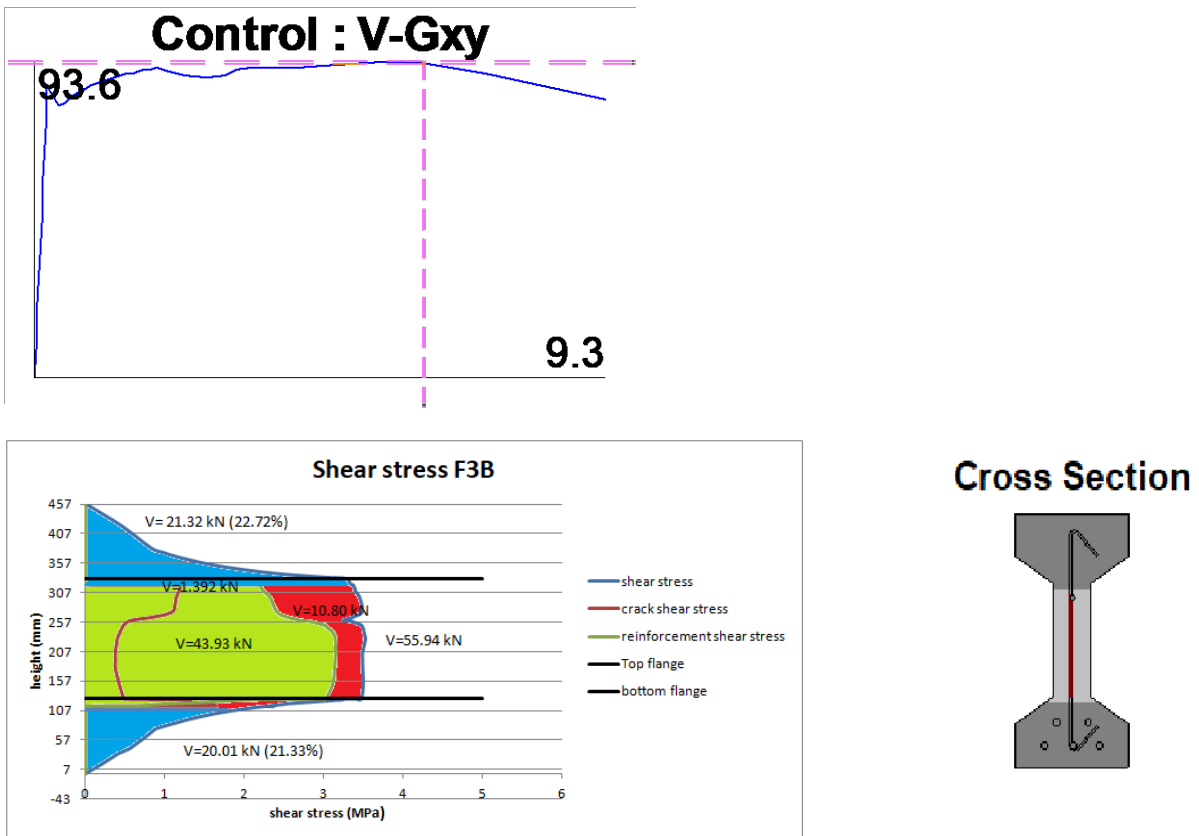


Figure D.28, Contribution of the concrete and steel part to the shear stress over the beam for F3B

F4A

After diagonal tension cracking the load drops a bit and the reinforcement on the crack yield immediately. Then the load increases while the maximum shear on the crack decreases and also the principal compressive capacity starts decreasing. The maximum shear resistance is reached at the first moment of slipping of the crack. After this the shear resistance decrease, as well as the principal compressive capacity. The principal compressive capacity ($\epsilon_c = -2.478 > -2.15$), while the stirrup stress does not reach its maximum. The failure mechanism is crushing of the web concrete this is in agreement with the experimental failure mechanism as described in table 6 of (Hanson & Hulbos, 1965).

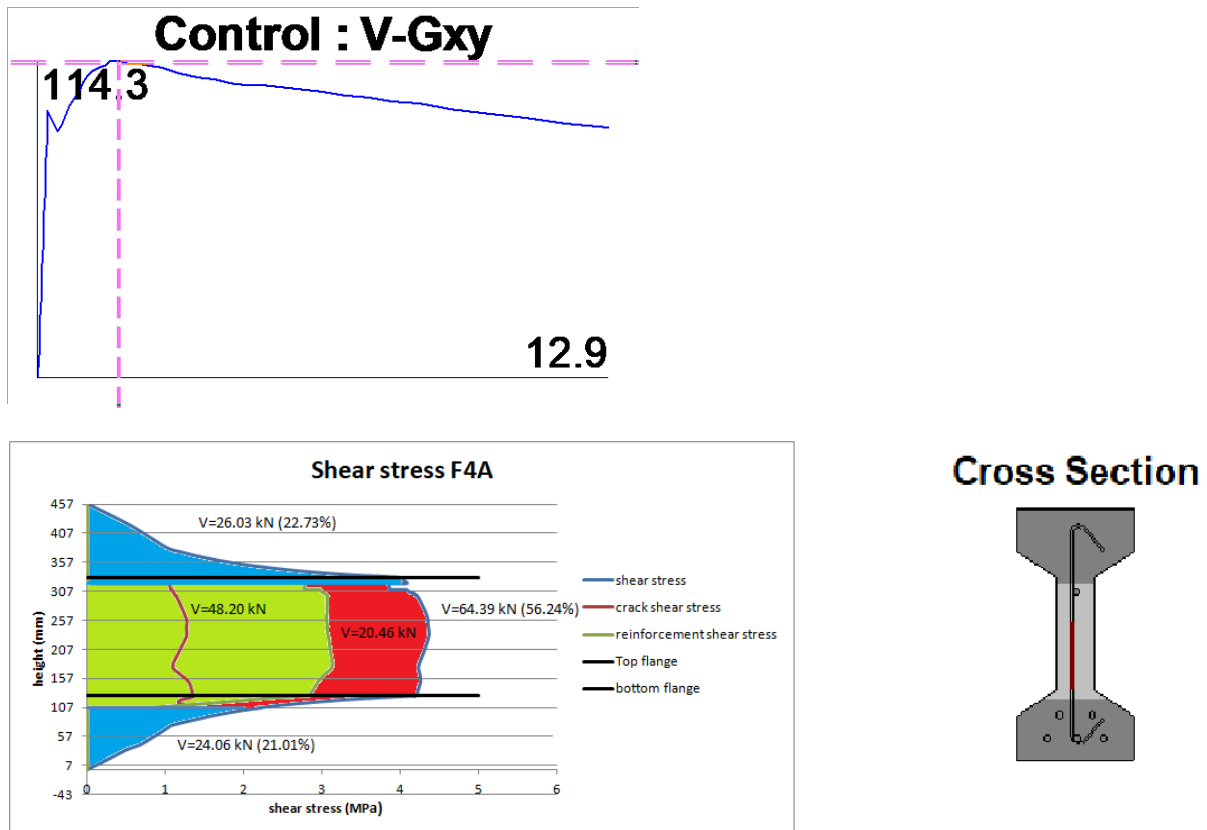
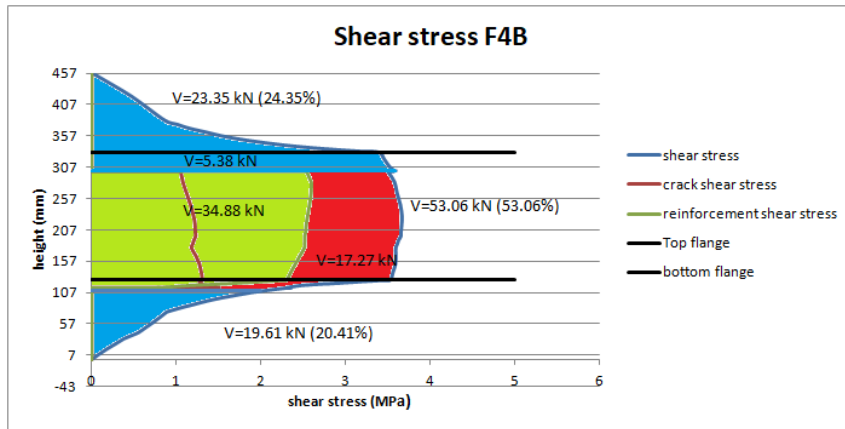
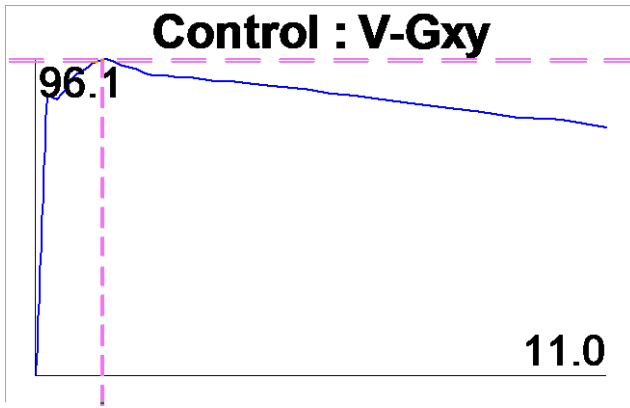


Figure D.29, Contribution of the concrete and steel part to the shear stress over the beam for F4A

F4B

After diagonal tension cracking the load drops a bit and the reinforcement on the crack yields immediately. Then the load increases while the maximum shear on the crack decreases and also the principal compressive capacity starts decreasing. The maximum shear resistance is reached at the first moment of slipping of the crack. After this the shear resistance decrease, as well as the principal compressive capacity. The principal compressive capacity ($\epsilon_c = -2.22 > -2.15$), while the stirrup stress does not reach its maximum ($444.1 < 591$). The failure mechanism is crushing of the web concrete this is not in agreement with the experimental failure mechanism which is Rupture of the stirrups as described in table 5 of (Hanson & Hulbos, 1965).



Cross Section

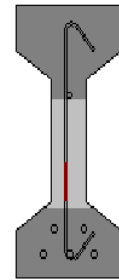
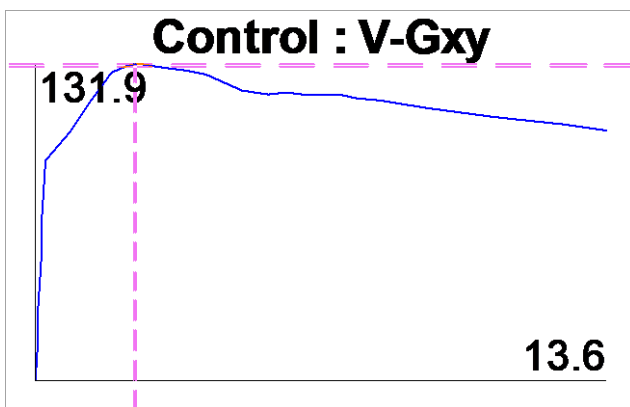


Figure D.30, Contribution of the concrete and steel part to the shear stress over the beam for F4B

F5A

The load increases after diagonal tension cracking and the reinforcement on the crack yields while the maximum shear on the crack and the principal compressive capacity decrease. The maximum load is reached at the moment of first slipping of the crack. At this moment the principal compressive stress and the stirrup stress at the crack do not reach their capacity. After this the shear resistance decreases and the principal compressive stress reaches its capacity ($\epsilon_c = -3.76 > -2.16$), while the stirrup stress at the crack does not reach its maximum ($436.9 < 591$). The failure mechanism is crushing of the web concrete this is not in agreement with the experimental failure mechanism which is denoted as shear compression failure as described in table 6 of (Hanson & Hulbos, 1965).



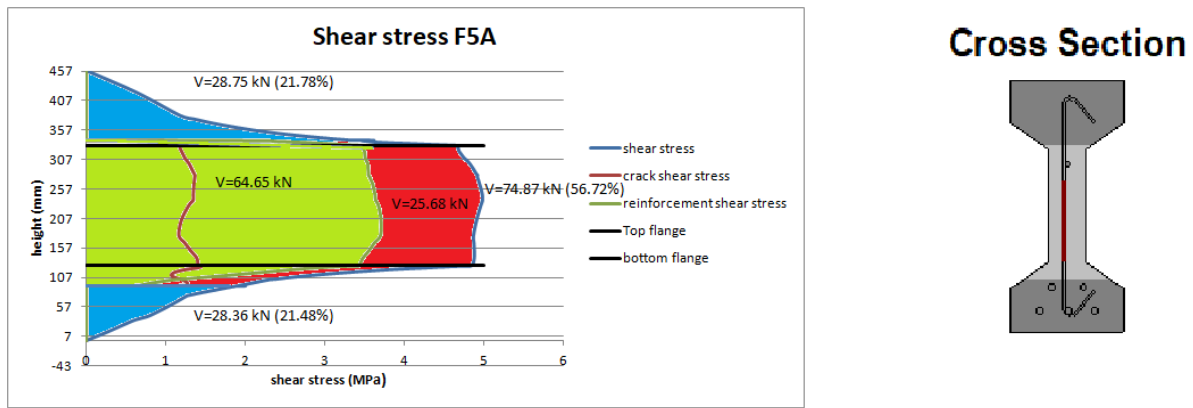
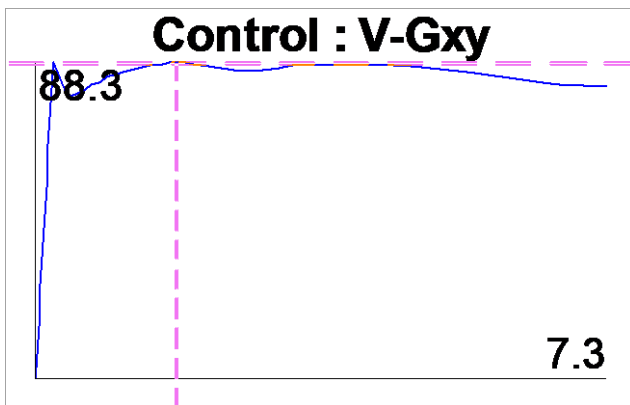
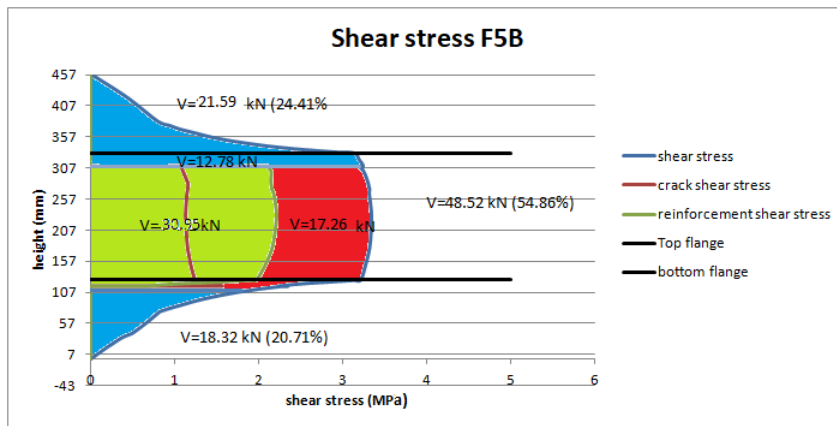


Figure D.31, Contribution of the concrete and steel part to the shear stress over the beam for F5A

F5B

After diagonal tension cracking the load drops a bit and the reinforcement on the crack yields immediately. Then the load increases while the maximum shear on the crack decreases and also the principal compressive capacity starts decreasing. The maximum shear resistance is reached at the first moment of slipping of the crack. After this the shear resistance decrease, as well as the principal compressive capacity. The stirrup stress at the crack increases till the rupture stress is reached after this the principal compressive capacity is also reached. The failure mechanism is rupture of the stirrups this is not in agreement with the experimental failure mechanism which is crushing of the web concrete as described in table 5 of (Hanson & Hulbos, 1965).





Cross Section

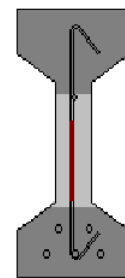
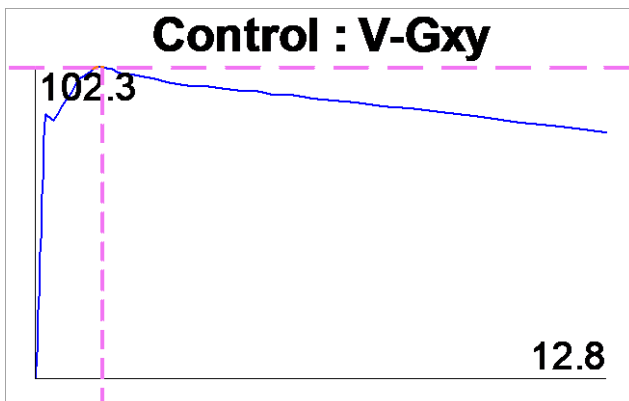


Figure D.32, Contribution of the concrete and steel part to the shear stress over the beam for F5B

F7A

After diagonal tension cracking the load drops a bit and the reinforcement on the crack yields immediately. Then the load increases while the maximum shear on the crack decreases and also the principal compressive capacity starts decreasing. The maximum shear resistance is reached at the first moment of slipping. After this the shear resistance decrease, as well as the principal compressive capacity. The principal compressive capacity ($\epsilon_c = -2.229 > -2.18$), while the stirrup stress does not reach its maximum ($442.7 < 591$). The failure mechanism is crushing of the web concrete this is in agreement with the experimental failure mechanism as described in table 6 of (Hanson & Hulbos, 1965).



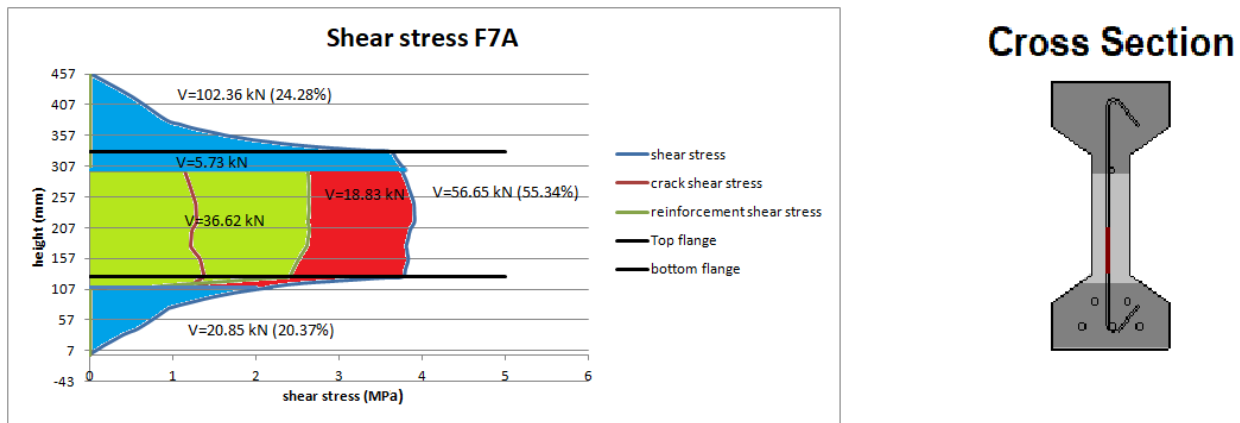


Figure D.33, Contribution of the concrete and steel part to the shear stress over the beam for F7A

F10A

After diagonal tension cracking the load drops a bit, the reinforcement on the crack yields. When the shear resistance starts to increase again the maximum shear on the crack starts decreasing as well as the principal compressive capacity. When the crack slips, the stirrup stress at the crack also starts to increase. The maximum shear resistance is reached when the reinforcement stress on the crack reaches the ultimate strength of the reinforcement, the concrete is near crushing at that moment ($\epsilon_c = -1.428 > -2.23$). The failure mechanism is rupture of the stirrups this is in agreement with the experimental failure mechanism as described in table 6 of (Hanson & Hulbos, 1965).

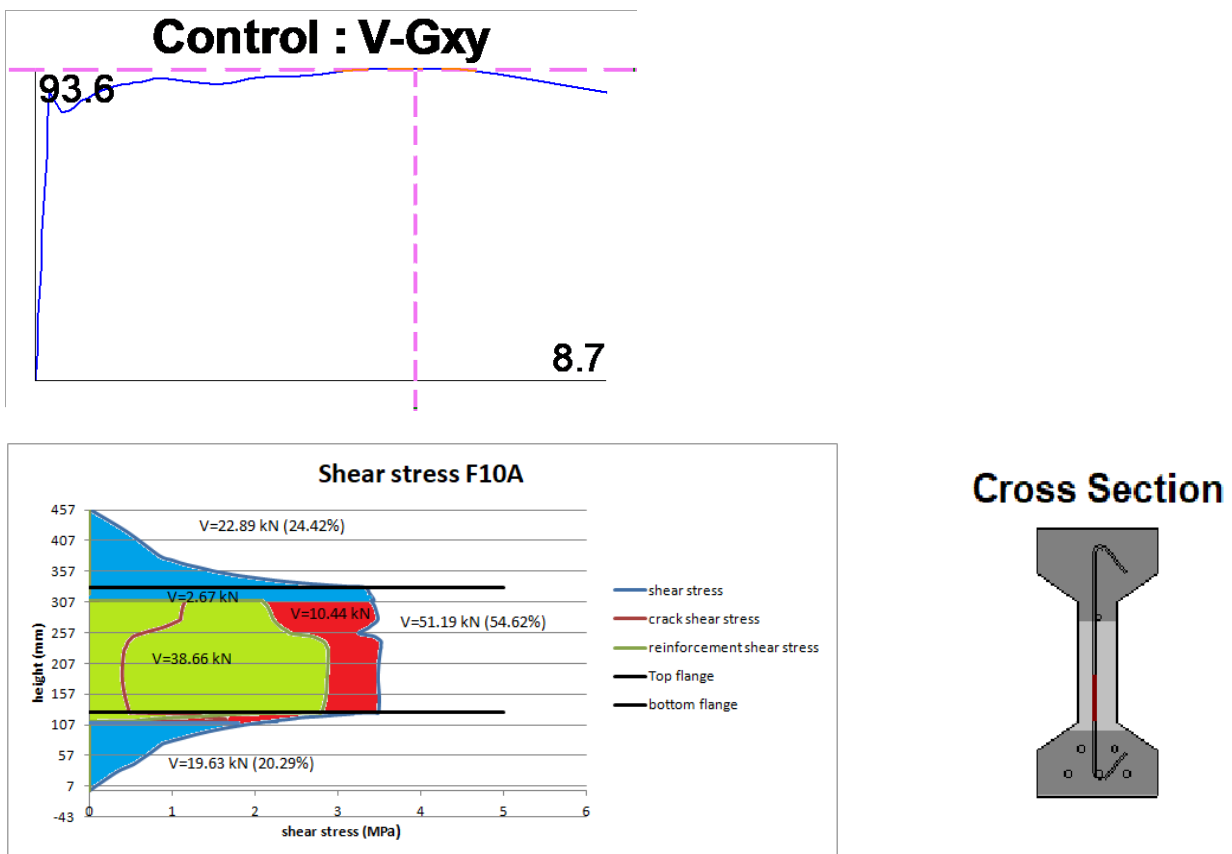
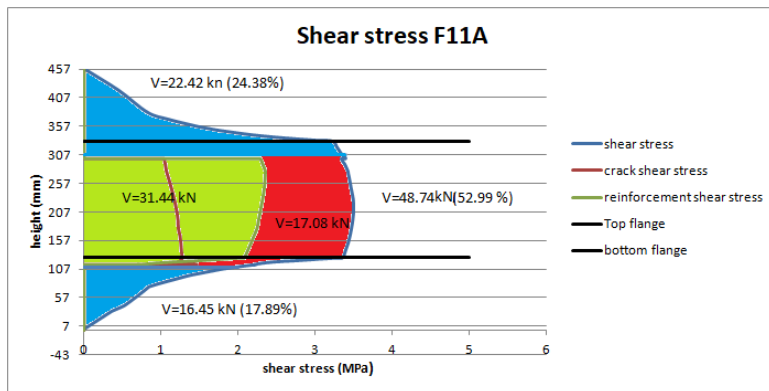
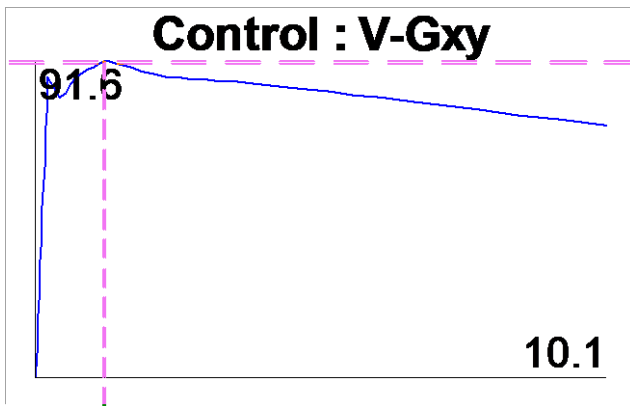


Figure D.34, Contribution of the concrete and steel part to the shear stress over the beam for F10A

F11A

After diagonal tension cracking the load drops a bit and the reinforcement on the crack yields immediately. Then the load increases while the maximum shear on the crack decreases and also the principal compressive capacity starts decreasing. The maximum shear resistance is reached at the first moment of slipping. After this the shear resistance decrease, as well as the principal compressive capacity. The principal compressive capacity ($\epsilon_c = -2.237 > -2.12$), while the stirrup stress does not reach its maximum ($444.0 < 591$). The failure mechanism is crushing of the web concrete this is not in agreement with the experimental failure mechanism which is Rupture of the stirrups as described in table 6 of (Hanson & Hulbos, 1965).



Cross Section

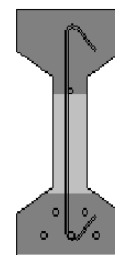
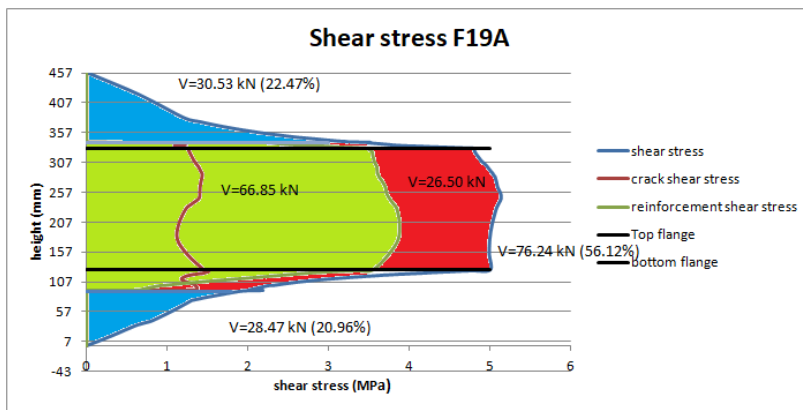
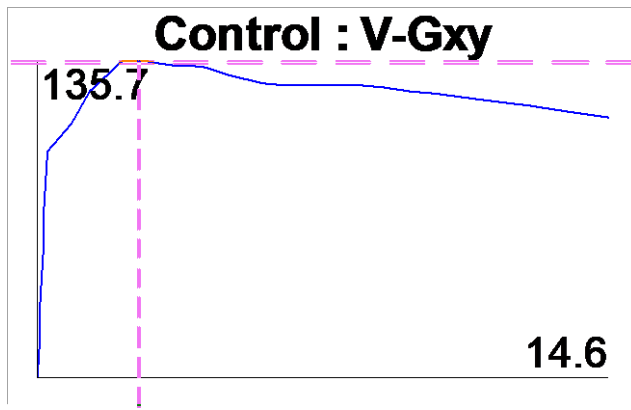


Figure D.35, Contribution of the concrete and steel part to the shear stress over the beam for F11A

F19A

The load increases after diagonal tension cracking, the reinforcement on the crack yields and while the maximum shear on the crack and the principal compressive capacity decrease. The maximum load is reached at the moment of first slipping. At this moment the principal compressive stress and the stirrup stress at the crack do not reach their capacity. After this the shear resistance decreases and the principal compressive stress reaches its capacity ($\epsilon_c = -3.223 > -2.26$), while the stirrup stress at the crack does not reach its maximum ($441.8 < 591$). The failure mechanism is crushing of the web concrete this is in agreement with the experimental failure mechanism as described in table 6 of (Hanson & Hulbos, 1965).



Cross Section

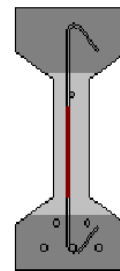
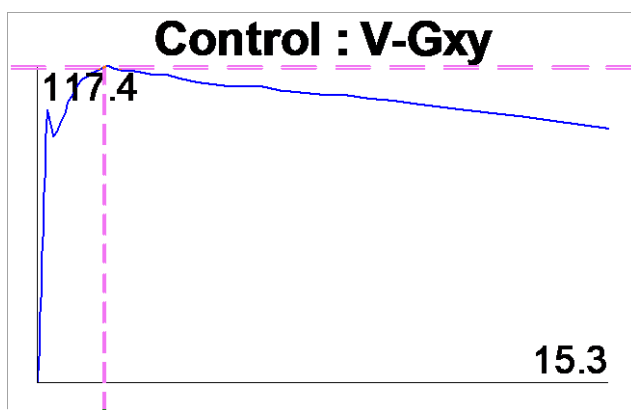
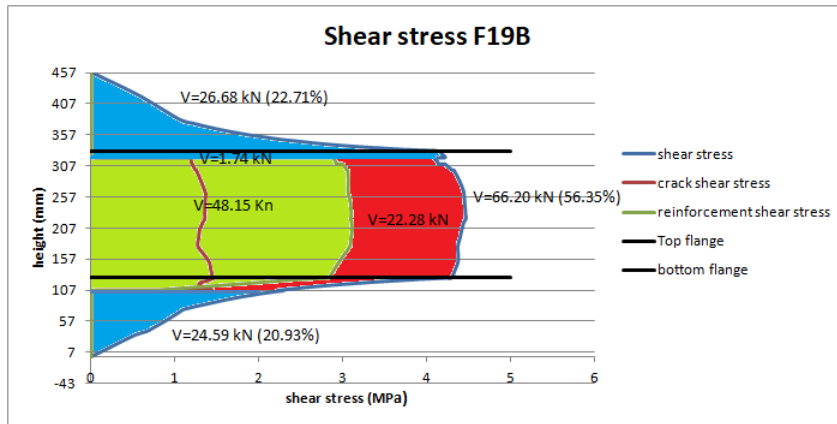


Figure D.36,Contribution of the concrete and steel part to the shear stress over the beam for F19A

F19B

After diagonal tension cracking the load drops a bit and the reinforcement on the crack yields immediately. Then the load increases while the maximum shear on the crack decreases and also the principal compressive capacity starts decreasing. The maximum shear resistance is reached at the first moment of slipping. After this the shear resistance decrease, as well as the principal compressive capacity. The principal compressive capacity ($\epsilon_c = -2.929 > -2.26$), while the stirrup stress does not reach its maximum ($444.0 < 591$).The failure mechanism is crushing of the web concrete, this is not in agreement with the experimental failure mechanism which is rupture of the stirrups as described in table 5 of (Hanson & Hulbos, 1965).





Cross Section

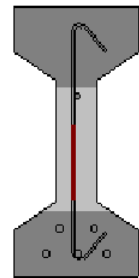


Figure D.37, Contribution of the concrete and steel part to the shear stress over the beam for F19B

D.4 Leonhardt

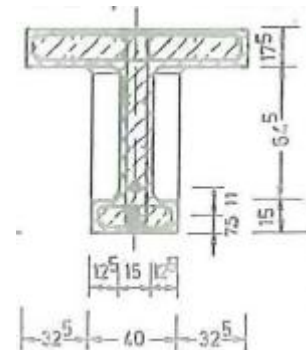
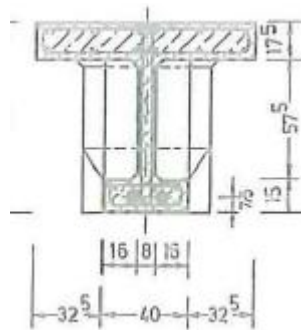
The beams TP2 and TP4 are entered in Response with the following parameters, from Leonhardt (Leonhardt, Koch, & Rostasy, 1973).

Concrete

cross-section

	TP2	TP4
h (mm)	970	900
h_{f top} (mm)	175	175
h_{f bot} (mm)	150	150
b_{f top} (mm)	1050	1050
b_{f bot} (mm)	400	400
b_{web} (mm)	150	80

Table D.16, Concrete cross-section



Concrete properties ((Leonhardt, Koch, & Rostasy, 1973)table 4.3)

	f_{cm} (MPa)	f_t (automatic) (MPa)	ε_{c'} (mm/m)	a_g (mm)
TP2	22.8	1.57	1.88	30
TP4	46.6	2.09	2.20	15

Table D.17, Concrete properties

Reinforcement

Longitudinal reinforcement

Place	kind	Distance from the bottom (mm)
Top	2x6Ø14	936 and 827 (TP2) 866 and 757 (TP4)
web	2x2Ø8	421 and 590 (TP2) 325 and 536 (TP4)
Bottom	5Ø8 (TP4) 6Ø8 (TP2)	34

Table D.18, Longitudinal reinforcement configuration

Stirrups

Place	kind	Distance from the bottom (mm)	Distance from the top (mm)
Web	Ø10@85 (TP4) Ø10@150(TP2)	25	25

Table 6.19, Transverse reinforcement configuration

Reinforcement properties

	f_y (MPa)	f_u (MPa)	ϵ_{sh} (mm/m)	ϵ_u (mm/m)	E_s (MPa)
Ø10	423	545	2.1	157	198094
Ø8	451	556	2.3	150	193191
Ø14	389	507	1.9	169	202998

Table D.20, Reinforcement properties

Prestress

	A_p (p. 126) (mm ²)	f_u (MPa)	ϵ_u	A	B	C	Dist bottom 1 (mm)	Dist bottom 2 (mm)	P (kN)
TP2	2x 1401	1337	16	0.083	160.8	10	75	110	1912
TP4	2x1401	1337	16	0.083	160.8	10	75	75	1780

Table D.21, Prestress properties

Results

TP2

After diagonal tension cracking the force increases, the stirrup on the crack does not yield immediately. When the reinforcement on the crack yields, the shear on the crack starts increasing while the maximum shear on the crack decreases. The reinforcement does not slip when the maximum load is reached. The principal compressive stress and the stirrup stress at the crack do not reach their capacity at maximum load. After this the shear resistance decreases and the principal compressive stress reaches its capacity ($\epsilon_c = -2.735 > -1.88$), while the stirrup stress at the crack does not reach its maximum ($431.6 < 545$). The failure mechanism is crushing of the web concrete this

is in agreement with the experimental failure mechanism as described in chapter 8 (Leonhardt, Koch, & Rostasy, 1973).

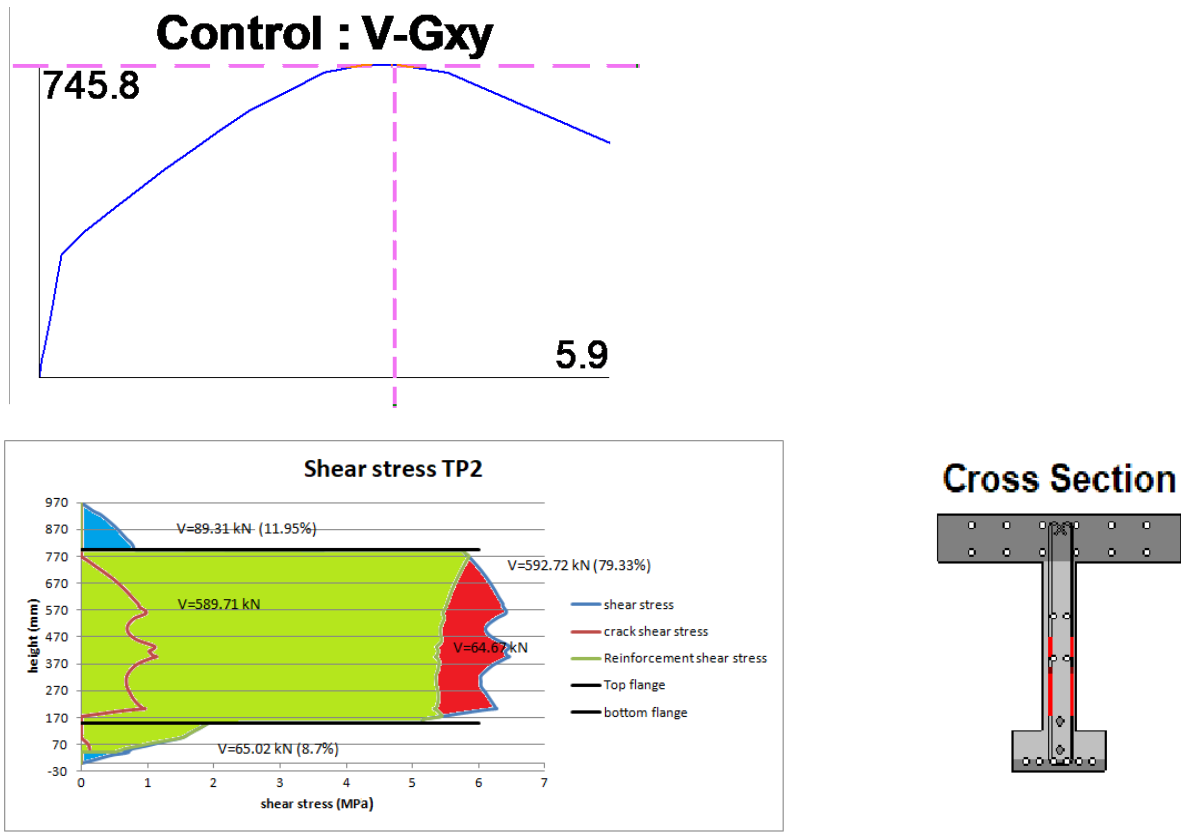
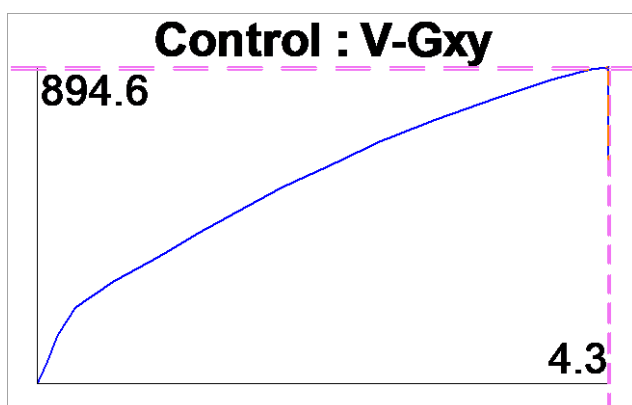


Figure D.38, Contribution of the concrete and steel part to the shear stress over the beam for TP2

TP4

After diagonal tension cracking the force increases, the stirrup on the crack does not yield immediately. When the reinforcement on the crack yields the shear on the crack starts increasing while the maximum shear on the crack decreases. The reinforcement does not slip when the maximum load is reached. The principal compressive stress reaches the principal compressive capacity at the maximum load ($\epsilon_c = -2.261 > -2.20.$), while the stirrup stress at the crack does not reach its maximum ($426.9 < 545$). The failure mechanism is crushing of the web concrete this is in agreement with the experimental failure mechanism as described in chapter 8 of (Leonhardt, Koch, & Rostasy, 1973).



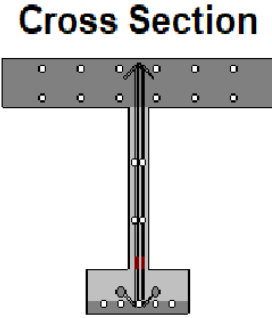
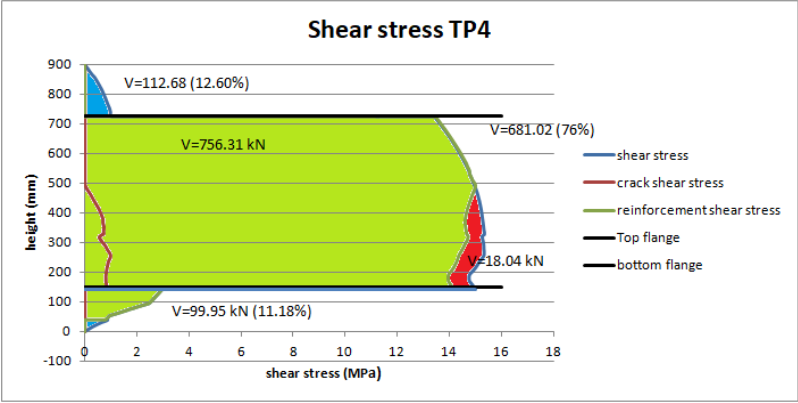


Figure D.39, Contribution of the concrete and steel part to the shear stress over the beam for TP4

E shear tension model accuracy

Table E.1 gives an overview of the accuracy of each beam for the proposed shear tension model compared to the experiments.

Table E.1, Shear tension model accuracy overview

Beam	V_{exp} (kN)	V_{yield} (kN)	V_{crush} (kN)	V_{max} (kN)	V (kN)	V_{exp}/V
LB2	172	139.5	125	620.6	139.5	1.23
LB3	149	129	123	612.3	129	1.15
LB6	155.8	151	132	649.0	151	1.03
LB7	137.8	132.5	129	649.0	132.5	1.04
LB8	134.3	139	130	647.4	139	0.97
LB10	215	210	229.5	645.4	229.5	0.94
HAP1TE	632	508	539.5	1787.8	539.5	1.17
HAP1TW	749	509	539.76	1787.8	539.76	1.39
HAP2TW	605.3	494.26	537	1881.9	537	1.13
HCP1TE	779	494	532.52	1591.7	532.52	1.46
HCP1TW	741	495.5	533.55	1591.7	533.55	1.39
HCP2TE	721	485	533.21	1768.2	533.21	1.35
HCP2TW	683	486	533.55	1768.2	533.55	1.28
FX1A	167	98.7	98	391.7	98.7	1.69
FX1B	142	98.7	98	391.7	98.7	1.434
F1A	286	190	206	401.1	206	1.39
F1B	267	123.5	140	401.1	140	1.90
F2A	214	196	236	385.8	236	0.91
F2B	178	97.2	98	385.8	98	1.82
F3A	224	152	163	402.8	163	1.37
F3B	178	84	74	402.8	84	2.12
F4A	177	109	117.5	373.0	117.5	1.51
F4B	169	96	95	373.0	96	1.76
F5A	179	121	139	377.2	139	1.29
F5B	143	81	71.7	377.2	81	1.77
F7A	154	102	103.2	390.0	103.2	1.49
F10A	129	90.5	82.5	414.8	90.5	1.43
F11A	129	91.2	90.8	355.0	91.2	1.41
F19A	178	126.2	141.5	436.1	141.5	1.26
F19B	176	113.5	119.4	436.1	119.4	1.47
Tp2	746	727.65	722.51	882.4	727.65	1.03
Tp4				879.4	879.4	1.00
totaal						1.36